

ПЛОВДИВСКИ УНИВЕРСИТЕТ „ПАИСИЙ ХИЛЕНДАРСКИ“
UNIVERSITY OF PLOVDIV „PAISII HILENDARSKI“

**НАУЧНИ
ТРУДОВЕ
ТОМ 38, кн. 5, 2011**

Химия

УНИВЕРСИТЕТСКО ИЗДАТЕЛСТВО „ПАИСИЙ ХИЛЕНДАРСКИ“

НАУЧНИ ТРУДОВЕ, ТОМ 38, КН. 5, 2011 – ХИМИЯ
UNIVERSITY OF PLOVDIV „PAISII HILENDARSKI“ – BULGARIA
SCIENTIFIC PAPERS, VOL. 38, BOOK 5, 2011 – CHEMISTRY

Редакционна колегия:

Председател: доц. д-р Илиян Иванов

Членове: доц. д-р Мария Стоянова

доц. д-р Виолета Стефанова

ISSN 0204–5346

СЪДЪРЖАНИЕ

APPLICATION OF BARE AND SILICA-COATED $MnFe_2O_4$ MAGNETIC NANOPARTICLES AS A SORBENT FOR SOLID PHASE EXTRACTION AND ICP-OES TRACE ELEMENTS DETERMINATION	7
<i>D. Georgieva, V. Stefanova, V. Kmetov, I. Roman, N. Kovachev, A. Canals</i>	
APPLICATION OF CLASSICAL METHODS TO ISOLATION OF RUTIN FROM ORIENTAL TOBACCOS.....	23
<i>M. Docheva, S. Dagnon</i>	
ЕКСТРАКЦИЯ НА ЛИПИДНИ КОМПОНЕНТИ ОТ БИОМАСА НА ПСИХРОФИЛНИ ДРОЖДИ.....	29
<i>С. Димитрова, Л. Луканов, К. Павлова</i>	
ОПРЕДЕЛЯНЕ НА КОЛИЧЕСТВА ОТ ХЕРБИЦИДА ФЛУМИОКСАЗИН В ЧЕРЕШИ ЧРЕЗ ИЗПОЛЗВАНЕ НА ВИСОКОЕФЕКТИВНА ТЕЧНА ХРОМАТОГРАФИЯ	37
<i>Д. Божилков, Ил. Козанова, С. Даньо, З. Ранкова, Ст. Николова, Ил. Иванов</i>	
СПЕКТРОФОТОМЕТРИЧЕН МЕТОД ЗА ОПРЕДЕЛЯНЕ НА ФРУКТАНИ В ХРАНИ	45
<i>Н. Петкова, М. Саватинова, Б. Витанова, П. Денев</i>	
RELATIONSHIP BETWEEN MOLYBDENUM AND NITRATE NITROGEN IN PLANTS AND THEIR YIELD.....	55
<i>D. Kostova, D. Haytova</i>	
AUTOMATIC GENERATION OF TAUTOMERS.....	65
<i>N. Kochev, V. Paskaleva, N. Jeliazkova</i>	
EXCITED-STATE REACTION PATHS OF CYTOSINE AND ISOCYTOSINE: C=O ELONGATION	71
<i>P. Kancheva, V. Delchev</i>	

THE NUCLEOPHILIC SUBSTITUTION REACTION OF SULFINIC ACIDS WITH HALONITROALKANES	81
<i>S. Ivanova, D. Koleva</i>	
SELECTIVE ACETOXYLATION OF CYCLODODECENE BY DIOXIGEN CATALYZED BY PALLADIUM(II) ACETATE, HYDROQUINONE AND IRON(II) PHTHALOCYANINE	87
<i>A. Kolev, E. Balbolov</i>	
SYNTHESIS AND ANTIMICROBIAL EVALUATIONS OF SOME NOVEL DERIVATIVES OF BENZIMIDAZOLE	95
<i>M. Staykova, S. Statkova-Abeghe, S. Kostadinova, M. Marhova, V. Stoyanova</i>	
MULTIFUNCTIONAL MECHANOCHEMICALLY-SYNTHESIZED Fe₂O₃-ZnO MIXED OXIDE.....	101
<i>N. Kostova, Al. Eliyas, M. Fabian, B. Kunev, N. Velinov, P. Balaz</i>	
PHOTOCATALYTIC TESTING OF MECHANOCHEMICALLY- SYNTHESIZED CADMIUM SELENIDE	111
<i>Al. Eliyas, M. Achimovičová, N. Kostova, A. Zorkovská, P. Baláž</i>	
ROLE OF THE PREPARATION METHOD ON CATALYTIC ACTIVITY OF Ag/CeO₂ FOR OXIDATION OF CO, CH₃OH AND (CH₃)₂O	119
<i>T. Tabakova, D. Dimitrov, K. Ivanov, V. Idakiev</i>	
PHOTOCATALYTIC ACTIVITY OF SPRAYED TiO₂ FILMS DEPOSITED ON DIFFERENT SUBSTRATES	133
<i>I. Stambolova, V. Blaskov, M. Shipochka, S. Vassilev, A. Loukanov</i>	
DECOLORIZATION OF REACTIVE BLACK 5 DYE ON TiO₂ HYBRID FILMS DEPOSITED BY SOL GEL METHOD	145
<i>V. Blaskov, I. Stambolova, M. Shipochka, S. Vassilev, N. Kaneva, A. Loukanov</i>	

THERMODYNAMIC DESCRIPTION OF THE Cu-Mg-Sn SYSTEM AT THE Cu-Mg SIDE	157
<i>J. Miettinen, G. Vassilev</i>	
ЕЛЕКТРОХИМИЯ НА МИОГЛОБИН ХЕМИСОРБИРАН ВЪРХУ ПОЗЛАТЕН ГРАФИТ	167
<i>Д. Георгиева, Т. Додевска, Ел. Хорозова, Н. Димчева</i>	
СИНТЕЗ НА ФЕРИТИ ОТ СИСТЕМАТА $MeO-Fe_2O_3$ ($Me=Zn, Cd$) И ИЗСЛЕДВАНЕ НА ТЯХНАТА РАЗТВОРИМОСТ В H_2SO_4.....	177
<i>А. Пелтеков, Б. Боянов</i>	
WASTE TONERS AND CARTRIDGES – UTILIZATION OPTION.....	191
<i>G. Patronov, D. Tonchev</i>	
RISK ASSESSMENT OF CYCLODODEC-2-EN-1-YL ETHERS IN THE ENVIRONMENT.....	197
<i>As. Kolev, Y. Koleva</i>	
АНТИОКСИДАНТЕН КАПАЦИТЕТ НА ПЛОДОВЕ НА ЧЕРНА БОРОВИНКА	205
<i>Р. Динкова, М. Георгиева, К. Василев, К. Михалев, Н. Йончева, Х. Динков</i>	
ЛИПИДЕН СЪСТАВ НА СЕМЕНА ОТ КИПАРИС.....	213
<i>М. Ангелова-Ромова, М. Златанов, Г. Антова, О. Тенева</i>	
FATTY ACIDS COMPOSITION AND FAT SOLUBLE VITAMINS CONTENT OF BIGHEAD CARP (ARISTICHTHYS NOBILIS).....	221
<i>А. Merdzhanova, D. Dobрева, М. Stancheва</i>	
ORGANOCHLORINE PESTICIDES AND POLYCHLORINATED BIPHENYLS IN FRESHWATER FISH.....	233
<i>St. Georgieva, M. Stancheва, L. Makedonski</i>	

APPLICATION OF BARE AND SILICA-COATED MnFe_2O_4 MAGNETIC NANOPARTICLES AS A SORBENT FOR SOLID PHASE EXTRACTION AND ICP-OES TRACE ELEMENTS DETERMINATION

*D. Georgieva^a, V. Stefanova^a, V. Kmetov^a, I. Roman^b,
N. Kovachev^b, A. Canals^b*

*^aDepartment of Analytical Chemistry and Computer Chemistry,
University of Plovdiv „Paisii Hilendarski“,
24 Tzar Assen, Str., 4000 Plovdiv, Bulgaria
e-mail: georgieva@uni-plovdiv.bg*

*^bDepartment of Analytical Chemistry and Food Science,
and University Materials Institute, University of Alicante,
P. O. Box 99, 03080 Alicante, Spain*

ABSTRACT

Magnetic nanosized sorbent material based on MnFe_2O_4 (MnNPs) was synthesized by co-precipitation. Silica coated nanoparticles (SMnNPs) were obtained and both types coated and non-coated nanoparticles were tested for solid phase extraction of V, Co, Cr, Ni, Cu, Zn, Pb and Cd complexes with ammonium pyrrolidine dithiocarbamate (APDC).

The analytes restoration into the final solution was achieved by treatment with 7 mol L^{-1} nitric acid at 25°C . The elution of elements for 10 min from

both kinds of nanoparticles and complete digestion of the bare ones for 4h were compared with respect to the recovery and the level of matrix effects in ICP-OES.

The observed matrix suppression of emission signals in the range 12% (Cu) to 37% (Cd, Pb) was caused by the high acid concentration. Dilution of the final solution prior instrumental analysis to 2.8 mol L⁻¹ nitric acid gives matrix effect reduction by a factor of 3 to 5, but also decreases the enrichment factor. There were no spectral interferences when SMnNPs eluates were measured. Due to the presence of Fe and Mn the obtained emission spectrum was significantly complicated in the case of bare MnNPs, hence special attention should be paid to the emission line selection and spectral interference corrections.

The elution of non-modified MnNPs was preferred instead of total digestion to reduce the matrix effects.

Using SMnNPs quantitative recoveries were obtained for Co, Cu and Ni, while for other elements R% were in range 60% – 85%. For all analytes R%≥90% were achieved with the exception of Cd (R=72%) applying bare MnNPs.

At the optimized SPE conditions an enrichment factor of 10 was obtained which allows detection limits decrease by factors 2–7 (SMnNPs) and 3–8 (MnNPs), in comparison to direct ICP-OES determination.

Key words: *magnetic nanoparticles, solid phase extraction, trace elements, ICP-OES*

INTRODUCTION

The utilization of nanoparticles in the solid phase extraction procedure for separation and pre-concentration of target analytes is a topic of growing interest¹⁻³. The application of magnetic nanoparticles (MNPs) is promising because they combine the general advantage of active surface of nanosized materials having high area to volume ratio with superparamagnetic properties which allows easy separation from the sample solution by means of external magnet and can simplify the analytical procedure^{1,3,4}.

Among different nanoparticles with magnetic properties⁵ only the surface modified magnetite (Fe₃O₄) have been exploited as a sorbent in

the solid phase extraction procedures (SPE) for trace elements⁶⁻¹⁵ and speciation¹⁶⁻¹⁸ analysis.

The mechanisms for elements retention on the surface of nanoparticles could be summarized as follow: i) chemical bonding of the analytes with active groups linked to the surface^{7-12, 14-18} or ii) sorption of the element complexes, preliminary formed in sample solution^{6, 13}. To the best of our knowledge the sorption of the hydrophobic complexes on the surface of non-modified magnetic nanoparticles has not been studied yet.

Different approaches for surface modification of the sorbent could be distinguished. A modification with active ligands as: polyacrylic acid was used for group SPE of Mn, Co, Cu, Zn, and Pb⁸; 1-(2-pyridylazo)-2-naphthol (PAN) was used for SPE of Mn⁹ and morin was used for Zn¹⁰ and Cu¹⁵.

Surfactants anchored chemically or physically adsorbed on the surface of nanoparticles may form single or double layer (hemimicelles, mixed hemimicelles, and admicelles) which stabilizes the solid phase in suspension and improves extraction efficiency^{6, 13}. The modification of magnetic nanoparticles with decanoic acid and sodium dodecyl sulphate have been developed from Faraji et al.^{6, 13} for SPE of Cd, Co, Cr, Ni, Pb, Zn as hydrophobic PAN complexes and mercury-Michler's thioketone complexes respectively.

Most of the methods incorporate two modification steps: preliminary covering of the nanoparticles with silica layer and further surface modification with complexing agent. The silica layer ensures sorbent protection in acidic media, decreases the agglomeration propensity but at the expense of loss of magnetic properties¹. Silica coated nanoparticles additionally modified with γ -mercaptopropyltrimethoxysilane have been applied for fast and selective SPE of trace amounts of Cd, Cu, Hg, and Pb¹²; for speciation of inorganic Te¹⁷ and for microextraction of Cd, Pb, and Hg from HepG2 cells⁷. The same group used the silica covered Bismuthiol-II – immobilized magnetite nanoparticles for SPE of trace amounts of Cr, Cu and Pb¹⁴ and amino-modified silica-coated magnetic nanoparticles for speciation of inorganic As¹⁸. Wu et al. reported application of the silica-coated Fe₃O₄ nanoparticles modified with N-(2-aminoethyl)-3-aminopropyltrimethoxy-silane for speciation of Cr¹⁶. Magnetite nanoparticles modified with 3-(trimethoxysilyl)-1-propanthiol and subsequent immobilized with 2-amino-5-mercapto-1,3,4-

thiadiazole have been employed for separation and preconcentration of trace amounts of Ag, Cd, Cu, and Zn¹¹.

In most of the published papers MNPs-SPE methods were combined with ICP-OES^{6, 9–11, 13, 14} or ICP-MS^{8, 12, 17, 18} as instrumental techniques for detection. However the study of non-spectral and spectral matrix effect in solutions obtained after SPE was not found.

Substituted iron oxides such as CoFe_2O_4 ¹⁹ or MnFe_2O_4 ²⁰ have been recently applied for SPE of UV filters from cosmetic samples and bovine serum albumin (BSA) respectively. Hu et al²¹ investigated the properties of substituted ferrites with common formula MeFe_2O_4 (where Me =Mn, Mg, Zn, Cu, Ni and Co) for removal of Cr(VI) from synthetic electroplating wastewater. The authors reported that among all tested sorbents MnFe_2O_4 nanoparticles have shown the strongest magnetic properties and the highest surface area which makes them promising for SPE. In our previous investigation²² sorption of the hydrophobic complexes of V, Co, Ni, Cu, Zn, As, Se, Cd, Pb with ammonium pyrrolidine dithiocarbamate (APDC) on non-modified Fe_3O_4 and MnFe_2O_4 nanoparticles was studied. Optimized SPE method for group pre-concentration was applied for ICP-MS determination of target analytes in urine samples. Both types of evaluated MNPs were found to be effective as sorbents for Me-APDC complexes and final solutions were compatible with ICP-MS.

The aim of present study was to compare the applicability of bare and silica coated MnFe_2O_4 nanoparticles as sorbents for group SPE of V, Co, Cr, Ni, Cu, Zn, Pb and Cd by means of sorption of their APDC complexes preliminary formed into the sample solution combined with subsequent ICP-OES determination.

EXPERIMENTAL

Instrumentation

An inductively coupled plasma optical emission spectrometer ICP-OES Optima 4300 DV Perkin Elmer (Perkin Elmer Corporation, Shelton, CT) equipped with flow focusing nebulizer OneNeb[®] (Ingeniatics S. L. Seville, Spain) was used in this study. The instrumental conditions are presented in Table 1.

For size characterization of studied MnNPs and SMnNPs a JEM-2010 high resolution transmission electron microscopy (HR-TEM) coupled to an

Inca Energy TEM100 energy dispersive X-ray spectrometer (EDS) from Oxford Instruments (Marlow, United Kingdom) was used.

Table 1. *The instrumental conditions of ICP-OES analysis*

Plasma gas flow rate	15 L min ⁻¹
Auxiliary gas flow rate	1.5 mL min ⁻¹
Frequency of RF generator	40 MHz
RF generator power	1.55 kW
Observation mode	Axial
Nebulizer	OneNeb® (Ingeniatics S. L. Seville, Spain)
Sample flow rate	0.5 mL min ⁻¹
Element /Wavelength (nm)/	Cd(I) ^a 228.802 (R); Cd(II) 214.440; Cd(II) 226.502; Co(II) 228.616 (R); Co (II) 230.786; Cr(II) 267.716 (R); Cr(II) 205.560; Ni(II) 231.604 (R); Ni(II) 221.648; Ni(I) 232.003; Cu (I) 327.39 (R); Cu(II) 213.597; Pb(II) 220.353 (R); Pb (I) 217.000; V (II) 290.880 (R); Zn(II) 206.200 (R); Zn(I) 202.548

^a in brackets: I is indication for atom emission line; II is indication for ion emission line
R is recommended by the manufacturer analytical line.

An 800 Series Digital hot plate stirrer from VWR (Darmstadt, Germany) and an UP200S-Stand-Mounted ultrasonic processor from Dr. Hielscher (Teltow, Germany) with 200W effective power/amplitude output and working frequency of 24 kHz, and with a S7 titanium sonotrode (7mm diameter, 100mm length) were used for MNPs synthesis and surface modification. A micro pH 2002 pH-meter from Crison (Alella, Spain) was used for the pH measurements.

Reagent and samples

Sodium hydroxide and ammonium hydroxide solution (25% (w/v), d=0.91g mL⁻¹) reagent-grade used for nanoparticles synthesis and pH adjustment were purchased from Scharlau (Barcelona, Spain). Manganese dichloride tetrahydrate (MnCl₂·4H₂O) from VWR BDH Prolabo (UK) and iron trichloride hexahydrate (FeCl₃·6H₂O) from Sigma–Aldrich (Steinheim, Germany) were used as a precursor salt for synthesis. Tetraethyl orthosilicate (TEOS) Sigma–Aldrich, ethanol and acetic acid LC-grade from Scharlau were used for nanoparticles surface modification.

The complexing agent – ammonium pyrrolidine dithiocarbamate (APDC), (Sigma Aldrich) was added as 2% solution in water (daily prepared). ICP multi-

element standard solution IV Merck (Darmstadt, Germany) and single element solutions of V 1000 mg L⁻¹ High Purity Standards (Charleston, UK) after appropriate dilution were used to prepare a model solution for SPE procedure optimization as well as for the preparation of calibration standards.

Ultra-pure water (resistivity $\geq 18\text{M}\Omega\text{cm}$) obtained by a NANOpure II system from Barnstead (Boston, MA, USA) was used for the preparation of all solutions.

Magnetic nanoparticles synthesis and surface modification

Magnetic nanoparticles were synthesized by co-precipitation of solution containing Mn²⁺ and Fe³⁺ ions in basic media. Before the synthesis, the precursor solution (V=500 mL) with concentrations of metal ions 0.017 mol L⁻¹ for Mn²⁺ and 0.033 mol L⁻¹ Fe³⁺ (molar ratio Mn²⁺: Fe³⁺ = 1:2) was heated to 30°C and then 0.25 mol L⁻¹ NaOH was added at once until pH~11 was reached. The produced suspension was additionally stirred keeping the temperature ~ 80°C for 3 hours.

The magnetic nanoparticles were separated from a supernatant solution by means of external magnet and washed with double distilled water until pH=7 was reached then once more with ethanol. Nanoparticles were stored as suspensions in 50 mL double distilled water and were stable up to 6 months.

A part of the produced MnNPs was subjected to the surface modification following the procedure described for CoFe₂O₄ nanoparticles¹⁹. Briefly, separated and washed MnNPs were dispersed in 450 mL of ethanol using the ultrasound processor (the pulse and the amplitude was set for all the synthesis process at 100% and 80%, respectively). The solution was purged with argon to remove dissolved oxygen. Chilled (for 10 min at - 18°C) solution of 10.5 mL of ammonia in 140 mL of ultrapure water was added to the suspension. The mixture was sonicated for 15 min, and then chilled TEOS solution (22.5 g in 75 mL ethanol) was added near to the sonotrode with a pipette. After 60 min, the argon flow and the ultrasound energy were stopped and the particles were separated by means of external magnet.

Magnetic nanoparticles based SPE procedure

Solid phase extraction procedure was performed in a batch mode presented on Fig. 1. Parameters of procedure such as solution pH, sorbent and ligand amounts as well as time for separation were previously optimized²². Approximately 10 mg of the nanoparticles were transferred into a conical test tube (V = 50 mL). Model solutions and 25 mg APDC (as a 2% m/v solution) were added and then pH was adjusted at five. The extraction of metal chelates was performed by continuous shaking for 5 min. Magnetic nanoparticles with the adsorbed metal complexes

were separated by means of permanent magnet for 5 min and then the supernatant solution was completely decanted. The separated solid phase was washed with 10 mL ultra-pure water.

For the analyte restoration in final solution 7 mol L^{-1} nitric acid was used at ambient temperature. Two approaches were tested: i) elution with 2 mL acid for 10 min for both types of nanoparticles (in this case non modified MnNPs were partially dissolved) and ii) prolonged treatment for 4 hours (for bare MnNPs only), that led to complete dissolution of solid phase.

The three different final solutions namely eluates obtained from SMnNPs and MnNPs and completely dissolved MnNPs were diluted with ultrapure water to final volume 5 mL and subjected to ICP – OES analysis.

ICP-OES determination of solutions obtained after SPE

The plasma axial observation mode was used for detection of analyte emission lines. The concentration of analytes into the final solutions obtained after SPE was calculated using matrix match calibration approach, where the calibrations standards (in interval $0\text{--}1 \text{ mg L}^{-1}$) were prepared by addition of spikes from multi-element aqua standards into the procedural blank.

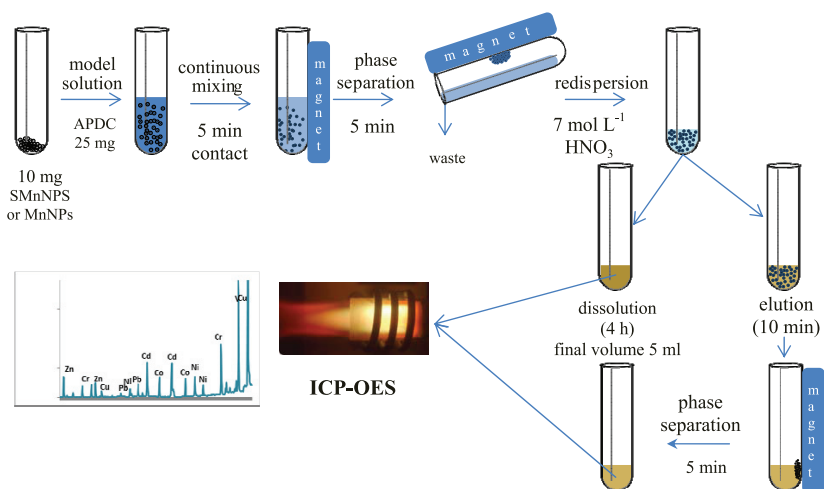


Figure 1. Principal scheme of the magnetic nanoparticles based solid phase extraction procedure.

RESULTS AND DISCUSSION

Magnetic nanoparticles characterization

Both synthesized magnetic nanoparticles (bare and silica coated) were characterized by TEM (Fig. 2A, B). Two fractions with mean diameters ~ 2 nm and ~ 20 nm could be distinguished for bare particles (Fig. 2C). The modification by silica layer led to the increased size and the finest fraction cannot be distinguished. Probably the smallest particles are agglomerated during the modification, but the mean size of the silica-coated manganoferrite nanoparticles is still below 50 nm. Finally it was proven by EDS analysis that manganoferrite particles were with desired molar ratio Mn:Fe = 1:2 which corresponds to the formula MnFe_2O_4 .

Optimization of ICP-OES determination

Three different final solutions obtained after SPE were subjected to ICP-OES analysis, namely final solutions obtained after SPE and: i) elution of analytes from SMnNPS, ii) elution of analytes from MnNPS for 10 min and iii) complete dissolution of solid phase (for MnNPS) for 4h. The matrix effects (spectral and non-spectral) were examined in all mentioned cases and correction approaches were proposed.

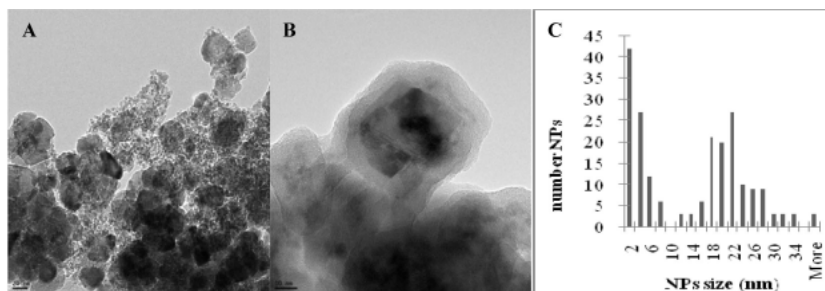


Figure 2. TEM images of MnNPs (A) and SMnNPs (B) with size distribution diagram for MnFe_2O_4 NPs. (C)

For estimation of the non-spectral matrix effect (Eq.1) sensitivities of analytes obtained in every sample fraction were compared to the common external calibration using aqua standard solutions containing only 1% (v/v) HNO_3 (0.14 mol L^{-1}) needed for stabilization.

$$MatrixEffect \% = \frac{Sens_{Matrix} - Sens_{AquaStd}}{Sens_{AquaStd}} \times 100 \quad (1)$$

where: $Sens_{Matrix}$ is the slope of calibration line in the presence of studied matrix; $Sens_{AquaStd}$ is the slope of calibration line obtained using aqua standards containing $0.14 \text{ mol L}^{-1} \text{ HNO}_3$.

Both borderline cases without dissolved solid phase (SMnNPs eluted with $7 \text{ mol L}^{-1} \text{ HNO}_3$) and with completely dissolved solid phase (4h treatment of MnNPs) were compared. (Fig. 3) For all monitored emission lines the non-spectral matrix effect was comparable when eluats from SMnNPs and completely dissolved MnNPs were directly measured. Observed matrix suppression was within the interval 12% (Cu) to 37% (Cd, Pb) and it was caused mainly by the high acid concentration. Further dilution up to 2.8 mol L^{-1} led to the reduction of matrix effect by factor 3–5, but enrichment factors were lowered in this case. All further measurements were performed after dilution of the final solution prior instrumental analysis up to 5 mL. Even in this case matrix suppression up to 15% for Cd, Cr and Ni was detected. In order to solve the problem with matrix effects we choose to work with calibration standards prepared in procedural blank (Matrix matched calibration).

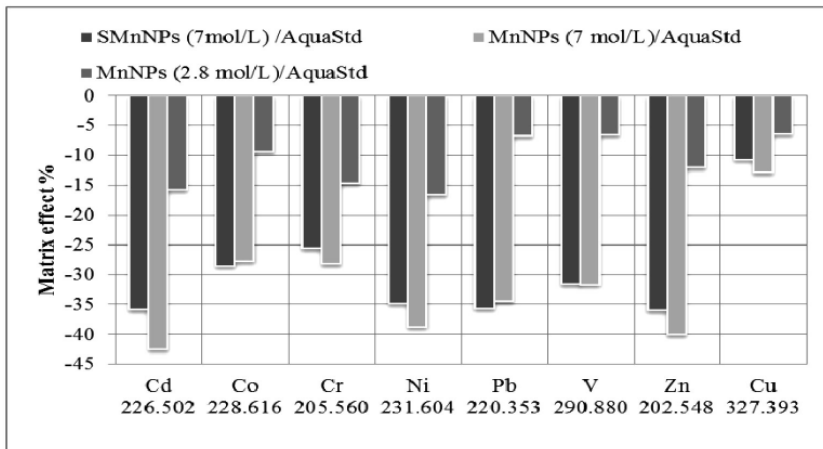


Figure 3. Non spectral matrix effect on the analytes sensitivity in solutions after SPE procedure, compared to external calibration using aqueous standards.

Spectral matrix effect was not observed when SMnNPs were used as a sorbent. Completely different behavior was detected in the case of non-modified MnNPs because of the presence of matrix elements (Fe and Mn) in the final solution. Elevation of the background signal was recorded in the both cases when non modified MnNPs were used for SPE (Fig. 4).

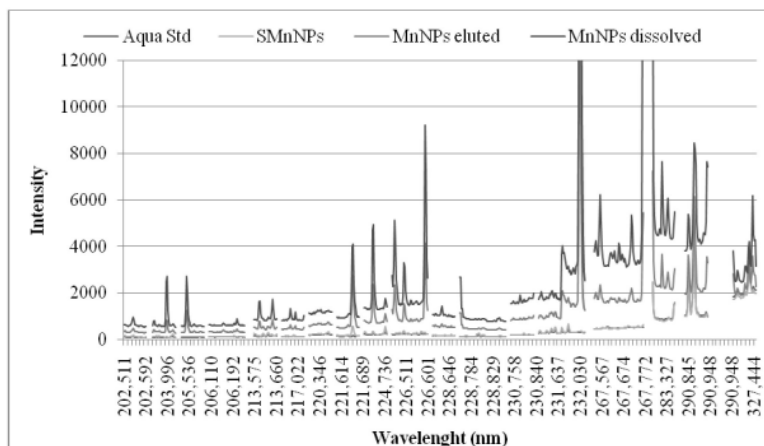


Figure 4. Emission signals of the analytes in blank solutions obtained after SPE using three approaches for analytes restoration: elution from SMnNPs, MnNPs and dissolution of MnNPs.

The mean enhancement of background (in comparison to aqua standard) was by factor of 3 for eluted MnNPs, and by factor of 6 when solid phase was completely dissolved. Probably this behavior is due to the band emission spectra of molecules or radicals formed by matrix components (i.e. Fe and Mn) in cooler regions of the plasma tail. As could be seen from figure 4 the obtained emission spectrum was significantly complicated due to the presence of Fe and Mn especially in the case of bare MnNPs. With increasing the concentration of matrix components even less sensitive emission lines of Fe and Mn could be detected.

For estimation of the spectral interferences at least two emission lines per analyte were monitored. Free from spectral interferences were the emission lines of Co 228.616 nm; Pb 220.353 nm; Zn 202.548 nm and V 290.880 nm. Spectral lines caused by matrix elements were observed near to the emission lines of Cd 214.440 nm and 226.502 nm; Cr 205.560 nm; Cu 327.390 nm and 213.597 nm; Ni 232.003 nm (Fig. 5).

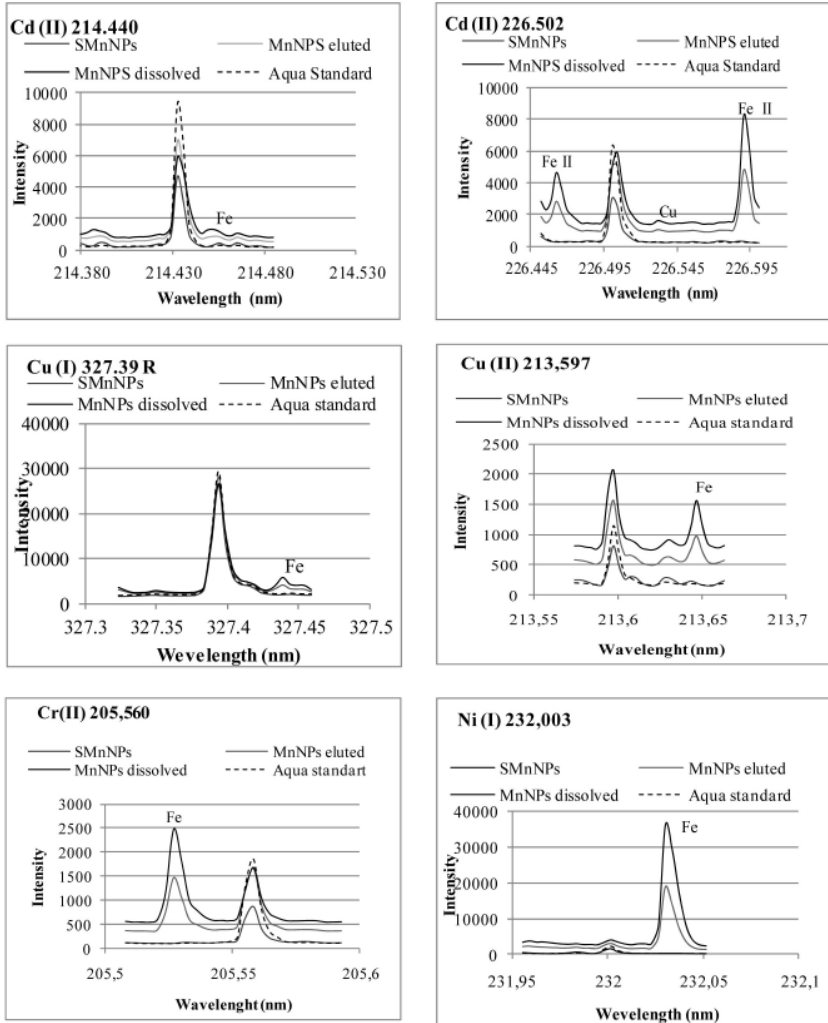


Figure 5. The emission lines for analytes measured in solutions after SPE with SMnNPs and MnNPs compared to the corresponding aqua standard. Concentration of the elements in all solutions is 0.5 mg L^{-1}

Nevertheless these lines could be used for analysis. To avoid any overlap of adjacent peaks of the analyte and interfering component it is recommended to measure the intensity at the analyte peak maximum, instead of the spectral peak area. The recommended by the instrument manufacturer emission line Cr 267.716 nm was overlapped by Mn 267.725 nm. The similar case was found for the line of Pb 217.000 nm interfered by Fe 216.995 nm. The last two lines are not suitable for analysis in the presence of manganoferrite matrix (Fig. 6).

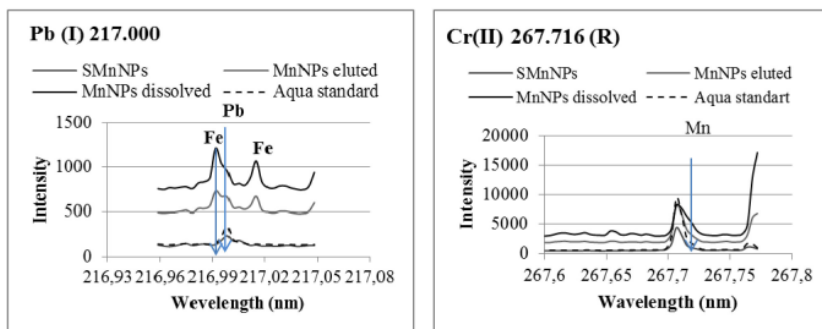


Figure 6. The emission lines of analytes directly overlapped by the matrix components in solutions after SPE with SMnNPs and MnNPs compared to the corresponding aqua standard. Concentration of the elements in all solutions is 0.5 mg L^{-1}

Analytical figures of merit

The recoveries (Table 2) obtained for model solutions of target analytes subjected to SPE-ICP-OES were calculated by equation (2).

$$R\% = \frac{Q_{\text{SPE}}}{Q_{\text{initial}}} \times 100 \quad (2)$$

where: R% – recovery; Q_{initial} is the initial analyte quantity in the model solution; Q_{SPE} – is the analyte quantity, measured after SPE procedure

When the MnNPs were used for SPE (for both restoration protocols) recoveries above 90% were observed for all tested elements with exception of Cd (R% = 78), while in the case of SMnNPs the recoveries above 90% were obtained only for Co, Cu, Ni and Pb, which proves that the surface of bare manganoferrite particles shows better adsorption properties towards Me-APDC complexes than siliconated ones.

For assessment of the method limits of detection MLOD (Table 3) in SPE the signals corresponding to 3 times standard deviation of blank solution were calculated as concentrations, using the calibration equations obtained by the method of matrix-matched calibration (standards prepared in procedural blank). Obtained values were lowered by the achieved pre-concentration factor. With the proposed SPE-ICP-OES procedure detection limits were decreased by factors in the range 2–7 (SMnNPs) and 3–8 for MnNPs. In respect to the MLOD the siliconated SMnNPs give better result, which is mainly due to the less pronounced matrix effect, but in this case incomplete recovery must be corrected by adequate calibration procedure. While for bare manganoferrite NPs, the sorption process is not problematic, but elution protocol should be kept as soft as possible in order to decrease the spectral interferences inherent for the matrix reach with Fe and Mn.

Table 2. Recoveries (R%) of the studied elements, with corresponding standard deviations (n=5), obtained for both types of MNPs and different restoration protocols.

R%±SD	Cd 214.440	Co 230.786	Cr 205.560	Cu 327.393	Ni 231.604	Pb 220.353	V 290.880	Zn 202.548
SMnNPs	72 ± 3	92 ± 4	60 ± 2	93 ± 4	95 ± 4	93 ± 3	71 ± 2	69 ± 3
MnNPs Eluted	78 ± 2	97 ± 4	93 ± 3	91 ± 3	99 ± 3	100 ± 2	100 ± 1	91 ± 3
MnNPs Dissolved	78 ± 1	97 ± 3	97 ± 2	90 ± 3	98 ± 2	99 ± 1	99 ± 2	90 ± 2

Table 3. Method limits of detection (MLOD) in µg L⁻¹ obtained by SPE procedure using bare and silica coated MnNPs compared to the instrumental limits of detection in aqua standards.

	Cd 214.440	Co 230.786	Cr 205.560	Cu 327.393	Ni 231.604	Pb 220.353	V 290.880	Zn 202.548
Aqua standards	0.35	0.89	1.71	0.67	0.74	6.97	7.73	0.80
SMnNPs	0.19	0.16	0.36	0.25	0.29	0.97	1.43	0.23
MnNPs Eluted	0.18	0.33	0.46	0.27	0.29	1.15	0.95	0.25
MnNPs dissolved	1.77	0.39	0.41	0.24	0.64	2.78	1.32	0.42

CONCLUSIONS

SPE with bare and silica covered MnFe_2O_4 magnetic nanoparticles proved to be effective for the group pre-concentration of APDC complexes of V, Co, Cr, Ni, Cu, Zn, Cd and Pb. Silica modified MnFe_2O_4 NPs applied as a sorbent allows free from spectral interferences ICP-OES analysis, but with lower recoveries. Bare MnNPs are more effective sorbent for Me-APDC complexes, but the dissolved matrix during elution, causes a number of spectral interferences in ICP-OES. Hence, keeping the soft conditions during elution of analytes is strongly recommended in order to reduce the matrix effect. For analytical data handling, the maximum of spectral peak is suggested as more appropriate.

The optimized SPE method combines a simple synthesis, small amount of sorbent phase (10 mg), easy performance and good compatibility with ICP-OES.

ACKNOWLEDGMENTS

The current work has been developed as a part of project DO 02–70 (GAMA) financed from National Science Fund of Bulgaria. Authors are thankful also for the financial support of EC 7FP Project 245588 (BioSUPPORT); NS11-HF-007 and the Spanish Ministry of Science and Innovation (Project CTQ2008-06730-C02-01 and Regional Government of Valencia Projects ACOMP/2009/144, ACOMP2010/047 and A-04/09.).

REFERENCES

1. M. Faraji, Y. Yamini and M. Rezaee, *Journal of the Iranian Chemical Society*, 2010, **7**, 1–37.
2. R. Lucena, B. M. Simonet, S. Cárdenas and M. Valcárcel, *Journal of Chromatography A*, 2011, **1218**, 620–637.
3. A. Simón de Dios and M. E. Díaz-García, *Analytica Chimica Acta*, 2010, **666**, 1–22.
4. J.-H. Lin, Z.-H. Wu and W.-L. Tseng, *Analytical Methods*, 2010, **2**, 1874–1879.
5. S. P. Gubin, ed., *Magnetic Nanoparticles*, WILEY-VCH Verlag GmbH & Co. KGaA, Weinheim, 2009.
6. M. Faraji, Y. Yamini, A. Saleh, M. Rezaee, M. Ghambarian and R. Hassani, *Analytica Chimica Acta*, 2010, **659**, 172–177.
7. B. Chen, S. Heng, H. Peng, B. Hu, X. Yu, Z. Zhang, D. Pang, X. Yue and Y. Zhu, *Journal of Analytical Atomic Spectrometry*, 2010, **25**, 1931–1938.
8. P.-L. Lee, Y.-C. Suna and Y.-C. Ling, *Journal of Analytical Atomic Spectrometry*, 2009, **24**, 320–327.
9. M. Khajeh and E. Sanchooli, *Journal of Food Composition and Analysis*, 2010, **23**, 677–680.
10. M. Khajeh, *Journal of Hazardous Materials*, 2009, **172**, 385–389.
11. M. H. Mashhadizadeh and Z. Karami, *Journal of Hazardous Materials*, 2011, **190**, 1023–1029.
12. C. Huang and B. Hu, *Spectrochimica Acta Part B*, 2008, **63**, 437–444.
13. M. Faraji, Y. Yamini and M. Rezaee, *Talanta*, 2010, **81**, 831–836.
14. J. S. Suleiman, B. Hu, H. Peng and C. Huang, *Talanta*, 2009, **77**, 1579–1583.
15. M. Khajeh, *International Journal of Environmental Analytical Chemistry*, 2009, **89**, 479–487.
16. Y. W. Wu, J. Zhang, J. F. Liu, Z. L. Deng, M. X. Han, F. Jiang, D. Z. Wang, H. K. Wang and H. Z. Yuan, *Atomic Spectroscopy*, 2011, **32**, 41–47.
17. C. Huang and B. Hu, *Journal of Separation Science*, 2008, **31**, 760–767.

18. C. Huang, W. Xie, X. Li and J. Zhang, *Microchimica Acta*, 2011, **173**, 165–172.
19. I. P. Román, A. Chisvert Alberto and A. Canals, *Journal of Chromatography A*, 2011, **1218**, 2467–2475.
20. H. F. Liang and Z. C. Wang, *Materials Chemistry and Physics*, 2010, **124**, 964–969.
21. J. Hu, I. M. C. Lo and G. Chen, *Separation and Purification Technology*, 2007, **56**, 249–256.
22. V. Stefanova, D. Georgieva, V. Kmetov, I. Roman and A. Canals, 2011, **submitted for publication**.

APPLICATION OF CLASSICAL METHODS TO ISOLATION OF RUTIN FROM ORIENTAL TOBACCOS

M. Docheva¹ and S. Dagnon²

*¹Tobacco and Tobacco Products Institute, Markovo 4108, Plovdiv,
Bulgaria, margarita_1980@abv.bg*

*²Faculty of Chemistry Dep. of Organic chemistry „Tzar Assen“ str. 24,
Plovdiv 4000, Bulgaria, dagnon@uni-plovdiv.bg*

ABSTRACT

Major commercial sources of rutin include *Sophora japonica*, *Eucalyptus* spp., *Fagopyrum sculentum* and *Ruta graveolens*. However, the necessity of identifying a better cheaper commercial source of rutin is still valid. Tobacco is a rich source of this medicinally important flavonoid. Especially the Oriental tobaccos grown in Bulgaria contain large amount of rutin, approximately 1% and potentially can be used commercially to obtain a product rich of this natural antioxidant. In this study the classical methods of extraction and isolation of rutin from Oriental tobaccos were investigated. By using analytical HPLC, the amounts of rutin present in the tobacco leaves and extracts were determined. The largest amount of rutin was obtained by water extraction with heat reflux and liquid-liquid extraction with ethyl acetate. The results of the quantitative determinations by HPLC of rutin show the amounts of 0.93% or 9.3 mg/g rutin in tobacco leaves and 0.7 mg/g in the obtained extract.

Key words: *polyphenols, HPLC, rutin, tobacco*

ВЪВЕДЕНИЕ

Ориенталските тютюни са основен тип тютюни, отглеждани в България. Те са дребнолистни и изсушените листа са съдържателни с нежна структура и тънък главен нерв, цвят жълто-оранжев, оранжев, оранжево-червен до червен със слаб зеленикав оттенък. Листата имат висок цигарен рандеман, отлична горяемост, много фин, приятен и уникален по своята си същност аромат. Басмите се отличават и с високото си съдържание на полифеноли [3].

Полифенолите са известни със своята биологична активност. Те притежават противовъзпалителни, антиалергични, антивирусни, противогъбични, антиоксидантни, кардиопротективни, противотуморни свойства, както и съдоразширяващ ефект. Делят се на четири основни групи: фенолни киселини, флавоноиди, танини, стилбени и лигнани. Флавоноидите са най-голямата група полифеноли – включват над 4000 представителя, като броят им непрекъснато расте [1].

Основните компоненти на полифенолния комплекс при Басмите са фенолните киселини – хлорогенова киселина и нейните изомери – неохлорогенова киселина и 4-О-кафеоилхинова киселина, и флавоноидите рутин и кемпферол-3-рутинозид [2, 5].

Рутинът принадлежи към групата на флавоноидите. Основното му действие е заздравяването на стените на капилярите. Има изразени антиоксидантни, противовъзпалителни, противоалергични и антивирусни свойства. Рутинът усилва действието на витамин С. Има индикации, че той подтиска туморните клетки на дебелото черво [1]. В аптечната мрежа се предлагат хранителни добавки от рутин предвид свойствата, които притежава.

Основните природни източници на рутин са Японска акация (*Sophora japonica*), Евкалипт (*Eucalyptus* spp.), Обикновена елда (*Fagopyrum esculentum*) и Седефче (*Ruta graveolens*). Тютюните от сортова група Басми отглеждани в България са богат източник на този флавоноид. Съдържанието му е приблизително 1% (10 mg/g) [2, 3]. Тези тютюни се отглеждат на плитките почви с ниско хумусно съдържание (до 1 – 2%) и не е необходимо торене, и поливане като постоянни практики. Предвид не сложната и икономична агротехника, Басмите представляват евтин източник на рутин, който може да бъде използван за промишлено му получаване [4].

Целта на изследването е да се извлече максимално количество рутин от тютюна и той да бъде изолиран и пречистен от фенолните киселини – хлорогеновата киселина и нейните изомери неохлорогенова киселина и 4-О-кафеоилхинова киселина.

МАТЕРИАЛ И МЕТОДИ

Изследването се извърши с ферментиран, смлян на прах тютюн от сортова група Басми, екотип Джебел Басма, реколта 2010 г. Адекватна проба от тютюна беше анализирана за съдържание на полифеноли по описания метод с ВЕТХ от Dagnon, Edreva, 2003 [2]. За целта беше използван течен хроматограф Клауер с кватернерна помпа, детектори: DAD и флуоресцентен RF 10Ax1 и аналитична колона Purosper[®]star RP-18e 25 cm x 4.6 mm i.d., 5 µm particle size (Merck, Germany).

Методи за извличане и изолиране на рутин от тютюна

Описанието на методите, които използвахме за извличане и изолиране на рутин от тютюна, както и съответните добиви на рутин са дадени в Таблица 1.

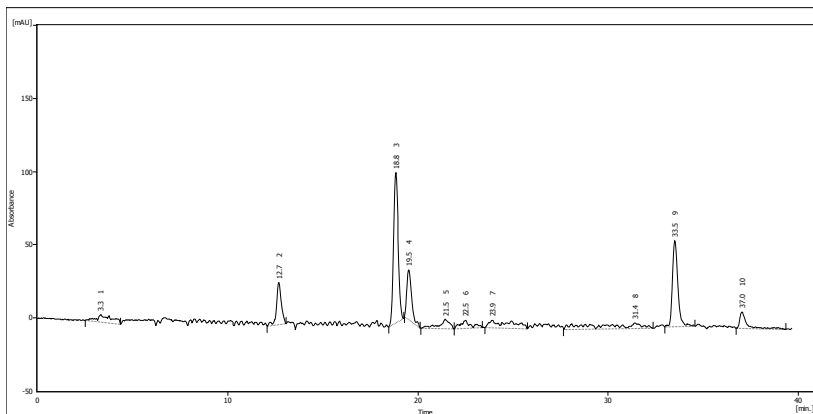
Присъствието на рутин в получените екстракти и фракции беше проследено с помощта на тънкослойна хроматография, а количеството му беше определено по метода за полифеноли с ВЕТХ.

Таблица 1. *Методи на извличане и изолиране на рутин от тютюн от екотип Джебел Басма*

Методи за екстракция	Методи за изолиране	Рутин mg/g
Вода при кипене 30 min	Течно-течна екстракция с етилацетат Колонна хроматография със силикагел Етилацетат: метанол: вода	0.08
Вода при кипене 120 min	Течно-течна екстракция с етилацетат	0.70
60% метанол	Колонна хроматография със силикагел Етилацетат: метанол	0.62
70% метанол	Течно-течна екстракция с етилацетат	0.34
Етилацетат: метанол (1:1 v/v)	-	9.05
Етилацетат: метанол (1:1 v/v)	Колонна хроматография със силикагел Етилацетат: метанол	2.02
Метанол	-	Следи
Етилацетат	-	Следи

РЕЗУЛТАТИ И ДИСКУСИЯ

Хроматографският профил на полифенолния комплекс в тютюн от сортава група Басми, екотип Джебел Басма е представен на Фигура 1.



Фигура 1. ВЕТХ анализ на полифеноли на тютюн.

Пикове с $t_R=12.7$, $t_R=18.5$ и $t_R=19.5$ (2, 3, 4) са идентифицирани като фенолни киселини, хлорогенова киселина и изомери.

Пика с $t_R=33.5$ (9) е идентифициран като рутин, а пика с $t_R=37.0$ (10) като кемферол-3-рутинозид.

Таблица 2 съдържа получените резултати от количествения анализ на полифенолите в тютюна.

Таблица 2. Съдържание на полифеноли (mg/g) при тютюн от екотип Джебел Басма

Полифеноли	mg/g
Неохлорогенова киселина	2,07
Хлорогенова киселина	11,1
4-о-кафеилхинова киселина	4,14
Рутин	9,37
Кемферол-3-рутинозид	1,62

Сравнявайки данните за рутин в Таблица 1 и Таблица 2 се вижда, че пълно извличане на рутин (9,05 mg/g) се постига със смес от етилацетат: метанол (1:1 v/v). Данните за съдържанието на полифеноли в получения екстракт са дадени в Таблица 3.

Таблица 3. *Съдържание на полифеноли в екстракт от тютюн, извлечени със смес от етилацетат:метанол (V/V = 1:1)*

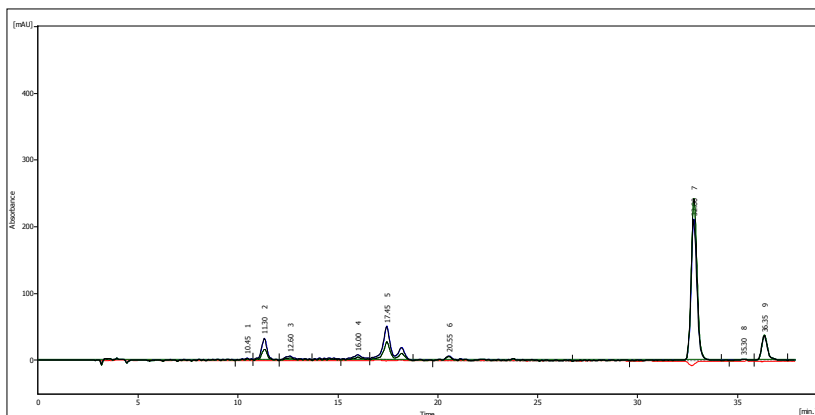
Полифеноли	mg/g
Неохлорогенова киселина, Хлорогенова киселина, 4-о-кафеoilхинова киселина	6,28
Рутин	9,05
Кемферол-3-рутинозид	следи

При този метод на екстракция селективно се извлича рутина, докато количеството на фенолните киселини е около една трета от тяхното съдържание в тютюна (Таблица 1 и Таблица 3). В Таблица 4 са представени резултатите за съдържанието на рутин и фенолни киселини във фракцията получена при колонната хроматография на силикагел и елуенти етилацетат: метанол.

Таблица 4. *Съдържание на полифеноли във фракцията получена с колонна хроматография със силикагел и елуенти етилацетат: метанол*

Полифеноли	mg/g
Неохлорогенова киселина, Хлорогенова киселина, 4-о-кафеoilхинова киселина	0,74
Рутин	2,02
Кемферол-3-рутинозид	следи

Съдържанието на рутин във фракцията е 2,02mg/g, докато количеството на фенолните киселини и кемпферол-3-рутинозид намалява значително до следи (Таблица 4). Хроматограмата получена при ВЕТХ анализ на фракцията от колонната хроматография показва, че тя е обогатена на рутин (Фигура 2). На нея ясно се вижда намаленото количество на фенолните киселини.



Фигура 2. ВЕТХ анализ на фракцията обогатена на рутин.

ЗАКЛЮЧЕНИЕ

Извършено е изследване при което е установена аналитична техника за селективно извличане на рутин от тютюн със смес от етилацетат: метанол (1:1 v/v). Определени са параметрите за изолиране на рутин от тютюн чрез колонна хроматография със силикагел и елуенти етилацетат: метанол.

Изследванията са финансирани по проект от Фонд „Научни изследвания“ към Пловдивски университет МУ 11 ХФ 003.

ЛИТЕРАТУРА

1. B. H. Havsteen, *Pharmacology&therapeutics*, 96 (2002) 67–202.
2. S. Dagnon, A. Edreva, *Beitr. Tabakforsch. Int.*, 20 (2003) 355–359.
3. S. Dagnon, D. Dimanov, *Bulgarian Journal of Agricultural Science*, 13 (2007) 459–466.
4. F. Fathiazad, A. Delazar, R. Amiri, S. D. Sarker, *Iranian Journal of Pharmaceutical Research* 3 (2006) 222–227.
5. H. Wang, M. Zhao, B. Yang, Y. Jiang, G. Rao, *Food Chemistry*, 107 (2008) 1399–1406.

ЕКСТРАКЦИЯ НА ЛИПИДНИ КОМПОНЕНТИ ОТ БИОМАСА НА ПСИХРОФИЛНИ ДРОЖДИ

С. Димитрова*, Л. Луканов*, К. Павлова**

*Медицински университет-Пловдив,
Фармацевтичен факултет, катедра „Химия и биохимия“

**Институт по Микробиология – БАН,
Лаборатория по приложни биотехнологии

ABSTRACT

A method for the extraction of β -carotene, coenzyme Q_{10} and ergosterol from biomass of psychrophilic yeast strains was described. The investigation substances were derived from the *Sporobolomyces salmonicolor* AL_1 and *Cryptococcus laurentii* AS_{58} biomass with n-hexan:acetone at a ratio of 1:1 at room temperature after two repeated extraction. This combination of solvents was better for simultaneously extraction of mentioned substances than each of n-hexan, acetone, CH_3OH , i-PrOH, EtOH and CH_2Cl_2 .

Key words: *Sp. salmonicolor* AL_1 , *Cr. laurentii* AS_{58} , Coenzyme Q_{10} , β -carotene, ergosterol

УВОД

Липидни компоненти са липоразтворимите витамини А, D, Е, К, коензим Q_{10} (CoQ_{10}) и стеролите. Те участват в състава на мембранните

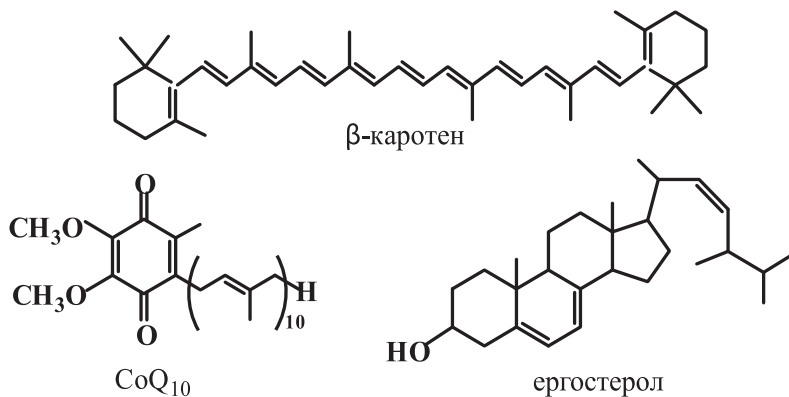
липиди заедно с висшите мастни киселини, триацилглицеролите, фосфолипидите и сфинголипидите.

Растения и микроорганизми синтезират предимно каротеноиди от тетраерпенов тип, най-широко разпространен от които е β -каротенът-прекурсор на витамин А. Съдържа се в жълто и оранжево оцветени плодове и зеленчуци (1, 2). Продуцира се и от гъби, бактерии, алги, дрожди (3, 4). Той е известен антиоксидант, който намалява клетъчни или тъканни увреждания, предизвикани от свободни радикали (6, 7, 8). Използва се в хранителната и фуражната промишленост като оцветител на хранителни продукти и аквакултури (5).

В човешкия организъм и в клетките на някои микроорганизми (бактерии-*Agrobacterium*, *Rhodobacter*; *Paracoccus* и дрожди-*Candida*, *Rhodotorula*, *Saitoella*) се синтезира CoQ_{10} (9). Той участва в митохондриалната дихателна верига. Основен компонент е в АТФ-генериращия стадий на процеса на окислителното фосфорилиране и антиоксидант, предотвратяващ липидното пероксидиране (10).

Стеролите по произход биват зоо-, фито – и микостероли. Представяват едновалентни полициклични алкохоли от клас стероиди. В дрождите преобладава главно ергостерол, който се използва като източник за получаването на витамин D_2 и суровина за синтез на стероидни хормонални препарати (11, 12).

Дрожди от родовете *Sporobolomyces*, *Sporidiobolus*, *Rhodotorula*, *Cryptococcus* имат способността да продуцират тези биологичноактивни вещества (11, 13, 16), структурите на които са показани на фиг. 1.



Фигура 1. Структури на β -каротен, CoQ_{10} и ергостерол

В литературата са посочени редица методи за екстракция на тези вещества от различни обекти, например каротеноиди от растителни (14) или биологични (15) проби, каротеноиди и CoQ_{10} от биомаса на микроорганизми (16) или каротеноиди и ергостерол от промишлени дрожди (11). Като екстрагенти са цитирани ацетон, n-хексан, метанол, i-пропанол, етанол, дихлорметан, диметилсулфоксид или комбинация от тях (17). Методите за екстракция на биологичноактивни вещества от биомаса на микроорганизми се осъществява след завършване на ферментационния процес и отделянето ѝ от супернатанта, изсушаване и следваща екстракция с различни разтворители в зависимост от това кое от веществата се цели да бъде извлечено максимално. Могат да се варират и условията на екстракция: време, температура, предварително третиране на ферментационната среда и др. (18).

Целта на настоящата работа е да се изследва комбинация от разтворители, която позволява най-пълно, бързо и едновременно екстрахиране на β -каротен, CoQ_{10} и ергостерол от биомасата на психрофилни дрожди.

МАТЕРИАЛИ И МЕТОДИ

1. Микроорганизми, хранителна среда и условия на култивиране

Щамовете *Sp. salmonicolor* AL₁ и *Cr. laurentii* AS₃₈ са изолирани от почвени проби от територията на българската база на остров Ливингстон – Антарктида.

Ферментационната среда съдържа, (g/L) – захароза – 40, $(\text{NH}_4)_2\text{SO}_4$ – 2.5, KH_2PO_4 – 1.0, $\text{MgSO}_4 \cdot 7\text{H}_2\text{O}$ – 0.5, NaCl – 0.1, $\text{CaCl}_2 \cdot 2\text{H}_2\text{O}$ – 0.01, дрождев екстракт – 1.0. Началната стойност на рН е 5.3 и средата е стерилизирана при 112°C за 30 min. Дълбочинното култивиране се провежда в 7 литров лабораторен биореактор (Sartorius) с работен обем от 5L и протича при аерационен поток от 0.5 v/v/m и разбъркване 400 rpm при 22°C в продължение на 120 часа. След завършване на ферментацията биомасата се центрофугира, двукратно се промива с дестилирана вода и се изсушава чрез лиофилизация.

2. Екстракция и HPLC – анализ на ергостерол, β -каротен и CoQ_{10}

Към 20mg много добре стрита лиофилизирана биомаса се прибавят 2 ml от всеки от разтворителите n-хексан, ацетон, дихлорметан,

i-пропанол, етанол, метанол и комбинация от n-хексан/ацетон в съотношение 1:1 и се разбърква на Vortex 2 min, след което се центрофугира 5 min при 3000 g. Течната фаза се отделя и се изпарява под вакуум. Температурата е съответно 50°C за хексановия, ацетоновия, метаноловия и дихлорметановия и 70°C за етаноловия и изопропаноловия екстракти. По този начин се провеждат три последователни екстракции. Полученият сух остатък се разтваря в 1ml подвижна фаза и се анализира по HPLC-метод, описан в предишна публикация (19).

3. Статистически анализ

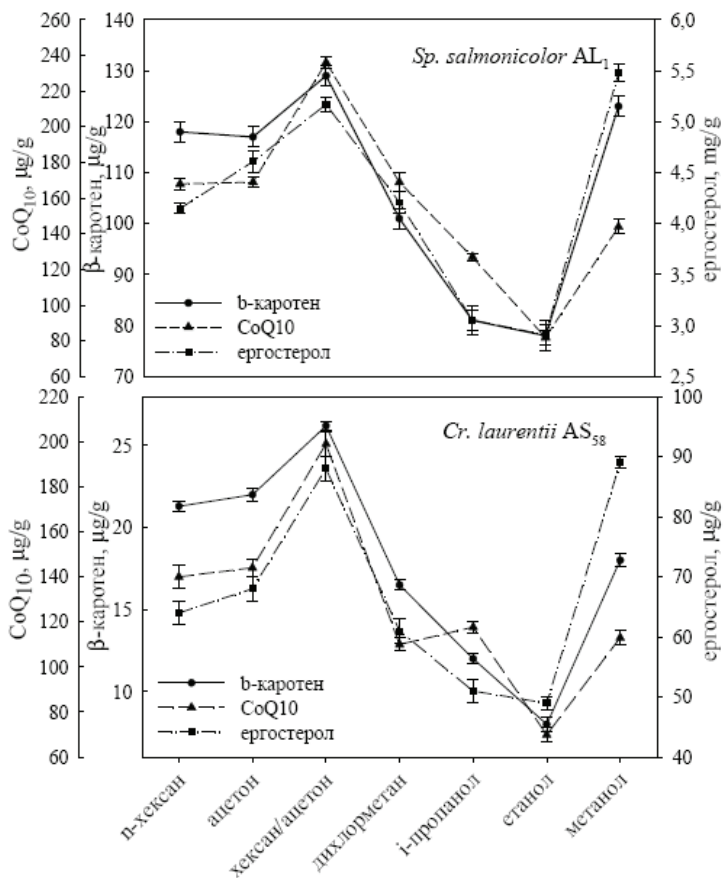
Статистическата обработка на резултатите е направена с SPSS (ver.11), при ниво на значимост $\alpha < 0.05$. Използван е вариационен анализ (ANOVA) като сравнението между групите е направено с теста на Tukey-Kramer. Резултатите са представени като средна стойност \pm стандартно отклонение.

РЕЗУЛТАТИ И ОБСЪЖДАНЕ

Използвани са биомаси на *Sp. salmonicolor* AL₁, селектиран като активен продуцент на екзополisahарид със значимо приложение в козметичната промишленост (20) и на *Cr. laurentii* AS₅₈ – проучван за синтез на биологичноактивни вещества (19).

На фиг. 2 са показани количествата екстрахирани ергостерол, β -каротен и CoQ₁₀ с помощта на различни разтворители от биомасите. Установи се, че всеки от тях екстрахира в различна степен изследваните вещества в зависимост от тяхната природа.

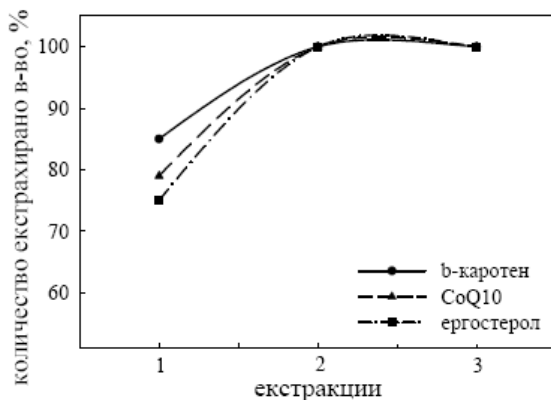
Максимално извличане на β -каротен се постига с комбинацията n-хексан/ацетон в съотношение 1:1 съответно 129.2 \pm 7.3 μ g/g суха биомаса за *Sp. salmonicolor* AL₁ и 26.2 \pm 0.9 μ g/g за *Cr. laurentii* AS₅₈. Подобни стойности се получават при екстракция с метанол (123.0 \pm 6.9 μ g/g и 18.3 \pm 0.7 μ g/g) и най-ниски с етанол. Комбинацията n-хексан/ацетон екстрахира в най-голяма степен и CoQ₁₀ съответно 236.1 \pm 12.1 μ g/g и 198.6 \pm 9.3 μ g/g. Ергостерол се екстрахира еднакво с метанол и n-хексан/ацетон – 5.4 \pm 0.2 mg/g и 5.2 \pm 0.2mg/g от биомасата на *Sp. salmonicolor* AL₁ и 89.0 \pm 5.1 μ g/g и 88.0 \pm 4.9 μ g/g от биомасата на *Cr. laurentii* AS₅₈. Всеки от разтворителите n-хексан и ацетон приблизително в еднаква степен екстрахират и трите вещества, но заедно в съотношение 1:1 дават много по-добър резултат. Незадоволителни резултати се получават при екстракция с дихлорметан, i-пропанол и етанол.



Фигура 2. Количества β -каротен, CoQ_{10} и ергостерол, получени при екстракция с различни разтворители

Проведени бяха три последователни екстракции за по-пълно извличане на веществата. На фиг. 3 е дадена степента на екстракция на β -каротен, CoQ_{10} и ергостерол от биомаса на *Sp. salmonicolor* AL₁ с n-хексан/ацетон 1:1. При първата се постига екстракция от 85% на β -каротен или 109.7 $\mu\text{g/g}$, 79% на CoQ_{10} или 186.4 $\mu\text{g/g}$ и 75% на ергостерол или 3.9 mg/g. При втората се получават съответно 129.2

$\mu\text{g/g}$, $236.1 \mu\text{g/g}$ и 5.2 mg/g , които стойности се потвърждават и при третата екстракция. Следователно двукратна екстракция е достатъчна за максималното извличане на изследваните вещества.



Фигура 3. Степен на екстракция на β -каротен, CoQ_{10} и ергостерол от биомаса на *Sp. salmonicolor* AL_1 с *n*-хексан/ацетон 1:1

Проучването е финансирано по проект ДТК 02/46, Фонд, „Научни изследвания“ МОНТ.

ЛИТЕРАТУРА

1. Sass-Kiss A., Kiss J., Milotay P., Kerek M., Toth-Markus M. (2005) Differences in anthocyanin and carotenoid content of fruits and vegetables. *Food Research International*, 38, 1023–1029
2. Melerndez-Marturnez A., Vicario I., Heredia F. (2007) Provitamin A carotenoids and ascorbic acid contents of the different types of orange juices marketed in Spain. *Food Chemistry*, 101 177–184
3. Ben-Amotz A. (1998) Case study: *Dunaliella* algal-derived β -carotene. *Phytochemicals*, 113–128
4. Aksu Z., Eren A. (2005) Carotenoids production by the yeast *Rhodotorula mucilaginosa*: Use of agricultural wastes as carbon source. *Process Biochemistry*, 40, 2985–2991
5. Frengova G., Beshkova D. (2009) Carotenoids from *Rhodotorula* and *Phaffia* yeasts of biotechnological importance. *J Ind Microbiol Biotechnol*, 36, 163–180
6. Henneckens C. (1997) β -carotene supplementation and cancer prevention. *Nutrition*, 13, 697–699.
7. Wang X. (1994) Absorption and metabolism of β -carotene. *J. Am. Coll. Nutr.*, 13, 314–325.
8. Edge R., McGarvey D., Truscott T. (1997) The carotenoids as antioxidants – a review. *Journal of Photochemistry and Photobiology B: Biology*, 41, 189–200
9. Kawamukai M. (2009) Biosynthesis and bioproduction of coenzyme Q₁₀ by yeasts and other organisms. *Biotechnol. Appl. Biochem.*, 53, 217–226
10. Frederick L., Crane D. (2001) Biochemical Functions of Coenzyme Q₁₀. *Journal of the American College of Nutrition*, 20, 591–598
11. Marova I., Crarnecka M., Halienova A., Breierova E., Koci R. (2010) Production of carotenoid/ergosterol-supplemented biomass by red yeast *Rhodotorula glutinis* grown under external stress. *Food Technol Biotechnol* 48, 56-61
12. Tuller G., Nemeč T., Hrastnik C., Daum G. (January 1999) Lipid composition of subcellular membranes of an FY 1679 derived haploid yeast wild-type strain grown on different carbon sources. *Lipid Analysis-Intermediate Report, S. cerevisiae* – EUROFAN 2 – Node N4

13. Dimitrova S., Pavlova K., Lukanov L., Savova I. (2008) Chemical composition of lipids and other lipophilic compounds from antarctic yeasts strains. *Comptes rendus de l'Academie bulgare des Sciences*, 61, 481–486
14. Hui Xu, Li Jia (2009) Capillary liquid chromatographic analysis of fat-soluble vitamins and β -carotene in combination with in-tube solid-phase microextraction. *Journal of Chromatography B*, 877, 13–16
15. Qing Su, Rowley K., Balazs N. (2002) Carotenoids: separation methods applicable to biological samples. *Journal of Chromatography B*, 781, 393 – 418
16. Yurkov A., Vustin M., Tyaglov B., Maksimova I., Sineokiy S. (2008) Pigmented basidiomycetous yeasts are a promising source of carotenoids and Ubiquinone Q₁₀. *Microbiology*, 77, 1–6
17. Rodriguez-Amaya D. B. (2001) A guide to carotenoid analysis in foods. International Life Science Institute Press, Washington
18. Roukas T., Mantzouridou F. (2001) An improved method for extraction of β -carotene from *Blakeslea trispora*. *Appl Biochem Biotechnol*, 90, 37 – 45
19. Dimitrova S., Pavlova K., Lukanov L., Zagorchev P. (2010) Synthesis of Coenzyme Q₁₀ and β -carotene by yeasts isolated from Antarctic soil and lichen in response to ultraviolet and visible radiations. *Appl Biochem Biotechnol*, 162, 795–804
20. Kuncheva M., Pavlova K., Panchev I., Dobрева S. (2007) Emulsifying power of mannan and glucomannan produced by yeasts. *Int J Cosmetic Science*, 29, 377–384

ОПРЕДЕЛЯНЕ НА КОЛИЧЕСТВА ОТ ХЕРБИЦИДА ФЛУМИОКСАЗИН В ЧЕРЕШИ ЧРЕЗ ИЗПОЛЗВАНЕ НА ВИСОКОЕФЕКТИВНА ТЕЧНА ХРОМАТОГРАФИЯ

*Д. Божилков¹, Ил. Козанова², С. Данъов¹, З. Ранкова²,
Ст. Николова¹, Ил. Иванов¹*

*¹Химически факултет, кат. Органична химия, „Цар Асен“ 24,
Пловдив 4000, България, dagnon@uni-plovdiv.bg*

*²Институт по овощарство „Остромила“ 12,
Пловдив 4004, България*

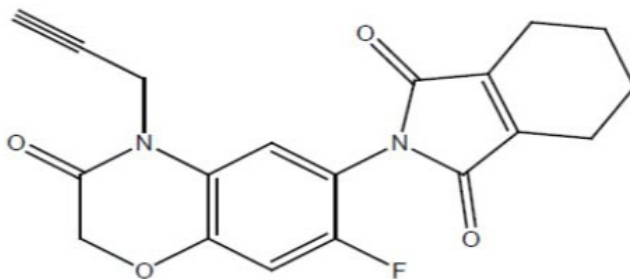
ABSTRACT

Cherries fresh fruit were tested for residues of herbicide flumioxazine. High-performance liquid chromatography (HPLC) with photodiode array detector was used. The signal of flumioxazine is linear at 220 nm in the range of 0.1 µg/ml to 10 µg/ml with 0.999 correlation coefficient. The method is selective for detection limit of flumioxazine in cherries 0.02 mg/kg. Recovery of added amounts of 0.1 mg/kg flumioxazine in fruit reaches 60%. After three years treatment of the cherry trees with herbicide Pledge 50 HR were not found any quantities of flumioxazine, higher than the M.R.Ls of 0,05 mg/kg.

Key words: *HPLC, herbicides, flumioxazine, cherries.*

ВЪВЕДЕНИЕ

Флумиоксазин N-(7-флуоро-3,4-дихидро-3-оксо-4-проп-2-инил-2Н-1,4-бензоксазин-6-ил)циклохекс-1-ен-1,2-дикарбоксимид (IUPAC) е активното вещество на препарата Пледж 50 ВП (50%). Той е селективен хербицид с широк спектър на действие срещу различни едногодишни и многогодишни плевели и треви. Флумиоксазин е регистриран от United States Environmental Protection Agency и е въведен за употреба през Април 2001 година.



flumioxazin

Флумиоксазин принадлежи към групата на N-фенилфталимидите, които са инхибитори на протопорфириноген оксидаза. Тези съединения са сред най-често патентованите класове хербициди през последното десетилетие. Протопорфириноген оксидазата е ензим, който катализира превръщането на протопорфириноген IX до протопорфирин IX като част от пътя за биосинтез на тетрапирола [1, 2]. Ензимното инхибиране води до загуба на хлорофил и каротеноиди и уврежда необратимо функцията и структурата на клетъчната мембрана. Чувствителните растения развиващи се на почви, третирани с флумиоксазин стават некротични и умират скоро след излагане на слънчева светлина [3]. Установено е, че устойчивостта на Пледж 50ВП в почвата е от 4 до 6 месеца [4].

За безопасността на храните, човешкото здраве и опазването на околната среда, дистрибуцията на хранителни стоки третирани с пестициди трябва да бъде строго контролирана. Нормативните документи регулиращи контрола на остатъци от пестициди в храните определят максималните допустими количества (МДК). Агенцията за контрол на

храните и лекарствата забранява продажбата на храни, съдържащи остатъчни количества пестициди, надвишаващи МДК. Максимално допустими количества на остатъци от флумиоксазин в череши за нашата страна са 0,05 mg/kg (изм. и доп. – ДВ, бр. 29 от 2008 г.).

Методите за контрол на замърсеността на плодовете с пестицидни остатъци постоянно се развиват и усъвършенстват. Много контролни органи разработват аналитични техники за определяне на многокомпонентни пестицидни остатъци, които се основават на различни хроматографски методи-ТСХ, ГХ, ВЕТХ [5–10]. Един ефективен мултиследови метод трябва да бъде специфичен и чувствителен, с малко или никакво матрично влияние при различни култури. Подготовката на пробата е от съществено значение при анализа на остатъчни количества от пестициди. Течно-течната екстракция е често използван метод, използващ разтворители като ацетон, ацетонитрил, хексан, етилацетат и смес от петролев етер:дихлорметан [12]. Съвременна ефективна техника за пречистване на пробата е твърдофазната екстракция, широко използвана при анализа на остатъчни количества от пестициди [5, 7]. Идентификацията на следи от широк спектър полярни и неполярни пестициди в комплексни матрици е трудна задача. В последните години се разработиха много методологии, използващи GC-MS и LC-MS/MS техники за подобряване надеждността и чувствителността за идентификация и количествено определяне [5, 7, 8, 10, 11].

Методът на Shu-Jen Tuan et al., 2009 [12] е подходящ за използване при рутинна проверка на остатъци от 176 пестициди в плодове и зеленчуци преди прибиране на реколтата. Той не включва определяне на остатъчни количества от флумиоксазин в череши. В литературата не се намериха данни за миграция на флумиоксазин от третирани с хербицид почви в плодовете на черешата.

Цел на нашето изследване е да се разработи метод за определяне на остатъчни количества от флумиоксазин в череши, използващ високоефективна течна хроматография (ВЕТХ) и детектиране с детектор с фотодиодна матрица. Да се изследват плодове от череши, растящи на почви, третирани с хербицида Пледж 50 ВП (50%).

МАТЕРИАЛ И МЕТОДИ

В периода 2009 – 2011 г. в черешовото насаждение на територията на Института по овощарство е заложен полски опит за проучване влиянието на селективния контактен хербицид с почвено и листно действие Пледж 50 ВП върху заплевеляването, вегетативните и продуктивните прояви на различни сорто-подложкови комбинации череша и риска от замърсяване с остатъчни количества от активното вещество на плодородната продукция.

Третирането с Пледж 50 ВП в доза 40g/dka е извършвано в началото на месец април, при наличие на поникнали плевелни растения. Продължителността на почвено хербицидно действие на Пледж 50 ВП е 5 месеца. Външни симптоми на фитотоксичност и депресия в растежа на дърветата не бяха наблюдавани.

За целите на изследването са използвани средни проби от череша от следните сортове:

1. Сорт Каталин/Гизела 5 (контрол) – череша от дървета растящи на нетретирана с Пледж 50 ВП почва.
2. Сорт Каталин/Гизела 5 (третирана) – череша от дървета растящи на третирана с Пледж 50 ВП почва.

Химикали и консумативи

Флумиоксазин (94.3%, HPLC) от фирма; Sigma-Aldrich

Органични разтворители: ацетон (Merck), дихлорметан (Merck), ацетонитрил (HPLC; Sigma-Aldrich),

NaCl (30%); NaHCO₃ (12%) и безв. Na₂SO₄;

Мембранен филтър 0.45 µm.

Стандартни разтвори

Изходният стандартен разтвор на флумиоксазин е приготвен с концентрация 100µg/ml в ацетонитрил (HPLC grade). Работните стандартни разтвори са получени чрез серийно разреждане на изходния стандартен разтвор с концентрации 10µg/ml, 5µg/ml, 2.5µg/ml, 1µg/ml, 0.5µg/ml и 0.1µg/ml. Всички разтвори са съхранявани при 4°C.

Подготовка на пробите

За подготовка на пробите е адаптиран метода описан от Shu-Jen Tuan et al., 2009 [12]. Средни проби от пресни череша са намалени чрез квартуване и са нарязани. Порция от 20g се хомогенизира с 80ml

ацетон за 1 min. Хомогената се филтрува под вакуум (11 μm). Разтворът се концентрира до 3–5 ml в облодънна колба на ротационен изпарител и след добавяне на 1.5 g NaCl се прехвърля във фуния за три течно-течни екстракции. Разтворът на пробата се екстрахира с 10 ml дихлорметан за 1 минута. Органичната фаза се събира, а водният слой се екстрахира както по-горе. След това към водния слой преди повторение на третата разделяща стъпка се добавят 1 ml 12% разтвор на NaHCO_3 и 5 ml 30% разтвор на NaCl. Към комбинираните органични слоеве се добавя 20 g безводен Na_2SO_4 , след което разтворът се филтрува. Филтратът се изпарява до сухо при 40°C. Остатъкът се разтваря в 2.5 ml ацетонитрил и се филтрува през мембранен филтър 0.45 μm . Анализира се чрез ВЕТХ.

ВЕТХ анализ

Използвана е HPLC система Кнауер в обърната фаза (RP) с колона Purospher C18 (250 \times 4.6 mm, 5 μm), кватернерен смесител Smartline Manager 5000, помпа Smartline 1000 и PDA 2800 детектор. Подвижната фаза А е вода: ацетонитрил, (60:40) и за 20 мин в градиент се променя до 100% ацетонитрил, фаза В. Скоростта е 1 ml/min. Дължината на вълната на фотодиодния детектор е фиксирана на 220 nm и хроматографията е проведена при стайна температура. Инжекционният обем е 10 μl за всички проби.

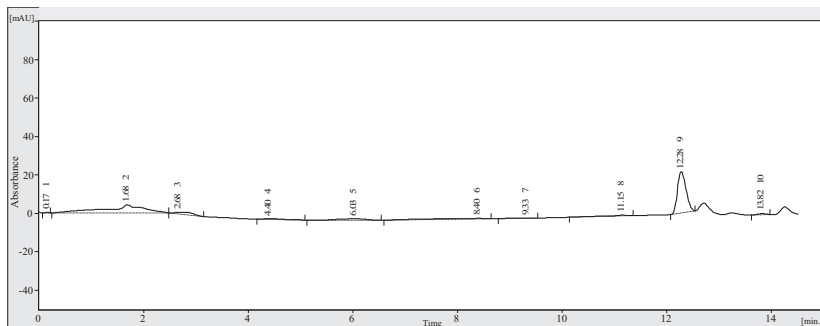
РЕЗУЛТАТИ

Извличане на флумиоксазин от черешите

При екстракцията на флумиоксазин от черешите е избран ацетон поради неговата ефективност към полярни и неполярни пестициди от различни матрици [12, 13]. Ацетонът е разтворител с ниска токсичност и сравнително ниска цена, напълно е смесим с водата и лесно се изпарява. Флумиоксазинът напълно се разтваря в дихлорометан, който го извлича от водната фаза при течно-течната екстракция. При количества 0.05 mg/kg – 0.1 mg/kg флумиоксазин в черешите, аналитичният добив варира от 30% до 60%. Тези резултати показват недостатъчната ефективност на течно-течната екстракция за адекватно извличане на остатъчни количества от флумиоксазин.

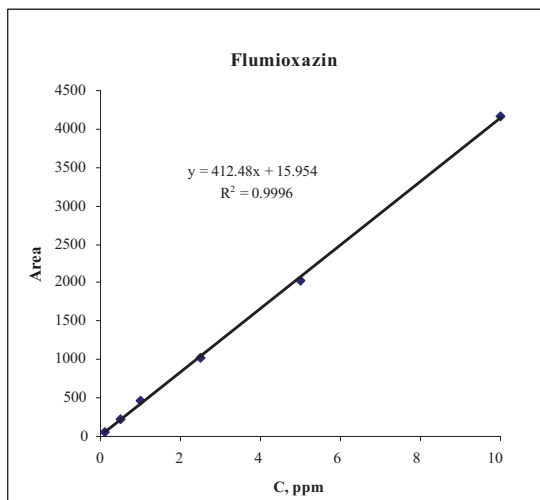
Разделяне и детектиране

Времето на задържане на флумиоксазин е 12.5 min и поглъщането му е при максимум на дължина на вълната 216 nm (Фиг. 1).



Фигура 1. Хроматограма на стандарт на флумиоксазин

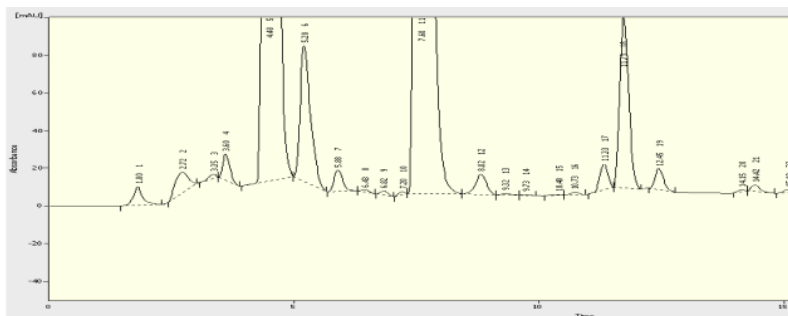
Сигналът на флумиоксазин при 220nm е линеен в областта от 0.1 µg/ml до 10 µg/ml и се характеризира с коефициент на корелация 0.999 (Фиг. 2).



Фигура 2. Линеиност на сигнала на флумиоксазин в зависимост от концентрацията

Границата на детектиране е при концентрация $0.1 \mu\text{g/ml}$ флумиоксазин, която отговаря на остатъчни количества от 0.02mg/kg в черешите. Получените резултати показват, че чувствителността на метода удовлетворява изискването за МДК (0.05mg/kg) при условие, че подготовката на пробата гарантира адекватно извличане на флумиоксазина от черешите.

На Фигура 3 е представена хроматограмата на проба череши с добавено количество 0.1mg/kg флумиоксазин.



Фигура 3. Хроматограма на проба череши с добавено количество от 0.1mg/kg флумиоксазин.

Не е идентифициран пик със същото време на задържане при двата варианта проби (контрола и третирана).

ЗАКЛЮЧЕНИЕ

При направените изследвания се установи, че използваният метод за подготовка на пробата на Shu-Jen Tuan et al., 2009 не дава достатъчно стабилни и адекватни резултати за определяне на остатъчни количества от флумиоксазин в череши. Предстоят експерименти за разработване на метод с използване на твърдофазна екстракция.

ЛИТЕРАТУРА

1. Duke, S. O., U. B. Nandihalli, H. J. Lee, and M. V. Duke. Amer. Chem. Soc. Symp. Ser. 559 (1994) 191–2004.
2. Dayan, F. E., and S. O. Duke. 1997a. Overview of protoporphyrinogen oxidase – inhibiting herbicides. Proc. Brighton Crop Protection Conf. – Weeds pp 83–92.
3. Vencill, W. K. 2002. Herbicide Handbook. Eighth edition. Weed Sci. Soc. Am. Lawrence, KS.
4. Rebecca Grace English, William K. Vencill. 2003. The basis of selectivity for flumioxazin use in peanut and associated weeds.
5. Balinova, A., Mladenova, R. and Shtereva, D. Journal of Chromatography A, 1150 (2007) 136–144.
6. Jae-Han Shimb, A. M. Abd El-Atyc. Journal of Chromatography A, 1218 (2011) 4366– 4377
7. Stajnbaher, D. and Zupancic-Kralj, L. Journal of Chromatography A, 1015 (2003) 185–198.
8. Hiemstra, M. and de Kok, A. Journal of Chromatography A, 1154 (2007) 3–25.
9. Yoshichika Hirahara et. al. Journal of Health Science 51 (2005) 617–627
10. E. Schrecka, F. Gereta, L. Gontierb, M. Treilhoua. Talanta 77 (2008) 298–303
11. Ortelli. D., Edder, P. and Corvi, C. Analytica Chimica Acta 520 (2004) 33–45.
12. Shu-Jen Tuan, Hsiu-Mei Tsai, Shang-Mei Hsu, Hong-Ping Li, Journal of Food and Drug Analysis, 17 (2009) 163–177.
13. Fenoll, J., Hellin, P., Martinez, C. M., Miguel, M. and Flores, P. Food Chemistry 105 (2007) 711–719.

СПЕКТРОФОТОМЕТРИЧЕН МЕТОД ЗА ОПРЕДЕЛЯНЕ НА ФРУКТАНИ В ХРАНИ

Н. Петкова, М. Саватинова, Б. Витанова, П. Денев

*Катедра „Органична химия и микробиология“
Университет по хранителни технологии,
бул. Марица 26, гр. Пловдив 4002;
E-mail: petkovanadejda@abv.bg, denev57@abv.bg*

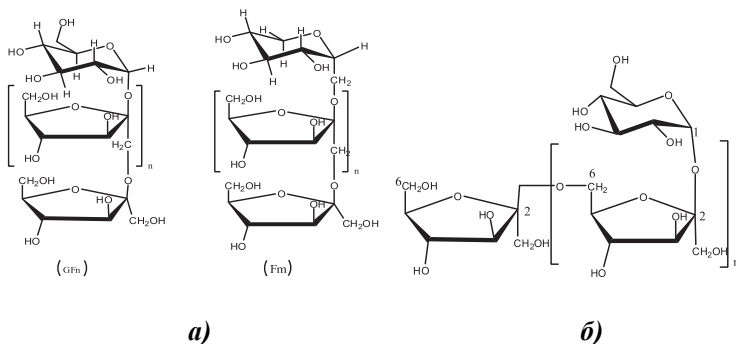
ABSTRACT

A simple, rapid and sensitive spectrophotometric method was developed for determination of fructans in food products (chewing candies with inulin). The proposed method is based on the familiar Seliwanoff test for ketoses. The presence of monosaccharides glucose and galactose did not show any interference in the analysis. The best operating conditions for development and measurement of a colored compound formed by interaction of fructans with resorcinol and thiourea in the hydrochloric acid medium was heating the samples for 8 min at 80°C. The producing red colored product is measured spectrophotometrically at 480 nm and the color is stable more than 60 min. Beer's law was obeyed in concentration range of fructose $0,5 \div 20 \mu\text{g}\cdot\text{cm}^{-3}$ ($R^2=0,997$). The proposed method was tested and validated for various parameters according to the ICH (International Conference on Harmonization) guidelines. The results demonstrated that the method is accurate, reproducible, cheap and less time consuming.

Ключови думи: *инулин, олигофруктози, фруктоза, спектрофотометрия, реакция на Селиванов.*

ВЪВЕДЕНИЕ

Фруктаните са широко разпространени резервни въглехидрати в растенията. Тяхната молекула съдържа една или повече фруктозил-фруктозни връзки. В зависимост от типа на свързване между фруктозните остатъци фруктаните могат да бъдат класифицирани в пет отделни групи: инулин, леван (Фиг. 1), смесени левани (граминан), инулин неосерия и неосерия левани (Таблица. 1). Инулинът е полидисперсен полизахарид, чиято верига е съставена основно от β -(2 \rightarrow 1) фруктозил-фруктозни остатъци (F_m), която обикновено, но не винаги, завършва с един глюкопиранозен остатък в редуциращия си край (GF_n) (Фиг. 1) [6]. Степента на полимеризация (DP) на фруктозата в инулина варира между 2 и 70. Олигофруктозите са фруктани от инулинов тип с DP между 2 и 12. Инулинът и олигофруктозите спадат към групата на диетичните влакнини и намират широко приложение в хранителните продукти като подсладители, сгъстителни или текстуриращи агенти [8].



Фигура 1. Фруктани: а) инулин и б) леван

Таблица 1. Типове фруктани срещани се в растенията

Тип фруктан	Вид на фруктозил-фруктозната връзка	Разпространение	Начален тризахарид
Инулин	2 \rightarrow 1	Топинамбур (гулия), цикория, далия	1 – кестоза
Леван	2 \rightarrow 6	<i>Dactylis glomerata</i>	6-кестоза
Разклонен (граминан)	2 \rightarrow 1 и 2 \rightarrow 6	Жито, ечимик	1 – кестоза и 6 – кестоза

Инулин неосерия	2→1	Аспержи и лук	6G – кестотриоза
Леван неосерия	2→6	Овес и <i>Lolium</i>	6G – кестотриоза

В практиката за определянето на инулин се използват колориметрични (спектрофотометрични) [1–5, 9], ензимни [8] и HPLC [10] методи за анализ. Повечето от съществуващите колориметрични методи се прилагат за определяне на инулин в кръв и урина като индикация за гломерулната филтрация на бъбреците [4, 9]. Други от тях се използват за стандартизация на изолиран инулин [3, 4] или за определянето му в растителни екстракти [1, 2, 5]. За анализа на инулин и олигофруктози в хранителни продукти се използват ензимни и HPLC методи. И двата метода обаче изискват наличие на специализирано и скъпоструващо оборудване, използване на пречистени ензими, а понякога е необходима продължителна пробоподготовка.

МАТЕРИАЛИ И МЕТОДИ

Всички химикали и реактиви използвани за метода са чисти за анализ. Те включват: D-фруктоза, глюкоза и галактоза (anhydrous, Fluka, 99% puriss); D-лактоза (monohydrate, Fluka, puriss), олигофруктози Frutafit CLR и инулин Frutafit TEX (Roosendaal, the Netherlands), резорцинол (Fluka, puriss >99%), тиокарбамид (VEB YENAPHARM pro Analysi – Laborchemie APOLDA) и дъвчащи бонбони за отслабване (без захар, със захарни алкохоли, олигофруктози и екстракт от сена), закупени от търговската мрежа. Използваните инструменти и апаратура включват автоматични пипети Ахурет (Ахуген), аналитична везна Kern ABJ, спектрофотометър Samspec M107, центрофуга – MLW T23 и магнитна бъркалка MSH 300 (BOECO, Germany).

Определяне на абсорбционния максимум

За определяне на абсорбционния максимум се приготвят стандартни разтвори на глюкоза, фруктоза, галактоза, лактоза, олигофруктоза, инулин – всички с концентрация $1,00 \text{ mg.cm}^{-3}$. В мерителна колба от 100 cm^3 се прибавят последователно $1,00 \text{ cm}^3$ проба, $1,00 \text{ cm}^3$ резорцинол (1 mg.cm^{-3}), $1,00 \text{ cm}^3$ тиокарбамид (0,1 %), $8,00 \text{ cm}^3$ етанол, $9,00 \text{ cm}^3$ к.НСl. Колбата се нагрява на водна баня в продължение на 8 min при 80°C . Следва охлаждане, доливане до марката с дест. вода и измерване на абсорбцията на съответната проба при различна дължина на вълната в диапазон от 340 до 660 nm, спрямо дест. H_2O .

Построяване на стандартна права

За построяване на калибрационна права са използвани стандартни разтвори на фруктоза с концентрации от $0,5 \mu\text{g}\cdot\text{cm}^{-3}$ до $20 \mu\text{g}\cdot\text{cm}^{-3}$.

Подготовка на пробата за анализ

Претегля се $2,50 \text{ g}$ дъвчащ бонбон, към него се прибавят 25 cm^3 дестилирана вода и пробата се разбърква на магнитна бъркалка при температура 50°C . Разтворената проба се прехвърля в мерителна колба от 50 cm^3 , долива се до марката с дестилирана вода и се филтрува през хартиен филтър с диаметър на порите $0,45 \mu\text{m}$. Полученият бистър филтрат се прехвърля в центрофужна епруветка от 50 cm^3 с винт и се екстрахира двукратно с по 5 cm^3 петролеев етер за извличане на липидите. Пробата се центрофугира двукратно в продължение на 15 min при 2000 min^{-1} с последващо отделяне на етерния слой. От водния слой се взема 1 cm^3 и се разработва по описания по-горе начин. Измерва се абсорбцията при 480 nm с три повторения. Извършва се и снемане на спектъра на поглъщане при различна дължина на вълната в диапазона от 340 nm до 660 nm .

Процедурата по валидирането на спектрофотометричния метод за вътрешно-лабораторни анализи е извършена според указанията на Международната конференция за хармонизация (ICH) [7], като са определени: линейност, прецизност и точност на метода.

Прецизността на метода е изразена чрез повторяемостта и междинната прецизност (intermediate precision). Те се изразяват чрез относителното стандартно отклонение (RSD) и се изчисляват по формула (1):

$$RSD = \frac{S}{\bar{X}} 100\% \quad (1)$$

където: S – стандартно отклонение от измерванията на 6 отделно претеглени, паралелно разработени и анализирани проби от един и същ аналитик в един и същи ден (за повторяемост); S – стандартно отклонение от измерванията на 6 отделно претеглени, разработени и анализирани проби в различни дни и от различни аналитици (за междинната прецизност); \bar{X} – средно аритметично съдържание на фруктани в пробата, $\text{g}/100 \text{ g}$.

За оценка на точността на метода е използвана относителната грешка, изчислена по формула (2). Обикновено точността се представя и се определя чрез метода на аналитичния добив (recovery), за който се използват три подхода, един от които е методът на стандартната добавка. Още в началото на разработване на пробата към 1,5 g бонбон разтворен в 50 cm³ дестилирана вода се добавят съответно 4; 8 и 10 μg.cm⁻³ фруктоза. Пробите се разработват по описаната методика и резултатите се изчисляват по формулите (2) и (3):

$$\text{Относителна грешка (\%)} = \frac{V_0 - V_s}{V_s} \times 100 \quad (2)$$

където: V_0 – определеното съдържание на фруктани в пробата; g/100 g;

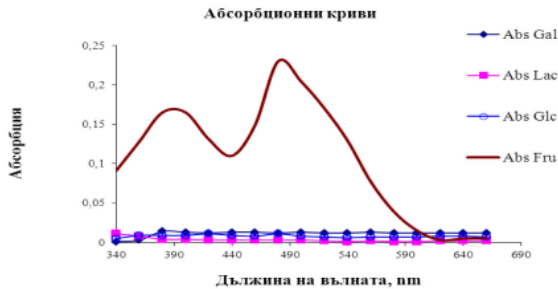
V_s – реалното (истинското) съдържание на фруктани в пробата. Стойността им се изчислява от правата построена по метода на стандартната добавка, g/100 g

$$\text{Точност (\%)} = 100 - [\text{Относителна грешка}] \quad (3)$$

РЕЗУЛТАТИ

От представените на фигура 2 абсорбционни спектри на формираното цветно съединение, получено при взаимодействието на фруктоза, глюкоза, галактоза и лактоза с резорцинол в кисела среда, ясно проличава високата специфичност на използвания реактив към кетози. Следователно присъствието на гореизброените алдози в изследваната проба няма да окажат пречещо влияние при спектрофотометричното определяне на фруктани. От снетата абсорбционна крива $Abs = f(\lambda)$ на фруктоза се забелязва, че полученият хромоген има максимална абсорбция при дължина на вълната 480 nm.

Изследвани са и абсорбционните спектри на дъвчащи бонбони, съдържащи олигофруктози, както и на разтвори на търговска марка инулин и олигофруктози. Получените резултати представени в таблица 2 показват, че и трите продукта в присъствие на резорцинол в кисела среда дават хромоген, който се характеризира с максимална абсорбция при 480 nm, както при фруктозата. Следователно фруктаните в тези продукти могат да бъдат анализирани при точно тази дължина на вълната, като определянето им се сведе до определяне на фруктоза в пробата.



Фигура 2. Абсорбционни спектри на комплексните съединения получени при взаимодействие на фруктоза, глюкоза, галактоза и лактоза, всички с концентрация $10 \mu\text{g}\cdot\text{cm}^{-3}$ с резорцинол

Таблица 2. Абсорбция на хранителни продукти и съставки при различна дължина на вълната

Дължина на вълната, nm	Абсорбция на дъвчащи бонбони	Абсорбция на Frutafit CLR, $10 \mu\text{g}\cdot\text{cm}^{-3}$	Абсорбция на Frutafit TEX, $10 \mu\text{g}\cdot\text{cm}^{-3}$
340	0,184	0,062	0,076
360	0,237	0,089	0,099
380	0,302	0,127	0,129
400	0,301	0,125	0,127
420	0,229	0,098	0,098
440	0,182	0,101	0,084
460	0,225	0,205	0,108
480	0,327	0,213	0,154
500	0,288	0,201	0,140
520	0,241	0,115	0,121
540	0,181	0,089	0,095
560	0,117	0,059	0,066
580	0,034	0,037	0,029
600	0,009	0,023	0,029
620	0,005	0,017	0,022
640	0,002	0,014	0,019
660	0,001	0,013	0,018

Стандартната права е построена с цел определяне линейността на спектрофотометричния метод (Фиг. 3) Получена е строга линейна зависимост между абсорбцията на формирания хромоген при 480 nm и концентрацията на фруктоза, $\mu\text{g}\cdot\text{cm}^{-3}$. Полученият корелационен коефициент е по-висок от 0,995 в концентрационния интервал на фруктоза от $0,5 \mu\text{g}\cdot\text{cm}^{-3}$ до $20 \mu\text{g}\cdot\text{cm}^{-3}$.



Фигура 3. Стандартна права на зависимостта между абсорбцията на формираното комплексно съединение и концентрацията на фруктозата

Прецизността на спектрофотометричния метод за определяне на фруктани беше оценена чрез повторемостта и междинната прецизност, изразени чрез стандартното отклонение и относителното стандартно отклонение (RSD) на фруктозата, определена в 6 отделно претеглени, разработени и анализирани проби. Отчетено е влиянието на човешкия фактор при извършване на анализа. От представените в таблица 3 резултати се вижда, че методът се отличава с много добра повторемост и междинна прецизност.

Таблица 3. Оценяване на прецизността на предложения метод

Номер на пробата	Съдържание на инулин и олигофруктози в дъвчащ бонбон, g/100g		
	Повторемост	Междинна прецизност *	Междинна прецизност **
1	3,6	4,0	3,3
2	4,6	4,4	4,3
3	3,8	4,6	4,1
4	4,4	3,6	4,3

5	4,2	4,0	4,4
6	3,4	3,8	4,7
Средно, g/100g	4,0	4,0	4,2
SD	0,5	0,4	0,5
RSD, %	11,6	8,9	11,9

*анализ на различно разработени проби в различни дни от един и същи аналитик

**анализ на различно разработени проби в различни дни от различни аналитици

В таблица 4 са представени резултати от оценката за точността на спектрофотометричния метод, изразена чрез относителната грешка. Представени са и данните от стандартната права построена в резултат на прилагане на метода на стандартната добавка. Разработеният метод се отличава с една добра точност, като се вземе предвид използването на реална проба с цялата си сложност на матрицата и наличие на интерфериращи компоненти.

Таблица 4. *Оценяване на точността на спектрофотометричния метод изразена чрез относителната грешка за определяне на фруктани*

Vs, g/100 g	Vo, g/100 g	Относителна грешка, %	Точност, %
4,8	5,0	5,3	94,7

ЗАКЛЮЧЕНИЕ

Разработеният спектрофотометричен метод за определяне на фруктани, базиран на реакцията на Селиванов, е бърз, опростен и подходящ за рутинни анализи в ежедневната лабораторна практика. Характеризира се с добра линейност $R^2 = 0,997$ и е специфичен само за кетози (фруктани). Методът се отличава със сравнително висока прецизност RSD около 8–12% и се характеризира с относителна грешка 5,3 %. Пробоподрготовката и времето за анализ са сравнително кратки, а себестойността на метода е сравнително ниска.

БЛАГОДАРНОСТИ

Авторите изказват благодарност на Фонд „Наука“ (проект по НИС, договор 10/11-Н), Университет по хранителни технологии – гр. Пловдив за оказаната финансова помощ.

ЛИТЕРАТУРА

1. Оленников, Д. Н.; Танхаева, Л. М.; Химия Растительного сырья; 2008; 69
2. Оленников, Д. Н.; Танхаева, Л. М.; Химия Растительного сырья; 2008; 95–99
3. Денев, П., Делчев, Н., Добрев Г., Панчев И., Кирчев, Н., Изолиране и характеристика на инулин от топинамбур, ХВП, 2010, 3, 48–51
4. Anan`ina, N., A., Andreeva O., A., Mycots, L. P., Oganesyanyan E., T., *Farmaceutical Chemistry Journal*, vol. 43, No.3, 2009, 157
5. Ashwell, G., In: *Methods in enzymol* 3, (Edscolowick, SJ and Kaplan, NO) Academic Press New York; 1957, 75
6. Van Laere, A. and Van Den Ende, Inulin metabolism in dicots: chicory as a model system, *Plant, Cell and Enviroment*, 2002, 25, 803–813
7. International Conference on Harmonization (ICH) of Technical Requirements for the Registration of Pharmaceuticals for Human Use, validation of analytical procedures: Methodology, adopted in 1996, Geneva
8. McCleary et al., Measurement of total fructan in food by enzymatic/Spectrophotometric method Collaborative Study, *Journal of AOAC International* Vol. 83, 2000
9. Nolin, Th. D., et al. Rapid microtiter plate assay for determination of inulin in human plasma and dialysate, *J of Pharm & Biomed. Anal.*, 28 (2002), 209–315.
10. Vendrell-Pascuas, S. et al., Determination of inulin by high-performance liquid chromatography with refractive index detection, *J of chromatography A*, 881, 2002

RELATIONSHIP BETWEEN MOLYBDENUM AND NITRATE NITROGEN IN PLANTS AND THEIR YIELD

D. Kostova, D. Haytova*

*Agricultural University – Plovdiv,
12 Mendeleev Str., 4000 Plovdiv, Bulgaria
E-mail: deny_kostova@yahoo.com

ABSTRACT

The influence of leaf fertilizer Fitona, Hortigrow and Humustim upon the content of molybdenum in the fruit of marrows has been investigated. The researches show that in soil and leaf fertilization the highest molybdenum content responds to the highest amount of nitrate nitrogen, which is being assimilated by plants. The influence of the incorporated in different fertilizers nitrogen upon the content of molybdenum in the fruit has been investigated as well. A relationship between the content of molybdenum in the fruit and the obtained yield in leaf and mixed fertilization has been traced out. The experimental data show that in leaf fertilization the yield decreases with the increase of the amount of molybdenum. A positive influence of molybdenum upon the yield has been determined in soil and leaf fertilization.

Key words: *molybdenum, triphenyltetrazolium chloride, plants, fertilization*

INTRODUCTION

Molybdenum is a micronutrient required by plants in very small amounts. Molybdenum complex is part of both nitrate reductase, whereby nitrate is re-

duced to nitrite, and nitrogenase whereby nitrogen-fixing bacteria convert nitrogen gas into ammonia.

The transition element molybdenum is essential for most organisms and occurs in more than 60 enzymes catalyzing diverse oxidation-reduction reactions. Several molybdoenzymes including nitrogenase, nitrate reductase, aldehyde oxidase are of significance to plants. Because of its involvement in the processes of N_2 fixation, nitrate reduction, and the transport of nitrogen compounds in plants, molybdenum plays a crucial role in nitrogen metabolism of plants [1–3].

The essential nature of molybdenum as a plant nutrient is based solely on its role in the NO_3^- reduction process via nitrate reductase. This enzyme occurs in most plant species as well as in fungi and bacteria, and is the principal molybdenum protein of vegetative plant tissues. However, the requirement of molybdenum for nitrogenase activity in root nodules is greater than the requirement of molybdenum for the activity of nitrate reductase in the vegetative tissues. Because nitrate is the major form of soil nitrogen absorbed by plant roots, the role of molybdenum as a functional component of nitrate reductase is of greater importance in plant nutrition than its role in N_2 fixation [4,5].

Molybdenum and nitrate are both required for the induction of nitrate reductase in plants, and the enzyme is either absent [6], or its activity is reduced [7], if either nutrient is deficient.

The objective of this study is to explore the influence of molybdenum upon the nutritious value of fruit of marrows and to clarify the opportunity of using 2,3,5-triphenyltetrazolium chloride (TTC) [8–15] as a reagent for determination of microquantities of molybdenum in plant samples.

MATERIAL AND METHODS

The experiment was carried out in eight variants: non fertilized, leaf fertilization and mixed fertilization (soil with leaf).

Variants of the experiment:

1. Control – non fertilized
2. Leaf fertilization 0.3 % Fitona
3. Leaf fertilization 0.3 % Hortigrow
4. Leaf fertilization 0.3 % Humustim
5. Soil fertilization $N_{16}P_{16}K_{16}$
6. $N_{16}P_{16}K_{16}$ + Fitona 0.3 %
7. $N_{16}P_{16}K_{16}$ + Hortigrow 0.3 %
8. $N_{16}P_{16}K_{16}$ + Humustim 0.3 %

Apparatus

Spectrophotometer UV-VSU with 1-cm light path quartz cells; Flame Atomic Absorption Spectrophotometer „Perkin Elmer“ (Germany)

Determination of molybdenum(VI) in plant samples

1g from the plant material was reduced to ashes in an oven in 450 – 500° C. The dry residuum was dissolved in a dilute hydrochloric acid (1:1). Obtained solution was transferred into a volumetric flask of 50 mL and diluted to the mark with distilled water. Aliquot parts of this solution were taken for analysis.

The following solutions were introduced into a separatory funnel of 100 mL: 0.5 mL of phosphoric acid, 2×10^{-2} M; 0.5 mL of TTC, 1×10^{-3} M; and an aliquote of the prepared plant sample solution. The mixture was diluted up to 10 mL with distilled water. Then 3 mL of 1,2-dichloroethane were added and the funnel was shaken for 30 sec. The organic phase was filtered through a dry paper into a 1 cm cuvette and the absorbance was measured at 250 nm [8]. A blank was run in parallel. A calibration graph was constructed with similarly treated standards.

RESULTS AND DISCUSSION

The influence of leaf fertilizer Fitona, Hortigrow and Humustim upon the content of molybdenum in the fruit of marrows has been investigated (Table 1). Molybdenum in plant samples was determined with an extraction-spectrophotometric method with TTC [8]. The accuracy of the method was checked up using atomic-absorption spectrometry (AAS). The experimental data (Table 1) show a good agreement between the results obtained by the two methods.

The leaf feeding up was done with 0.3% solutions of these fertilizers. The experimental data (Fig. 1) show that the highest amount of Mo 3.99 mg/kg can be accumulated in the fruit of marrows in leaf feeding-up with Fitona. The content of molybdenum is lowest 3.42 mg/kg in fertilization with Humustim, as in the control (non fertilized) the content of molybdenum is almost the same.

In mixed fertilization (soil and leaf) the content of molybdenum increases in the same variants of fertilization with the leaf fertilizers Fitona, Hortigrow, Humustim. All this indicates that soil fertilization commonly helps accumulation of higher amount molybdenum in the fruit of plants in leaf fertilization. In the control sample it was fertilized only with $N_{16}P_{16}K_{16}$ and the content of molybdenum was low 3.37 mg/kg. This value was approximately like that

in variant 6 ($N_{16}P_{16}K_{16}$ + Fitona). In the variants of fertilization 7 ($N_{16}P_{16}K_{16}$ + Hortigrow) and 8 ($N_{16}P_{16}K_{16}$ + Humustim) the molybdenum content in the fruit increased.

Table 1. Content of molybdenum in the fruit of marrows in leaf fertilization and mixed fertilization

№	Variants	Mo, mg kg ⁻¹ TTC method	RSD* %	Mo, mg kg ⁻¹ AAS	Nitrate mg/kg
1	Control – non fertilized	3.46	1.1	3.55	120
2	0.3 % Fitona	3.99	1.7	3.80	90
3	0.3 % Hortigrow	3.94	1.5	4.00	250
4	0.3 % Humustim	3.42	1.8	3.60	175
5	$N_{16}P_{16}K_{16}$	3.37	1.2	3.50	115
6	$N_{16}P_{16}K_{16}$ + 0.3 % Fitona	3.28	1.9	3.15	135
7	$N_{16}P_{16}K_{16}$ + 0.3 % Hortigrow	4.32	1.2	4.45	100
8	$N_{16}P_{16}K_{16}$ + 0.3 % Humustim	4.35	1.4	4.40	250

*Relative Standard Deviation for TTC method (based on 5 determination)

Indices:

N_{16} – introduced as NH_4NO_3 (34 % N)

P_{16} – introduced as $Ca(H_2PO_4)_2$ (46 % P_2O_5)

K_{16} – introduced as K_2SO_4 (50 % K_2O)

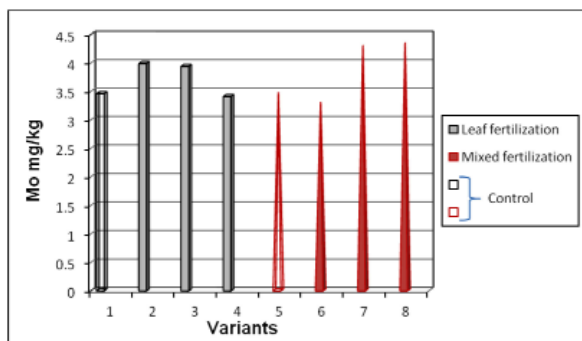


Figure 1. Content of Mo in the fruit of marrows in leaf and mixed fertilization (soil and leaf) fertilization. Variants: 1 – Control; 2 – Fitona; 3 – Hortigrow; 4 – Humustim; 5 – Control ($N_{16}P_{16}K_{16}$); 6 – $N_{16}P_{16}K_{16}$ + Fitona; 7 – $N_{16}P_{16}K_{16}$ + Hortigrow; 8 – $N_{16}P_{16}K_{16}$ + Humustim

Molybdenum is of great significance for the circum rotation of nitrogen and its assimilation by plants. Being incorporated in the composition of the enzyme nitrate_reductase, molybdenum itself ensures the assimilation of the nitrate nitrogen sources by plants. In this respect a subordination was traced out between the content of molybdenum and nitrate nitrogen in the fruit of marrows in leaf fertilization and mixed (soil and leaf) fertilization. The experimental data (Fig. 2) show that in leaf fertilization the nitrate nitrogen can be assimilated to the highest extent, 250 mg/kg, in the content of Mo, 3.94 mg/kg, in the fruit of marrows. In soil and leaf fertilization the highest content of Mo, 4.35 mg/kg, responds to the highest amount of nitrate nitrogen, 250 mg/kg, which is being assimilated by plants.

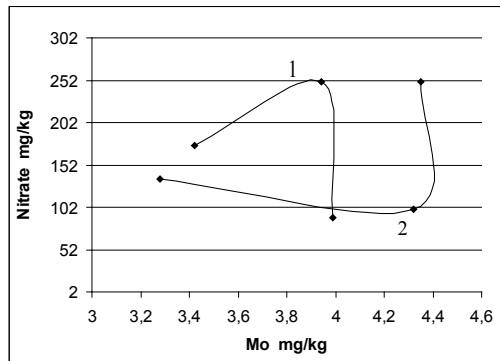


Figure 2. A subordination between the content of Mo and nitrate nitrogen ($NO_3 - N$) in the fruit of marrows:
1 – leaf fertilization; 2 – soil and leaf fertilization

In order to trace out what is the influence of the different fertilization leaf and mixed one, we have investigated the influence of nitrogen that is being incorporated in different fertilizers upon the content of molybdenum in the fruit of marrows. A certain subordination is traced between the content of nitrogen in the leaf fertilizers Humustim, Fitona and Hortigrow and the assimilation of molybdenum by plants. The subordination between Mo in fruit and nitrogen in fertilizer is represented in Fig. 3. The experimental data (Fig.3, curve 1) show that at the lowest content of nitrogen in leaf fertilizer (3%) the content of Mo in fruit is also lowest (3.42 mg/kg). With the increase of the percentage of nitrogen in fertilizer, the content of Mo increased to 3.99 mg/kg for 7.2 % nitrogen, and respectively 3.94 mg/kg Mo for 20 % nitrogen in leaf fertilizer.

Consequently the higher content of nitrogen in fertilizer helps the accumulation of higher amount of molybdenum in the fruit of plants.

The subordination between molybdenum in the fruit of marrows and nitrogen in leaf fertilizer in mixed fertilization is represented in Fig. 3, curve 2. It cannot be seen a definite subordination between the two parameters if leaf fertilization is done together with soil one ($N_{16}P_{16}K_{16}$).

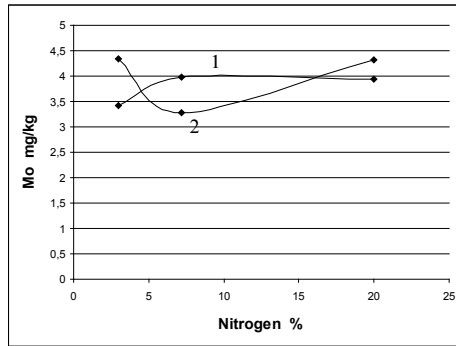


Figure 3. A subordination between the content of Mo in the fruit of marrows and nitrogen in leaf fertilizer in 1 – leaf fertilization and 2 – soil and leaf fertilization

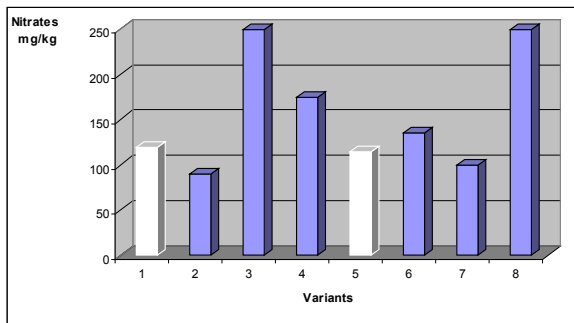


Figure 4. Content of nitrate nitrogen ($NO_3 - N$) in the fruit of marrows. Variants: 1 – non fertilized, 2 – Fitona, 3 – Hortigrow, 4-Humustim, 5 – $N_{16}P_{16}K_{16}$, 6 – $N_{16}P_{16}K_{16}$ + Fitona, 7 – $N_{16}P_{16}K_{16}$ + Hortigrow, 8 – $N_{16}P_{16}K_{16}$ + Humustim

The influence of the different kind of fertilization is investigated upon the content of nitrates in the fruit of marrows. In leaf fertilization the highest amount of nitrates, 250 mg/kg, is accumulated in the fruit in fertilization with Hortigrow, which comprises 20% nitrogen (Fig. 4, variants 1–4). It should be mentioned that leaf fertilizer Hortigrow has highest nitrogen amount in comparison with Fitona and Humustim. This fact explains the high content of nitrates in the fruit. The content of nitrates in the fruit in mixed fertilization (soil N_{16}, P_{16}, K_{16} and leaf fertilization) is presented in Fig. 4, variants 5–8. The experimental data show that plants accumulate the biggest amount of nitrates, 250 mg/kg, in fertilization with $N_{16}, P_{16}, K_{16} +$ Humustim.

Molybdenum is one of the main nutritious elements for vegetable crops. That is the reason for which molybdenum is a factor that has an influence on yield and its quality. In this respect a certain subordination is traced out between the content of Mo in the fruit of marrows and the obtained yield in leaf and mixed fertilization.

The experimental data (Fig. 5) show that in leaf fertilization the yield decreases with the increase of the amount of Mo accumulated by plants. In soil and leaf fertilization there has been determined a positive influence of molybdenum upon the yield of marrows (Fig. 6). As distinct from leaf fertilization, mixed fertilization has a positive influence not only upon the content of molybdenum in the fruit of marrows, but upon the yield. With the increase of the content of molybdenum in the fruit of marrows the yield increases. This could be explained with the additional introduction of the main nutritious elements N, P and K in soil.

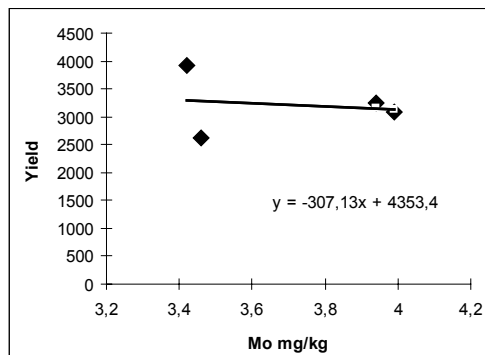


Figure 5. A subordination between yield and the content of Mo in the fruit of marrows in leaf fertilization; Correlation coefficient: $r = -0.17$

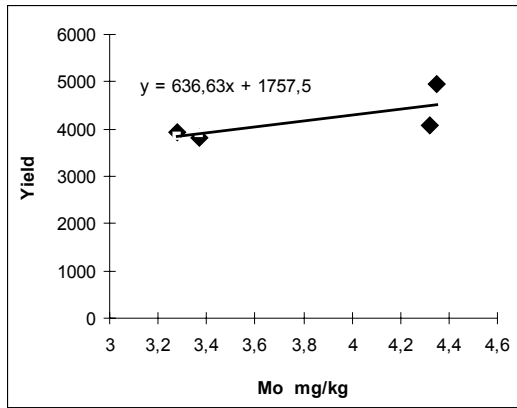


Figure 6. A subordination between yield and the content of Mo in the fruit of marrows in mixed fertilization (soil and leaf);
Correlation coefficient: $r = 0,73$

ACKNOWLEDGMENT

The authors would like to thank the Research Fund of the Agricultural University for financial support.

REFERENCES

1. Mendel R., G. Schwarz G., Molybdoenzymes and molybdenum cofactor in plants, *Crit. Rev. Plant Sci.*, 1999, 18, 33–69.
2. Zimmer W., Mendel R., Molybdenum metabolism in plants, *Plant Biol.*, 1999, 1, 160 – 168.
3. Srivastava P., Biochemical significance of molybdenum in crop plants, In: U. C. Gupta, ed., *Molybdenum in Agriculture*, New York: Cambridge University Press, 1977, pp. 47–70.
4. Parker M., Harris H., Yield and leaf nitrogen of nodulating and non-nodulating soybean as affected by nitrogen and molybdenum, *Agron. J.*, 1977, 69, 551–554.
5. Mengel K., Kirkby E., *Principles of Plant Nutrition*, 4th ed. Bern, Switzerland: International Potash Institute, 1987, pp. 551–558.
6. Li Z., Gresshoff P., Developmental and biochemical regulation of constitutive nitrate reductase activity in leaves of nodulating soybean, *J. Exp. Bot.*, 1990, 41, 1231–1238.
7. Randall P., Changes in nitrate and nitrate reductase levels on restoration of molybdenum to molybdenum-deficient plants, *Aus. J. Agric. Res.*, 1969, 20, 635–642.
8. D. Kostova, Triphenyltetrazolium chloride as a new analytical reagent for molybdenum(VI): Application to plant analysis *Journal of Anal Chem.*, 2011, 66, 4, 384 – 388.
9. A. Alexandrov, M. Kostova,, Triphenyltetrazoliuchlorid als Extraktionsreagens für Molybdän(VI), *Mikrochimica Acta (Wien)*, 1976, I, 487–492.
10. A. Aleksandrov, M. Hadzhieva, Extraction investigations of ternary ion-associated complex of molybdenum(VI) with pyrogalllic acid and triphenyltetrazolium chloride, *Nauch. Tr. Plovdiv Univ. Chem.*, 1979, 17, 11–23.
11. S. Kostova, A. Dimitrov, Extraction-Spectrophotometric studies of Molybdenum(VI) Ion-Association Complexes with some Polyphenols and Tetrazolium Salts, *Bulg. Chem. Ind.* 2000, 71(1–2), 44.
12. Gavazov K., Lekova V., Dimitrov, The use of tetrazolium salts in inorganic analysis, *Russian Chemical Reviews*, 2007, 76(2), 169–179.

13. K. Gavazov, V. Lekova, B. Boyanov, A. Dimitrov, DTA and TGA Study of Some Tetrazolium Salts and their Ion-association Complexes with the Molybdenum (VI) – 4-Nitrocatechol Anionic Chelate, *Journal of Thermal Analysis and Calorimetry*, 2009, 96(1), 249–254.
14. D. Kostova, An Influence of Molybdenum Upon The Content of Antioxydants in the Fruits of Tomatoes, BALWOIS 2010 – Ohrid, Republic of Macedonia – 25, 29 May 2010 http://balwois.com/balwois/administration/full_paper/ffp-1360.pdf.
15. D. Kostova, Determination of molybdenum with triphenyltetrazolium chloride in plant samples, University of Plovdiv „Paissii Hilendarski“ – Bulgaria, *Scientific works. Chemistry*, 2010, 37(5), 43–48.

AUTOMATIC GENERATION OF TAUTOMERS

N. Kochev^{a1}, V. Paskaleva^a, N. Jeliazkova^b*

*a) University of Plovdiv, Department of Analytical Chemistry
and Computer Chemistry,*

b) Ideaconsult Ltd, 4 A. Kanchev str., Sofia 1000, Bulgaria,

ABSTRACT

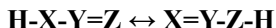
A software module for automatic generation of tautomers is introduced. The software is implemented on top of Chemistry Development Kit (CDK) Library. The program enumerates all possible tautomeric forms of a given molecule. All places for double bond/hydrogen atom shift are identified and combined via exhaustive combinatorial algorithm. Different tautomerism cases are described as rules represented in the form: $H-X-Y=Z \leftrightarrow X=Y-Z-H$, where the states are coded as SMILES strings and the H atom positions are denoted as well. For a particular target molecule, each rule is applied by means of exhaustive substructure searching of the rule fragments against given target structure. As a result all possible locations for a shift are recognized. The tautomeric forms in this sense could be described as binary numbers where each digit represents the „shift“ state of each recognized location.

Key words: *tautomer, automatic generation, SMILES, substructure, isomorphism*

^{1*} *correspondence author: nick@uni-plovdiv.bg*

INTRODUCTION

Tautomerism is a process of dynamic isomerization of one tautomer converting itself into another. The IUPAC definition [1] generalizes the Tautomerism in the form:



where X, Y and Z are typically C, O, N or S atoms and H is the moving group. When the moving group is H⁺ the tautomerism is called „prototropic“. Computer-based applications often handle tautomers as different structures because of their different topological representation (i.e. double bond positions are changed). Tautomerism can influence the calculations of pKa, LogP and solubility and also can change the stereochemistry of a compound. Different tautomers have different ligand-receptor interactions. Also structure similarity searching is affected because of the differentiations of tautomeric fingerprints [2]. Software for automatic generation of tautomers is a valuable tool for scientists working in the areas of structure-based drug discovery, design and optimization, structure elucidation and spectra prediction. The latter is the basic motivation for developing yet another software tool for automatic tautomer generation.

SOFTWARE IMPLEMENTATION

The program was implemented using object oriented language Java on top of the open source library CDK [3]. Our software uses the CDK model for structure representation. Figure 1 shows the flow chart of tautomer generation algorithm.

First the molecular structure is inputted into the system as a SMILES string. All possible fragment states for each rule are searched against the target structure thus all rule positions are identified using the AMBIT isomorphism algorithm [4].

Each rule has typically two states coded as 0 and 1. The found locations match one of the states (0 or 1) for each rule. The other state is generated by the software. Then all possible combinations of fragments' states are iterated to generate all possible tautomers (see figure 1).

Currently the software uses eleven rules described by means of SMILES line notation. They cover the range of 1,3 shifting of the moving group. For example the first rule describes the most common type of Tautomerism, keto-enol one, and has two possible states of the molecule. All other rules are listed in table 1.

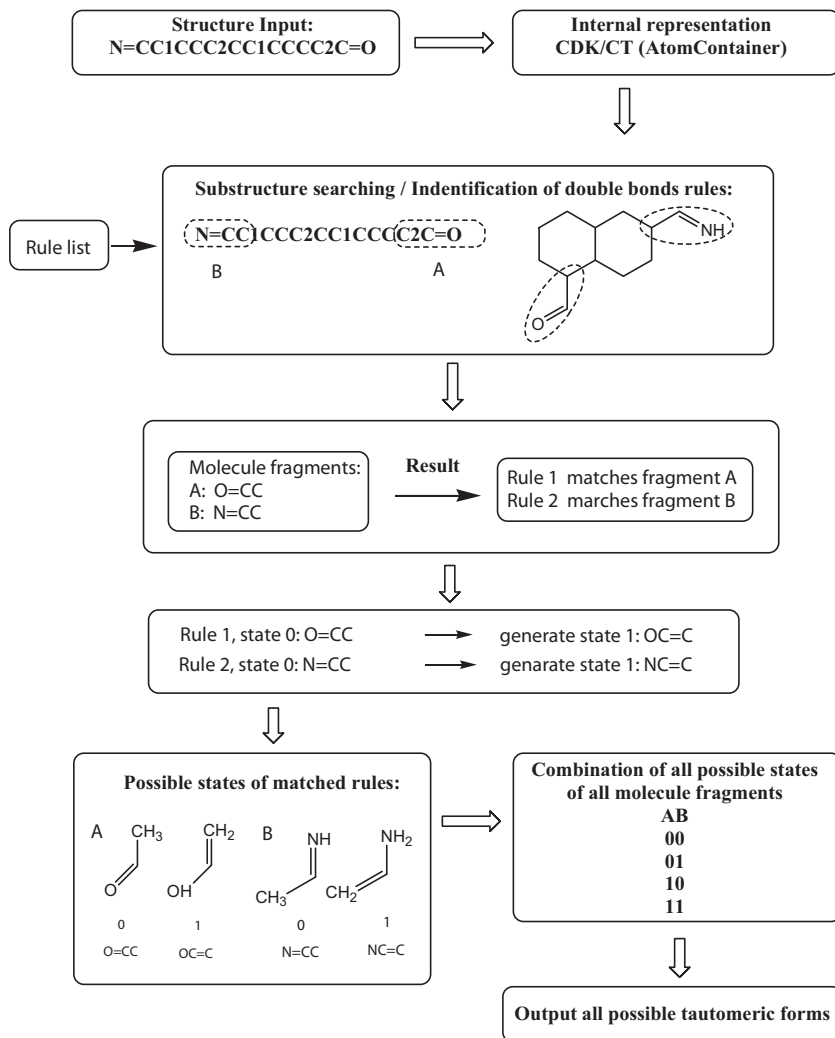


Figure 1. Flow chart of the tautomer generation algorithm.

Table 1. Tautomer rule list

	NAME	STATES		H-position
1	keto/enol	O=CC	OC=C	3,1
2	amin/imin	N=CC	NC=C	3,1
3	amide/imid	O=CN	OC=N	3,1
4	nitroso/oxime	O=NC	ON=C	3,1
5	azo/hydrazone	N=NC	NN=C	3,1
6	thioketo/thioenol	S=CC	SC=C	3,1
7	thionitroso/ thiooxime	S=NC	SN=C	3,1
8	amidine/imidine	N=CN	NC=N	3,1
9	diazoamino/ diazoamino	N=NN	NN=N	3,1
10	thoamide/ aminothiols	S=CN	SC=N	3,1
11	nitrosamine/ diazohydroxide	O=NN	ON=N	3,1

EXAMPLE OF SOFTWARE APPLICATION

For illustration purposes we use the molecule of 6-(iminomethyl) decahydronaphthalene-1-carbaldehyde shown in Figure 2. It contains two fragments A and B which correspond accordingly to the rules: 1 – keto/enol rule and 2 – amino/imino rule.

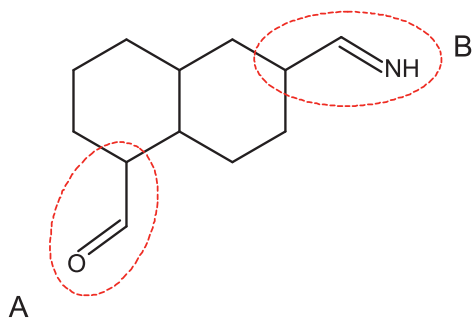


Figure 2. Rule application for the molecule of 6-(iminomethyl) decahydronaphthalene-1-carbaldehyde. Fragments A and B are identified.

Fragment A (keto/enol rule) is found in state 0 – „keto“. Fragment B (amino/imino rule) is found in state 1 – „imino“.

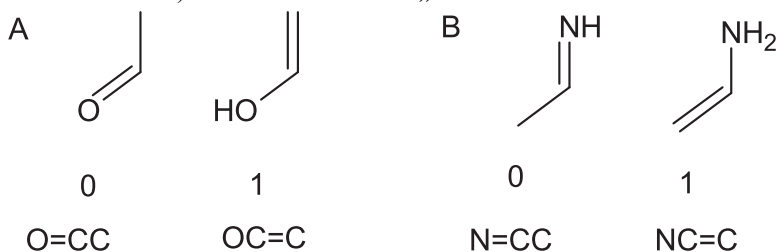


Figure 3. Rule states of fragments A and B and their codes.

To get all possible tautomeric forms for the molecule all combinations of states of fragments A and B are generated: 00 – keto, imino; 01 – keto, amino; 10 – enol, imino; 11 – enol, amino.

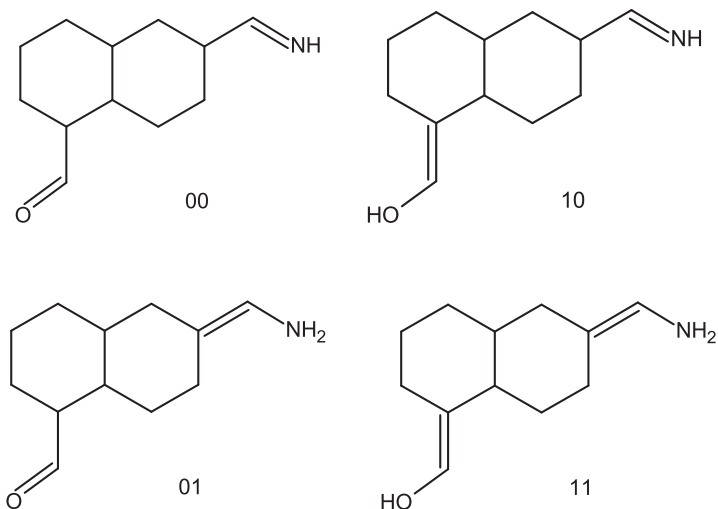


Figure 4. Result (generated) tautomeric forms.

CONCLUSIONS

Described software module handles well the basic forms of tautomerism and can be used for handling small organic structures. This is the first version

of a bigger project for automatic generation of tautomers. The software module is part of AMBIT software platform for Chemoinformatics. Current version of the software handles well molecules for which the described rules from table 1 are not overlapped. Also 1,5 shifts or higher distances shifts are not regarded.

REFERENCES

1. IUPAC Compendium of chemical terminology (electronic version). <http://goldbook.iupac.org/T06252.html>, accessed 18 Nov, **2011**.
2. Milleti F., Storchi L., Sforza G., Cruciani G.; Tautomer enumeration and stability prediction for virtual screening on large chemical databases. *J. Chem. Inf Model*, **2009**, 49(1), 68–75
3. Chemistry Development Kit (CDK); http://almost.cubic.uni-koeln.de/cdk/cdk_top
4. Nina Jeliaskova, Nikolay Kochev, AMBIT-SMARTS: Efficient Searching of Chemical Structures and Fragments; *Molecular Informatics*, 30 (8), **2011**, 707–720. <http://ambit.sourceforge.net>, accessed 18 Nov, **2011**.

EXCITED-STATE REACTION PATHS OF CYTOSINE AND ISOCYTOSINE: C=O ELONGATION

P. Kancheva, V. Delchev

*Dept. Physical Chemistry, University of Plovdiv,
Tzar Assen 24 Str., 4000-Plovdiv, Bulgaria,
Email: vdelchev@uni-plovdiv.bg*

ABSTRACT

We investigated the excited-state reaction paths for the C=O elongation in the most stable oxo-amino tautomers of cytosine and isocytosine. They were studied at the B3LYP (TD) level of theory and aug-cc-pVDZ basis functions. As expected for this kind of reactions no conical intersections S_0 - S_1 were found for both compounds. We explained the ps-relaxation of cytosine with the population of the ${}^1n_o\pi^*$ excited state via conical intersection ${}^1n_o\pi^*/{}^1\pi\pi^*$ and subsequent fluorescence to the S_0 state at C=O = 1.443 Å. For isocytosine we found a channel for the population of the ${}^1\pi\sigma^*$ excited state, which would contribute to the photochemical dissociation of this compound. This is the first step for the formation of the hydroxo tautomer of isocytosine.

Ключови думи: *Възбудени състояния, DFT изчисления, Изоцитозин, Цитозин.*

ВЪВЕДЕНИЕ

Цитозинът е основна градивна единица на макромолекулите на нуклеиновите киселини (ДНК и РНК). Той се свързва комплементарно,

чрез водородни връзки, с гуанина и по този начин участва в процесите на кодиране и предаване на генетичната информация [1]. Експерименталните изследвания показват, че аминоксо формата на цитозина е най-стабилна [2–5]. Въпреки наличието на голям брой теоретични изследвания на реакционните механизми [6–8], в които участва цитозинът, все още липсва яснота за влиянието на карбонилната група върху фотохимичните трансформации на съединението.

Изследването на кристалната структура на изоцитозина дава сведения за съществуването на два стабилни аминоксо тавтомера: 1Н и 3Н [9]. Този факт показва, че изоцитозинът много лесно тавтомеризира. Наличието и на други тавтомерни форми (хидроксо) е доказано също от анализа на вибрационните спектри на съединението в газова фаза [10]. Изоцитозинът и механизмите на реакциите, в които той участва са значително по-слабо изучени, отколкото тези на цитозина. Липсват данни също така за влиянието на С=О групата върху фотохимичните трансформации на това съединение.

Целта на настоящото изследване е да се изучат реакционните пътища на възбудените състояния на цитозина и изоцитозина при удължаване на С=О връзката. Този реакционен механизъм е важен за населването на триплетните състояния на пиримидиновите производни. Предполагано е, че фосфоресцентните ивици в спектрите на някои пиримидини се дължат на преходи $S_1 \rightarrow T_1$, които често се извършват при удължаване на С=О връзки [11].

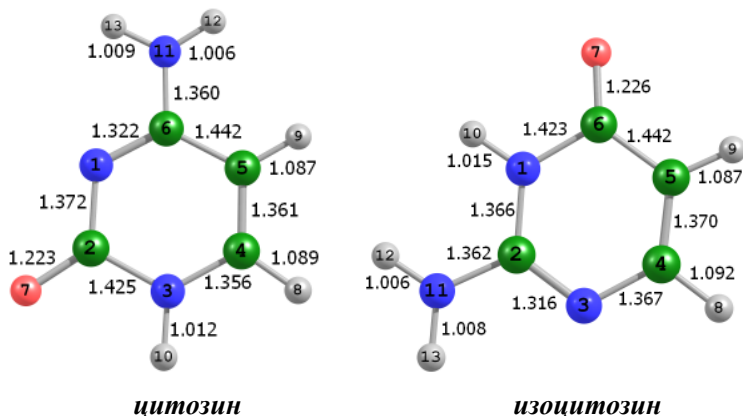
МЕТОДИ

Структурите на оксо-амино тавтомерите на цитозина и изоцитозина са оптимизирани с помощта на теорията за функционала на плътността (B3LYP) и базисни функции aug-cc-pVDZ. Използвана е програмата GAUSSIAN 03 [12]. Релаксационните (реакционните) пътища на възбудените състояния са изучени при удължаване на С=О връзката в двете съединения: от нейната равновесна стойност до около 1.45 Å.

РЕЗУЛТАТИ И ДИСКУСИЯ

Оптимизираните структури на основното състояние на цитозина и изоцитозина са представени на фиг. 1. Както се вижда, те имат равнинни геометрии, което показва, че аминоксо групата е спрегната с ароматния

пръстен. Връзките C=O в двете съединения са приблизително равни, въпреки, че в цитозина карбонилната група е свързана за два азотни атома от пръстена.



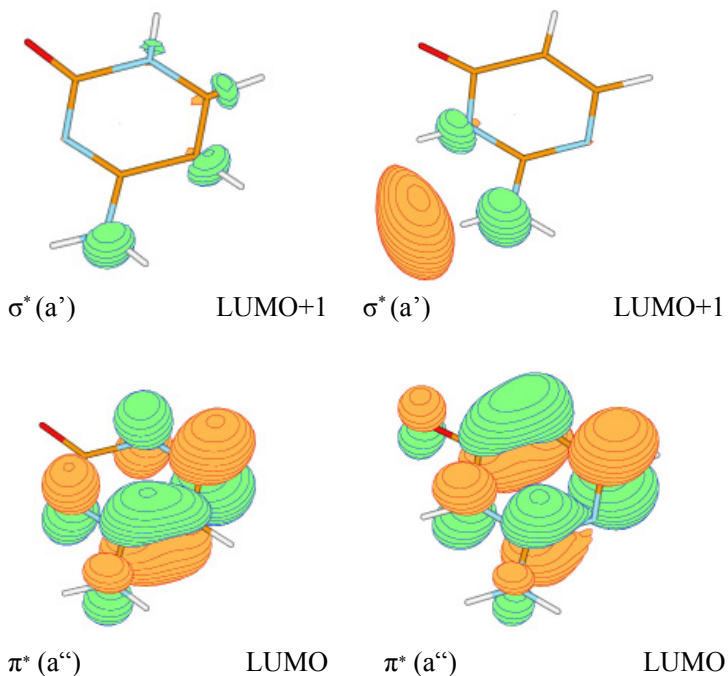
Фигура 1. Оптимизирани структури на цитозина и изоцитозина.

Вертикалните енергии на възбуждане на ниско лежащите възбудени състояния и експерименталните УВ-абсорбционни максимуми на двете съединения са представени в таблица 1. Поради равнинния строеж на молекулите на съединенията е възможно класифицирането на молекулните орбитали и възбудените състояния по симетрия, в рамките на точковата група C_s . Така например, орбиталите n_o , σ , и σ^* имат симетрия a' , а орбиталите π и π^* са със симетрия a'' (фиг. 2). Респективно, основното състояние S_0 и възбуденото състояние ${}^1\pi\pi^*$ имат симетрия A' , а възбудените състояния ${}^1n_o\pi^*$, ${}^1\sigma\pi^*$, и ${}^1\pi\sigma^*$ са със симетрия A'' . Съгласно правилата за запазване на симетрията при електронните преходи, електронните състояния със симетрия A'' се класифицират като „тъмни“ и абсорбционни ивици за тях не би трябвало да се наблюдават в УВ-спектъра (или ако се наблюдават са ниско интензивни). Симетрията на ${}^1\pi\pi^*$ възбуденото състояние го класифицира като „светло“ електронно състояние, със значителна сила на осцилатора. Следователно, абсорбционните ивици на цитозина и изоцитозина се дължат предимно на $\pi \rightarrow \pi^*$ електронни преходи в молекулите на съединенията.

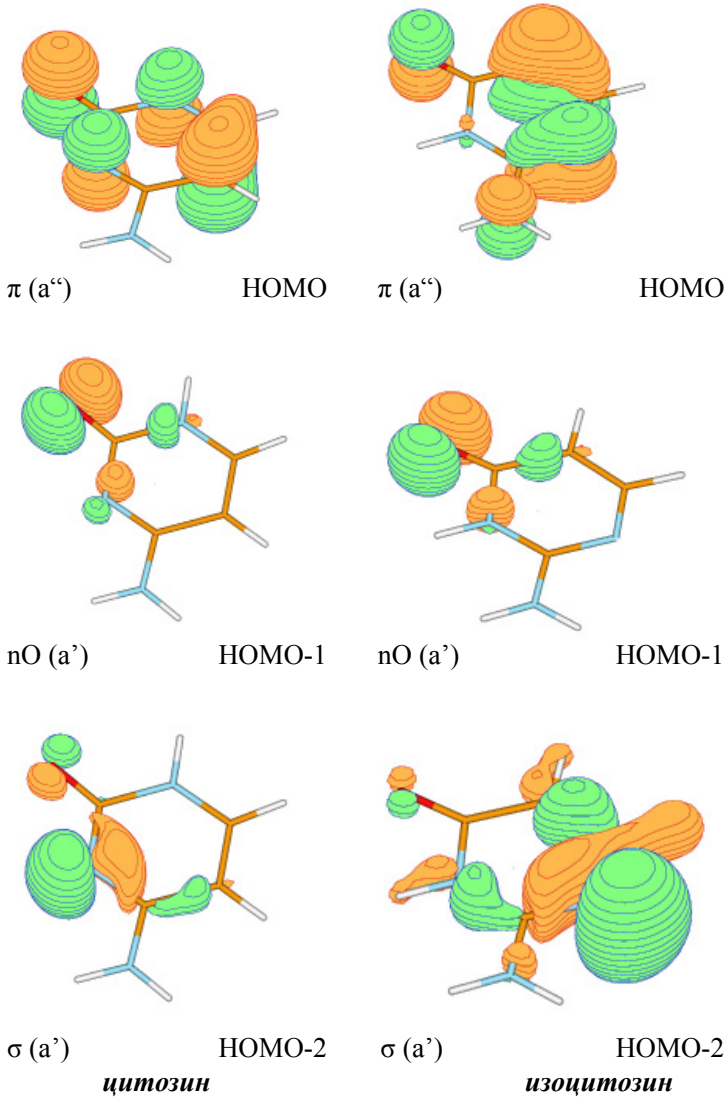
Таблица 1. Вертикални енергии на възбуждане на цитозина и изоцитозина.

възбудено състояние	ЦИТОЗИН			ИЗОЦИТОЗИН			
	eV	nm	експ. eV	възбудено състояние	eV	nm	експ. eV
${}^1\pi\pi^*$	4.58	271	4.6 ^a / 4.65 ^b	${}^1\pi\pi^*$	4.64	267	4.79 ^a
${}^1n_o\pi^*$	4.72	263		${}^1\pi\sigma^*$	4.77	260	
${}^1\sigma\pi^*$	5.09	244		${}^1n_o\pi^*$	4.85	256	
${}^1\pi\sigma^*$	5.15	241		${}^1\sigma\pi^*$	5.42	229	
${}^1\pi\pi^*$	5.26	236	5.2 ^a	${}^1\pi\sigma^*$	5.66	219	

^a Лит. [13,14], ^b воден разтвор [15,16], ^a ацетонитрил [15].



Фигура 2. (продължава)



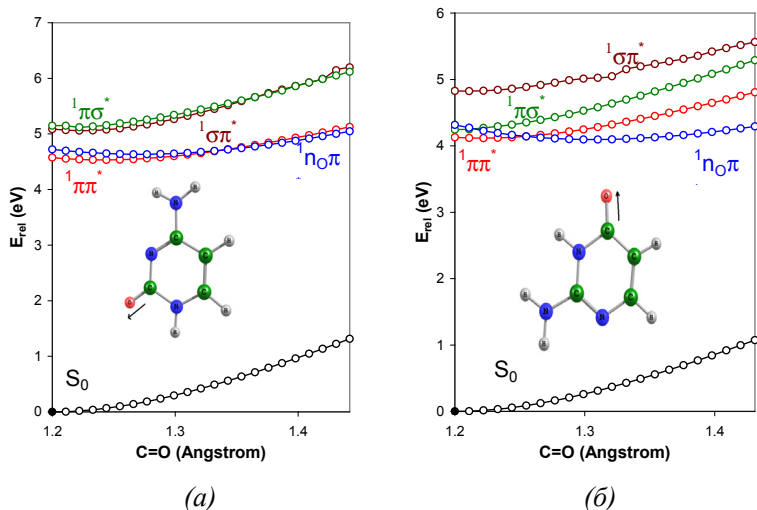
Фигура 2. Оптимизирани орбитали на цитозина и изоцитозина, които участват в електронните преходи.

Както се вижда от таблицата изчислените вертикални енергии на възбуждане на ${}^1\pi\pi^*$ възбудените състояния са доста близки до УВ-абсорбционните максимуми на двете съединения [13–16]. При молекулните орбитали π и π^* от фиг. 2 вълновата функция се анулира в молекулната равнина и показва максимуми под и над нея, но с различен знак. Второто по енергия електронно състояние в двете съединения е „тъмно“, като при цитозина то е ${}^1n_o\pi^*$, а при изоцитозина е ${}^1\pi\sigma^*$ – при около 4.7 eV. Наличието на ниско лежащо ${}^1\pi\sigma^*$ възбудено състояние в изоцитозина е предпоставка за N-H дисоциация на молекулата. Както е известно базите на нуклеиновите киселини участват в процеси на NH-дисоциация през ${}^1\pi\sigma^*$ възбудени състояния по т. нар. PIDA (*photo-induced dissociation-association*) механизъм [17–19].

Възбуденото ${}^1\pi\sigma^*$ електронно състояние на цитозина е с по-ниска енергия от второто „светло“ ${}^1\pi\pi^*$ възбудено състояние, което показва, че е възможно населване на ${}^1\pi\sigma^*$ електронното състояние през конично сечение ${}^1\pi\pi^*/{}^1\pi\sigma^*$ при подходящ реакционен път на тези две състояния.

На фиг. 3 са представени реакционните пътища на четири възбудени състояния на цитозина и изоцитозина при удължаване на C=O връзките. От фиг. 3а се вижда, че реакционните пътища на възбудените състояния на цитозина при удължаването на C=O връзката не водят до конични сечения от типа S_0 - S_1 . Обаче, при разстояние C=O = 1.366 Å се наблюдава конично сечение ${}^1n_o\pi^*/{}^1\pi\pi^*$. Това конично сечение е индикация за населване на „тъмното“ ${}^1n_o\pi^*$ възбуденото състояние на цитозина от „светлото“ ${}^1\pi\pi^*$ възбудено състояние чрез вътрешна конверсия.

Този процес може да ускори последващото населване на T_1 възбуденото състояние (интеркомбинация), което да доведе до фосфоресценция на цитозина. Подобен механизъм е предложен от Marian за 6-азаурацила [11]. По-вероятно е да се наблюдава флуоресцентен преход от населеното ${}^1n_o\pi^*$ възбуденото състояние на цитозина до основно състояние. Както е известно от експеримента цитозина показва две релаксационни времена на възбудените състояния: в ps-скала (1.86 ps) и в fs-скала (160 fs) [20]. Според нас, по-дългото релаксационно време 1.86 ps се дължи на флуоресценция ${}^1n_o\pi^* \rightarrow S_0$. При около C=O = 1.3 Å реакционният път на ${}^1n_o\pi^*$ възбуденото състояние показва плитък минимум. Обаче, флуоресцентният преход се осъществява при C=O = 1.443 Å, където енергетичната разлика ${}^1n_o\pi^* - S_0$ е 3.383 eV. Експериментът е показал, че флуоресцентният максимум на цитозина е при 325 nm (3.818 eV) [21,22]. Флуоресценция през ${}^1\pi\pi^*$ възбуденото състояние не се наблюдава, тъй като това състояние се дезактивира чрез вътрешна конверсия до S_0 [19,23–25].



Фигура 3. Реакционни пътища на възбудените състояния на (а) цитозина и (б) изоцитозина при удължаване на C=O връзката. Плътните точки на двете фигури посочват оптимизираната структура, докато контурните точки съответстват на геометрия на съединението при дадено C=O разстояние на оптимизираната структура.

Реакционните пътища на $^1\sigma\pi^*$ и $^1\pi\sigma^*$ възбудените състояния на цитозина (фиг. 3а) показват повишаване на енергията към края на реакционната координата и пресичане в конично сечение $^1\sigma\pi^*/^1\pi\sigma^*$. Тези два реакционни пътя нямат никакъв особен принос към флуоресцентните и фосфоресцентните процеси на цитозина от гледна точка на C=O реакционната координата.

На фиг. 3б са представени реакционните пътища на възбудените състояния на изоцитозина. Прави впечатление, че във Франк-Кондоновата област първите три възбудени състояния са квазиизродени, като все пак $^1\pi\pi^*$ възбуденото състояние е с най-висока енергия. Още в началото на реакционния път (C=O между 1.237 – 1.248 Å) се наблюдава конично сечение $^1\pi\pi^*/^1\pi\sigma^*$, което е предпоставка за населването на $^1\pi\sigma^*$ възбудено състояние. Както е известно [17,19], през това състояние се осъществява NH-дисоциацията на базите на нуклеиновите киселини. Следователно, при изоцитозина NH-дисоциацията на молекулата по PIDA механизма би следвало да е осъществима.

Населването на ${}^1n_o\pi^*$ възбуденото състояние на изоцитозина се осъществява от „светлото“ ${}^1\pi\pi^*$ възбудено състояние през конично сечение ${}^1n_o\pi^*/{}^1\pi\pi^*$ (фиг. 3б). Както се вижда от фигурата това конично сечение е при $C=O = 1.281 \text{ \AA}$. Реакционният път на ${}^1n_o\pi^*$ възбуденото състояние на изоцитозина показва по-дълбок минимум (0.218 eV изчислен спрямо вертикалната енергия на възбуждане), отколкото в цитозина (0.084 eV изчислен спрямо вертикалната енергия на възбуждане). Това показва, че флуоресцентният преход ${}^1n_o\pi^* \rightarrow S_0$ при изоцитозина би могъл да се очаква от минимума на реакционния път на ${}^1n_o\pi^*$ възбуденото състояние. За съжаление липсват данни за експериментален флуоресцентен спектър на изоцитозина, за да се потвърди или отхвърли това наше твърдение.

Реакционният път на ${}^1\sigma^*$ възбуденото състояние на изоцитозина няма принос към дискутираните по-горе механизми на възбудените състояния при удължаване на $C=O$ връзката. Прави впечатление обаче, че този реакционен път е независим от реакционния път на ${}^1\pi\sigma^*$ възбуденото състояние.

ЗАКЛЮЧЕНИЕ

Изследваните механизми на удължаване на $C=O$ връзките в цитозина и изоцитозина показаха, че липсват конични сечения от типа S_0-S_1 за двете съединения. При цитозина посочихме канал за населване на „тъмното“ ${}^1n_o\pi^*$ възбуденото състояние през конично сечение ${}^1n_o\pi^*/{}^1\pi\pi^*$, което вероятно е причина за наблюдаване на релаксационен процес в ps-ната времева скала. Тази флуоресценция през ${}^1n_o\pi^*$ възбуденото състояние се извършва при $C=O = 1.443 \text{ \AA}$. За изоцитозина установихме възможност за населване на ${}^1\pi\sigma^*$ възбуденото състояние във Франк-Кондоновата област, което е предпоставка за фотохимична дисоциация на молекулата. С други думи, очакваме цитозина да бъде фотохимично стабилен, докато изоцитозинът би могъл да тавтомеризира до хидроксо или имино тавтомери.

БЛАГОДАРНОСТИ

Единият от авторите (ВБД) благодари на поделение НПД при ПУ „Паисий Хилендарски“ за финансовата подкрепа (проект НИ11-ХФ-007) при разпечатване на постера, с който тези изследвания бяха представени на **9-тата научна конференция по химия с международно участие 2011**, ПУ.

ЛИТЕРАТУРА

1. Lehninger, A., in *Principles of Biochemistry* – 4 ed., 2004, Freeman. pp. 608.
2. Jeffrey, G. A.; Kinoshita, Y., *Acta Cryst.*, 1963, 16, 20–28.
3. Kobayashi, R., *J. Phys. Chem. A*, 1998, 102, 10813–.
4. Les, A.; Adamowicz, L.; Bartleu, R. J., *J. Phys. Chem.*, 1989, 93, 4001–4005.
5. Gorb, L.; Podolyan, Y.; Leszczynski, J., *J. Mol. Struct. (THEOCHEM)*, 1999, 487, 47–55.
6. Civcir, P.Ü., *J. Mol. Str. (THEOCHEM)*, 2000, 532, 157–169.
7. Tian, S. X.; Zhang, C. F.; Zhang, Z. J.; Chen, X. J.; Xu, K. Z., *Chem. Phys.*, 1999, 242, 217–225.
8. Gould, I. R.; Burton, N. A.; Hall, R. J.; Hiller, I. H., *J. Mol. Struct.*, 1995, 331, 147–154.
9. McConnell, J. F.; Sharma, B. D.; Marsh, R. E., *Nature*, 1964, 203, 399–400.
10. Vranken, H.; Smets, J.; Maest, G., *Spectrochim. Acta A*, 1994, 50, 875–889.
11. Etinski, M.; Marian, C. M., *Phys. Chem. Chem. Phys.*, 2010, 12, 15665–15671.
12. Frisch, M., et al., *Gaussian03*, Revision D.01, Gaussian, Inc., Wallingford, CT, 2004.
13. Fülcher, M. P.; Roos, B. O., *J. Am. Chem. Soc.*, 1995, 117, 2089–2095.
14. Ismail, N.; Blancafort, L.; Olivucci, M.; Kohler, B.; Robb, M. A., *J. Am. Chem. Soc.*, 2002, 124, 6818–6819.
15. Morita, H.; Nagakura, S., *Theoret. Chim. Acta (Berl.)*, 1968, 11, 279–295.
16. Brown, D. J.; Lyall, J. M., *Australian J Chem.*, 1962, 15, 851–857.
17. Chmura, B.; Rode, M.; Sobolewski, A.; Lapinski, L.; Nowak, M., *J. Phys. Chem. A*, 2008, 112, 13655–13661.
18. Sobolewski, A.L., *Chem. Phys. Lett.*, 1993, 211, 293–299.
19. Delchev, V. B.; Sobolewski, A. L.; Domcke, W., *Phys. Chem. Chem. Phys.*, 2010, 12, 5007–5015.
20. Canuel, C.; Mons, M.; PiuZZi, F.; Tardivel, B.; Dimicoli, L.; Elhanine, M., *J. Chem. Phys.*, 2005, 122, 074316(6).

21. Sharonov, A.; Gustavsson, T.; Carre, V.; Renault, E.; Markovitsi, D., *Chem. Phys. Lett.*, 2003, 380, 173–180.
22. Callis, P. R., *Chem. Phys. Lett.*, 1979, 61, 563–567.
23. Matsika, S., *J. Phys. Chem. A*, 2004, 108, 7584–7590.
24. Matsika, S., *J. Phys. Chem. A*, 2005, 109, 7538–7545.
25. Perun, S.; Sobolewski, A. L.; Domcke, W., *J. Phys. Chem. A*, 2006, 110, 13238–13244.

THE NUCLEOPHILIC SUBSTITUTION REACTION OF SULFINIC ACIDS WITH HALONITROALKANES

S. Ivanova, D. Koleva

*Department of Organic Chemistry,
Asen Zlatarov University of Bourgas,
1, Prof. Yakimov str., BG-8010 Bourgas, Bulgaria,
e-mail: viperorg@abv.bg*

ABSTRACT

Arylsulfonylnitromethanes were obtained by nucleophilic substitution reaction. The suggested method of obtaining arylsulfonylnitromethanes has some important advantages over the methods know so far: it is a relatively short, one stage process; no by-products are obtained, so there is no need of further procedures to separate the main products from the reaction mixture, the final compounds possess a good degree of purity. The structure of the new products were confirmed by ^1H NMR, IR and elemental analysis.

Key words: *arylsulfonylnitromethanes, synthesis, structure.*

INTRODUCTION

α – Nitrosulfones were obtained by the oxidation of α – nitrosulphides¹, an interaction between sulfonylcarbanion and organic nitrate, or a reaction of metal sulfides and sulfinic acids with α – chloro-, α – bromo-, α

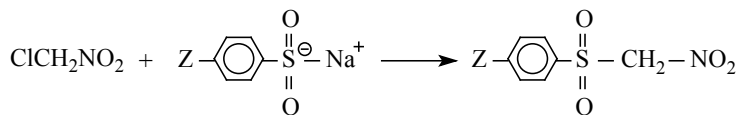
– iodonitroalkanes². In one particular case alone, a direct nitration of arylsulfone was made resulting in α – nitrosulfone. Zeilstra *et al* suggested a method of obtaining α – nitrosulfones based on the reaction between potassium nitronate and p-toluene sulfonylbromide³. Publications describing a method of obtaining α – nitrosulfones by nitration in the presence of bases are also available. Studies on the chemical behaviour of α – nitrosulfones show that they readily take part in reactions of nucleophilic addition². As a result, α – nitroesters, nitroacetonitriles, bis(phenylsulfonyl)methane and bis(alkylsulfonyl)methanes are obtained. They react readily with aldehydes, and alcohols, alkenes or bisadducts are obtained. Arylnitromethylethylsulfones can also be used to obtain bis(arylsulfonyl)furans⁵. Wade *et al* found out that phenylsulfonylnitromethane takes part in C-alkylation reaction resulting in a series of α – nitrosulfones. Studies on the conformation of aromatic α – nitrosulfones were also made⁴.

The present work proposes a original method of obtaining arylsulfonylnitromethanes.

Structure of the new compounds were elucidated on the basis of elemental analysis and spectral data.

RESULTS AND DISCUSSION

Arylsulfonylnitromethanes were obtained by a nucleophilic substitution reaction.



Z = H (1); Z = 4-Me (2); Z = 4-MeO (3);
Z = 4-Cl (4); Z = 4-Br (5); Z = 4-I (6).

Scheme 1.

The suggested method of obtaining arylsulfonylnitromethanes has some important advantages over the methods known so far: it is a relatively short, one stage process; no by-products are obtained, so there is no need of further procedures to separate the main products from the reaction mixture, the final compounds possess a good degree of purity.

Arylsulfonylnitromethanes 1–6 were synthesized by mixing equimolar quantities of the corresponding reagents in ethanol at 18–20 °C from 12 to 72 hours. These compounds are colourless, crystalline substances, very soluble in chloroform, acetone and dioxane. They are stable for long storage periods and melt without decomposing. The compounds obtained were identified by TLC.

All the products 1–6 were purified by recrystallization or flash column chromatography on silica gel with a benzene as the eluent. The structure of compounds 1–6 confirmed by ¹H – and ¹³C-NMR, IR spectra, and elemental analysis (Table 1, 2).

Table 1. Characterization Data of the New Synthesized Compounds

Comp. №	Mp., °C (solvent)	Color Yield %	Mol. formula mol.wt	Calcd. / found %			
				C	H	N	S
1	76–77 (EtOH)	White 81	C ₇ H ₇ NO ₄ S (201.14)	43.60	3.71	7.06	15.60
				43.54	3.68	6.98	15.53
2	73–74 (EtOH)	White 78	C ₈ H ₉ NO ₄ S (215.16)	44.20	3.95	6.72	14.58
				44.15	3.89	6.66	14.49
3	79–80 (EtOH)	White 75	C ₈ H ₉ NO ₅ S (231.13)	41.57	3.65	5.80	13.95
				41.53	3.59	5.73	13.90
4	138–139 (EtOH/ Dioxane)	White 82	C ₇ H ₆ ClNO ₄ S (235.58)	35.55	2.40	5.76	13.45
				35.49	2.35	5.70	13.39
5	159 (EtOH/ Dioxane)	White 74	C ₇ H ₆ BrNO ₄ S (280.12)	29.75	2.45	5.38	11.65
				29.73	2.40	5.32	11.61
6	186–187 (EtOH/ Dioxane)	White 86	C ₇ H ₆ INO ₄ S (327.03)	25.50	1.56	4.38	9.70
				25.43	1.50	4.33	9.67

Table 2. Spectral Data of Some New Synthesized Compounds

Comp. №	Spectral Data
1	¹ H NMR (δ, ppm): 5.52 (d, J = 5.8 Hz, 2H), 7.24 – 7.80 (m, 5H); ¹³ C (δ, ppm): 32 (methylene), 131 (Ar-C); IR(ν, cm ⁻¹): 1550, 1340 (NO ₂), 1310, 1150 (SO ₂), 2930, 2850, 1450 (CH ₂).
	¹ H NMR (δ, ppm): 2.42 (s, CH ₃), 5.50 (d, J = 5.6 Hz, 2H), 7.20 – 7.85 (m, 4H); ¹³ C (δ, ppm): 33.2 (methylene), 130 (Ar-C); IR(ν, cm ⁻¹): 1545, 1345 (NO ₂), 1305, 1140 (SO ₂), 2920, 2845, 1450 (CH ₂).

3	^1H NMR (δ , ppm): 2.40 (s, CH_3), 5.51 (d, $J = 5.6$ Hz, 2H), 7.25 – 7.75 (m, 4H); ^{13}C (δ , ppm): 32.4 (methylene), 131 (Ar-C); IR (ν , cm^{-1}): 1550, 1340 (NO_2), 1310, 1145 (SO_2) 2920, 2845, 1470 (CH_2).
4	^1H NMR (δ , ppm): 5.53 (d, $J = 5.8$ Hz, 2H), 7.20 – 7.85 (m, 4H); ^{13}C (δ , ppm): 32.6 (methylene), 130 (Ar-C); IR (ν , cm^{-1}): 1560, 1345 (NO_2), 1305, 1150 (SO_2), 2925, 2855, 1455 (CH_2).
5	^1H NMR (δ , ppm) 5.51 (d, $J = 5.8$ Hz, 2H), 7.23 – 7.84 (m, 4H); ^{13}C (δ , ppm): 31.8 (methylene), 130 (Ar-C); IR (ν , cm^{-1}) 1555, 1340 (NO_2), 1300, 1140 (SO_2), 2930, 2860, 1460 (CH_2).
6	^1H NMR (δ , ppm): 5.52 (d, $J = 5.8$ Hz, 2H), 7.20 – 7.78 (m, 4H); ^{13}C (δ , ppm): 32.2 (methylene), 131 (Ar-C); IR (ν , cm^{-1}): 1550, 1335 (NO_2), 1305, 1145 (SO_2), 2920, 2850, 1460 (CH_2).

The ^1H (^{13}C) –NMR spectra of arylsulfonylnitromethanes contain an aromatic multiplet at 7.24 – 7.85 (130–131) ppm. The shifts of methylene protons can be seen at 5.50 – 5.53 (31.4–33.2) ppm. The chemical shift of the methyl group in the benzene nucleus is at 2.40 ppm. The presence of a methyl group does not effect substantially the position of the aromatic multiplet.

The IR spectra of the compounds obtained contain intensive absorption bands of nitro – and sulfonyl groups. Asymmetric and symmetric valence vibrations of nitro groups can be seen at 1560–1545 and 1345–1335 cm^{-1} , while the asymmetric and symmetric vibrations of sulfonyl group are at 1310–1300 and 1150–1140 cm^{-1} . These bands are highly intensive since the sulfonyl group are not situated on the same plane as the other substitutes. The absorption bands at 3100–3000 cm^{-1} are assigned to valence C-H aryl vibration. A triplet characterized by a decreasing intensity of the high-frequency bands can be seen in this interval because the molecules of the compounds under study contain monosubstituted benzene nuclei. The skeleton vibrations of the arene nucleus at 1640–1600 and 1480–1450 cm^{-1} . There is an absorption band of a monosubstituted benzene nucleus at 700 cm^{-1} , and an absorption band of a p-disubstituted nucleus at 810–800 cm^{-1} . A characteristic band of valence C-N vibration can be seen at 850–840 cm^{-1} . The methylene group is identified by the absorption maximums of valence asymmetric and symmetric vibrations at 2930–2845 cm^{-1} and deformation

vibrations at 1470–1450 cm^{-1} . The absorption band of asymmetric and symmetric valence vibrations at 2950–2850 cm^{-1} is due to the methyl group in p-position in the arene nucleus. The presence of a methoxy group in the benzene nucleus is proved by the absorption bands of valence vibrations of the methyl group at 2840 cm^{-1} and the valence asymmetric and symmetric vibrations of C-O-C bond at 1270 and 1030 cm^{-1} . The presence of a halogen atom in the phenylsulfonyl group result in characteristic band at 800–580 cm^{-1} . An absorption band of medium intensity corresponding to valence S-aryl vibrations is characteristic of all arylsulfonylnitromethanes at 1090–1080 cm^{-1} .

CONCLUSIONS

There new compounds (3, 5, 6) were synthesized by means of $\text{S}_{\text{N}}2$ reaction. The obtained series of arylsulfonylnitromethanes are very important from preparative point of view since these compounds are active methylene components. Part of these compounds was tested antifungal activity and found that they are potential growth inhibitors causal fungal.

EXPERIMENTAL

Melting points were determined on a Kofler hot stage and are uncorrected. The elemental analysis were carried out in the Microanalytical Center at University Prof. A. Žlatařov. The infrared spectra were recorded on a Specord spectrometer using KBr discs in the range 4000 to 400 cm^{-1} . $^1\text{H-NMR}$ (chemical shifts measured in deuterated solvent are given in ppm from TMS) spectra were recorded with a Bruker 250 MHz spectrometer, using CDCl_3 solution.

PREPARATION OF 1 – 6

An equimolar quantity of chloronitromethane dissolved in ethanol (25 ml) was added to the sodium salt of sulfinic acid (0,01 mol). The reaction mixture was rapidly stirred and then allowed to stay from 12 to 72 hours at a room temperature. The crystals obtained were separated from the reaction mixture and were recrystallized from ethanol and ethanol/dioxane.

ACKNOWLEDGMENT

The authors want to acknowledge the support of the project by the National Science Fund of Ministry of Education and Science – Bulgaria.

REFERENCES

1. N. Kharasch, J. L. Camerson, *J. Am. Chem. Soc.* 73 (1951) 3864–3869.
2. J. J. Zeilstra, J. B. F. N. Engberts, *Recueil*. 93 (1974) 11–14.
3. J. J. Zeilstra, J. B. F. N. Engberts, *J. Org. Chem.* 39 (1974) 3215–3219.
4. J. L. Kelley, E. W. McLean, K. F. Williard, *J. Heterocyclic Chem.* 14 (1977) 1415–1420.
5. P. A. Wade, S. D. Morrow, S. A. Hardinger, M. S. Saft, H. R. Hinney, *Chem. Comm.* (1980) 288–291.

SELECTIVE ACETOXYLATION OF CYCLODODECENE BY DIOXIGEN CATALYZED BY PALLADIUM(II) ACETATE, HYDROQUINONE AND IRON(II) PHTHALOCYANINE

A. Kolev¹, E. Balbolov²

*¹Atmospheric Vacuum Distillation-1, LUKOIL Neftochim Burgas
E-mail address: asekolev@yahoo.com*

*²Department of Organic Chemical Technology,
University „Prof. Assen Zlatarov“, 1 Prof. Yakimov str.,
8010 Burgas, Bulgaria
E-mail address: balbolov@btu.bg*

ABSTRACT

Selective palladium-catalyzed aerobic oxidation of cyclododecene with the aid of a metal macrocycle-quinone system was conducted. This involves a multistep electron transfer with three catalysts (Palladium(II) acetate, hydroquinone and iron(II) phthalocyanine). The triple catalytic system was applied to acetoxylation of cyclododecene to cyclododec-2-en-1-yl acetates in high selectivity (93.4%) and a conversion of cyclododecene up to 93–98%.

Key words: *acetoxylation, cyclododec-2-en-1-yl acetate*

ВЪВЕДЕНИЕ

Алиловите ацетати са основни междинни съединения в органичния синтез, особено след като беше установено, че метални соли и комплекси катализират лесно и с висока избираемост заместването на ацетоксигрупата с разнообразни нуклеофили. По този начин на основа циклододец-2-ен-1-ил ацетат могат да се получат циклододец-2-ен-1-ол, циклододец-2-ен-1-он, 1-алкоксицикло-додец-2-ен. Всички те, както и самите ацетати се използват в парфюмерийната промишленост [1 – 6].

В работите на някои автори беше показано [7], че циклододецен могат да се ацетоксилират селективно до алилови моноацетати. Реакцията е проведена в разтвор на ледена оцетна киселина в присъствие на 5% Pd(OAc)₂ като катализатор, в комбинация с окислителна система II, състояща се от 20% бензохинон и 110–200% манганов диоксид по отношение на субстрата. Добивът на циклододец-(E)-2-ен-1-ил ацетата при степен на превръщане 77% (43h реакционно време и температура 60°C) е 72%.

От друга страна представляваше интерес да се проучи възможността за получаване на циклододец-2-ен-1-ил ацетат с висок добив при значително намаляване на времето на реакцията. За тази цел проведохме окислително ацетоксилиране на циклододецен с използване на каталитична система I Pd(OAc)₂-хидрохинон-FePc-молекулен кислород при вариране на температурата на реакцията от 313 до 353K и налягане на кислорода от 0.1 до 1.0 MPa [9].

Целта на настоящата работа е да се определи, коя от използваните каталитични системи в предни наши работи [9, 13] има най-голям потенциал за получаване циклододец-2-ен-1-ил ацетата.

МАТЕРИАЛИ И МЕТОДИ

Методика за окисление на циклододецен с каталитична система Pd(OAc)₂ – 1,4-бензохинон – Fe(Pc) – O₂ в ледена оцетна киселина.

Реакцията се провежда в температурния интервал 313–353 K и налягане на въздуха 0.1 ÷ 1.0 MPa. Към реактора е осигурено хранване с инертен газ и вакуум линия. Въздухът за окисление под високо налягане постъпва директно от метална бутилка. Свързаният към реак-

тора термостат служи за поддържане на реакционна температура. В реактора се зарежда смес от 0.1167–0.3368 g (0.52–1.5 mmol) $\text{Pd}(\text{OAc})_2$, 0.2333–0.6603 g (2.12–6.0 mmol) хидрохинон, 0.2944÷0.8492 g (0.52÷1.5 mmol) $\text{Fe}(\text{Pc})$ и 0.5304÷1.5304 g (5.2÷15.0 mmol) $\text{Li}(\text{OAc})_2 \cdot 2\text{H}_2\text{O}$ в 70 ml ледена оцетна киселина. С пипета се добавя 2.87–5.74 ml (15–30 mmol) от субстрата. Следва внимателно пристягане на капака на реактора и пускане на термостата. След достигане на желаната температура се подава въздух от бутилката, докато налягането в реактора достигне желаната стойност. Началото на реакцията се отчита след пускане на бъркалката. На съответните интервали от време се вземат проби за анализ.

*Методика за окисление на циклододецен
или 1,5,9-циклододекатриен с каталитична система
 $\text{Pd}(\text{OAc})_2$ – 1,4-бензохинон – MnO_2 в ледена оцетна киселина.*

В 500 ml термостатиран стъклен двугълен реактор снабден с обратен хладник и магнитна бъркалка се поставят 1.122 g (5 mmol) $\text{Pd}(\text{OAc})_2$, 2.162 g (20 mmol) p-бензохинон, 17.4 g (200 mmol) MnO_2 в 250 ml ледена оцетна киселина. Сместа се нагрява при температура на реакцията 40°C при разбъркване в продължение на 30 минути. 100 mmol циклододецен или 1,5,9-циклододекатриен се прибавят и се разбърква при посочената температура в продължение на 72 часа. След охлаждане до стайна температура се прибавят 250 ml пентан-етер (1:1) и се разбърква още 30 минути. Сместа се филтрува през шотов филтър, след това органичната фаза се екстрахира три пъти с 250 ml пентан-етер (1:1). След дестилация на разтворителя се получава продукт, който се почиства чрез колонна хроматография.

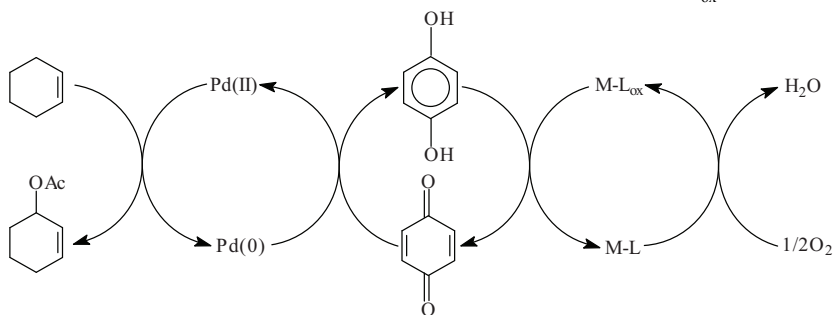
*Методика за окисление на циклододецен
или 1,5,9-циклододекатриен с каталитична система
 $\text{Pd}(\text{OAc})_2$ – $\text{Cu}(\text{OAc})_2$ – въздух в ледена оцетна киселина.*

еакцията се провежда в температурния интервал 358–383 K и налягане на въздуха 2.5 MPa. Към реактора е осигурено хранване с инертен газ и вакуум линия. Въздухът за окисление под високо налягане постъпва директно от метална бутилка. Свързаният към реактора термостат служи за поддържане на реакционна температура. В реактора се зарежда смес от 0.2245–0.3368 g (1.0–1.5 mmol) $\text{Pd}(\text{OAc})_2$, 0.4991–1.4974 g (2.5–7.5 mmol) $\text{Cu}(\text{OAc})_2 \cdot \text{H}_2\text{O}$ и 70 ml ледена оцетна киселина. С пипета се добавя 2.87–5.74 ml (15–30 mmol) от субстрата.

Следва внимателно пристягане на капака на реактора и пускане на термостата. След достигане на желаната температура се подава въздух от бутилката, докато налягането в реактора достигне 2.5 МРа. Началото на реакцията се отчита след пускане на бъркалката. На съответните интервали от време се вземат проби за анализ.

РЕЗУЛТАТИ И ОБСЪЖДАНЕ

Практически интерес за нас представлява намирането и използването на каталитична система за получаване на циклододец-2-ен-1-ил ацетат, чрез окислително ацетоксилиране на циклододецен. Възможността за бързо реокисление на образуващия се хидрохинон до бензохинон с кислород при меки условия, води до повишаване на концентрацията на каталитично активния комплекс. Прякото окисление на хидрохинона с молекулен кислород при стайна температура е много бавна реакция и това се отразява на другите стадии на каталитичния процес. В научната литература се появиха съобщения [8], че макроциклични комплекси на преходните метали (ML) могат да активират кислорода и окислението протича като многостепенно пренасяне на електрони в присъствие на тройна окислително-редукционна система-Pd(II)/Pd(0)-бензохинон/ хидро хинон-ML_{ox}/ML:



Това е една изключително умерена система, която успешно се използва за алилово окисление на циклични алкени, поради възможността за бързо реокисление на образуващия се хидрохинон до бензохинон с кислород при меки условия. В литературата се срещат и съобщения за използване на въздух вместо молекулен кислород [10, 11]. Най-добър резултат е получен с железен фталоцианин Fe(Pc). Въпреки ниската си разтворимост в повечето органични разтворители, той е много ефективен при активиране на кислорода без следа от разграждане. Реакциите

протичат по-бързо и по ефективно, като се получават високи добиви при умерени условия.

Посочените по-горе реокислителни окисляват паладия достатъчно бързо при меки условия, но трябва да се вземат в стехиометрични количества (I каталитична система). Използването на каталитична система II, а така също $\text{Cu}(\text{OAc})_2$ и въздух (в каталитична система III) превръща процесите на стехиометрично окисление в каталитични, което би позволило преминаване от лабораторни или полупромишлени към многотонажни инсталации. В предишни изследвания в последните години [12, 13], се съобщава за провеждане на ацетоксилиране на диклододец-ен-1 и 1,5,9-циклододекатриен в присъствието на $\text{Pd}(\text{OAc})_2$ - $\text{Cu}(\text{OAc})_2$ при $353\div 373$ K и 2.5 MPa атмосферен въздух.

Най-добрите резултати от проведените реакции с трите каталитични системи са посочени в таблица 1.

Таблица 1. Реакционни условия, конверсия и селективност при реакция окислително ацетоксилиране на циклододец-ен-2 до циклододец-2-ен-1-ил-ацетат в разтвор на ледена оцетна киселина, в присъствие на каталитични системи: $\text{Pd}(\text{OAc})_2$ -бензохинон- $\text{Fe}(\text{Pc}) - \text{O}_2$; $\text{Pd}(\text{OAc})_2$ -бензохинон - MnO_2 ; $\text{Pd}(\text{OAc})_2$ - $\text{Cu}(\text{OAc})_2 - \text{въздух}$

№	Каталитична система	Налигане на кислорода, MPa	Температура, K	Време на реакцията, h	Добив на циклододец-2-ен-1-ил-ацетат, %	Конверсия на циклододец-ен-2, %	Селективност, %
I.	$\text{Pd}(\text{OAc})_2$ -бензохинон- $\text{Fe}(\text{Pc}) - \text{O}_2$	1.0	333	12	87.6	93.8	93.4
		0.1	333	12	37.0	39	95
II.	$\text{Pd}(\text{OAc})_2$ -бензохинон - MnO_2	-	333	43	72	77	93.5
III.	$\text{Pd}(\text{OAc})_2$ - $\text{Cu}(\text{OAc})_2 - \text{въздух}$	2.5	373	12	44	63	71

От таблица 1 се вижда се, че реакцията на ацетоксилиране при използване на каталитична система I се получава най-голям добив по циклододец-2-ен-1-ил-ацетат при селективност над 93.4%. Максимал-

на активност на каталитичната система се наблюдава при 333 К в продължение на 13 часа. Колкото е по-висока температурата на реакцията, толкова по-малко е времето на реакцията, при което започва нелинейно увеличаване на степента на превръщане. При температура 353 К каталитичните частици от система I бързо и почти необратимо се дезактивират. Значение за достигане на достатъчно висока и икономически ефективна степен на превръщане на субстрата има и налягането на кислорода (таблица 1). Наличието на два изомера на циклододецена в изходната реакционна смес и различната реакционна способност на транс – и цис-двойни връзки са причина за получаване на три алилови моноацетати.

При проведения предварителен експеримент с каталитична система II, условията на реакцията са много близки до тези посочени в [7], при което беше определено процентното влияние на превръщане на циклододецена върху състава на продуктите. При степен на превръщане на циклододецена (съдържащ: транс – 62.9%, цис – 25.9% изомери) от 68.2 до 97.0% селективността по алиловия ацетат се понижава от 88.0 до 83.4%. Изменението е незначително, което позволява провеждане на процеса при степен на превръщане на субстрата над 80%. Потвърждава се по-високата реакционна способност на транс-изомера.

Селективността при каталитична система III на процеса окисление зависи съществено от протичането на последователни и паралелни превръщания на субстрата до целевия и странични продукти. При всички опити с тази каталитична система селективността по алиловите моноацетати е по-висока от тази на монокетоните и се променя в интервала 56÷71%

ИЗВОДИ

От разгледаните три каталитични системи най-голям потенциал за получаване на ацетати на циклододецена в промишлена среда има каталитичната система I Pd(OAc)₂-хидрохинон-FePc-молекулен кислород. Интегрирането на тази система за работа с въздух, също би спомогнало за реализацията на системата в промишлеността.

ЛИТЕРАТУРА

1. Ger. Patent, 2, 719, 976 (1978); C. A. Vol.90, 86872d.
2. Jap. Patent 45,548(1985).
3. G. Ohloff, J. Liebigs Ann. Chem., (1957), 606, 100.
4. US Patent, 3,929,677 (1975); C. A. Vol.84, 165076b.
5. GB Patent, 2,002,358 A (1978).
6. Ger. Patent, 2, 852, 344 A1 (1980).
7. S. Hansson, A. Heumann, T. Rein and B. Akermark, J. Org. Chem., (1990), 55, 975.
8. J. E. Backvall, B. R. Hopkins, H. Grennberg, M. M. Mader, K. A. Awasth, J. Amer. Chem. Soc., (1990), 112, 5160; F. Notheisz, A. Zsigmond, Zs. Szegletes, J. E. Backvall, Stud. Sur. Sci. Catal., (1995), 94, 728.
9. A. K. Kolev, M. Skumov, E. Balbolov, React. Kinet. Catal. Lett., (2003), 78 (2), 325–330.
10. A. N. Capbell; P. B. White; I. A. Guzei, S. S. Stahl. J. Am. Chem. Soc. (2010), 132, 15116–15119
11. C. J. Engelin, P. Fristrup, Molecules (2011), 16, 951–969
12. E. Balbolov, S. D. Dimitrov., J. Mol. Catal., (1997), 126, 37.
13. E. Balbolov, M. Mitkova., Oxid. Commun., (1999), 126, 37.

SYNTHESIS AND ANTIMICROBIAL EVALUATIONS OF SOME NOVEL DERIVATIVES OF BENZIMIDAZOLE

*M. Staykova¹, S. Statkova-Abeghe¹, S. Kostadinova²,
M. Marhova², V. Stoyanova²*

¹ *Department of Organic Chemistry, University of Plovdiv,
24 „Tzar Assen“ Str., 4000, Plovdiv, Bulgaria*

² *Department of Biochemistry and Microbiology,
University of Plovdiv, 24 „Tzar Assen“ Str., 4000, Plovdiv, Bulgaria*

ABSTRACT

N-Acyliminium reagents derived from benzimidazole have been successfully used in reactions with active methylene nucleophiles. A series of cyclic enaminketones or dimedone were selectively amidoalkylated at the α -carbon atom of the enaminketone. The new 2-substituted derivatives of 2,3-dihydrobenzimidazole are interesting both from synthetic point of view and as potential bioactive compounds.

All the synthesized benzimidazole derivatives were assayed for antimicrobial activity using standardized tests (DM and DDM) against seven strains microorganisms. Eight compounds displayed antimicrobial activity against *Staphylococcus aureus*, *Enterobacter aerogenes*, *Candida albicans*.

Key words: *N-acyliminium ions; enaminketones; antimicrobial activity*

INTRODUCTION

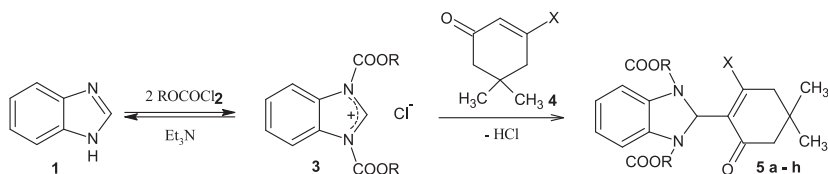
The α -amidoalkylation of carbon nucleophiles with *N*-acyliminium compounds is a long-established method for C–C bond formation [1–2]. This reaction can be used for the synthesis of various heterocyclic derivatives.

Benzimidazole ring is an important heterocyclic pharmacophore in drug discovery. Benzimidazoles are regarded as a promising class of bioactive heterocyclic compounds that exhibit a range of biological activities – antiviral [3–4], antitumor [5–6], anticancer [7], antimicrobial activity against *Staphylococcus aureus*, *Bacillus subtilis*, *Escherichia coli* and *Candida albicans* [8], antibacterial activity against *Staphylococcus aureus*, *Escherichia coli*, *Enterococcus faecalis* and fungicidal activity against *Candida albicans* and *Aspergillus* [9–11]. Benzimidazoles are potential enterovirus inhibitors [12].

The last several years we used successfully adducts of cyclic imines and acyl chlorides as electrophilic reagents in an intermolecular α -amidoalkylation reaction toward aromatics and methylene active carbonyl compounds [13–16].

RESULTS AND DISCUSSION

A series of cyclic enamino ketones or dimedone **4** were selectively amidoalkylated with *N*-acyliminium compounds **3** derived from benzimidazole **1**. Enaminones, as defined by Greenhill, are monoenamines of 1,3-dicarbonyl compounds [17] and they combine the ambident electrophilicity of enones with the ambident nucleophilicity of enamines.



R = Me, Et

X = OH, NHR₁

R₁ = Me, Et, Pr, Ph, Bz, C₆H₅CH₂CH₂, 4-ClC₆H₄CH₂, 3,4-(MeO)₂C₆H₃CH₂CH₂

Scheme 1.

To determine the influence of the acyl component, we initially studied the reactions of two different N-acyliminium compounds **3** with enaminones **4**. The reactions were carried out for 1 h at r.t. in 1,2-dichloroethane. The substituents R₁ were varied in a series of enaminones. The yields were from 11% (R = C₂H₅, X = CH₃NH) to 87% (R = CH₃, X = C₆H₅NH) and all of the studied examples proceeded regioselectively at the α-carbon of the enaminone as indicated by the disappearance of the characteristic vinyl signal in the ¹H-NMR spectra.

All the synthesized benzimidazole derivatives were evaluated for antimicrobial activity. Antimicrobial effects were assessed in standard disk diffusion method according to recommendations of CLSI [18] and agar well diffusion method [19]. For second test a wells were prepared in the agar plates with the help of sterile borer (ø 6 mm). The effect of compound to be tested was determined by measuring the diameter of zone of inhibition. All experiments were done three times and mean value was presented. All newly synthesized compounds to be tested were dissolved in DMSO to 0.4% and DMSO was used as negative control. In resent investigation effects were estimated for two Gram positive strains (*Enterococcus faecalis*; *Staphylococcus aureus*), four Gram negative strains (*Escherichia coli*; *Enterobacter aerogenes*; *Salmonella abony*; *Pseudomonas aeruginosa*) and one yeast strain (*Candida albicans*).

The following strains were used in this study: *Escherichia coli* ATCC 25922; *Enterobacter aerogenes* ATCC 25029; *Salmonella abony* ATCC 6017; *Pseudomonas aeruginosa* ATCC 27853; *Enterococcus faecalis* ATCC 29212; *Staphylococcus aureus* ATCC 33592 (MRSA); *Candida albicans* ATCC 10231.

The following agar media were used for the antimicrobial test: Mueller-Hinton agar (*S. aureus*, *P. aeruginosa*, *E. coli*, *E. aerogenes*, *S. abony*, *E. faecalis*) and Saboraud-dextrose (*C. albicans*). All the culture media were prepared and treated according to the manufacturer guidelines.

There was no inhibition observed for used strains except for *E. aerogenes*, *S. aureus* and *C. albicans*. Tested compounds have more bacteriostatic than bactericidal effect on *E. aerogenes*. Clear bactericidal effect on *S. aureus* has **5c**. Data of antimicrobial effects of tested compounds are presented in table 1.

Table 1. Antimicrobial effects of synthesized benzimidazole derivatives

Compound \ Strain			Zone of inhibition, ø mm					
			<i>E. aerogenes</i>		<i>S. aureus</i>		<i>C. albicans</i>	
5	R	X	DDM	DM	DDM	DM	DDM	DM
a	C ₂ H ₅	NHCH ₂ CH ₂ C ₆ H ₅	NI	12	NI	NI	NI	NI
b	C ₂ H ₅	NHCH ₂ C ₆ H ₅	NI	I	NI	NI	NI	10
c	C ₂ H ₅	NHC ₃ H ₇	NI	13	NI	13	NI	NI
d	C ₂ H ₅	NHC ₂ H ₅	NI	12	NI	NI	NI	NI
e	C ₂ H ₅	NHCH ₃	NI	12	NI	NI	NI	NI
f	CH ₃	NHCH ₂ C ₆ H ₅	NI	NI	NI	NI	NI	12
g	C ₂ H ₅	OH	NI	13	NI	NI	NI	NI
h	CH ₃	OH	NI	11	NI	NI	NI	NI

DDM – disc diffusion method, 80 µg; DM – agar well diffusion method, 200 µg; NI – no inhibition; I (intermediate sensitivity) – slight growth inhibition

We didn't find observable prevalence in the effects of tested compounds neither for Gram negative nor for Gram positive microorganisms included in this study.

Results which we obtained from two methods were different. Some of possible reasons for this may be the different amount of the compounds which applied in test or particular characteristics of the compounds or solvent. It seems that agar well diffusion test will be more appropriate to use for further investigation of antimicrobial activity of benzimidazole derivatives with suitable for bioassay solvents.

In conclusion, the scope of application of the intermolecular reaction of α-amidoalkylation has been successfully expanded. A series of cyclic enamino ketones were selectively amidoalkylated at the α-carbon atom in reactions with acyliminium reagents derived from benzimidazole.

Eight of synthesized benzimidazole derivatives displayed antimicrobial activity against three strains microorganisms. For some of the compounds was registered clear bactericidal effect on *Staphylococcus aureus*, bacteriostatic effect against *Enterobacter aerogenes* and antimicotyc activity against *Candida albicans*.

ACKNOWLEDGMENTS

We acknowledge financial support from the fund for scientific research of Plovdiv University – MU11 HF 003.

REFERENCES

1. Speckamp, W. N., Moolenaar, M. J. *Tetrahedron*, 2000, 56, 3817–3856
2. Hiemstra, H., Speckamp, W. N. *Incomprehensive Organic Synthesis*, Pergamon: Oxford, 1991, 2, 1047–1082
3. Garuti, L., Roberti, M., Gentilomi, G. *Il Farmaco*, 2000, 55, 35–39
4. Goda, F. E. et al. *Saudi Pharmaceutical Journal*, 2008, 16(2), 103–111
5. Kamal, A., Praveen Kumar, P., Sreekanth, K., Seshadri, B. N. and Ramulu, P. *Bioorganic & Medicinal Chemistry Letters*, 2008, 18, 2594–2598
6. Abdel-Mohsen T. H., Ragab F., Ramla M. M., El Diwani H. *European Journal of Medicinal Chemistry*, 2010, 45, 2336–2344
7. Gowda, Th., Kavitha, C. V., Chiruvella, K. K., Joy, O., Rangappa, S. K., Raghavan, C. S. *Bioorganic & Medicinal Chemistry Letters*, 2009, 19, 4594–4600
8. Tulug, T. M. K., Nurten, A. *European Journal of Medicinal Chemistry*, 2009, 44, 1024–1033
9. Shingalapur, R. V. et al. *European Journal of Medicinal Chemistry*, 2009, 44, 4244–4248
10. Jafar, A. A. et al. *Orbital*, 2009, 1(4), 306–309
11. Al-Tel, Taleb H. *European Journal of Medicinal Chemistry*, 2010, 45, 5848–5855
12. Xue, F. et al. *Bioorg. Med. Chem.*, 2011, 19, 2641–2649
13. Statkova-Abeghe, S., Angelov, P., Ivanov, I., Nikolova, St. *Tetrahedron letters*, 2007, 48, 6674–6676
14. Venkov, A. P., Statkova-Abeghe, S. M., Donova, A. K. *Cent. Eur. J. Chem.*, 2004, 2 (1), 234–246
15. Donova, A. K., Statkova-Abeghe, S. M., Venkov, A. P., Ivanov, I. *Synth. Commun.*, 2004, 34 (15), 2813–2821
16. Statkova-Abeghe, S., Gueorgiev, D., Ivanov, I., Nikolova, St. *University of Plovdiv „Paisii Hilendarski“, Scientific papers – Chemistry*, 2006, 34 (5), 95–98
17. Greenhill, J.V. *Chem. Soc. Rev.*, 1977, 6, 277–294

18. Performance standards for antimicrobial disk susceptibility tests; Approved standard – 9th ed.; CLSI document M2-A9. 26:1; Clinical Laboratory Standards Institute, 2006, Wayne, PA.
19. Perez, C., Pauli, M., Bazevque, P. *Acta Biologiae et Medicinae Experimentalis*, 1990, 15:113–115

MULTIFUNCTIONAL MECHANOCHEMICALLY-SYNTHESIZED Fe₂O₃-ZnO MIXED OXIDE

*N. Kostova¹, Al. Eliyas¹, M. Fabian²,
B. Kunev¹, N. Velinov¹, P. Balaz²*

*¹Institute of Catalysis, Bulgarian Academy of Sciences,
1113 Sofia, Bulgaria*

*²Institute of Geotechnics, Slovakian Academy of Sciences,
043 53, Kosice, Slovakia*

ABSTRACT

Fe₂O₃-ZnO mixed oxide with 1% wt. Fe has been synthesized using the mechanochemical activation method. The catalytic properties of Fe₂O₃-ZnO mixed oxide as catalyst has been investigated using the decomposition of isopropanol as model reaction. The photocatalytic activity of the Fe₂O₃-ZnO mixed oxide, using ethylene as a model air pollutant, has been carried out in a gas-phase flat-bed continuous flow photocatalytic reactor. Ethylene conversion degree was taken as a measure of the photocatalytic activity of the sample. The performance of the Fe₂O₃-ZnO photocatalytic material is compared with the standard reference photocatalyst Degussa P25 (75% anatase TiO₂ + 25% rutile TiO₂).

Key words: *mixed oxides, mechanochemical synthesis, photocatalytic activity*

INTRODUCTION

Mixed oxides, which contain more than one kind of metal atom are important class of catalysts that are widely used in several fields of investigation related to catalysis [1–4]. ZnO and TiO₂ have been widely used as photocatalyst owing to their high activities, low costs and environment-friendly properties [5]. However, the photocatalytic activities of ZnO and TiO₂ are limited to irradiation wavelengths in the UV-region because of their wide band-gaps and they can absorb only UV light. Some problems still remain to be solved in their application, such as the fast recombination of photogenerated electron-hole pairs. Therefore, improving the photocatalytic activity by modification of the material has become a topic among researchers in recent years. One approach is to dope transition metals into ZnO [6–8]. Some of the recent publications on Fe-doped ZnO systems using different methods of sol–gel techniques have examined the influence of Fe doping on the nanostructures and optical properties [9, 10]. The mechanochemical method for preparation of mixed oxides becomes more widely used at present due to its relative simplicity and availability [11, 12].

The contamination of air with various volatile organic compounds, originating from the petrochemical industry, presents a serious environmental problem due to the intrinsic toxicity and stability of some of these compounds. The photocatalytic degradation of organic compounds using semiconductor particles, most often nanometer-sized transition metal oxides, represents a promising solution to this environmental problem. Ethylene or its chlorinated derivatives have often been selected as target pollutants in air by many researchers in view of the large-scale production in the petrochemical plants (ethylene is the most widely produced petrochemical) causing air pollution in such industrial sites. Ethylene emissions are of concern because its release can lead to the formation of extremely toxic oxides.

The purpose of this work was to investigate the multifunctional properties of the mechanochemically prepared Fe₂O₃-ZnO (1%wt. Fe) mixed oxide. Its acid-base properties were studied using isopropanol decomposition as catalytic test reaction. In the second case of air purification the mechanochemically prepared mixed oxide is applied as film coating on a support to oxidize photocatalytically ethylene as model pollutant in air.

EXPERIMENTAL

Mechanochemical synthesis of Fe₂O₃-ZnO mixed oxides was performed in a laboratory planetary mill Pulverisette 6 (Fritsch, Germany) by high-energy milling of hematite and ZnO. The following experimental conditions were applied for the mechanochemical synthesis: loading of the mill, 50 balls of 10 mm in diameter; material of milling chamber and balls was tungsten carbide; volume of milling chamber, 250 mL; room temperature; rotational speed of the mill planet carrier, 400 min⁻¹; milling time, 20 min.

X-ray powder diffraction patterns (XRD) of the samples were registered at room temperature with a TUR M62 apparatus with PC management and data accumulation, using HZG-4 goniometer with CoK_α radiation. The XRD lines were identified by comparing the measured patterns to the JCPDS data cards.

Catalytic performance of the samples was performed on a flow reactor-gas chromatography system under atmospheric pressure by using isopropanol decomposition as reaction probe. 0.2 g of catalyst was charged into the reactor. Argon was used carrier gas. Isopropanol was put in saturator. The temperature of saturator was kept at 273 K. The reactor was directly connected to a 2 m GC column filled with Chromosorb W (60–80 mesh) with 20 % Carbowax 400 at 313 K [13]. Isopropanol conversion to propene was used as a measure of acidity and that to acetone is a measure of basicity of the sample.

The measurement of the photocatalytic activity of material Fe₂O₃-ZnO has been carried out in a gas-phase flat-bed continuous flow POLITEF photocatalytic reactor, using ethylene as a model air pollutant. The course of the photocatalytic reaction of complete oxidation of ethylene was monitored by means of a gas-analyzer (LANCOM III, Land Instruments Co., England), equipped with a sensor for total hydrocarbon content in a gaseous mixture (ppm C_xH_y). The inlet mixture is fed into the reactor by a 4-channel mass flow regulator (Matheson Model 8249), having the following composition: 10000 ppm C₂H₄, 10% O₂, 90% N₂. The nitrogen was fed into the reactor via two channels – the first channel feed N₂ directly into the reactor (dry N₂), while the second channel feeds the nitrogen flow to the water vapor saturator (distilled H₂O) to saturate the stream (moist N₂) and then further to the reactor. The use of two independently regulated channels for feeding nitrogen to the reactor enables the variation of the humidity of the inlet

gaseous mixture, which is a very important parameter of a photocatalytic process of oxidation.

During our previous experimental runs with other photocatalyst samples it was established that the optimal relative humidity RH is 30% [15].

Feeding ethylene and oxygen through two other independently regulated channels allows varying the ratio $C_2H_4 : O_2$ – in all our experimental runs the oxygen concentration is in large excess with respect to the amount of oxygen needed stoichiometrically to achieve 100% conversion degree of ethylene. So we can accept that at moderate conversion degrees the oxygen concentration C_{O_2} is practically unchanged comparing the inlet and the outlet compositions. In this specific case C_{O_2} is incorporated into the value of the effective kinetic constant k_{eff} in the kinetic equation:

$$R_{C_2H_4} = k_{\text{eff}} \cdot C_{C_2H_4} / (1 + K_{O_2} \cdot C_{O_2} + K_{C_2H_4} \cdot C_{C_2H_4}) \quad (1)$$

In the equation (1) $R_{C_2H_4}$ is the rate of consumption of ethylene (mol/h.g-cat), $C_{C_2H_4}$ is the concentration of ethylene at the outlet of the reactor (mol/cm³), while K_{O_2} and $K_{C_2H_4}$ are the adsorption-desorption equilibrium constants of oxygen and ethylene respectively. The equation (1) corresponds to a mechanism of the type of Langmuir-Hinshelwood, which means that both the reactants react on the surface of the photocatalyst in adsorbed state and there is no inhibiting effect by the reaction products – CO₂ and H₂O. This is often applied in the so called „formal kinetic approach“. The maximum contact time of ethylene τ_c under our experimental conditions is 4 min (such is the capacity of the experimental set-up i.e. the possibilities of the four-channel mass flow controller) – at this value of τ_c we achieve the maximum possible conversion degree of ethylene (if the relative humidity is also optimal and oxygen is in large excess). For avoiding under-pressure in the reactor and improving the precision of the analyses a GC flow splitter was used. It was placed between the reactor outlet and the gas-analyzer and the coefficient of dilution was measured to be 53.47 using CO₂ standard. The standard concentration of CO₂ in the cylinder was 19.25% and the gas-analyzer measured concentration 0.36% CO₂, on the basis of which the dilution coefficient was evaluated to be 53.47. Therefore the reading of the gas-analyzer for total hydrocarbons C_xH_y has to be multiplied by the coefficient to obtain the real concentration at the reactor inlet (the value measured in the dark) and at the reactor outlet (the value measured under irradiation).

1. Types of illumination and illumination intensity

a. UV-A light

The width of the flat rectangular quartz glass illumination window (the dimensions are: 5 cm x 15 cm x 0.5 cm) of the reactor enables the use of two linear lamps simultaneously (4-Watt UV-A lamps Philips model TL4W/08 F4T5/ BLB with total power of illumination 8 Watts, placed lying directly upon the window (distance 0 cm) – the intensity of illumination is 0.014 W/cm². This is polychromatic kind of illumination with wavelength range 320–400 nm and a maximum at 365 nm.

b. UV-C light

Two lamps Philips TUV 4W/G4 T5 (monochromatic light $\lambda = 254$ nm) of light power 4 Watts (making a total of 8 Watts), placed lying directly upon the window (distance 0 cm) – the intensity of illumination is the same – 0.014 W/cm², however this kind of illumination is a high frequency one i.e. the photons have much higher energy.

c. Visible light

This irradiation was accomplished using a linear halogen lamp Tungfram 500 Watts K1R7s giving intensity of illumination 8.9 mW/cm² (9700 Lm) at 50 cm from the surface of the illumination window. This kind of lamp causes considerable heating of the quartz window and reducing the distance of illumination could be risky in view of the inflammability of ethylene air mixtures. The other experimental conditions (the flow rates and the contact time) are the same as in the experiments with UV-light.

2. Deposition of thin film photocatalytic coating on TLC sheet

Merck aluminum foil, pre-coated with silica gel (0.2 mm) was used as support for the photocatalytic coating of the powder nano-sized material. It is available commercially and used for the purposes of thin layer chromatography (TLC Merck Art.5554 Kieselgel 60 F₂₅₄). The commercial sheet has dimensions 25 cm x 25 cm. A rectangular piece is easily cut out (4.2 cm x 13.4 cm) to fit with the dimensions of the accommodation nest drilled in the bed of the POLITEF photocatalytic reactor. The total geometric illuminated surface area amounts to 56 cm². An amount of 56 mg of the powder nanosized photocatalytic material is weighed exactly, in order to obtain a coating of 1mg/cm², in a weighing funnel. The amount was transferred quantitatively by rinsing it with de-ionized water in a volumetric

flask of 5 ml and filled up to the mark. The flask, containing the suspension (56 mg of $\text{Fe}_2\text{O}_3\text{-ZnO}$ in 5 ml H_2O), is immersed in a large beaker with water and fixed firmly in it, without touching the walls of the beaker. The sonotrode of an ultrasonic processor Hielscher UP 200S is also immersed in the water beaker. The ultra-sonnic bath treatment (24 kHz) is carried out at maximal amplitude in continuous mode (cycle 1) to disintegrate the agglomerates for 1 hour. After the sonication the suspension is deposited on the TLC sheet uniformly using a directing air stream all over the surface. Then the film is dried with until a constant weight is obtained. The sample is ready for measuring the photocatalytic activity.

RESULTS AND DISCUSSION

Figure 1 shows XRD patterns of undoped ZnO as well as 1 % wt. Fe doped ZnO, respectively.

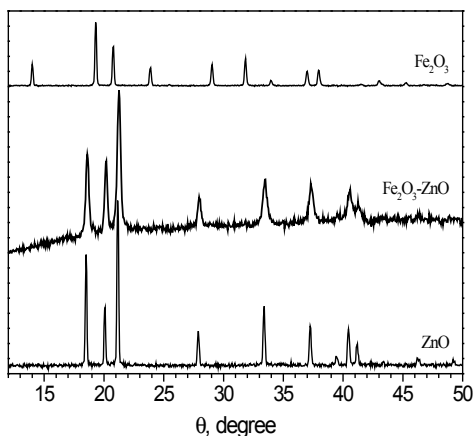


Figure 1. X-ray diffraction pattern of the initial ZnO and Fe_2O_3 and $\text{Fe}_2\text{O}_3\text{-ZnO}$ mechanochemically synthesized mixed oxide.

It had been found that all samples exhibit the hexagonal wurtzite structure in correspondance with the JCPDS database of card number 36–1451. Apart from a small decrease in peak intensity, the Fe-doping does not affect the ZnO wurtzite structure. The relative decrease in intensity of all XRD peaks in Fe-doped mixed oxide can be attributed to incorporation of Fe ions into the ZnO lattice and the resultant decrease of crystallite size.

This is also evidenced by the increase in the full width at half maxima (FWHM) of the XRD peaks in Fe-doping in the ZnO sample. This effect is due to the fact that Fe³⁺ ion has smaller radius (0.055 nm) than Zn²⁺ ion (0.074 nm) and doping results in contraction of the lattice parameters [6–8]. The spectra show only diffraction peaks of ZnO without any addition of other diffraction peaks. This might be due to a small quantity of iron, which can substitute the position of Zn ions in the ZnO structure. Therefore there is not change of peak positions, when doping ZnO with iron in this study.

Isopropanol is probe for selectivity in catalysts, because it can undergo both dehydrogenation to acetone and dehydration reaction to propene [14]. The results of catalytic test are summarized in Table 1. At it is seen in Table 1 the initial ZnO was not selective for propene formation. Fe₂O₃ is selective towards both acetone and propene formation. The selectivity to propene increased after introduction of small amount of iron into catalyst Fe₂O₃-ZnO (sample 2) in comparison to pure ZnO.

Table 1. *Catalytic performance in isopropanol conversion (wt.%)*

No	Sample	T, °C	propene	acetone	isopropanol
1	ZnO	280	–	60	40
		350	1	96	3
2	Fe ₂ O ₃ -ZnO	280	2	63	35
		350	8	82	10
3	Fe ₂ O ₃	280	5	12	83
		350	18	56	16

The potential catalytic activity of the samples was evaluated in gas phase by using isopropanol as a probe molecule. Gas chromatographic analysis of the reaction products indicates the production of expected organic products, acetone and propene, with all catalysts. The conversion of isopropanol proceeds through dehydration to propene and dehydrogenation to acetone with the selectivity depending on the type of materials. Pure zinc oxide exhibited dehydrogenation of isopropanol at 280–320°C. Its dehydrating efficiency to propene was less than dehydrogenating activity of initial ZnO and started only at 300°C. Acetone was the main product with the pure hematite. The selectivity to propene for hematite was 22% at 430°C at 100 5 isopropanol conversion.

The results from the photocatalytic activity testing using different kind of light for the illumination are represented in Table 2.

Table 2. Degrees of photocatalytic conversion of ethylene (10 000 ppm C_2H_4 , feed concentration) under illumination with different kinds of light, contact time $\tau_e = 4$ min, 30% RH and O_2 excess over Fe_2O_3 -ZnO and Degussa 25 TiO_2 for comparison

Photocatalyst coating 1mg cm^{-2}	Conversion of C_2H_4 , %	Type of illumination	Intensity of illumination $W\ cm^{-2}$	Distance of illumination cm
Fe_2O_3 -ZnO	4	UV-A	0.014	0
Fe_2O_3 -ZnO	9	UV-C	0.014	0
Fe_2O_3 -ZnO	12	Visible	8.9	50
Degussa 25 TiO_2	26.5	UV-A	0.014	0
Degussa 25 TiO_2	40	UV-C	0.014	0
Degussa 25 TiO_2	0	Visible	8.9	50

All the data in the table refer to maximal contact time of ethylene (4 min), optimal humidity (30% RH) and large excess of oxygen in the feed mixture. The degree of conversion of ethylene was taken as a measure of the photocatalytic activity of the sample. For the sake of comparison the performance of the Fe_2O_3 -ZnO photocatalytic material is juxtaposed with previous results, obtained with the standard reference photocatalyst Degussa P25 (75% anatase TiO_2 + 25% rutile TiO_2) [15]. It can be seen that Degussa P25 is superior in case of using UV light, while the composite Fe_2O_3 -ZnO material has also some activity with visible light, where Degussa displays zero activity.

The obtained results can be explained with the fact that the band gap of the Fe_2O_3 component is narrow (2.2 eV, corresponding to $\lambda=564$ nm i.e. activation by visible light), while the wide band gap of anatase TiO_2 (3.2 eV, corresponding to $\lambda=388$ nm) shows that it can be excited only by UV light. For this reason anatase TiO_2 displays zero activity with visible light, while the Fe_2O_3 -ZnO has some moderate activity with visible light. To the contrary – under UV light irradiation the TiO_2 has higher photonic efficiency than the Fe_2O_3 -ZnO composite material. At one and the same illumination intensity the UV-C lamps are more efficient than the black light blue lamps (UV-A light) probably because of the higher photon energy.

The mechanochemical technique can ensure obtaining the designed phases and structures by single step processing of materials in a closed activation chamber at room temperature. The multi-step character of mechanochemical activation involves the accumulation of energy due to

the formation of new surfaces, structural disorder in the bulk phase and even the change in the chemical composition of a solid.

CONCLUSIONS

Fe-doped ZnO mixed oxides were prepared by high energy ball milling and analyzed for structural, catalytic and photocatalytic properties. The XRD spectrum shows samples that exhibit wurtzite crystal structure which is not affected by Fe doping.

The reactivity of Fe₂O₃-ZnO mixed oxide as catalysts was investigated using the decomposition of isopropanol as model reaction. Pure ZnO is highly selective towards acetone formation. Dehydration and dehydrogenation of isopropanol are performed over Fe₂O₃-ZnO mixed oxide. The dehydrogenation of isopropanol to acetone was found to be dependent on the chemical composition of the samples.

The effect of the illumination on the photocatalytic activity of mechanochemically activated Fe₂O₃-ZnO mixed oxide (1% wt. Fe) was studied. The mechanochemically prepared Fe₂O₃-ZnO mixed oxide, shows absorption capacity in the visible region as well as in UV-region of solar spectrum that make this composite a promising heterojunction-type photocatalyst for solar light applications both for air purification from organics due to hole transfer from Fe₂O₃ valence band to ZnO valence band. The Fe₂O₃-ZnO mixed oxide is an effective photocatalyst for treatment of organic pollutant in air.

ACKNOWLEDGEMENTS

The authors are grateful to National Science Fund of Bulgaria (project DO 02-295/2008) and bilateral project between the Slovak Academy of Sciences and the Bulgarian Academy of Sciences for financial support.

REFERENCES

1. A. Perez, J. F. Lamonier, J.M. Giraudon, R. Molina, S. Moreno, *Catal. Today* 176, 286-291 (2011).
2. M. C. I. Bezen, C. Breitkopf, J. A. Lercher, *Appl. Catal. A: General* 399, 93–99 (2011).
3. N. G. Kostova, K. Ivanov, M. Achimovicova, E. Dutkova, P. Balaz, *Nanoscience & Nanotechnology* Eds. E. Balabanova, I. Dragieva, Sofia vol. 9, 37–39 (2009).
4. D. Carriazo, M del Arco, E. Garcia-Lopez, G. Marci, C. Martin, L. Parmisano, V. Rives, *J. Mol. Catal. A: Chemical*, 342-343, 83–90 (2011).
5. D. Li, H. Haneda, *Chemosphere* 51,1123–137 (2003).
6. Z. C. Chen, L. J. Zhuge, X. M. Wu, *Thin Solid Films* 515, 5462 (2007).
7. C. Wang, Z. Chen, Y. He, L. Li, D. Zhang, *Appl. Surf. Sci.* 255, 6881 (2009).
8. T. Rattana, S. Suwanboon, P. Amornpitoksuk, A. Haidoux, P. Limsuwan, *J. Alloys and Comp.* 480, 603 (2009).
9. A. K. Srivastava, M. Deepa, N. Bahadur, M. S. Goyat, *Mat. Chem. Phys.* 114, 194 (2009).
10. Y. Zhang, L. Wu, H. Li, J. Xu, L. Han, B. Wang, Z. Tuo, E. Xie, *J. Alloys and Comp.* 473, 319 (2009).
11. N. G. Kostova, E. Dutkova and P. Balaz, *J. Balkan Tribol. Assoc.* 15, 72–78 (2009).
12. Peter Balaz, „Mechanochemistry in Nanoscience and Minerals Engineering“ Springer 2008 pp. 413.
13. Yu. Kalvachev, A. Spojakina, N. Kostova, L. Dimitrov, in *Acid-Base Catalysis II*. Editors: H. Hatori, M. Misono, Y. Ono, *Stud. Surf. Sci. Catal.* 90, 413–418, Elsevier, Amsterdam (1994).
14. D. K. Chakrabarty, B. Viswanathan, *Heterogeneous Catalysis*, New Age International Ltd, Publishers, New delhi, pp.185, 2008.
15. A. Eliyas, K. Kumbilieva, L. Petrov, *Nanoscience & Nanotechnology* Eds. E. Balabanova, I. Dragieva, Sofia vol. 9, 50–53 (2009).

PHOTOCATALYTIC TESTING OF MECHANOCHEMICALLY-SYNTHESIZED CADMIUM SELENIDE

*Al. Eliyas¹, M. Achimovičová², N. Kostova¹,
A. Zorkovská², P. Baláž²*

*¹Institute of Catalysis, Bulgarian Academy of Sciences,
1113 Sofia, Bulgaria*

*²Institute of Geotechnics, Slovak Academy of Sciences,
043 53, Košice, Slovakia*

ABSTRACT

Spectroscopic and optical properties of highly luminescent II–VI semiconductor CdSe nanocrystals have been extensively studied due to their application in electrical and opto-electrical devices. CdSe nanocrystals are prepared by chemical wet process mainly. However, mechanochemical synthesis in planetary ball mill produces surface clean semiconductor nanoparticles without the influence of organic ligands coming from chemical process and such nanoparticles can be investigated as photocatalyst.

The aim of the present investigation was to test the photocatalytic activity of mechanochemically synthesized CdSe semiconductor with UV-C (monochromatic $\lambda=254$ nm) light and to compare this activity with the activity of the standard reference photocatalyst TiO₂ Degussa P25 (75% anatase + 25% rutile, average anatase particle size 25 nm). The second aim of the study was to test the photocatalytic activity of CdSe with visible light. The photocatalytic activity of the samples was tested in a batch reactor with Chromium Acidic Black Diazo Dye (Colour Index

Acid Black 194), which is used for colouring textiles. It appears in waste waters from textile factories and the new environmental regulations have forbidden discharging it into the waterways strictly.

The relatively low conversion degrees over CdSe, compared to the TiO₂ Degussa P25, can be explained by the low specific surface area of the CdSe sample. In order to increase the conversion degree sonication pretreatment of the CdSe is required as it falls at the bottom of the reactor as sediment, probably due to formation of agglomerates of large size. The sonication, prior to the photocatalytic activity test improves considerably the performance of the CdSe semiconductor. The result with model waste water is encouraging and the investigation could be extended to monitor the performance of CdSe for contaminated air purification in a gas-phase flat-sheet continuous flow steady state photocatalytic reactor. In view of the band gap of CdSe ($\Delta E = 1.7$ eV corresponding to band gap absorption edge wavelength of 730 nm) the investigation can be extended also in the direction of photocatalytic performance of CdSe with visible light to test the photonic efficiency (quantum yield) of this nanosized semiconductor material.

Key words: *Photocatalysis, mechanochemistry, Cadmium selenide*

INTRODUCTION

Cadmium selenide belongs to the group of metal chalcogenides A^{II}B^{VI}. CdSe is an n-type semiconductor and due to its band gap energy from 1.65 to 1.8 eV it can be used for various optoelectronic applications. According to Frame and Osterloh metal chalcogenides are promising as catalysts for photocatalytic water reduction because their bandgaps allow absorption in the visible region of the spectrum [1]. Many other metal chalcogenides can be used as photocatalysts for hydrogen evolution from water or water solutions by using solar light or UV-Vis irradiation [2–5]. CdSe nanocrystals are prepared by chemical wet process mainly [6–9]. However, recently Tan and co-authors synthesized CdSe nanocrystals by mechanical alloying process that is a safe, low cost and easy way to fabricate semiconductor nanocrystals, and can be easily extended to mass production [10]. Mechanochemical synthesis in planetary ball mill also produces surface clean semiconductor nanoparticles without the influence of organic ligands coming from chemical process and such nanoparticles can be investigated as photocatalyst.

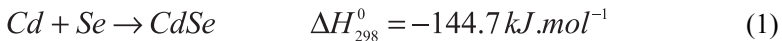
Verifying of photocatalytic activity of selenide semiconductor is possible by testing with the various dyes and the pollutants that are appearing in waste waters especially from textile factories. Song and co-authors [11] have tested

photocatalytic activity of S-doped BiSe photocatalyst by photocatalytic oxidation of methylene blue under visible-light irradiation ($\lambda > 400$ nm). Photocatalysis is so called Advanced Oxidation Process (AOP) whose a main feature is the generation of reactive hydroxyl radicals ($\text{OH}\cdot$), which are the precursors of degradation of any organic or inorganic compound. These hydroxyl species possess a higher oxidation potential (2.80V) compared to the other common oxidants like atomic oxygen (2.42 V), O_3 (2.07 V), H_2O_2 (1.78 V), hydroperoxy radicals (1.70 V) and chlorine dioxide (1.57 V) [12]. TiO_2 with wide band gap energy 3.2 eV is generally used for photocatalytic degradation reactions in UV light range because of non-toxic nature, simple synthesis, low costs, and can be used for comparative study.

In this paper we report the photocatalytic activity testing of mechanochemically synthesized CdSe with UV-light and visible light. The results are compared with photocatalytic activity of the standard reference photocatalysts TiO_2 (Degussa P25).

EXPERIMENTAL

Mechanochemical synthesis of cadmium selenide was performed in a laboratory planetary mill Pulverisette 6 (Fritsch, Germany) by high-energy milling of cadmium powder (99 %, Aldrich, Germany) and selenium powder (99.5 %, Aldrich, Germany) in argon atmosphere according to the reaction



which is thermodynamically possible due to the negative values of enthalpy change, ΔH_{298}° . The following experimental conditions were used for the mechanochemical synthesis: loading of the mill, 50 balls of 10 mm in diameter; material of milling chamber and balls, tungsten carbide; volume of milling chamber, 250 mL; mass of Cd and Se for reaction (1), 2.94 g and 2.06 g, respectively; ball-to-powder ratio, 73:1; room temperature; rotational speed of the mill planet carrier, 500 min^{-1} (8 Hz); milling time, 30 min.

X-ray diffraction measurements were carried out using a D8 Advance diffractometer (Bruker, Germany) equipped with a Θ/Θ goniometer, $\text{Cu K}\alpha$ radiation (40 kV, 40 mA), a secondary graphite monochromator, and a scintillation detector. The diffraction data were collected over an angular range $20 < 2\Theta < 70^\circ$ with steps 0.03° and a counting time of 5 s/step.

The XRD lines were identified by comparing the measured patterns to the JCPDS data cards.

Specific surface area was determined by the low temperature nitrogen adsorption method in a Gemini 2360 sorption apparatus (Micromeritics, USA).

The photocatalytic activity of TiO₂ (Degussa P25) and mechanochemically synthesized CdSe was tested with Chromium Acidic Black Diazo Dye (Colour Index Acid Black 194) which is known to be especially stable to UV-light and with 4-chlorophenol that is also common pollutant of waste waters. The UV-light source was Phillips lamp TUV 4W/G4 T5 (UV-C light monochromatic, $\lambda=254$ nm) and the intensity of illumination of the water surface was 0.05 Watts/cm². The distance of illumination (between the lamp and the water surface of the reactor) was 1.5 cm. The batch reactor contains 200 ml of the aqueous solution of Acid Black 194 – 20 ml of the stock standard solution (0.001 M) were diluted to obtain 0.0001M solution. The batch reactor was equipped with a magnetic stirrer (400 rpm). The diameter of the reactor is 10 cm and the water surface area is 78.5 cm². The air flow was bubbled through the solution passing through 2 frits to scatter the air in tiny bubbles to saturate the solution in oxygen. At the same time the stirrer and the tiny air bubbles prevented agglomeration of the nanosized semiconductor particles resulting in ideal mixing slurry reactor without any need of ultrasonic treatment in advance. Prior to the photocatalytic activity measurement the photocatalyst sample was stirred for 30 min in the dark in air flow in order to reach the adsorption-desorption equilibrium of the dye on the photocatalyst sample surface before switching on the illumination. Ultrasonic pretreatment of the selenide suspension was carried out for 5 min with Ultrasonic Processor UP200S (Hielscher, Germany) immersing the sonotrode directly in the photocatalytic reactor.

The conversion degree (degree of decoloration) is calculated on the basis of the formula:

$$X_3 = (C_0 - C_3) \cdot 100 / C_0 \quad (2)$$

where C_0 corresponds to initial concentration based on the calibration curve, initial extinction (absorbance) at $\lambda_{\max} = 570$ nm corresponds to E_0 , C_3 correspond to concentration after 3 hours of illumination (extinction (absorbance) after 3 hours of illumination = E_3).

The concentration of the working solution is checked spectrophotometrically by a single beam CamSpec M501 spectrophotometer at wavelength of the maximum $\lambda_{\max} = 570$ nm – the extinction (absorbance) should be $E_0 = 1.091$ Abs corresponding to initial concentration $C_0 = 0.0001$ M.

The analysis was carried out by a Total Organic Analyzer (TOC Shimadzu VCSH), based on total combustion of organics in a quartz reactor at 680°C and

detection of CO₂ by non-dispersive infrared gas analyzers. The result is given in mg of carbon per liter of water.

RESULTS AND DISCUSSION

The X-ray diffraction pattern of mechanochemically synthesized CdSe is shown in Fig. 1. The XRD peaks were identified based on the JCPDS card 19–191 and correspond to cubic cadmium selenide – CdSe phase. The large broadening of X-ray diffraction reflections also confirms the nanocrystalline nature of the cadmium selenide prepared by mechanochemical synthesis. The value of specific surface area, S_A of mechanochemically synthesized CdSe is also displayed in Fig. 1. The specific surface area value of TiO₂ is 50 m²g⁻¹.

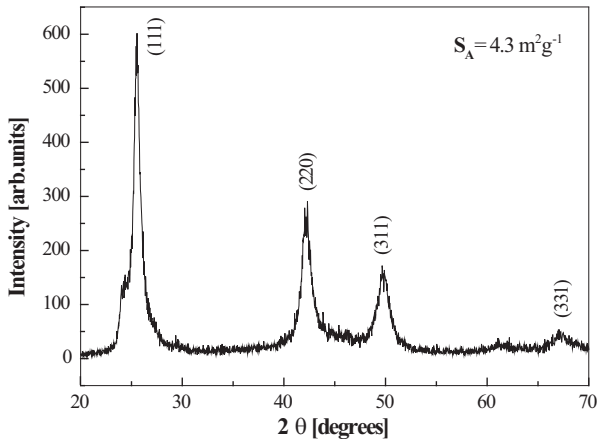


Figure 1. *X-ray diffraction pattern of CdSe mechanochemically synthesized for 30 min.*

TiO₂ and CdSe samples were tested with Chromium Acidic Black Diazo Dye (Colour Index Acid Black 194), which is used for colouring textiles and 4-Chlorophenol that was chosen as a model pollutant of waste waters as it is used for the synthesis of azodyes and it always appears in wastewaters from azodyes production. They appear in waste waters from textile factories and the new environmental regulations have forbidden them strictly. The dye is manufactured by the BULCOLOR Co. in the town Kostenetz, which is known to be especially stable to UV-light. The chemical structures of the dye and chlorophenol are shown in Fig. 2.

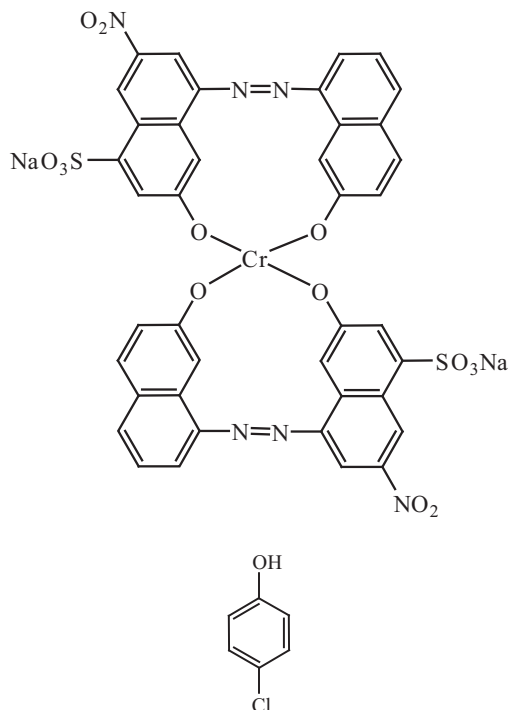


Figure 2. Structural formulae of Chromium Acidic Black Diazodye (Colour Index C.I. Acid Black 194) and 4-Chlorophenol.

Table 1. Comparison of conversion degrees of wastewater model pollutants Acid Black 194 (A) and 4-Chlorophenol (C) in aqueous solutions over nanosized TiO₂ Degussa P25 and mechano-chemically prepared CdSe in a batch photocatalytic reactor under UV-C irradiation ($\lambda=254$ nm) at illumination intensity 0.05 W/cm².

Type of photocatalyst	TiO ₂	CdSe
Photocatalyst amount [mg]	200	400
Initial absorbance – E_0 [Abs]	1.200	1.833
Initial concentration – $C_0(A)$ [M]	0.0001083	0.0001679
Initial concentration – $C_0(C)$ [mgC/L]	1285	1 333
Absorbance after 3 h of illumination – E_3 [Abs]	0.533	1.245

Concentration after 3 h of illumination – $C_3(A)$ [M]	0.0000488	0.000114
Concentration after 3 h of illumination – $C_3(C)$[mgC/L]	470	745
Conversion degree X_3 of (A) [%]	55.0	32.1
Conversion degree X_3 of (C) [%]	63.4	44.1

The conditions and the results of photocatalytic activity testing of TiO₂ Degussa P25 and mechanochemically synthesized CdSe are shown in Table 1. The relatively low conversion degrees over CdSe, compared to the TiO₂ Degussa P25, can be explained by the low specific surface area of the CdSe sample. In order to increase the conversion degree sonication of the CdSe is required as it falls at the bottom of the reactor as sediment, probably due to formation of agglomerates of large size. The sonication, prior to the photocatalytic activity test improves considerably the performance of the CdSe semiconductor.

The experimental runs with visible light (8.9 Watts/cm² illumination intensity) showed zero activity of TiO₂, which should be expected in advance in view of the wide band gap of TiO₂ (3.2 eV). However the CdSe semiconductor sample gave some moderate activities – 9% conversion of Acid Black 194 and 13.5% conversion of 4-chlorophenol preserving the rest of the experimental conditions the same as those shown in Table 1.

CONCLUSIONS

The result with model waste water is encouraging and the investigation could be extended to monitor the performance of CdSe for contaminated air purification in a gas-phase flat-sheet continuous flow steady state photocatalytic reactor. The nanosized CdSe semiconductor photocatalytic material displays some moderate activities in regard to Acid Black 194 and 4-Chlorophenol decontamination in model wastewaters, being superior in this respect to the TiO₂ photocatalyst. Future research work should be focused on composite CdSe-TiO₂ photocatalytic materials to utilize both the UV and the visible light components of the solar spectrum.

ACKNOWLEDGEMENTS

The authors are grateful to National Science Fund of Bulgaria (project DO 02-295/2008, project DO 02/252/2008), the Slovak Grant Agency VEGA (the projects 2/0043/11, 2/0009/11), the Slovak Research and Development

Agency APVV (project 0189–10), Centre of Excellence of Advanced Materials with Nano – and Submicron – Structure (NanoCexMat I) and Infrastructure Improving of Centre of Excellence of Advanced Materials with Nano – and Submicron – Structure (NanoCexMat II), which are supported by the Operational Program „Research and Development“ financed through European Regional Development Fund for their financial support.

REFERENCES

1. F. A. Frame, F. E. Osterloh, *J. Phys. Chem. C* 114 (2010) 10628–10633.
2. Y. Bessekhoud, M. Mohammedi, M. Trari, *Sol. Energ. Mat. Solar. C.* 73 (2002) 339–350.
3. I. Tsuji, H. Kato, A. Kudo, *Chem. Mater.* 18 (2006) 1969–1975.
4. I. Tsuji, H. Kato, H. Kobayashi, A. Kudo, *J. Am. Chem. Soc.* 126 (2004) 13406–13413.
5. N. Zheng, X. Bu, H. Vu, P. Feng, *Angew. Chem. Int. Ed.* 44 (2005) 5299–5303.
6. A. L. Rogach, A. Kornowski, M. Gao, A. Eychmueller, H. Weller, *J. Phys. Chem. B* 103 (1999) 3065–3069.
7. J. E. Bowen Katari, V. L. Colvin, A. P. Alivisatos, *J. Phys. Chem.* 98 (1994) 4109–4117.
8. G. G. Yordanov, G. D. Gicheva, B.H. Bochev, C. D. Dushkin, E. Adachi, *Colloid Surface A* 273 (2006) 10–15.
9. G. G. Yordanov, H. Yoshimura, C. D. Dushkin, *Colloid Surface A* 322 (2008) 177–182.
10. G. L. Tan, J. H. Du, Q. J. Zhang, *J. Alloy Comp.*, 468 (2009) 421–431.
11. L. Song, S. Zhang, Ch. Chen, X. Hu, Q. Wei, *Chem. Eng. J.* 171 (2011) 1454–1457.
12. R. Vinu, G. Madras, *J. Indian Inst. Sci* 90 (2010) 189–230.

ROLE OF THE PREPARATION METHOD ON CATALYTIC ACTIVITY OF Ag/CeO₂ FOR OXIDATION OF CO, CH₃OH AND (CH₃)₂O

T. Tabakova¹, D. Dimitrov², K. Ivanov², V. Idakiev¹

*¹Institute of Catalysis, Bulgarian Academy of Sciences,
1113 Sofia, Bulgaria*

*²Department of Chemistry, Agricultural University,
4000 Plovdiv, Bulgaria*

ABSTRACT

The catalytic activity of Ag/ceria catalysts for oxidation of CO, CH₃OH and (CH₃)₂O has been studied. Two different techniques were used for preparation of the catalysts – deposition-precipitation and modified version of deposition – precipitation. HRTEM combined with EDS, X-ray diffraction, FTIR of CO at 90 and 300 K and XPS measurements were employed to obtain information about the effect of different synthesis procedures on the surface and on the bulk structure of the catalysts and to explain the differences observed in their catalytic performance.

Key words: *Silver catalysts, complete oxidation, CO, VOCs, ceria*

INTRODUCTION

The removal of volatile organic compounds (VOCs) emitted from industrial and domestic processes have drawn a lot of attention due to in-

creasing social and political concern in environment. A cheap and efficient way of VOCs removing is their complete catalytic oxidation to harmless products such as H_2O and CO_2 . Supported Pt and Pd are well established as efficient catalysts for VOCs combustion. However, due to the high cost and limited reserve of such noble metals, the quest for cheaper and more environmentally friendly catalytic materials are of an ever-increasing importance for tomorrow's applications. Recently, the promotion effect of Ag on the performance of NiO_x and CoO_x in reaction of total oxidation of CH_3OH as well as of mixture of CH_3OH , $(CH_3)_2O$ and CO – main components of waste gases from production of formaldehyde has been reported [1]. It was found that catalytic behaviour depends on the selection of support and NiO_x is more suitable support than CoO_x . CeO_2 is known as a very attractive support material, because of its ability to maintain a high dispersion of the active components and to change the oxidation state of the cation between +3 and +4 depending on the redox conditions [2].

The aim of present study was to examine the catalytic activity of Ag/ CeO_2 catalysts for abatement of air pollutants – CH_3OH , $(CH_3)_2O$ and CO in waste gases from formaldehyde production. HRTEM, X-ray diffraction, FTIR of CO at 90 and 300 K and XPS measurements were employed to obtain information about the effect of different synthesis procedures on the surface and on the bulk structure of the catalysts and to explain the differences observed in their catalytic activity.

EXPERIMENTAL

1. Catalyst preparation

Two different techniques were used for preparation of Ag/ceria catalysts: deposition-precipitation (DP) and modified version of deposition-precipitation (MDP). Deposition-precipitation took place by precipitation of a desired amount of $AgNO_3$ (at pH 9.0) with K_2CO_3 at 333 K on ceria suspended in water by ultrasound. Ceria, used as a support and also as reference was laboratory-made by precipitation of $Ce(NO_3)_3 \cdot 6H_2O$ with K_2CO_3 at 333 K (pH 9.0), ageing in a course of 1 h at the same temperature, drying and calcination in air at 673 K for 2 hours. The MDP involved precipitation of $AgNO_3$ at the pH value indicated above on cerium (III) hydroxide freshly precipitated and aged 1 hour at 333 K. In both cases, the resulting precipitates were aged 1 h at 333 K, then filtered and washed until no NO_3^-

– could be detected. Further, the precipitates were dried in vacuum at 353 K and calcined in air at 673 K for 2 hours. All the samples were synthesized in a „Contalab“ laboratory reactor enabling complete control of the reaction parameters (pH, temperature, stirrer speed, reactant feed flow, ect). The Ag loading for each catalyst was 3wt. %. „Analytical grade“ chemicals were used for catalysts preparation.

Depending on the preparation method, the samples were labelled as AgCeDP and AgCeMDP.

2. Characterization techniques

The BET surface areas of the catalysts were determined on a „Flow Sorb II-2300“ device.

HRTEM analysis was performed using a Jeol JEM 2010 (200 kV) microscope equipped with an EDS analytical system Oxford Link. The powdered samples were ultrasonically dispersed in isopropyl alcohol and the obtained suspensions were deposited on a copper grid, coated with a porous carbon film.

X-ray diffraction patterns were obtained on a DRON-3 automatic powder diffractometer using Cu K α radiation.

X-ray photoelectron data were recorded on a VG Scientific ESCAL-AB-210 spectrometer using unmonochromatized Mg K α radiation (1253.6 eV) from an X-ray source operating at 15 kV and 20 mA. The binding energy scale of the spectrometer was calibrated by setting the Ag 3d_{5/2} peak of a sputtered Ag foil to 368.27 eV. The working pressure was below 8.10⁻⁹ mbar. The hemispherical analyzer works at a constant pass energy of 20 eV for Ce 3d, Ag 3d, O 1s, C 1s regions and VB. All spectra were recorded at a photoelectron take-off angle of 90°. Charging effects were corrected by using the Ce 3d_{3/2} U''' line at 917.00 eV as reference [3]. Quantitative calculations were made using MULTILINE program [4].

The FTIR spectra were taken on a Perkin-Elmer 1760 spectrometer (equipped with a MCT detector) with the samples in self-supporting pellets introduced in a cell allowing thermal treatments in controlled atmospheres and spectrum scanning at controlled temperatures (from 90 to 300 K). The experiments were performed on sample preliminarily heated up to 673 K in dry oxygen and cooled down in the same atmosphere (oxidised sample) or reduced in hydrogen at 373 K and outgassed at RT (reduced sample). Band integration and curve fitting were carried out by „Curvefit“, in Spectra Calc

(Galactic Industries Co.) by means of Lorentzian curves. All the spectra were normalised on the weight of the pellets.

3. Catalytic activity measurements

The catalytic activity of the samples in CO and CH₃OH oxidation was measured using continuous flow equipment with fixed bed stainless steel reactor at atmospheric pressure. The following conditions were chosen: catalyst bed volume – 0.5 cm³ (particle size 0,6 – 1.0 mm), inlet CO and CH₃OH concentrations – 2.0 % balanced with air and space velocity 20000 h⁻¹.

Two types of equipments for DME oxidation measurements were used: (i) flow-line equipment with an isothermal reactor, allowing precise control of the methanol dehydration to (CH₃)₂O on Al₂O₃ and (ii) flow-line equipment with stainless steel reactor for deep oxidation of the preliminarily purified DME. The feed gas was 1.0 % DME balanced with air and the space velocity was 20000 h⁻¹.

The reactant and product gases were analyzed for methanol, DME, CO, CO₂, O₂ and N₂ by HP 5890 Series II gas-chromatograph, equipped with flame ionization and thermal conductivity detectors and Porapak Q and MS-5A columns.

RESULTS AND DISCUSSION

1. Physicochemical characterization of the catalysts

The XRD patterns of the catalysts prepared by different methods are shown in Fig. 1. They showed the presence of CeO₂ in the cubic crystal structure of fluorite-type. The average size of ceria particles calculated from the peak at 2θ = 28.6 is 4.5 nm, according to Scherrer's equation. This size remains almost unchanged after the deposition of Ag – 4.3 nm. AgMDP catalyst also contains ceria crystallites with similar size. No peaks related to the presence of Ag were discernible in the diffraction patterns. The absence of a signal for Ag could be attributed to the fact that the particles size is too small and also that the measurement is under the detection limit of the instrument.

HRTEM measurements confirm that in both samples ceria is highly crystalline after calcination at 673 K (Fig. 2). The analysis of the fringes observed in the micrographs revealed that the support has a cubic structure and that it mainly exposes the (111) face. The surface of AgCeDP is covered

by an AgOx layer, according to FTIR data (see below). Since silver is unstable under the electronic beam of the microscope, an agglomeration into metallic silver particles occurs during the first few minutes of exposure, thus producing a lot of small silver particles that coalesce to form big particles by increasing the time under the electronic beam. However, the results agree well with XRD data for presence of very small silver particles.

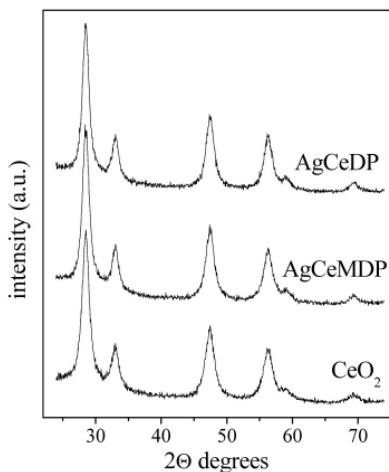


Figure 1. XRD patterns of studied samples

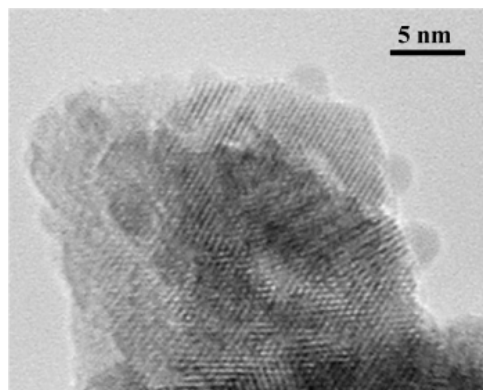


Figure 2. HRTEM image of AgCeDP (magnification of 800,000).

The absorption spectra of CO adsorbed at 90 K (fine curve) and at RT (bold curve) on AgCeDP oxidized sample are reported in Fig. 3. An intense band at 2149 cm^{-1} and a weaker one at 2168 cm^{-1} are observed in the spectrum in carbonylic region (Fig. 3a). On the basis of data already reported, the band at 2149 cm^{-1} can be assigned to CO on Ce^{4+} cations and on OH groups, while that at 2168 cm^{-1} is due to CO adsorbed on Ce^{4+} sites with a different coordinative unsaturation [5]. A very weak band at 2100 cm^{-1} could be seen in the spectrum, too. The low intensity of this band is in agreement with the reduction of Ag by the inlet of CO. This band could be tentatively assigned to Ag^0 sites stabilized by the support. However, a contribution of CO adsorbed on $\text{Ag}^{\delta+}$ sites to the band at 2168 cm^{-1} could also be suggested and supported by XPS measurements (see below). The formation of different carbonate and bicarbonate structures was observed in the carbonate region 1800–800 cm^{-1} (Fig. 3b). The appearance of bands at 1560, 1480, 1357, 1285, 1216 and 854 cm^{-1} after CO adsorption could be an indication for the reduction of Ag_xO .

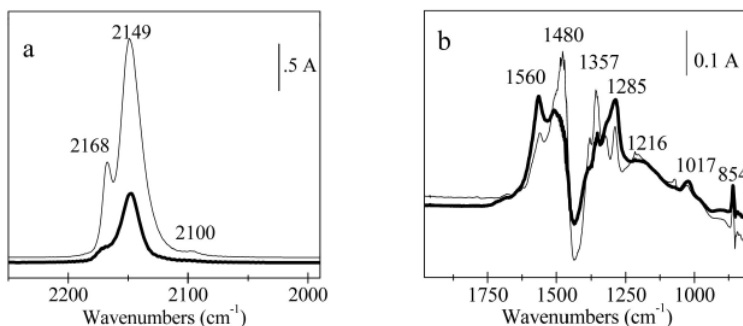


Figure 3. FTIR spectra of 5.0 mbar CO adsorbed at 90 K (fine curve) and at RT (bold curve) on oxidized AgCeDP in the carbonylic region (a) and in the carbonate region (b).

The inlet of CO at 90 K on AgCeDP catalyst reduced at 523 K (bold curve) produces in the carbonylic region a strong band at 2155 cm^{-1} that can be assigned to CO adsorbed on Ce^{3+} sites; another one at 2139 cm^{-1} due to liquid-like CO and a broadening from the low frequency side (Fig. 4). The reduction of the CO pressure causes a simultaneous decrease of the intensity of all the components and at RT only a very weak band at 2121 cm^{-1} is present (fine curve). The broad and weak adsorption at lower frequencies

can be tentatively related to Ag⁰ sites, possibly stabilised by ceria and able to adsorb small amounts of CO.

Very similar spectroscopic features were observed in the corresponding spectra of oxidized and reduced Ag/CeMDP, however bands were with lower intensity. These observations implied lower numbers surface sites, able to activate CO.

The admission of oxygen at RT on preadsorbed CO on the reduced samples produces a band at 2162 cm⁻¹ (not shown). According to previous results on Ag/titania, the band at 2162 cm⁻¹ can be assigned to CO on Ag^{δ+} sites exposed at the surface of the Ag_xO layer [6].

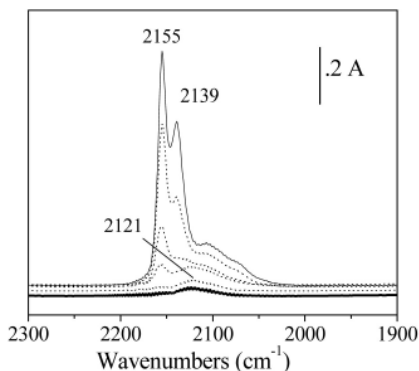


Figure 4. FTIR absorbance spectra of 5.5 mbar CO adsorbed on reduced Ag/CeDP during a gradual increase of the temperature from 90 up to 300 K (between fine and bold curves) in carbonilic region.

XPS technique was used to characterise the nature of the surface of the Ag/ceria catalysts. The analysis of Ce 3d XPS spectra of fresh (as-prepared) catalysts indicates the presence of stoichiometric CeO₂ on the surface. The binding energies of six peaks, corresponding to the three pairs of spin-orbit doublets obtained by curve fitting are in good agreement with the data for stoichiometric CeO₂ [7,8]. Upon reduction, two new peaks appear at 885.23 and 904.04 eV. Moreover, in combination with the appearance of these peaks, the relative areas of the peaks at 889.16 and 907.68 eV, as well as that at 917 eV, decrease. These changes are caused by the reduction of Ce⁴⁺ and the appearance of Ce³⁺. The XPS spectra of Ce 3d core electron levels of fresh and reduced silver-containing catalyst prepared by deposition-pre-

cipitation are illustrated in Fig. 5. The spectrum of pure ceria is also shown for comparison.

There are 8 peaks assignments in the spectra, labeled according to the convention established by Burroughs [9]. The peaks U, U'', U''' and V, V'', V''' refer to $3d_{3/2}$ and $3d_{5/2}$, respectively. These peaks are characteristic of the Ce(IV) 3d final state. At the same time, the peaks U' and V' (at about 903 and 885 eV) refer to $3d_{3/2}$ and $3d_{5/2}$, respectively. They are present for the Ce(III) 3d final state [10]. The increased intensity of the peaks at 884.93 and 903.53 eV in the XPS spectrum of reduced AgCeDP in comparison with those observed on the fresh catalyst is clearly seen. The decreased intensity of the peak at 917 eV is observed, too. The reduction of MDP-prepared silver-promoted catalyst causes similar changes on the surface, but Ce^{3+} content is lower than that on the surface of DP-prepared ones (not shown).

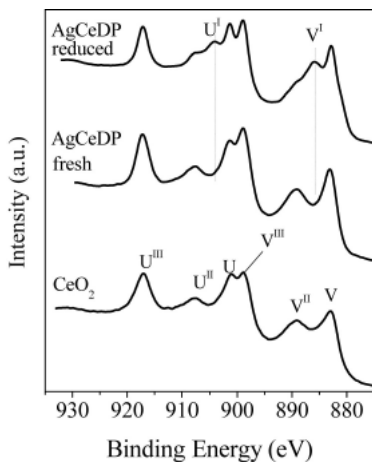


Figure 5. *Ce 3d XPS spectra of fresh CeO_2 and AgCeDP – fresh and reduced.*

The calculation of the Ce^{3+} concentration, according to equations in [10] evidences that the atomic content of Ce^{3+} on the catalysts surface increases after reduction (Table 1). The presence of Ce^{3+} on the surface of fresh samples may be caused by X-ray induced reduction of CeO_2 , in agreement with the data from the literature [10]. The promotion by silver enhances the oxygen mobility and facilitates the creation of surface oxygen vacancies. Moreover, the data reveal that the preparation method influences the surface

reduction of ceria and this effect is stronger on the catalysts prepared by deposition-precipitation.

Table 1. Surface concentration of Ag and Ce³⁺, calculated by XPS data

Catalysts	Surface concentration of Ag, (at. %)		Surface concentration of Ce ³⁺ , (at. %)	
	fresh	reduced	fresh	reduced
AgCeDP	2.19	2.16	0.19	0.44
AgCeMDP	0.60	0.60	0.18	0.31

The Ag 3d XPS peaks of fresh and reduced Ag/ceria catalysts are presented in Fig. 6. The BE of the 3d_{5/2} and 3d_{3/2} peaks (368.6 and 374.6 eV, respectively) of fresh and reduced samples are in agreement with those reported in the literature for metallic silver [11]. No shift of the peaks is observed after reduction. The only difference is that the peaks of fresh AgCeDP are broader (FWHM = 2.4) compared to that of the reduced sample (FWHM = 1.7). The decrease in the width of the peaks after reduction may be attributed to the presence of partially oxidized Ag cations or adsorbed oxygen species, as suggest our FTIR data. Moreover, structures due to chemisorbed and subsurface O species are observable in O 1s spectra of fresh silver/ceria catalysts (not shown). XPS measurements evidence also that the atomic concentration of Ag on the surface of the DP-prepared catalysts is higher than that observed on the catalyst prepared by MDP (Table 1). These results, as well as the higher Ce³⁺ surface concentration over reduced DP-prepared catalyst support the suggestion that nanosized metallic particles in close contact with oxygen defects in ceria are responsible for the higher catalytic activity of this catalyst.

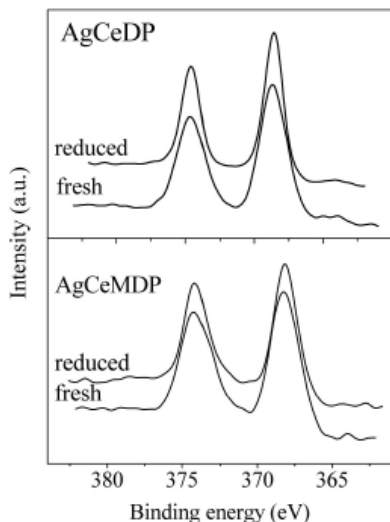


Figure 6. Ag 3d XPS spectra of fresh and reduced Ag/ceria catalysts prepared by DP and MDP methods.

2. Catalytic activity

Figs. 7–9 show the conversion curves vs. temperature over Ag/ceria catalysts. The figures demonstrate the role of two different synthesis procedures on the CO, CH₃OH and (CH₃)₂O oxidation activity of these catalysts. Ag/CeO₂ sample prepared by DP shows higher CO and CH₃OH oxidation activity than that of MDP – prepared. The most pronounced effect of different preparation methods was registered in the CO oxidation reaction (Fig. 7). The activity increased with increasing temperature and reached 50 % CO conversion at 373 K over DP-prepared sample and at 433 K over MDP-prepared. Almost 100 % CO oxidation was achieved over AgCeDP sample at 423 K and at 493 K over AgCeMDP.

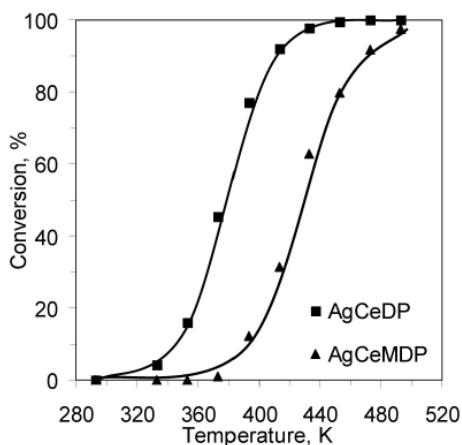


Figure 7. Temperature dependence of CO conversion over Ag/ceria catalysts prepared by DP and MDP methods.

The comparison of CH₃OH oxidation activity data for both investigated samples confirmed better behavior of AgCeDP. The results have shown that at 373 K were attained 90 and 15 % conversion over DP – and MDP-prepared Ag/CeO₂, respectively (Fig. 8).

The catalytic performance for (CH₃)₂O oxidation of the samples is demonstrated in Fig. 9. Both catalysts reached maximum conversion at about 413 K, 11 % and 6 % over MDP – and DP-prepared Ag/CeO₂, respectively. The increase of the reaction temperature to 540 K slightly improves the catalytic activity of AgCeDP.

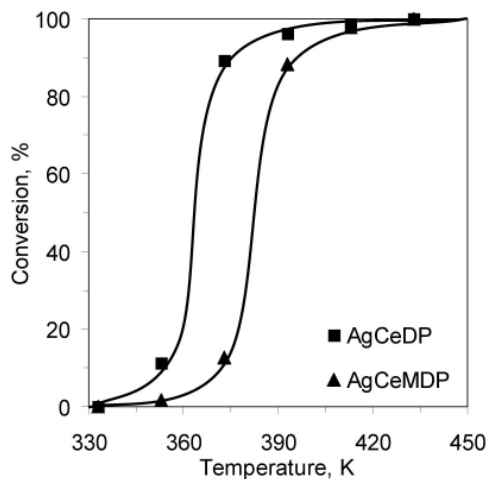


Figure 8. Temperature dependence of CH₃OH conversion over Ag/ceria catalysts prepared by DP and MDP methods.

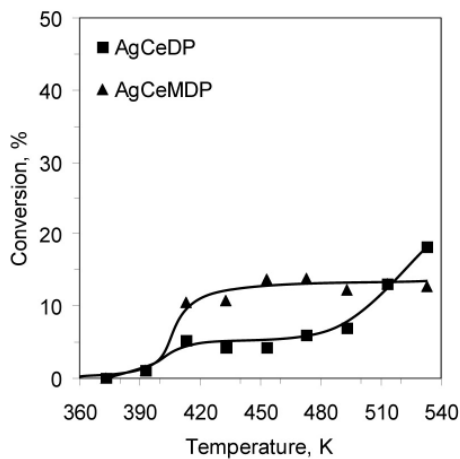


Figure 9. Temperature dependence of (CH₃)₂O conversion over Ag/ceria catalysts prepared by DP and MDP methods.

The catalytic data analysis reveals that deposition-precipitation is more suitable methods for synthesis of active ceria-based catalysts. Deposition-precipitation has the advantage over coprecipitation to allow preparation of catalysts with metallic particles localized mainly on the surface of the supports, avoiding encapsulation of active sites within the support. Recently, catalytic combustion of VOCs and preferential oxidation of CO (PROX) was studied over IB metal/ceria catalysts [12]. It was proposed that the presence of smaller crystallites of both IB metal and ceria result in a larger enhancement of mobility/reactivity of surface ceria oxygens, involved in both reactions through a Mars–van Krevelen mechanism.

The impact of the preparation method on the performance of Ag/ceria catalysts can be reasonably rationalized on the basis of different surface concentration of both silver nanoparticles and reactive ceria oxygens sites. It could be suggested that differences in perimeter interface around silver particles, acting as the site for oxidation reaction, affect the activity of the studied catalysts.

CONCLUSION

The application of two different preparation methods of Ag/CeO₂ catalysts leads to significant differences in their catalytic activity for oxidation of CO, CH₃OH and (CH₃)₂O. The experimental results revealed that deposition-precipitation is more suitable method for synthesis of Ag/ceria catalysts because it allowed significant part of metal promoter to be exposed at the catalyst surface. FTIR spectra of CO adsorbed on oxidized and reduced catalysts and XPS measurements evidenced higher concentration of Ag on the surface of the catalyst prepared by DP than that on the catalyst prepared by MDP. The higher surface concentration of silver nanoparticles and Ce³⁺ over reduced DP-prepared catalyst supports suggestion that nanosized metallic particles in close contact with oxygen defects on ceria are responsible for better catalytic performance of this catalyst.

ACKNOWLEDGMENT

Authors gratefully acknowledge the financial support by the National Science Fund (Project DDVU 02/7).

REFERENCES

1. S. Christoskova, M. Stoyanova, D. Dimitrov, D. Bojilov, K. Ivanov, *J. Int Sci. Publ.:Ecology & Safety* 3 (2009) 179.
2. A. Trovarelli, *Catal. Rev.-Sci. Eng.* 38 (4) (1996) 439.
3. L. Armelao, D. Barreca, *Surf. Sci. Spectra* 8 (2001) 247.
4. A. Jablonski, B. Lesiak, L. Zommer, M.F. Ebel, H. Ebel, Y. Fukuda, Y.Suzuki, S. Tougaard, *Surf. Interf. Anal.* 21 (1994) 724.
5. C. Binet, M. Daturi, J. C. Lavalley, *Catal. Today* 50 (1999) 207.
6. F. Boccuzzi, A. Chiorino, M. Manzoli, D. Andreeva, T. Tabakova, I. Ilieva, V. Idakiev, *Catal. Today* 75 (2002) 169.
7. B. Skarman, L. R. Wallenberg, P. Larsson, A. Andersson, J. Bovin, S. N. Jacobsen, U. Helmersson, *J.Catal.* 181 (1999) 6.
8. F. Zhang, P. Wang, J. Koberstein, S. Khalid, S.-W. Chan, *Surf. Sci.* 563 (2004) 74.
9. P. Burroughs, A. Hamnett, A. F. Orchard, and G. Thornton, *J. Chem. Soc. Dalton Trans.* 17 (1976) 1686.
10. A. Qi Wang, P. Panchaipetch, R. M. Wallace, T. D. Golden, *J. Vac. Sci. Techn.* 21 (2003) 1169.
11. J. F. Moulder, W.F. Stickle, P.E. Sobol, K.D. Bomben, *Handbook of X-Ray Photoelectron Spectroscopy*, Perkin-Elmer, Eden Prairie, 1992, p.120.
12. S. Scirè, P. M. Riccobene, C. Crisafulli, *Appl. Catal. B* 101 (2010) 109.

PHOTOCATALYTIC ACTIVITY OF SPRAYED TiO₂ FILMS DEPOSITED ON DIFFERENT SUBSTRATES

*I. Stambolova¹, V. Blaskov¹, M. Shipochka¹,
S. Vassilev², A. Loukanov³*

*¹Institute of General and Inorganic Chemistry,
BAS, Acad. G. Bonchev St, bl.11, 1113 Sofia, Bulgaria,
e-mail: stambolova@yahoo.com*

*²Institute of Electrochemistry and Energy Systems,
BAS, Acad. G. Bonchev bl. 10, 1113, Sofia, Bulgaria*

*³Dept. of Engineering geoecology,
University of Mining and Geology, Stoyan Edrev St.,
1700 Sofia, Bulgaria*

ABSTRACT

Thin photocatalytically active TiO₂ films are successfully deposited on glass and alumina foil substrates by spray pyrolysis method. The films are characterized by means of X-ray diffraction (XRD), Scanning Electron Microscopy (SEM), X-ray Photoelectron Spectroscopy (XPS), Thermal Analyses (TG-DTA). The XRD spectra of TiO₂ thin films, treated at 400°C showed formation of nanosize anatase phase. The films were studied with respect to the photo-initiated bleaching of azo dye Reactive Black 5 (RB5) under UV illumination. The influence of the substrate, treatment conditions and pH of the dye solution on the decoloration were investigated. It was found that the films, deposited on alumina foil revealed a better photocatalytic

activity than those on glass substrates, due to the furrowed surface of the alumina substrate. The highest rate of decoloration was obtained at low pH value of the dye solution for films treated at 400°C.

Key words: *TiO₂ films, photocatalysis, spray pyrolysis, azo dye*

INTRODUCTION

In the last decade the interest in photocatalysts applications has greatly grown, especially in the field of water purification. In this case, different wide band gap semiconductors have been studied as photocatalysts such ZnO [1], TiO₂ [2], BiVO₄ [3], Bi₂O₃ [4] etc. Among them, TiO₂ is the most suitable for degradation of organic pollutants in waste water due to its non toxicity, low cost, low water solubility and photochemical stability. The photocatalytic activity of TiO₂ has been found to vary with its structural form and is reportedly higher in the anatase form compared to the rutile form [5].

Up to today, several papers about photocatalytic properties of TiO₂ powders and thin films have been published [6]. The coatings overcome the disadvantage of the powders namely: the need of post-treatment separation in the photocatalytic reactor. Various methods are available for the preparation of TiO₂-based photocatalytic films, such as electrochemical methods [7–9], vacuum arc plasma evaporation [10], chemical vapour deposition (CVD) [11–13], as well as classical [14,15] and modified sol gel [16,17] methods.

Spray pyrolysis is an economical and fast chemical method, which is widely applied for formation of thin layers and particles of different compounds. Seabra et. al. prepared TiO₂ films from mixture of titania powder and polyester ink and studied the degradation of the azo dye Orange II [18]. Spray pyrolysis method have been successfully applied to obtain TiO₂ films, which exhibit good photocatalytic activity [19,20,21]. However, the studies about the technological and operational parameters affecting the photocatalytic performance of sprayed TiO₂ films are quite scarce [21,22].

Azo dyes are the most important class of synthetic organic dyes used in the textile industry. The photodegradation of aqueous solutions of different azo dyes have been reported by Soutsas et.al. [23]. Reactive Black

5 (RB5) dye is often used to colour cellulose fibers, which cause serious environmental problems [24]. This requires the development of effective photocatalysts for the degradation of this dye.

The aim of the present study is to investigate the influence of various parameters of TiO₂ sprayed films on the decoloration of Reactive Black 5 dye.

EXPERIMENTAL PROCEDURES

The alumina foil plates and glass substrates (75 x 25mm) were cleaned successively in hot ethanol and acetone. They were further used for the deposition of thin TiO₂ films. An alcoholic solution (EtOH–98% purity) of titanium tetraisopropoxide (TTIP) (98% purity, Acros) was hydrolyzed by a water-ethanol mixture in molar ratio TTIP:H₂O:C₂H₅OH=1:1:30. Acetyl acetone was added as a complexing agent (solution *A*). The solution *A* was dissolved in a mixture of isopropanol and butyl carbitol (C₄H₉OC₂H₄OC₂H₄OH) and then stirred intensively for 24 h at room temperature. The as prepared mixture were used for the spray procedure onto the heated substrates. After the spray coating procedure, one part of the deposits was progressively treated in air from 20 to 400°C for 1 or 2 hours with heating velocity 5°C/min in order to investigate the effect of thermal treatment temperature on the films properties.

The crystalline phase composition and size of the crystallites of the samples was studied by X-ray diffraction (XRD) using X-ray diffractometer Philips PW 1050 with CuK_α-radiation. The composition and electronic properties of the films were investigated by X-ray photoelectron spectroscopy (XPS) by VG ESCALAB II electron spectrometer using AlK_α radiation (1486.6 eV). The binding energies were determined with an accuracy of ±0.1 eV. A scanning electron microscope (SEM) JSM-5510 of JEOL was used for morphology observations of the films.

To study the photocatalytic activity of the films, experiments were conducted using an ultraviolet lamp with light intensity 5.10⁻⁵ W/cm² located in the centre of a vessel. The latter contained water solution of dye Reactive Black 5 with concentrations 10 ppm – 80ppm. The photocatalytic degradation is evaluated by taking aliquote of the solution and measuring the residual concentration by spectrophotometer type Boeco S26 in the wavelength range from 200 to 1100 nm at regular time intervals.

RESULTS AND DISCUSSION

Applied experimental way of preparation leads to formation of well crystallized anatase phase according to the X-ray analysis. X-ray diffracton line broadening (XRD-LB) measurements were carried out in order to estimate the TiO_2 crystallite size. Calculation was performed using the Scherrer's equation:

$$D = \frac{k\lambda}{\cos\theta} \quad (1)$$

where D is the crystallite size (nm), λ is the wavelength of $\text{CuK}\alpha$ radiation (nm), θ is the Bragg angle ($^\circ$), K is a constant (0.89) and B is the calibrated width of a diffraction peak at half-maximum intensity (rad).

The average crystallite size of the thin films as determined from half wide of full maximum (HWF) intensity of the (101) peak of the films. The average crystallite size, determined by the Scherrer's equation is about 20 nm. The size of the crystallites is typical for the films obtained by spray pyrolysis technique.

All film samples are characterized by X-ray photoelectron spectroscopy and the corresponding spectra are shown in Fig. 1. In the range of the $\text{O}1s$ state, the X-ray photoelectron spectrum (Fig. 1a) contains two peaks: the peak at 529.8 eV corresponds to the state of the oxygen atom O^{2-} in the TiO_2 oxide, and the low intensity peak at 531.9 eV characterizes the chemical bond of oxygen ion O^{2-} in the water molecule adsorbed on the surface of the TiO_2 film.

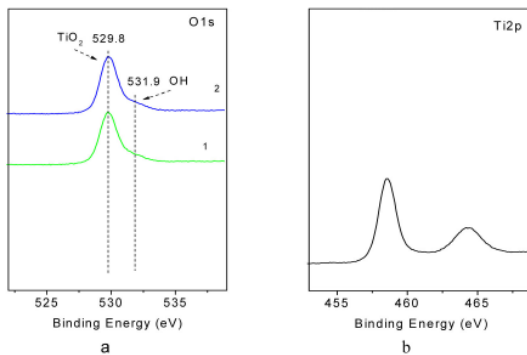


Figure 1. XPS spectra of sprayed TiO_2 film for $\text{O}1s$ lines(a) and $\text{Ti}2p$ (b).

For the Ti2p state, the spectrum (Fig. 1b) contains two peaks that reflect binding energies for electrons in the states Ti 2p_{1/2} and Ti 2p_{3/2}, respectively. These energies correspond to the Ti⁴⁺ state. The absence of other chemical shifts in the X-ray photoelectron spectrum makes it possible to believe that the synthesized TiO₂ films possess stoichiometric composition.

The XPS results proved that the films on glass substrate contain also Na and Si ions. This could be explained by interaction of the substrate with the films after thermal treatment similarly to the previously obtained by us ZrO₂ [25] and TiO₂-SnO₂ films [26].

Table 1. *Chemical composition of TiO₂ films, deposited on glass substrate*

Sample	O [at%]	Ti [at%]	Na [at%]	Si [at%]
TiO ₂ /glass	77.1	17.0	1.9	4.0

SEM photographs of the sprayed films on alumina foils, thermally treated at 400°C are shown on Fig. 2. The films morphology follows the uneven furrowed metallic plate surface. It consists of pores, which are probably formed by coalescence of several small pores. The structure of the TiO₂ films deposited on glass substrate is almost compact and very smooth (Fig. 3). The difference in the morphology of the films deposited on the glass and alumina foil could be explained with the surface nature of the substrates.

The photocatalytic studies showed that pH of the dye solution is very important parameter for the effective decoloration of the RB5 (Fig. 4). In our case the most suitable value of pH is 2. The catalyst also reveals relatively fast decoloration at pH=4. The reaction rate is very slow at pH 6. Similar dependence of degradation rates vs pH of azo dye by TiO₂ powders is proved by Augugliaro et.al. [27]. In the heterogeneous photocatalysis pH is very important operating parameter affecting the charge of the surface of the films and the positions of conductance and valence bands. The variation in the operating pH is known to influence the isoelectric point (PZC) and the surface charge of the photocatalyst used. The surface charge of TiO₂ is zero or neutral at pH_{pzc} in the range of pH 4.5–7.0, depending on the catalysts used, according to [28] At PZC of TiO₂, the interaction between the photocatalyst particles and water contaminants is minimal due to the absence of any electrostatic force. At low pH (pH < pH_{pzc}), TiO₂ particles possess positive charge, while a negative charge is expected at higher pH (pH > pH_{pzc}).

The majority of the reactive dyes (anionic dyes) found in the wastewater have water solubilizing sulfonic ($-\text{SO}_3^-$) groups, which are negatively charged. Therefore, acidic conditions would favor the electrostatic attraction between the positively charged TiO_2 surface and the reactive dyes, which would result in increased absorption and consequently in increased degradation of dyes.

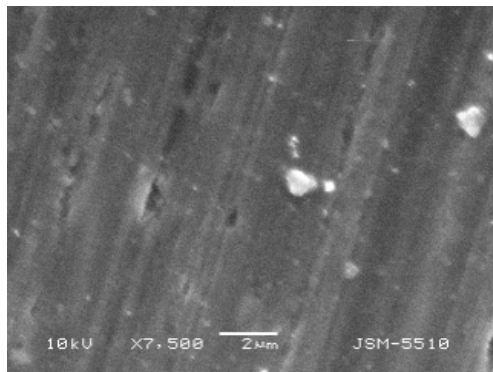


Figure 2. SEM photograph of TiO_2 film, deposited on alumina foil.

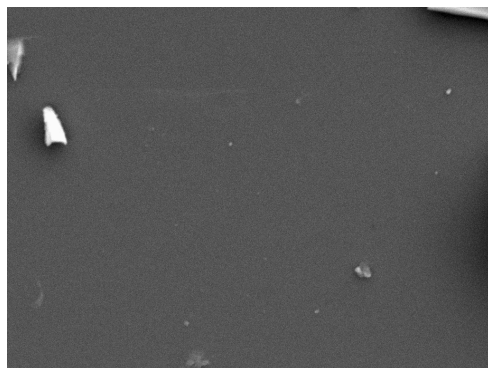


Figure 3. SEM photograph of TiO_2 film, deposited on glass substrate.

Fig. 5 shows the relationship between the decoloration rate and the volume of the sprayed solution. As can be seen the decrease in the sprayed volume leads to enhancement of the photocatalyst efficiency in the chosen interval.

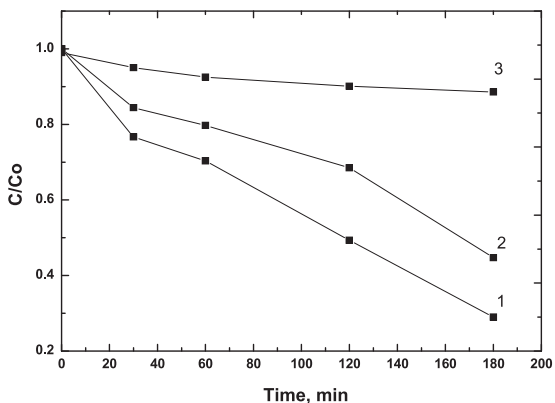


Figure 4. Kinetic curves of RB5 decoloration in coordinates $(C/C_0) = f(t)$ at different pH of the dye solution: pH=2 (1), 4 (2) and 6 (3). Films are deposited by spray of 25 ml solution, treated at 400°C.

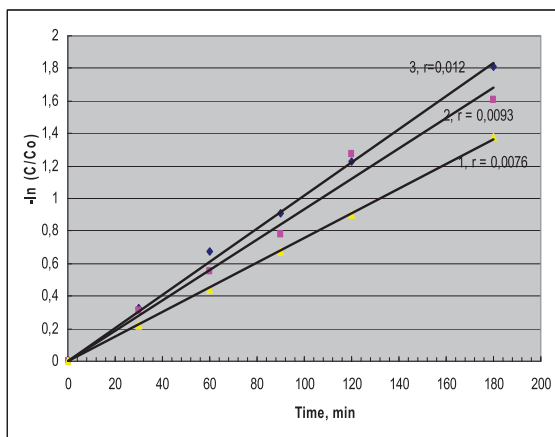


Figure 5. Kinetic curves of RB5 decoloration in coordinates $-\ln(C/C_0) = f(t)$ for films obtained by spraying of: 35 ml solution (1), 25 ml (2) u 15 ml(3); r is rate constant.

Deposition of the larger spray volume probably covers even deep grooves of the metallic surface leads to a formation of smoother film with

less number of active centers. For this reason the thin films (spray of 15 and 25 ml) are better catalysts than the thicker films, deposited by spraying of 35 ml, regardless of their lower TiO_2 content.

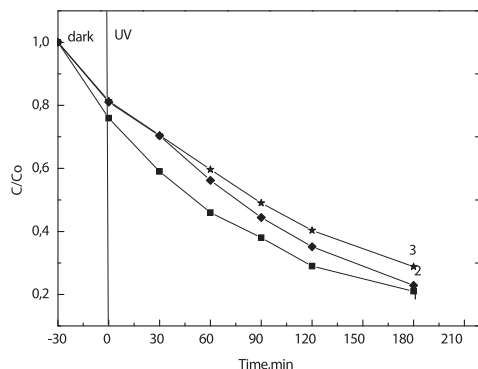


Figure 6. Kinetic curves of RB5 decoloration in coordinates $C/Co = f(t)$ The TiO_2 films are treated at $400^\circ\text{C}/1\text{ h}$ (1), $400^\circ\text{C}/2\text{ h}$ (2) not treated (3), RB5 concentration – 50 ppm

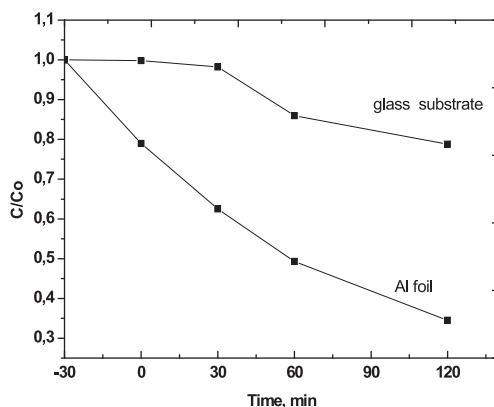


Figure7. Kinetic curves of RB5 decoloration in coordinates $C/Co = f(t)$ for TiO_2 films deposited on glass and Al foil.

The post deposition thermal treatment of the films has pronounced effect on the dye decoloration process (Fig 6). The films which are no treated

thermally after spray deposition have weaker efficiency than the treated films. The best results were obtained for the films treated at 400°C for 1 h, probably due to the better crystallization of the films. The prolongation of the isothermal heating up to 2 hours is not so effective due to the sintering effects.

The effect of the substrate used is shown on Fig. 7. The TiO₂ films on alumina foil are more effective photocatalysts than the films, deposited on glass substrate. This effect can be explained with the surface of the foil, which is not so smooth as the glass surface (Fig. 3 and Fig. 4). The uneven furrowed metallic surface causes better adsorption and adhesion of the dye. Another reason could be the temperature treatment of the glass substrate. It leads to a presence of Na and Si ions in the film, as was proved by XPS analysis (Table 1). According to the literature data [29] this element has detrimental effect on the photocatalytic efficiency.

CONCLUSIONS

Thin TiO₂ nanosize anatase films are prepared by spray pyrolysis of Ti(i-OPr)₄ solution. The films revealed high photocatalytic activity for decoloration of Reactive Black 5 azo dye and are effective at relatively high concentrations (up to 80 ppm). It was proved that the studied technological and operating parameters affect the photocatalytic properties. The pH of the dye solution influences considerably the photocatalytic activity. It was established that the films were most effective for the dye degradation in acidic medium (pH=2–4). The alumina foil seems to be more suitable than the glass substrate.

ACKNOWLEDGEMENTS

The authors thank to the Bulgarian Ministry of Science and Education for the financial support by project DVU 02/36 (2010).

REFERENCES

1. Hoffmann M., S. Martin, W. Choi, D. Bahnemann, *Chem. Rev.*, 95, 1995, 69.
2. Chong M. N., Bo Jin, C. W. K. Chow, C. Saint, *Water Research*, 44, 2010, 2997.
3. Zhang L., W. Wang, J. Yang, Zh. Chen, W. Zhang, L. Zhou, S. Liu, *Appl. Catal. A*, 308, 2006, 105.
4. Yin W., W. Wang, L. Zhou, S. Sun, L. Zhang, *J. Hazard. Mater.*, 173, 2010, 194.
5. Tsai S. J., S. Cheng, *Catal. Today* 33, 1997, 227.
6. Akpan U. G., B. H. Hameed, *J. Hazardous Mater.*, 170, 2009, 520.
7. Song W., W. Xiaohong, Q. Wei and J. Zhaohua, *Electrochim. Acta*, 53, 2007, 1883.
8. Wu X. H., Z. H. Jiang, H. L. Liu, X. D. Li and X. G. Hu, *Mater. Chem. Phys.*, 80, 2003, 39.
9. Karuppuchamy S., N. Suzuki, S. Ito, T. Endo, *Curr. Appl. Phys.*, 9, 2009, 243.
10. Miyata T., S. Tsukada and T. Minami, *Thin Solid Films*, 496, 2006, 136.
11. Babelon P., A. S. Dequiedt, H. Mostefa-Sba, S. Bourgeois, P. Sibillot, M. Sacilotti, *Thin Solid Films*, 322, 1998, 63.
12. Kim B. – H., J. – Y. Lee, Y. – H. Choa, M. Higuchi, N. Mizutani, *Mater. Sci. Eng.*, B107, 2004, 289.
13. Ghorai T. K., D. Dhak, S. K. Biswas, S. Dalai and P. Pramanik, *J. Mol. Catal. A: Chem.*, 273, 2007, 224.
14. Liao D. L., C. A. Badour, B. Q. Liao, *J. Photochem. Photobiol. A*, 194, 2008, 11.
15. Zhang X. and Q. Liu. *Mater. Lett.*, 62, 2008, 2589.
16. Andronic L. and A. Duta, *Mater. Chem. Phys.*, 112, 2008, 1078.
17. Liu C., X. Tang, C. Mo and Z. Qiang, *J. Solid State Chem.*, 181, 2008, 913.
18. Seabra M. P., E. Rego, A. Ribeiro, J. A. Labrincha, *Chem. Eng. J.*, 171, 2011, 175.
19. Lopez A., D. Acosta, A. I. Martinez, J. Santiago, *Powder Technol.*, 202, 2010, 111.

20. Okuya M., K. Shiozakia, N. Horikawaa, T. Kosugib, G. R. Asoka Kumara, J. Madarasz, S. Kaneko, G. Pokol, *Solid State Ionics*, 172, 2004, 527.
21. Abou-Helal M. O., W. T. Seeber, *Applied Surface Science*, 195, 2002, 53.
22. Uzunova-Bujnova M., R. Kralchevska, M. Milanova, R. Todorovska, D. Hristov, D. Todorovsky, *Catal. Today*, 151, 2010, 14.
23. Soutsas K., V. Karayannis, I. Poulos, A. Riga, K. Ntampeglitis, X. Spiliotis, G. Papapolymerou, *Desalination*, 250, 2010, 345.
24. Koyuncu I., *Desalination* 143, 2002, 243.
25. P. Peshev, I. Stambolova, S. Vassilev, P. Stefanov, V. Blaskov, K. Starbova, N. Starbov, *Mater Sci. Eng. B* 97 (2003) 106.
26. I. Stambolova, V. Blaskov, S. Vassilev, M. Shipochka, C. Dushkin, *J Alloys Comp.* 489(2010)257–261.
27. Augugliaro V., C. Baiocchi, A. B. Prevot, E. Garcia-Lopez, V. Loddo, S. Malato, G. Marci, L. Palisano, M. Pazzi, E. Pramauro, *Chemosphere*, 49, 2002, 1223.
28. Chong M. N., B. Jin, Ch. W. K. Chow, Ch. Saint, *Water Research* 44, 2010, 2997.
29. Fernández A., G. Lassaletta, V. M. Jiménez, A. Justo, A. R. González-Elipse, J. – M. Herrmann, H. Tahiri, Y. Ait-Ichou, *Appl. Catal. B*, 7, 1995, 49.

DECOLORIZATION OF REACTIVE BLACK 5 DYE ON TiO₂ HYBRID FILMS DEPOSITED BY SOL GEL METHOD

V. Blaskov^{1,}, I. Stambolova¹, M. Shipochka¹,
S. Vassilev², N. Kaneva³, A. Loukanov⁴*

*¹Institute of General and Inorganic Chemistry, BAS,
Acad. G.Bonchev St, bl.11, 1113 Sofia, Bulgaria, vblaskov@abv.bg*

*²Institute of Electrochemistry and Energy Systems, BAS,
Acad. G.Bonchev bl. 10, 1113, Sofia, Bulgaria*

*³Laboratory of Nanoparticle Science and Technology,
Faculty of Chemistry, University of Sofia,
1 J. Bourchier Blvd., 1164 Sofia, Bulgaria*

*⁴Dept. of Engineering geoecology,
University of Mining and Geology, St. Edrev St.,
1700 Sofia, Bulgaria*

ABSTRACT

Photocatalytically active TiO₂ films were successfully prepared by sol gel method. The solutions as well as suspensions enriched with Degussa P25 powder were spin coated on glass substrates. The phase composition and crystallite size of the films were characterized by means of X-ray diffraction (XRD). The morphology and chemical composition were studied by Scanning Electron Microscopy (SEM) and X-ray Photoelectron Spectroscopy (XPS). The XRD spectra of TiO₂ thin films annealed at 400° C

showed a formation of nanosize anatase phase. The decoloration of Reactive Black 5 (RB5) dye, used in the textile industry was investigated at different pH range. The pH of the dye solution influences significantly the photocatalytic properties of TiO₂ films. The films, obtained from suspensions by microwave-assisted drying and/or conventional heating have a rate of the RB5 degradation compatible with those of conventionally treated TiO₂ films.

Key words: *TiO₂ films, photocatalysis, sol gel, hybrid films, azo dye*

INTRODUCTION

Nanosized TiO₂ thin films have many different applications as photocatalysts [1–3], gas sensors [4–6], ceramic membranes [7], optical filters [8] etc. Sol gel method, spray pyrolysis and chemical vapor deposition are widely applied for the preparation of TiO₂ thin films. The sol gel method has many advantages over the other methods due to the possibility of producing materials with controlled porosity, phase and chemical composition on different substrates at relatively low temperatures [9–11]. However, it is difficult to prepare films without cracking. Prominently, the sol gel polymer/inorganic hybrid route is attractive and capable of producing homogeneous crack free films with variety of microstructures.

Only several authors reported about the deposition of composite TiO₂ films using a polymeric matrix which implies hydrolysis and condensation of titanium tetraethoxyde in the presence of hydroxypropylcellulose (HPC) or methylcellulose [4,12,13,14]. Recently our team has proposed a new modified sol–gel processing using TiCl₄ and diethylaminoethylcellulose (DEAE) for the preparation of an oriented pure brookite film [15]. The ethylcellulose, (EC) used in the present study as a polymer modifier, is a long chain and abundant in R-OH and R-O-R bonds. So it can be useful for the enhancement of homogeneity of metal ions in the precursor and thus for preventing the aggregation of particles during the heating.

The hybrid thin films prepared from suspensions of titanium precursor solutions with Degussa P25 powder seem also very promising photocatalysts probably due to the high photocatalytic activity of P25.

We present in this paper the results concerning the preparation of TiO₂ thin films by sol-gel method using solutions and suspensions, deposited onto glass substrates and study the photocatalytic properties of the films.

EXPERIMENTAL

The glass substrates (26 mm x 76 mm) were cleaned 10 min with ethanol in the ultrasonic bath. Finally they were dried in the furnace at 200°C for 10 min. Two titanium precursor solutions were applied: (i) Titanium tetrachloride TiCl₄, (Merck, 98%) dissolved in ethanol (*sol A*) and (ii) alcoholic solution (EtOH–98% purity) of titanium tetraisopropoxide (TTIP) (98% purity, Acros) hydrolized with water-ethanol mixture in a molar ratio TTIP:H₂O:C₂H₅OH=1:1:30. Acetyl acetone was added as a complexing agent. The as prepared solution was titled *sol B*. Ethylcellulose [C₆H₇O₂(OC₂H₅)₃]_n solution (1 wt%) dissolved in ethanol and was stirred 24h (*sol C*). This solution was added to *sol A* or *sol B* under vigorous 3 h stirring.

In order to obtain titania hybrid films powder TiO₂ Degussa P25 (75% anatase and 25% rutile) was used. This powder was added under vigorous stirring to Ti(OBu)₄ dissolved in butanol to obtain suspension.

The solutions/suspensions were deposited by spin coating at 1500 rpm. Each coating was treated by different manners. The films deposited from titanium precursor solutions were treated according to path A, while the hybrid films, obtained from suspensions with P25 were treated according to path A, B and B-C. (Fig. 1)

The phase composition and crystallites size of the samples were studied by X-ray diffraction (XRD) using X-ray diffractometer Philips PW 1050 with CuK_α-radiation. The composition and electronic properties of the films were investigated by X-ray photoelectron spectroscopy (XPS). The measurements were performed in VG ESCALAB II electron spectrometer using AlK_α radiation. A scanning electron microscope (SEM) JSM-5510 of JEOL was used for morphology observations of the films.

The photocatalytic experiments were conducted using an ultraviolet source (UV lamp) with light intensity 5.10⁻⁵ W/cm² located in the centre of a photocatalytic reactor. The latter contained 10 ppm water solution of the RB5. The photocatalytic degradation is evaluated with spectrophotometer type Boeco S26 (the wavelength range from 200 to 1100 nm). The pH of the solutions was adjusted using concentrated HCl before the experiments.

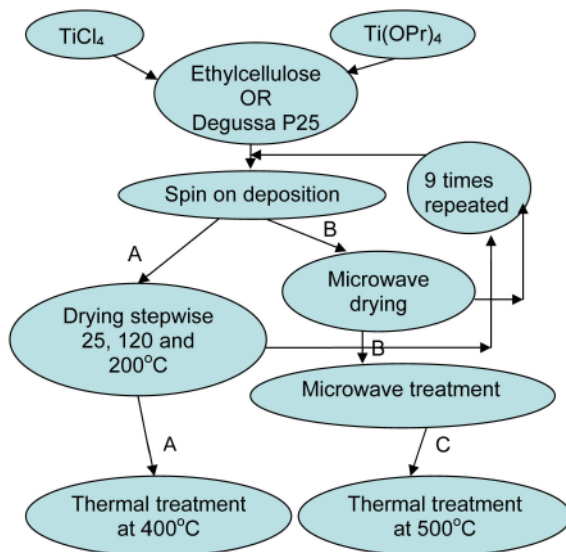


Figure 1. Scheme of the experimental procedures

RESULTS AND DISCUSSION

Fig. 2 illustrates XRD patterns of the TiO_2 thin films. The peaks clearly indicate the presence of anatase (crystalline) phase of TiO_2 . X-ray diffracton line broadening (XRD-LB) measurements were carried out in order to estimate the TiO_2 crystallite size. Calculation was performed using the Scherrer equation:

$$D = \frac{k\lambda}{\cos\theta} \quad (1)$$

where D is the crystallite size (nm), λ is the wavelength of $\text{CuK}\alpha$ radiation (nm), θ is the Bragg angle ($^\circ$), K is a constant (0.89) and B is the calibrated width of a diffraction peak at half-maximum intensity (rad).

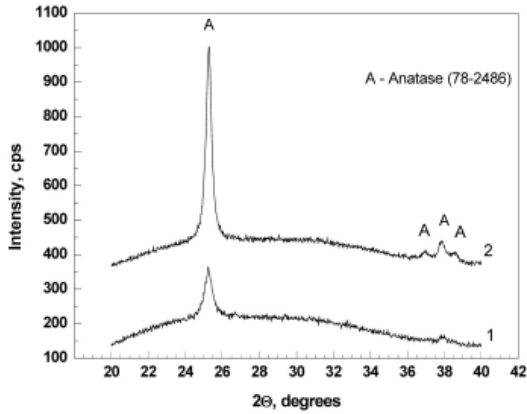


Figure 2. XRD of TiO₂ films obtained from: Ti(OPr)₄/EC (1) and TiCl₄/EC (2) solutions

The average crystallite size of the thin films as determined from half width of full maximum (HWHM) intensity of the (101) peak of the films, obtained from Ti(OPr)₄/EC and TiCl₄/EC solutions are: t_{101} =16.1 nm and t_{101} =22.8 nm, respectively.

The typical XPS spectrum of the TiO₂ films contains two peaks corresponding to states Ti 2p_{1/2} and Ti 2p_{3/2} (Fig. 3a). These energies correspond to the Ti⁴⁺ state. In the range of the O 1s state the peak at 529.8 eV corresponds to the state of the oxygen atom O²⁻ in the TiO₂ oxide. The low intensity peak at 531.9 eV characterizes the chemical bond of oxygen ion O²⁻ in the water molecule adsorbed on the surface of the TiO₂ film. The presence of OH– group is characteristic of the TiO₂ catalysis with developed specific area. The chemical composition of the films obtained from both titanium precursor solutions as well as corresponding O/Ti relations (in atomic percent) are shown in Table 1.

Table 1 Chemical composition of the TiO₂ films, according to XPS analyses

Solution composition	C [at.%]	O [at.%]	Ti [at.%]	Si [at%].	O/Ti
TiCl ₄ /EC	27.9	50.8	18.0	3.3	2.82
Ti(OPr) ₄ /EC	20.9	56.9	22.2	-	2.56

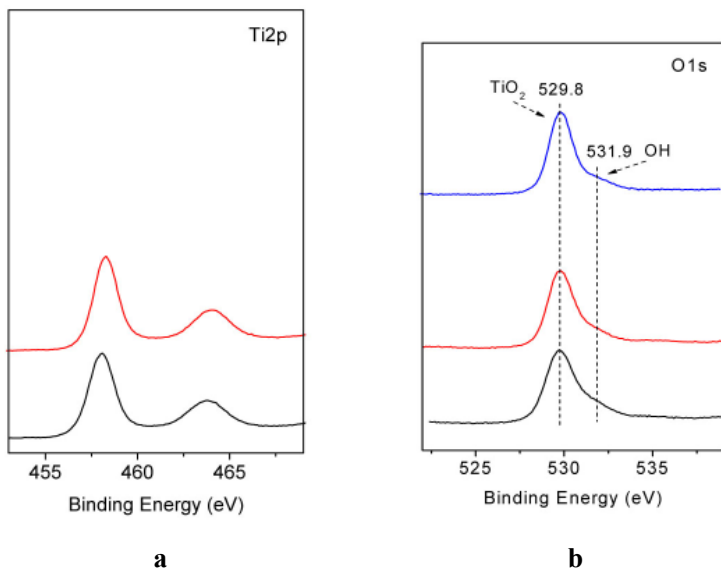


Figure 3. XPS spectra of Ti2p line (a) and O1s line (b) of TiO₂ sol gel layers

The SEM micrographs of the films from TiCl₄, treated at 400°C is shown in Fig. 4. The films possess flake like structure, which consists of fine particles agglomerates

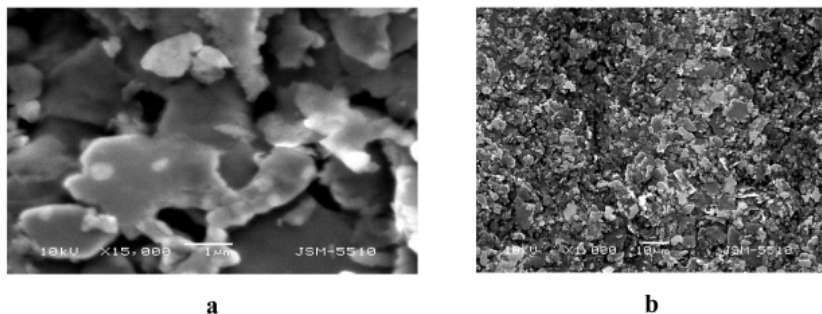


Figure 4. Morphology of TiO₂ films with 9 successive coatings from TiCl₄ and ethylcellulose, treated at 400°C, magnification 15000 (a) and 1000 (b)

The films have slightly different chemical composition. The samples prepared from TiCl₄/EC solution contain also small quantity of Si ions. Probably in the analyzed spot of the monochromatic X-rays the films are thinner. Consequently in the final composition we were observed ions from the substrate. This could be explained by interaction of the substrate with the films after thermal treatment, similarly to the previously obtained by us ZrO₂ [16] and TiO₂-SnO₂ films [17].

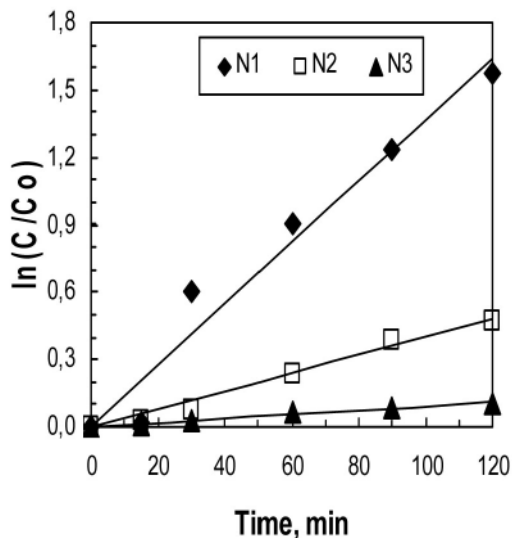


Figure 5. Kinetic curves of RB5 decolorization in coordinates $-\ln(C/C_0) = f(t)$ for films, deposited from $Ti(OPr)_4/EC$ at different pH: pH=2 (N1), pH=4(N2) and pH=6(N3)

The kinetic curves of RB5 decoloration on the TiO₂ films (where C₀ is initial concentration of RB5), deposited from Ti(OPr)₄ and TiCl₄ solutions at different pH of the dye solution under UV radiation are shown in Fig. 5 and Fig. 6. The degradation of the dye enhances with decreasing of the pH. This tendency is valid for the films obtained from both titanium precursor solutions. Similar dependence of degradation rates vs pH of the azo dye by TiO₂ powders is proved by Augugliaro et.al. [18]. In the heterogeneous photocatalysis pH is very important operating parameter affecting the charge of

the surface of the films and the positions of conductance and valence bands. The variation in the operating pH is known to influence the isoelectric point (PZC) or the surface charge of the photocatalyst used. The surface charge of TiO_2 is zero or neutral in the pH range of 4.5–7.0 according to [19]. At PZC of TiO_2 , the interaction between the photocatalyst particles and water contaminants is minimal due to the absence of any electrostatic force. At low pH ($\text{pH} < \text{pHpzc}$), TiO_2 particles possess positive charge, while a negative charge is expected at higher pH ($\text{pH} > \text{pHpzc}$). The majority of the reactive dyes possess water solubilizing sulphonic ($-\text{SO}_3^-$) groups which are negatively charged. Therefore, acidic conditions would favor the electrostatic attraction between the positively charged TiO_2 surface and the sulphonic groups of the dyes, which would result in increased absorption and degradation of dyes.

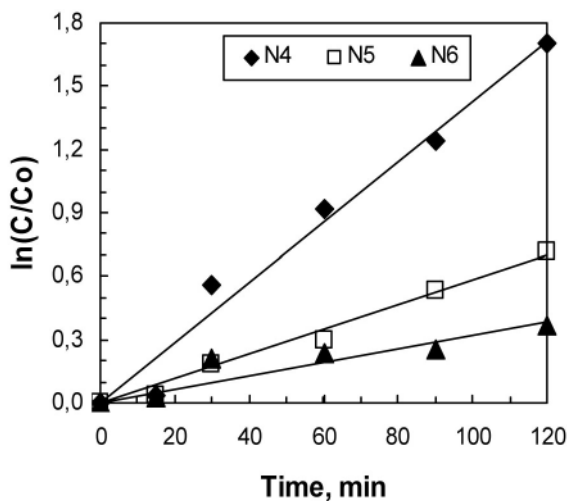


Figure 6. Kinetic curves of RB5 decolorization in coordinates $-\ln(C/C_0) = f(t)$ for films, deposited from TiCl_4/EC at different $\text{pH}=2(\text{N4}); \text{pH}=4(\text{N5}); \text{pH}=6(\text{N6})$

The photocatalytic properties of hybrid TiO_2 films are presented on Fig 7. It was established that the drying/heating way of the films influences significantly their characteristics. When the microwave oven is used in drying

and heating stage the films relatively slow degrade the dye, may be due to the incomplete incineration of the organics and low degree of crystallization. The films, dried in microwave oven and treated conventionally showed photocatalytic behaviour similar to those, obtained by conventional treatment. Application of microwave heating in sol gel method seems promising way to obtain photocatalytic active films at reduced temperatures and time, giving possibility to use substrates with low thermal stability (plastic etc.).

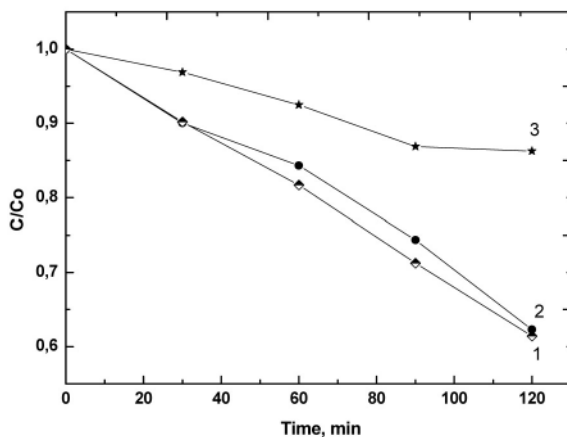


Figure 7. Kinetic curves of RB5 decolorization in coordinates $C/Co = f(t)$ for hybrid films, deposited from suspensions $Ti(OPr)_4$ – Degussa P25 by: conventional drying and treatment at 500° (1), microwave drying and conventional treatment at 500°C (2) and microwave drying and treatment (3).

CONCLUSIONS

Thin TiO₂ photocatalytic active films were obtained from polymer modified solutions and suspensions. The films treated at 400°C possess nanosize anatase phase.

It was established that the acidity of the dye solution influences significantly the photocatalytic activity towards degradation of the azo dye Reactive Black 5. The catalysts degrade faster the dye in acidic than in neutral

medium. The films deposited from TiCl_4 showed better activity than the films, obtained from titanium iso-propoxide solutions.

The TiO_2 hybrid films, obtained from suspensions and treated under microwaves, following by conventional treatment revealed degradation rate compatible with those of conventionally treated films. The TiO_2 thin films prepared by us are promising as efficient photocatalyst for degradation of Reactive Black 5 azo dye.

ACKNOWLEDGEMENTS

The authors thank to the Bulgarian Ministry of Science and Education for the financial support by project DVU 02/36 (2010).

REFERENCES

1. Dong F., W. Zhao, Z. Wu, S. Guo, J. Hazard. Mater., 162, 2009, 163.
2. Saylikan F., M. Asiltürk, N. Kiraz, E. Burunkaya, E. Arpaç, H. Saylikan, J. Hazard. Mater., 162, 2009, 1309.
3. Yu J., X. Zhao, Mater. Res. Bull., 35, 2000, 1293.
4. Garzella G., E. Comini, E. Tempesti, C. Frigeri, G. Sberveglieri, Sens. Act. B, 68, 2000, 189.
5. Ruiz M., G. Sakai, A. Cornet, K. Shimanoe, J. R. Morante, N. Yamazoe, Sens. Act. B, 93, 2003, 509.
6. Liu H.-M., Ch.-H. Keng, Ch.-Y. Tung, Nanostr. Mater., 9, 1997, 747.
7. Yan Y., S. R. Chaudhuri, A. Sarkar, J. Amer. Ceram. Soc., 79, 1996, 1061.
8. Zhai J., T. Yang, L. Zhang, X. Yao, Ceram. Int., 25, 1999, 667.
9. Brinker C. J., M. S. Harrington, Sol. Energy Mater. Sol. Cells 5, 1981, 159.
10. Vicente G. S., A. Morales, M. T. Gutierrez, Thin Solid Films 391, 2001, 133
11. Fan Q., B. McQuillin, A. K. Ray, M. L. Turner, J. Phys. D, Appl. Phys., 33, 2000, 2683
12. Kim K., H. Kim, J. Eur. Ceram. Soc. 23, 2003, 833

13. Nagpal V., R. Davis, S. Desu, J. Mater. Res.,10, 1995, 3068.
14. Habibi M. H., M. Nasr –Estafani, T.A. Egerton, J. Mater. Sci. 42, 2007,6027
15. Kuznetsova I. N., V. Blaskov, I. Stambolova, L. Znaidi, A. Kanaev, Mater. Lett. 59, 2005, 3820
16. P. Peshev, I. Stambolova, S. Vassilev, P. Stefanov, V. Blaskov, K. Starbova, N. Starbov, Mater Sci. Eng. B 97,2003, 106.
17. I. Stambolova, V. Blaskov, S. Vassilev, M. Shipochka, C. Dushkin, J Alloys Comp. 489,2010, 257.
18. Augugliaro V., C. Baiocchi, A.B. Prevot, E. Garcia-Lopez, V. Loddo, S. Malato, G. Marci, L. Palisano, M. Pazzi, E. Pramauro, Chemosphere, 49, 2002, 1223
19. Chong M. N., B. Jin, Ch. W. K. Chow, Ch. Saint, Water Research 44, 2010, 2997.

THERMODYNAMIC DESCRIPTION OF THE Cu-Mg-Sn SYSTEM AT THE Cu-Mg SIDE

*J. Miettinen**, *G. Vassilev***

** Aalto University, School of Chemical Technology,
Vuorimiehentie 2K, Fi-00076, Espoo, Finland*

*** University of Plovdiv, Faculty of Chemistry, 24 Tsar Asen str.,
4000 Plovdiv, Bulgaria*

ABSTRACT

Thermodynamic description of the Cu-Mg-Sn system at its Cu-Mg side is presented. The thermodynamic parameters of the binary sub-systems, Cu-Mg, Cu-Sn and Mg-Sn, are taken from the earlier CALPHAD-type assessments. The treatment of the Mg-Sn phases was somewhat changed. The adjustable parameters of the Cu-Mg-Sn system are optimized in this work. For this purpose experimental thermodynamic and phase equilibrium data were used and compared to calculated quantities.

Key words: *Thermodynamic description, Cu-Mg-Sn system, Phase diagrams*

INTRODUCTION

This study continues the recently started work for the development of a thermodynamic database for technically important copper alloys [1, 2]. Namely, thermodynamic description is presented for the ternary Cu-Mg-Sn system at its Cu-Mg side. Thermodynamic data are optimized for the

ternary system using the earlier assessed data of Cu-Mg [3], Cu-Sn [4] and Mg-Sn [5] (partially reassessed in this study), and applying the experimental thermodynamic and phase equilibrium data from the literature.

PHASES AND MODELS

In this work the optimizations of Coughanowr et al. [3], Miettinen [4], and Morioka and Hasebe [5] were retained for the Cu-Mg, Cu-Sn and Mg-Sn systems, respectively. The phase diagram Mg-Sn, however, was not represented so well, as the hcp solubility was somewhat too high and the melting point of Mg₂Sn was somewhat too low in regard to the measured values. Therefore, both the hcp and the Mg₂Sn parameters were modified slightly in this work, whereas the liquid state parameters were adopted from [5] as such. In the newly optimized Mg-Sn diagram, the liquid+Mg₂Sn region is worse established than by [5] but the improved agreement with the higher melting point value of Mg₂Sn [6] was preferred as it is so clearly supported by the experimental study on the ternary Cu-Mg-Sn system of Tesluk [7].

The phase equilibria of the Cu-Mg-Sn system have been reviewed by Chang et al. [8]. In the present Cu-Mg-Sn description, the following phases are considered: liquid, fcc, bcc, hcp (A3), gamma (γ), Cu₂Mg (Laves C15), CuMg₂, Cu₄₁Sn₁₁ (δ), Cu₃Sn (ϵ), Mg₂Sn, Cu₄MgSn (T₁) and CuMgSn (T₂). The disordered solution phases, i.e., liquid, fcc, bcc and hcp, and the ordered gamma phase (treated as a disordered solution phase by Miettinen [4, 9]), are described with the substitutional solution model. The fcc and hcp (A3) solid solutions contain mainly copper and magnesium, respectively. The bcc and gamma phases (γ) are copper-rich and originate from the binary Cu-Sn system. The first one (bcc) contains around 15 at. % Sn, while in the second the tin content varies from around 17 to approximately 27 at. % Sn.

The Cu₂Mg phase extending to the ternary system is described with the sublattice model and the rest of the phases, CuMg₂, Cu₄₁Sn₁₁, Cu₃Sn, Mg₂Sn, Cu₄MgSn and CuMgSn, are treated as stoichiometric phases.

The substitutional solution model was applied for the description of the molar Gibbs energy (G_m^ϕ) of the solution phases of the Cu-Mg-Sn system (i.e. liquid, fcc, bcc, hcp). The gamma phase (γ) was treated with this model as well.

The Gibbs energy (${}^oG_i^\phi$) of the pure component i in a phase ϕ is expressed relative to the enthalpy of the component in its stable phase at 298.15 K [10].

L_{ij}^ϕ is a binary parameter describing the interaction between components i and j in phase ϕ , and $L_{Cu,Mg,Sn}^\phi$ is a ternary interaction parameter of phase ϕ . For these parameters, ${}^oG_i^\phi$ is a function of temperature, and L_{ij}^ϕ and $L_{Cu,Mg,Sn}^\phi$ can be functions of temperature and composition.

The Cu_2Mg having ternary solubility is described as a semi-stoichiometric phase as $(Cu, Sn)_2Mg$ using the sublattice model. The Gibbs energy (per mol of formula unit) of that phase becomes

$$G_m^\phi = y_{Cu}^\phi {}^oG_{Cu:Mg}^\phi + y_{Sn}^\phi {}^oG_{Sn:Mg}^\phi + 2RT(y_{Cu}^\phi \ln y_{Cu}^\phi + y_{Sn}^\phi \ln y_{Sn}^\phi) + y_{Cu}^\phi y_{Sn}^\phi L_{Cu,Sn:Mg}^\phi \quad (1)$$

where ${}^oG_{Me:Mg}^\phi$ is the Gibbs energy of pure Me_2Mg ($Me=Cu,Sn$), y_{Me}^ϕ is the site fraction of Me atoms occupying the first sublattice, and $L_{Cu,Sn:Mg}^\phi$ is a parameter describing the interaction between Cu and Sn atoms in that sublattice. For copper and tin, the site fractions are expressed with mole fractions x_i as $y_i^\phi = x_i^\phi / (x_{Cu}^\phi + x_{Sn}^\phi)$, whereas for magnesium, $y_{Mg}^\phi = 3x_{Mg}^\phi = 1$.

The binary $CuMg_2$, $Cu_{41}Sn_{11}$, Cu_3Sn , Mg_2Sn phases and the ternary Cu_4MgSn and $CuMgSn$ phases are treated as stoichiometric phases. The Gibbs energy of formation of the binary compounds is expressed as

$${}^oG_{A:B}^\phi = a {}^oG_A^\alpha + b {}^oG_B^\beta + A + BT \quad (2)$$

where a and b are stoichiometric coefficients and ${}^oG_i^\phi$ is the Gibbs energy of the pure component i in its stable phase at 298.15K [10]. Similarly, for the ternary compounds, Cu_4MgSn and $CuMgSn$, the Gibbs energy of formation becomes.

$${}^oG_{Cu:Mg:Sn}^\phi = a {}^oG_{Cu}^{fcc} + b {}^oG_{Mg}^{hcp} + c {}^oG_{Sn}^{bct} + A + BT \quad (3)$$

RESULTS AND DISCUSSION

Chang et al. [8] have reviewed the experimental studies on the $Cu-Mg-Sn$ systems before 1979. Later studies seem not be available. Table 1 shows the experimental information [7, 8, 11–14] selected in the present optimization.

The thermodynamic description of the Cu-Mg-Sn system is presented in Table 2. The parameters marked with a reference code [2 – 5, 15 – 17] were adopted from the earlier SGTE assessments and those marked with *O or *E were optimized or estimated in the present study. By *O, the parameter was optimized using the experimental data of literature (Table 2) and by *E, the parameter was estimated arbitrarily, by applying no experimental data (since not available). The thermodynamic data for the pure components are given by [10] except for the gamma phase (see Table 2).

Table 1. *Experimental information applied in the optimization process*

Experimental information type	Ref.
Primary surfaces	
Three isopleths, at sections Cu-MgSn, Cu ₂ Mg-Mg ₂ Sn and CuMg ₂ -Mg ₂ Sn	[8]
Three isopleths, at Mg:Sn= 3.70, Mg:Sn= 0.41, 4% Sn (composition in weight pct)	[6]
Two isotherms, at 670 and 400°C	[11, 12]
	[13, 14]

In the following, calculated results are compared with the original experimental data to demonstrate the successfulness of the optimization. All calculations were carried out with the ThermoCalc software [18].

Calculated monovariant curves of primary solidification are presented in Fig. 1. They agree reasonably well with the curves assessed tentatively by Chang et al. [8].

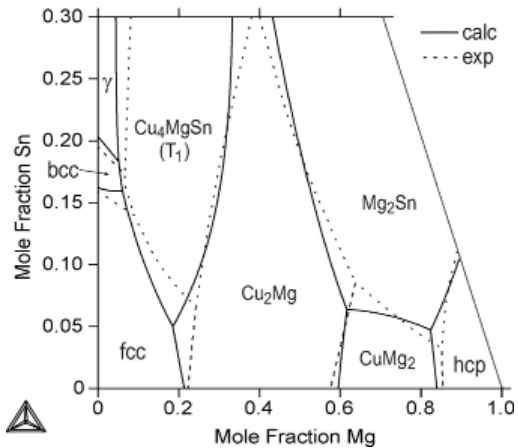


Figure 1. *Calculated primary (i.e. liquidus) surfaces (solid lines) at the Cu-Mg side of the Cu-Mg-Sn system, together with experimentally determined regions [8] (dashed)*

Fig. 2 shows a calculated isopleth, at a sections Cu-MgSn with ratio Mg:Sn=3.70 and Mg:Sn=0.41, and at a constant tin content of 4 wt%. The agreement with the experimental data [11, 12, 7] can be considered very satisfying. Finally, Fig. 3 shows a calculated isothermal section of the system, at temperatures of 670 °C. The results agree reasonably well with the observations of [14]. At 670 °C, the calculated fcc solubility at low tin contents was higher than indicated by the experimental data (see the three black triangles located in the fcc region in Fig. 3). When treating Cu_4MgSn (T_1) as a stoichiometric phase, one can improve the agreement only by introducing a strong composition dependent ternary interaction parameter for the fcc phase. Such a treatment, however, is not justified with the present tiny amount of experimental data.

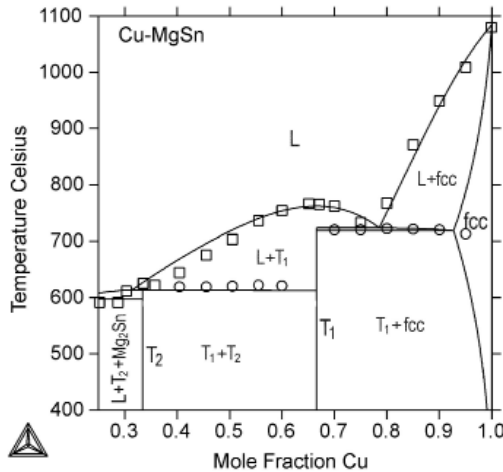


Figure 2. Calculated isopleth at the Cu-MgSn section together with experimental data [7]. The compounds Cu_4MgSn and CuMgSn are denoted as T_1 and T_2 , respectively. The symbol (\square) stays for an experimental liquidus point and the symbol (o) – for a thermal arrest.

No experimental thermodynamic data were available for the ternary system except for the enthalpy of formation of two ternary samples containing 33.33 at% Mg with 8.4 and 12.1 at% Sn. For these alloys, Predel and Ruge [19] gave values -10.3 and -13.5 kJ/mol, which are lower (less negative) than the calculated values, -14.2 and -15.2 kJ/mol.

Figure 3. Calculated isothermal section in the copper-rich part of the Cu-Mg-Sn system at 670° C, together with experimental data from Phillips and Ainsworth [14].

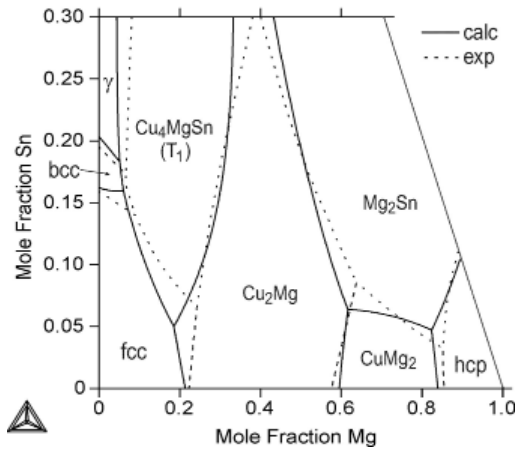


Table 2. Thermodynamic adjustable parameters for the Cu-Mg-Sn system obtained from the literature (reference code) and optimized (*O) or estimated (*E) in this study. All values are in J/mol. T is the absolute temperature (K). The thermodynamic data of the pure components are taken from Dinsdale [10] unless a parameter expression is shown in the Table.

Phase	Reference
liquid (1 sublattice, sites: 1, constituents: Cu,Mg,Sn) $L_{Cu,Mg}^L = (-35430+4.227T) + (-7454)(x_{Cu}-x_{Mg})$ $L_{Cu,Sn}^L = (-8124-6.553T) + (-23970+7.037T)(x_{Cu}-x_{Sn})$ $+ (-25124+13.566T)(x_{Cu}-x_{Sn})^2 + (-10213+10.042T)(x_{Cu}-x_{Sn})^3$ $L_{Mg,Sn}^L = (-49353+14.835T) + (-17571+7.906T)(x_{Mg}-x_{Sn})$ $L_{Cu,Mg,Sn}^L = (-10000+20T)x_{Cu} + (-10000+20T)x_{Mg}$ $+ (-50000+20T)x_{Sn}$	[3] [4] [5] *O
fcc (1 sublattice, sites: 1, constituents: Cu,Mg,Sn) $L_{Cu,Mg}^{fcc} = -23487+8.26T$ $L_{Cu,Sn}^{fcc} = (-10672-1.484T) + (-15331+6.954T)(x_{Cu}-x_{Sn})$ $L_{Mg,Sn}^{fcc} = L_{Mg,Sn}^{hcp}$ (fcc not stable in binary Mg-Sn)	[3] [15] *E
bcc (1 sublattice, sites: 1, constituents: Cu,Mg,Sn) $L_{Cu,Mg}^{bcc} = -6500$ (bcc not stable in binary Cu-Mg) $L_{Cu,Sn}^{bcc} = (-44822+51.216T) + (-6877-56.427T)(x_{Cu}-x_{Sn})$ $L_{Mg,Sn}^{bcc} = L_{Mg,Sn}^{hcp}$ (bcc not stable in binary Mg-Sn)	[16] [15] *E

<p>hcp (A3) (1 sublattice, sites: 1, constituents: Cu,Mg,Sn) $L_{Cu,Mg}^{hcp} = 10000$ [2] $L_{Cu,Sn}^{hcp} = (-26799-0.732T) + (-28065-0.029T)(x_{Cu}-x_{Sn})$ [15] $L_{Mg,Sn}^{hcp} = (-24000) + (-20000)(x_{Mg}-x_{Sn})$ *O</p>	
<p>Cu₃Sn (ε) (2 sublattices, sites: 0.75:0.25, constituents: Cu:Sn) ${}^{\circ}G_{Cu,Sn}^{\epsilon} = 0.75{}^{\circ}G_{Cu}^{fcc} + 0.25{}^{\circ}G_{Sn}^{bet} + (-8218-0.18T)$ [17]</p>	
<p>gamma (γ) (1 sublattice, sites: 1, constituents: Cu, Mg, Sn) ${}^{\circ}G_{Cu}^{\gamma} = {}^{\circ}G_{Cu}^{fcc} + 10$ [4] ${}^{\circ}G_{Mg}^{\gamma} = {}^{\circ}G_{Mg}^{hcp} + 10$ [2] ${}^{\circ}G_{Sn}^{\gamma} = {}^{\circ}G_{Sn}^{bet} + 10$ [4] $L_{Cu,Mg}^{\gamma} = 50000$ [2] $L_{Cu,Sn}^{\gamma} = (40039-32.912T) + (-232532+135.367T)(x_{Cu}-x_{Sn})$ $+ (210180-129.043T)(x_{Cu}-x_{Sn})^2$ [4] $L_{Mg,Sn}^{\gamma} = 50000$ (gamma not stable in binary Mg-Sn) *E $L_{Cu,Mg,Sn}^{\gamma} = -60000$ *O</p>	
<p>Cu₂Mg (C15) (2 sublattices, sites: 0.6667:0.3333, constituents: Cu,Sn:Mg) ${}^{\circ}G_{Cu,Mg}^{C15} = 0.6667{}^{\circ}G_{Cu}^{fcc} + 0.3333{}^{\circ}G_{Mg}^{hcp}$ $+ (-9270-42.588T+6.6537T \ln T-0.005732T^2)$ [2] ${}^{\circ}G_{Sn,Mg}^{C15} = 0.6667{}^{\circ}G_{Sn}^{bet} + 0.3333{}^{\circ}G_{Mg}^{hcp} + (0)$ *O $L_{Cu,Sn,Mg}^{C15} = -43500+18T$ *O</p>	
<p>CuMg₂ (2 sublattices, sites: 0.3333:0.6667, constituents: Cu:Mg) ${}^{\circ}G_{Cu,Mg}^{CuMg2} = 0.3333{}^{\circ}G_{Cu}^{fcc} + 0.6667{}^{\circ}G_{Mg}^{hcp} + (-9540+0.862T)$ [3]</p>	
<p>Cu₄₁Sn₁₁ (δ) (2 sublattices, sites: 0.788:0.212, constituents: Cu:Sn) ${}^{\circ}G_{Cu,Sn}^{\delta} = 0.788{}^{\circ}G_{Cu}^{fcc} + 0.212{}^{\circ}G_{Sn}^{bet} + (-6323.5-1.2808T)$ [15]</p>	
<p>Mg₂Sn (2 sublattices, sites: 0.6667:0.3333, constituents: Mg:Sn) ${}^{\circ}G_{Mg,Sn}^{Mg2Sn} = 0.6667{}^{\circ}G_{Mg}^{hcp} + 0.3333{}^{\circ}G_{Sn}^{bet} + (-26200+9T)$ *O</p>	
<p>Cu₄MgSn (T₁) (3 sublattices, sites: 0.666:0.167:0.167, constituents: Cu:Mg:Sn) ${}^{\circ}G_{Cu,Mg,Sn}^{T1} = 0.666{}^{\circ}G_{Cu}^{fcc} + 0.167{}^{\circ}G_{Mg}^{hcp} + 0.167{}^{\circ}G_{Sn}^{bet}$ $+ (-19600+5T)$ *O</p>	
<p>CuMgSn (T₂) (3 sublattices, sites: 0.334:0.333:0.333, constituents: Cu:Mg:Sn) ${}^{\circ}G_{Cu,Mg,Sn}^{T2} = 0.334{}^{\circ}G_{Cu}^{fcc} + 0.333{}^{\circ}G_{Mg}^{hcp} + 0.333{}^{\circ}G_{Sn}^{bet}$ $+ (-26400+10T)$ *O</p>	

On the other hand, the enthalpy of formation value of [19] for the binary Cu_2Mg is also quite low, i.e., -8.1 kJ/mol, whereas two other studies [20, 21] suggest values between -11 and -12 kJ/mol, which agree better with the calculated value of -10.8 kJ/mol. Consequently, the measurements of [19] may suffer from a systematic error. Shifting the dataset of [19] with the measurements of [20, 21] would improve the agreement clearly.

CONCLUSIONS

A thermodynamic description was optimized for the ternary Cu-Mg-Sn system applying the experimental phase equilibrium data of the literature. In this description, twelve phases, i.e., liquid, fcc, bcc, hcp, gamma, Cu_2Mg (Laves C15), CuMg_2 , $\text{Cu}_{41}\text{Sn}_{11}$ (δ), Cu_3Sn (ϵ), Mg_2Sn , Cu_4MgSn (T_1) and CuMgSn (T_2), were considered. The disordered solution phases, i.e., liquid, fcc, bcc and hcp, and the ordered gamma phase were described with the substitutional solution model, while the semi-stoichiometric Cu_2Mg phase was described with the sublattice model. The rest of the phases, the near-stoichiometric compounds, were treated as stoichiometric phases. In the optimization, the unary and binary thermodynamic data of the systems were taken from previous binary descriptions. Good or at least reasonable correlation was obtained between the calculated and the experimental thermodynamic and phase equilibrium data.

ACKNOWLEDGEMENTS

Financial support of Luvata Pori Oy and the Technology Development Center (TEKES, Finland) during the ADEV project (development of method for controlling structures in copper alloys) is gratefully acknowledged by J. Miettinen.

REFERENCES

1. Miettinen, J., Thermodynamic description of the Cu-Ni-Si system in the copper-rich corner above 700°C, *CALPHAD*, 2005, 29, 212–22.
2. Miettinen, J., Thermodynamic description of the Cu-Mg-Ni and Cu-Mg-Zn systems, *CALPHAD*, 2008, 32, 389–98.
3. Coughanowr, C.; Ansara, I.; Luoma, R.; Hämäläinen, M.; Lukas, H. L., Assessment of the Cu-Mg system, *Z. Metallkd.*, 1991, 82, 574–82.
4. Miettinen, J., Thermodynamic description of the Cu-Al-Sn system in the copper-rich corner, *Metall. Mater. Trans. A*, 2002, 33A, 1639–48.
5. Morioka, S.; Hasebe M., Thermodynamic constraints to describe Gibbs energies for binary alloys, *J. Phase Equilibria*, 1999, 20, 244–57.
6. Massalski, T.B.; Murray, J.L.; Bennett L.H.; Baker H., *Binary Alloy Phase Diagrams*, ASM International, 1986.
7. Tesluk, M.Yu., A study of the Mg-Cu-Sn ternary system, *Zb. Rob. Aspir. L'viv Derzh. Univ.* 1963, 42, 5–17.
8. Chang, Y.A.; Neumann, J.P.; Mikula, A. and Goldberg, D.; *The Metallurgy of Copper, Phase Diagrams and Thermodynamic Properties of Ternary Copper-Metal Systems*, INCRA Monograph VI, 1979.
9. Miettinen, J., Thermodynamic description of the Cu-Al-Zn and Cu-Sn-Zn systems in the copper-rich corner, *CALPHAD*, 2002, 26, 119–39.
10. Dinsdale, A.T., SGTE Data for Pure Elements, *CALPHAD*, 1991, 15, 317–425.
11. Venturello, O.; Fornaseri, M., Leghe rame-stagno-magnesio ricche in rame, *Met. Ital.* 1937, 29, 213–23.
12. von Dahl O., Über die Structur und die Vergütbarkeit der Cu-reichen Cu-Mg – und Cu-Mg-Sn – Legierungen, *Wiss. Veröf. Siemens-Konzern*, 1939, 6, 222–35.
13. Tesluk, M.Yu.; Gladyshevskii, E.I., Solubility of tin in the intermetallic phase CuMg₂, *Visn. L'viv Derzh. Univ., Ser. Khim.* 1955, 34, 84–96.

14. Phillips D. L.; Ainsworth, P. A., Eine vergütbare Zinn-Magnesium-Bronze, *Metall.*, 1969, 23, 804–15.
15. Shim, J-H.; Oh, C-S.; Lee, B-J.; Lee, D. N., Thermodynamic Assessment of the Cu-Sn System, *Z. Metallkd.*, 1996, 87, 205–12.
16. Liang, P.; Seifert, H. J.; Lukas, H. L.; Ghosh, G.; Effenberg, G.; Aldinger, F., Thermod. Modelling of the Cu-Mg-Zn Ternary System, *CALPHAD*, 1998, 22, 527–44.
17. J. Miettinen, Thermodynamic description of the Cu-Ni-Sn system at the Cu-Ni side, *CALPHAD*, 2003, 27, 309–18.
18. Andersson, J-O.; Helander, T.; Höglund, L.; Shi, P.; Sundman, B., Thermo-Calc and DICTRA, computational tools for mater. science, *CALPHAD* 2002, 26, 273–312.
19. Predel, B.; Ruge, H., About the Bond Relations in Laves Phases, *Mater. Sci. Eng.*, 1972, 9, 333–41.
20. King, R. C.; Kleppa, O.J., A Thermochemical Study of Some Selected Laves Phases, *Acta Metall.*, 1964, 12, 87–97.
21. Predel, B.; Bencker, H.; Vogelbein, W.; Ellner, M., Formation Enthalpies of Ternary Laves Phases of the $MgCu_2$ -Type in the System $MgCu_2$ - $MgZn_2$, *J. Solid State Chem.* 1979, 28, 245–57.

ЕЛЕКТРОХИМИЯ НА МИОГЛОБИН ХЕМИСОРБИРАН ВЪРХУ ПОЗЛАТЕН ГРАФИТ

Д. Георгиева¹, Т. Додевска², Ел. Хорозова¹, Н. Димчева¹

*¹ катедра Физикохимия, ПУ „П. Хилендарски“,
ул. „Цар Асен“ № 24, гр. Пловдив 4000;
E-mail: ninadd@uni-plovdiv.bg*

*² катедра Неорганична химия и Физикохимия, УХТ – гр. Пловдив,
бул. „Марица“ №26, Пловдив 4002;
E-mail: dodevska@mail.bg*

ABSTRACT

Redox protein myoglobin was immobilized on gold-plated graphite through self-assembly process. Its redox behavior was probed with cyclic voltammetry. The experimental results suggest irreversible binding of the protein to the gold layer due to the interaction of sulfur-containing amino-acid cysteine from the protein shelf with gold: $2HS-R + 2Au \rightarrow 2Au-S-R + H_2$. In addition to that, two separate peaks appear on the cathodic part of the cyclic voltammetric curve one of which being assigned to the redox transformation of heme-prosthetic group. The efficiency of the electron exchange between the chemisorbed myoglobin was found to be much bigger as compared to the one of physically adsorbed myoglobin. It was hypothesized that upon chemisorption, most of the myoglobin molecules bind to the gold layer in an orientation superior for direct electron communication with the underlying electrode surface.

The immobilized protein was found capable to electrocatalytically reduce H_2O_2 and Cl_3CCOOH in neutral aqueous solutions at room temperature. The electroreduction of Cl_3CCOOH was found to occur at much lower overpotentials compared to bare graphite electrode.

Ключови думи: *миоглобин, хемисорбция, директен електронен пренос, позлатен графитов електрод*

ВЪВЕДЕНИЕ

Целенасоченото изграждане на сложна електродна архитектура чрез структурирането на електродни повърхности представлява принципно нов подход при имобилизиране на биокомпоненти, целящ постигане на директна електрическа комуникация между биокатализатор и електрод посредством: 1) скъсяване на дистанцията между електродната повърхност и активния център на първия; и 2) ориентиране на биокатализатора в благоприятна за директен електронен пренос-DET конформация. В тази връзка, модифицирането на електродни материали с нано-частици от ZrO_2 [1], със Au наночастици [2–4], въглеродни нанотръбички (CNT) [5–8] и титанови нанотръбички (TiNT) [9], предхождащо имобилизацията на миоглобина, във всички случаи е довело до наличие на директна биоелектрокатализа [10,11]. Възможностите на тези биоелектрокаталитични системи се определят от уникалните свойства на наночастиците. Те се отличават с голямо съотношение повърхност/обем, предоставят стабилна повърхност за ориентирана адсорбция на биомолекулите при запазване на биологичната им активност. В много от случаите, самите наночастици представляват своеобразни нано-проводници, улесняващи електронния обмен между електрода и протеина, които предоставят възможност размерът и повърхностната им морфология да бъдат контролирани чрез вариране условията на получаването им. Това мотивира изследванията ни върху електрохимичното поведение на миоглобин, имобилизиран върху позлатен графит.

ЕКСПЕРИМЕНТАЛНА ЧАСТ

В настоящата работа беше използван миоглобин от конски сърдечен мускул (horse heartmyoglobine: Fluka Biochemika). Въглероден материал – спектрално-чист графит във вид на пръчки с диаметър 0,5 см

и дължина 8–10 см с надлъжна тефлонова изолация, беше използван като основа за ензимния електрод.

H_2O_2 и химикалите за приготвяне на буферните разтвори ($\text{K}_2\text{HPO}_4 \cdot 12\text{H}_2\text{O}$, лимонена киселина, конц. H_3PO_4 и Tris (hydroxymethyl – aminomethane), бяха закупени от Fluka. Разтвори на трихлороцетна киселина Cl_3CCOOH със спецификации чист за анализ (чза) и изходна концентрация 0,56 М бяха използвани като моделни нетипични субстрати на миоглобина, без допълнителна обработка. Останалите реактиви бяха с чистота над 98 % или със спецификация „спектрално чисти“ (Fluka) и не бяха подлагани на допълнителна обработка преди употреба. При получаването на водни и буферни разтвори беше използвана двойно дестилирана вода. Фосфатно-цитратен буфер с неутрално рН (7,0) и концентрация 0,1 М беше използван като работна среда, докато 0,1 М трис-буфер, рН= 7,0 се използваше за приготвянето на ензимните разтвори. Киселинността им беше контролирана с рН-метър Hanna Instruments, рН 211.

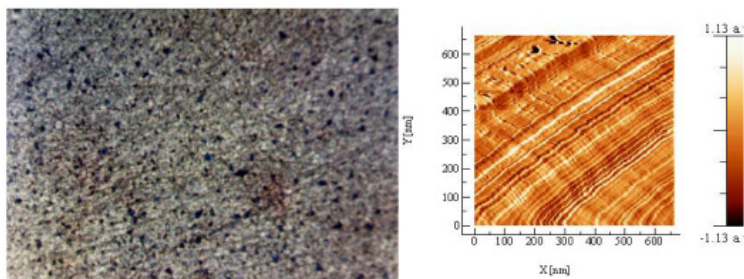
Стандартна, триелектродна стъклена клетка с неразделени електродни пространства и работен обем 10–20 cm^3 , сравнителен електрод – Ag / AgCl, 3 М KCl спомагателен електрод – платинов проводник и работен електрод от спектрално-чист графит, беше използвана при всички електрохимични изследвания. Измерванията бяха проведени с електрохимична работна станция Palm Sens с компютърен контрол и софтуер PS Trace 2.13 (Palm InstrumentsBV, Холандия). Отлагането на тънки филми от злато (дебелина до 1–2 μm) беше извършвано чрез кратковременна електролиза ($t=10$ s) от 2%-ен разтвор на HAuCl_4 в 0.1 М HCl при потенциал – 155 mV (vs. Ag/AgCl, 3М KCl).

РЕЗУЛТАТИ И ОБСЪЖДАНЕ

1. Електрохимична активност на миоглобин, хемисорбиран върху позлатен графит

Върху микроскопските изображения (фиг. 1) се вижда, че при електрохимичното модифициране на графита на повърхността му се отлага тънък, но плътен слой от злато, който повтаря релефа на носителя с всичките му структурни дефекти. Атомно-силовото микроскопско изображение на модифицирания графит свидетелства, че при модифицирането се формират 3D структури от злато с височина до около 100

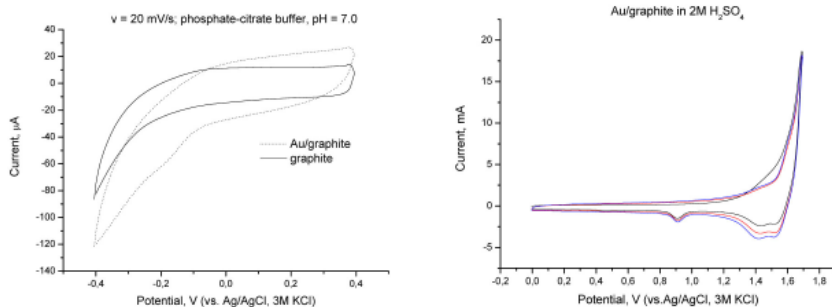
nm. Отлагането на тънък златен филм върху графита променя и вида на цикличните волтампереграми на електрода, заснети във фонов електролит ФЦБ, рН 7,0 (фиг. 2). Цикличните волтамперни криви на позлатения графитов електрод (фиг. 2, ляво) свидетелстват за по-развита електродна повърхност от тази на същия електрод, но преди модификацията. Тези резултати са в унисон с наблюденията от микроскопските изследвания – образуването на микро и нано-структури води до увеличаване на повърхността на електродите.



Фигура 1. *Ляво: Микроскопско изображение на филма от злато отложен потенциостатично върху графит при потенциал – 155 mV (vs. Ag/AgCl) за 10 s (металографски микроскоп, x 250); Дясно: 3D – топология на тънък филм злато отложен върху графит изследвана с AFM.*

Физичната и химичната сорбция (хемисорбция, при която енергията на връзките между сорбента и сорбата е от порядъка на енергията на химична връзка), са двата метода за имобилизация, при които се запазва напълно или в значителна степен каталитичната активност на биокатализатора като при тях в най-голяма степен се запазва както каталитичната им активност, така и пространствена конфигурация на молекулата най-близка до нативната. Освен това, хемисорбцията предлага и допълнително предимство – възможността обемистите протеинови глобули да се свързват винаги чрез точно определен фрагмент от макромолекулата си, като по този начин се постига точно определена еднотипна пространствена ориентация на биокатализатора. В тази връзка, хемисорбирането на миоглобина върху позлатен графит представлява един от най-удачните и прости в препаративно отношение подходи, при който се очаква запазване на каталитичната му активност

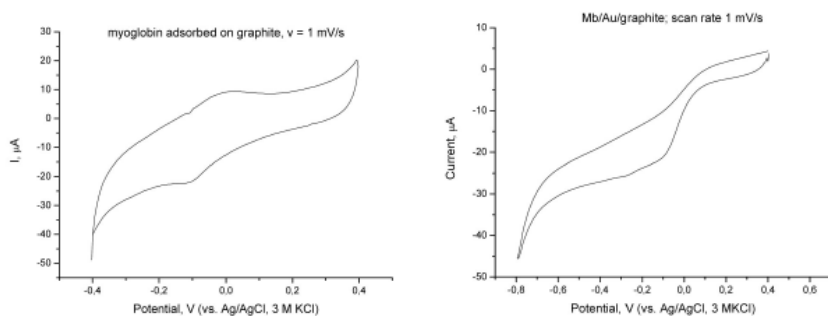
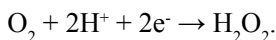
в значителна степен и за дълъг период от време. При предварителни експерименти беше установено, че хемисорбцията му върху позлатен графитов електрод завършва напълно за около 20 ч, и че процесът протича само върху предварително почистен електрохимично и промит с дестилирана вода електрод, който не е влизал в досег с въздух или буферни разтвори. В случаите, когато електродната повърхност е замърсена от адсорбирани газове или разтвори на соли, хемисорбцията на протеина или протича в незначителна степен, или изобщо не се наблюдава. Липсата или проявата на каталитичната активност при добавяне на водороден пероксид (т. е. отклика на ензимния електрод при добавяне на порции субстрат) беше приет като индикатор за степента на протичане на сорбцията.



Фигура 2. Ляво: Циклични волтамперни криви на спектрално чист графит (черно) и на графит с отложен тънък златен филм (сиво, пунктир) фонов електролит фосфатно-цитратен буфер, pH 7,0; скорост на сканиране $20 \text{ mV}\cdot\text{s}^{-1}$; Ag/AgCl, 3M KCl; Дясно: електрохимично почистване: първите три циклични волтамперни криви на графит с отложен тънък златен филм в $2\text{M H}_2\text{SO}_4$; скорост на сканиране $100 \text{ mV}\cdot\text{s}^{-1}$; Ag/AgCl, 3M KCl.

На фиг. 3 са сравнени циклични волтамперни криви на миоглобин, адсорбиран върху немодифициран и върху модифициран със златни отложения графит след електрохимично почистване на златния слой при много ниски скорости на изменение на потенциала. На показаните криви се наблюдават добре изразени максимуми както върху анодния, така и върху катодния ход на кривите, чиито потенциали на пика се изменят с изменение скоростта на сканиране. Волтамперограмите на

адсорбираня върху модифициран графит миоглобин се отличават с по-остри, ясно изразени максимуми (фиг. 3), в сравнение с кривите на миоглобин, адсорбиран върху немодифициран графит. С увеличаване скоростта на сканиране катодните пикове на редукция на адсорбираня върху модифициран графит миоглобин се изместват в отрицателна посока, както е и върху немодифициран графит. Видът на кривите подсказва, обаче, че процесите в случая са необратими. Анализът на данните показва, че окислително-редукционното превръщане на хемисорбираня върху модифицирания графит миоглобин протича с пренос на един електрон и е в резултат от протичането на реакцията:



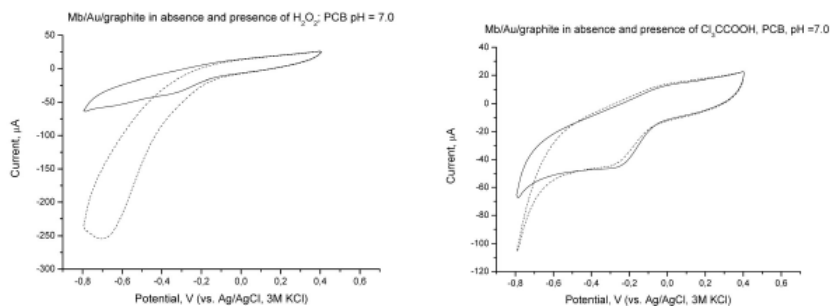
Фигура 3. Ляво: Циклични волтампетри криви на графитов електрод с адсорбиран миоглобин (ляво) и на миоглобин хемисорбиран върху позлатен графит (дясно) във фонов електролит фосфатно-цитратен буфер, pH 7,0; скорост на сканиране $1 \text{ mV}\cdot\text{s}^{-1}$; Ag/AgCl, 3M KCl.

Възможността да се регистрират продължително възпроизводими циклични волтампетри криви свидетелства, че миоглобинът се адсорбира необратимо върху модифициран със злато графит. Златните частици, отличаващи се с висока биосъвместимост, не само улесняват електронния трансфер между протеиновите молекули и електродната повърхност, но и предполагат образуването на здрава хемисорбиционна връзка между сярна-съдържащите аминокиселини от белтъчната глобула на миоглобина и модифицирания графит, съгласно уравнението: $2\text{HS-R} + 2\text{Au} \rightarrow 2\text{Au-S-R} + \text{H}_2$. При скорости на сканиране над 10 mV/s

върху катодния ход на волтамперограмите се наблюдава появата на втори максимум, който има формален редокс-потенциал $E = -350 \pm 10$ mV и не се наблюдава върху немодифициран графит. Потенциалът му практически не се влияе от скоростта на сканиране и по всяка вероятност не се отнася до хемисорбиран миоглобин.

2. Електрокаталитична активност на хемисорбиран миоглобин

Каталитичната активност на адсорбиран миоглобин върху модифициран със златни наночастици графит беше изследвана при електроредукция на H_2O_2 и на трихлороцетна киселина (фиг.4). Сравнението на цикличните волтамперни криви на електрода с хемисорбиран миоглобин (фиг. 4) в отсъствие (плътна) и в присъствие на висока концентрация на водороден пероксид (пунктир) доказват, че електрохимичната редукция на пероксида започва още при потенциал около 0 V, като формата на кривите е характерна за практически необратими електрохимични реакции. Въз основа на тези криви беше заключено, че потенциали в диапазона от 0 до $-0,350$ V са подходящи за амперометрично определяне на пероксида в неутрална водна среда. При тези експериментални условия електроредукцията му протича със значителна скорост и не протичат странични реакции, които да влияят върху електродния сигнал.



Фигура 4. Циклични волтамперни криви на електрод от позлатен графит с хемисорбиран миоглобин: Ляво – в отсъствие (плътна) и в присъствие (пунктир) на водороден пероксид; Дясно – в отсъствие (плътна) и в присъствие (пунктир) на трихлороцетна к-на; фонов електролит фосфатно-цитратен буфер, pH 7,0; скорост на сканиране $50 \text{ mV}\cdot\text{s}^{-1}$; Ag/AgCl, 3M KCl.

Съществуват литературни данни, че имобилизираният върху различни електродни материали миоглобин е ефективен редокс-катализатор на електрохимичната редукция на трихлорооцетна киселина [12,13]. При това редукционният процес протича при свръхнапрежение, което е поне с 0,8 V по-ниско, отколкото върху електродния материал без имобилизиран протеин.

В тази връзка, с помощта на метода циклична волтамперометрия беше изследвано поведението на миоглобина, хемисорбиран върху позлатен графит в отсъствие и в присъствие на трихлорооцетна киселина (фиг. 4). От представената фигура е видно, че върху цикличната волтамперограма, заснета в присъствие на трихлорното органично съединение, при потенциали по-отрицателни от $-0,5$ V се наблюдава рязко нарастване на тока в отрицателна посока, характерно за протичане на редукционни процеси. При това, изменението на тока спрямо фоновия сигнал е пропорционално на концентрацията на добавената трихлорооцетна киселина (не е показано).

Изследването на стабилността на ензимния електрод, получен при хемисорбция на редокс-протеина миоглобин върху тънък златен филм, отложен върху графит показва, че електродът може да бъде използван до 14 дни след приготвянето му, като запазва над 40 % от първоначалната си активност, при условие, че се съхранява в буферен разтвор и при ниски температури. Дискутираните дотук експериментални резултати показват, че избраният метод за закрепване на редокс-протеина към електродната повърхност позволява многократното му използване и предлага много по-дълъг живот на имобилизирания биокомпонент в сравнение с физичната адсорбция при значително съхранение на каталитична активност.

БЛАГОДАРНОСТ

Авторите изказват благодарност за финансовата подкрепа на Националния фонд „Научни изследвания“ (договор ДВУ – 02/38) и на фонд „Научни изследвания“ към ПУ (тема НИ11-ХФ-007).

ЛИТЕРАТУРА

1. G. Zhao, F. J.–Ju, X.J.–Juan, C. H.–Yuan: *Electrochem. Commun.*, 7, 724–729 (2005).
2. S. Liu, H. Ju: *Electroanalysis*, 15, 1488–1493 (2003).
3. L. S Duan, Q. Xu, F. Xil, S. F.Wang: *Int. J. Electrochem. Sci*, 3, 118–124 (2008).
4. S. Zhao, K. Zhang, Y. Bai, W. Yang, Sun C.: *Bioelectrochem.*, 69, 158–163, (2006).
5. S. Zhang, W. Yang, Y. Niu, Y. Li, M. Zhang, Sun C.: *Anal. Bioanal. Chem.*, 384, 736–741, (2006).
6. P. Yanez–Sedeno, J. M. Pingarron: *Anal. Bioanal. Chem.* 382, 884–886 (2005).
7. W. Sun, X. Li, Y. Wang, X. Li, C. Zhao, K. Jiao: *Bioelectrochem.*, 75, 170–175 (2009).
8. M. G. Esplandiu, M. Pacios, L. Cydanek, J. Bartroli, M. del Valle: *Nanotechnology*, 20 (35), paper 355502 (2009).
9. A. Liu, M. Wei, I. Honma, H. Zhou, *Anal. Chem.* 77, 8068–8074 (2005).
10. G. K. Ahirwal, C. K. Mitra: *Sensors*, 9, 881 – 894 (2009).
11. A. Christenson, N. Dimcheva, E. Ferapontova, Lo Gorton, T. Ruzgas, L. Stoica, S. Shleev, A. Yaropolov, D. Haltrich, R. Thorneley, S. Aust: *Electroanalysis*, 16, 1074 (2004).
12. Y. Wang, J. Wu, T. R. Zhan, W. Sun, K. Jiao: *Sensor Letters* 7 (6), 1106–1112 (2009).
13. Yancai Li., Weiwei Yang, Yu Bai, Changqing Sun: *Electroanalysis* 18 (5) 499–506 (2006).

СИНТЕЗ НА ФЕРИТИ ОТ СИСТЕМАТА MeO-Fe₂O₃ (Me=Zn, Cd) И ИЗСЛЕДВАНЕ НА ТЯХНАТА РАЗТВОРИМОСТ В H₂SO₄

А. Пелтеков, Б. Боянов

*Катедра „Химична технология“, ПУ „Паисий Хилендарски“
ул. „Цар Асен“ 24, Пловдив, България*

ABSTRACT

Ferrites from the MeO-Fe₂O₃ system, where Me = Zn, Cd, were synthesized using a ceramic technology. Their composition, structure and properties were studied by chemical, X-ray diffraction analysis, DTA-TGA, Mössbauer spectroscopy. The solubility of the ferrites in diluted sulfuric acid solutions (7–14 vol.%) was studied using microwave treating. The experimental results show that the solubility degree of Zn and Cd using microwave heating is higher than the one obtained by heating and leaching. On the basis of the data obtained a conclusion can be made that CdFe₂O₄ is less stable than ZnFe₂O₄ using the both ways of leaching.

The solubility of the mix ferrite Zn_{0.5}Cd_{0.5}Fe₂O₄ as well as of samples of zinc cake where the zinc is mainly as ZnFe₂O₄ is investigated after mechanical activation and followed by high-temperature acid leaching. The results obtained show that the degree of Zn and Cd solubility from ferrites and zinc cake increase significantly after mechanical treatment comparing to the initial non-treated samples.

Key words: ferrites, zinc cake, microwave heating, leaching, mechanical activation

ВЪВЕДЕНИЕ

Добиваните цинкови руди са полиметални и получените от тях цинкови концентрати, освен Zn, съдържат различни примеси [1,2]. Във високотемпературните находища основният цинков минерал – сфалеритът съдържа предимно Fe, Co, Cu, In, Sn и Se. Примесите в нискотемпературните находища са предимно Cd, Ga, Ge, Hg, Tl и др. [3]. Освен това от рудите при флотацията в концентратите преминават определени количества Pb, Fe, SiO₂, Al₂O₃, CaO, MgO, Ni, As, Sb, Cl, F. В резултат на това при окислителното пържене в пещи с кипящ слой протичат твърдофазни взаимодействия между оксидите на цинка и другите цветни метали с Fe₂O₃ (получен при окислението на FeS₂, (Zn,Fe)S, CuFeS₂), вследствие на което се получават ферити [4–6]. Те са много стабилни и трудно разтворими съединения. Получаването основно на ZnFe₂O₄ води до намаляване степента на извличане на цинка и необходимост от допълнителна преработка на цинк съдържащия кек.

При стандартната хидрометалургична технология може да се постигне високо извличане на цинка само при концентрати с много ниско съдържание на желязо (под 2–3%). Най-често в производствената практика се използват концентрати с 6–7% Fe, при което 10–15% от цинка остава в неразтворения остатък от сяроокиселото извличане (цинковите или оловно-цинкови кекове). В резултат на изчерпване на богатите цинкови суровини с ниско съдържание на желязо понастоящем се налага преработката на цинкови концентрати със съдържание на желязо достигащо понякога 12–14% [1,2]. Количеството на получаваните кекове рязко нараства и те съдържат до 20% Zn и около 25% Fe. Това налага тяхната преработка, както поради икономически съображения, така и поради екологични изисквания [7,8]. Намаляването на прякото извличане на цинка и увеличеното количество на кековете водят до нарастване на производствените разходи и влошаване на технико-икономическите показатели на извличането, а оттам и на цялото цинково производство [9].

Конвенционалната хидрометалургична технология за извличане на цинка от сулфидни концентрати има съществени недостатъци по отношение степента на извличане на цинка, получаването на значителни количества цинков кек, отпадъци и др. През последните години за оптимизиране на схемата са проведени теоретични и практически изследвания, които в различна степен са намерили промишлена реализация.

Провеждането на високотемпературно и висококиселинно „мокро извличане“ повишава разтворимостта на цинковия ферит, но се повишава и концентрацията на желязо в разтворите и свързаните с това сериозни затруднения в следващата очистка и филтруване на пулпата [10]. В тази връзка са разработени и практически реализирани три варианта на технологично решение за утаяване на желязото – ярозитен, гьотитен и хематитен процес [7, 11,12]. В някои отношения ярозитният метод има по-големи предимства и се прилага в повече заводи за производство на цинк в света. Все още в практиката на цинковата хидрометалургия обаче няма еднозначен отговор за предпочитан избор на една от съвременните схеми.

Съществен технологичен проблем на заводите е повишеното съдържание на желязо в преработваните цинкови концентрати и получаването в процеса на пържене на неразтворим при стандартни условия цинков ферит ($ZnFe_2O_4$), и ниската степен на извличане на цинка [13,14]. Феритът, който свързва около 15% от общото количество цинк, остава практически инертен при нискокиселинни условия на извличане [15]. Това налага разработване на различни и търсене на нови методи, с цел максимално привеждане на феритния цинк в разтворима форма.

В тази връзка целта на настоящата разработка е да провери в лабораторни условия влиянието на два недостатъчно изследвани метода за повишаване разтворимостта на цинковия ферит (синтезиран и получен в промишлени условия) – микровълново нагриване и механична активация.

МАТЕРИАЛИ И МЕТОДИ

С цел изучаване поведението и свойствата на феритите, в лабораторни условия са синтезирани феритите $ZnFe_2O_4$, $CdFe_2O_4$, $Zn_{0.5}Cd_{0.5}Fe_2O_4$ при $1000^\circ C$ за 10 h с използване на керамичната технология. Керамичната технология [16,17], приложена към производството на ферити, се явява полезна за синтезирането на ферити със състав и свойства близки до получаваните в промишлени условия. Тяхната характеристика е извършена с използването на различни методи.

Рентгенофазовият анализ е проведен с апарат „TUR-M62“ с Брег-Брентано геометрия и с компютърно управление на гониометър HZG-3, Co-K α лъчение, стъпка на сканиране на спектъра 0.05° и с повишено

време за събиране на импулсите на всеки канал – 5 s. Фазовата идентификация е направена с помощта на базата от данни JCPDS (International Center for Diffraction Data, Alphabetical Indexes, Pennsylvania 19073–3273, sets 1–86, 1997).

Мьосбауеровите спектри са снети на електромеханичен спектрометър (Wissenschaftliche Elektronik GMBN, Germany), работещ в режим на постоянно ускорение при стайна температура. Като източник е използван $^{57}\text{Co}/\text{Cr}$ (Активност $\cong 10 \text{ mCi}$), стандарт – Fe. Експериментално полученият спектър е обработен на програма, работеща по метода на най-малките квадрати.

Диференциално-термичният анализ на пробите е извършен с помощта на дериватограф на унгарската фирма „МOM“ (Derivatograph Q), работещ в динамичен режим при следните условия: чувствителност на DTA – 0,5 mV, DTG – 1,0 mV, TG – 100 mg, скорост на нагриване $10^\circ/\text{min.}$, температура на нагриване – до 1000°C . Масата на всички проби е 100 mg. Работи се във въздушна атмосфера и керамичен тигел.

Проведено е изследване върху разтворимостта на феритите и на цинков кек с използване на микровълново нагриване (МН) и конвенционално нагриване (КН), и последващо извличане с разтвори на H_2SO_4 . В това изследване МН е осъществено в микровълнова фурна „SANG-E20“ при мощност 800 W и работна честота 2.45 GHz, като изследванията са провеждани при 100% мощност на апарата. Електромагнитните вълни се генерират от магнетрон и по вълновод постъпват в камерата, в която се третира пробата.

Данни от научната литература показват, че разтворимостта на ZnFe_2O_4 се влияе съществено от концентрацията на киселината [10,18]. В това изследване са използвани разтвори на H_2SO_4 (7, 10,5 и 14 об.%), което е съобразено с практиката на извличането в хидрометалургията на цинка. За сравнение на получените резултати са провеждани опити и при обикновено нагриване.

И при двата вида нагриване се цели достигане на температура $90\text{--}95^\circ \text{C}$ [7,18,19], която при МН се постига много по-бързо, след което нагриването се прекратява.

Изследвано е дефектообразуването при МА с метода на Мьосбауеровата спектроскопия и е проследено изменението на разтворимостта на механично активиран цинков ферит в сярна киселина [20]. Установено е, че при МА на ZnFe_2O_4 още в началото се образуват деформирани магнитноподредени области. Наблюдава се плавен преход на изход-

ното вещество в деформирано състояние. Именно с тези деформирани области е свързано увеличаването на разтворимостта на $ZnFe_2O_4$.

Нарушаването на порядъка в кристалната решетка в хода на механичната активация води до магнитно подреждане, като тази част е енергийно богата и тя се извлича при обработването на феритите с киселини [21]. Механохимичната обработка на феритите е един от методите за стимулиране на химичните процеси, възможностите на които в последно време съществено се разширяват с появяването на високоефективна смилача техника [22]. В това изследване цинковият кек и смесеният ферит от вида $Zn_{0,5}Cd_{0,5}Fe_2O_4$ са механоактивирани в продължение на 60, 120 и 600 min с използване на планетарна мелница (FRITSCH, Германия) окомплектована с трибореактор и възможност за работа със сухи проби или за работа със суспензии.

Привеждането на трудно разтворими вещества в разтворимо състояние, което обикновено се осъществява чрез нагриване с концентрирани киселини, може да бъде ускорено чрез механохимична обработка на неразтворимите компоненти [23]. Всички тези предпоставки дават основание да се провери възможността за използване на механоактивацията в хидрометалургията на цинка.

Цинкът, разтворим в сярна киселина и във вода се определя на базата преминал цинк в разтвор при извличане на 2 g от кека в 100 ml 7 % разтвор на сярна киселина или вода.

Химичният състав на кека е определен по два метода. Общият, сярноразтворимият и водоразтворимият цинк са определени по обменен метод чрез титруване с комплексон III, стандартизиран спрямо цинк, а останалите компоненти от кека са анализирани чрез ААС.

Степента на извличане (η) на металите при изследването е изчислена по формулата:

$$\eta = \frac{G_{Me}}{G_{Me}^0} \cdot 100, \%$$

където:

G_{Me} – масата на метала, преминал в разтвора определен след титруване, g

G_{Me}^0 – масата на метала в изходната проба в g, определен след пълното извличане проведено по стандартна методика на КЦМ – АД, Пловдив.

РЕЗУЛТАТИ И ДИСКУСИЯ

Рентгенофазовият анализ (РФА) показва, че изходните ZnO и Fe₂O₃ са реагирали при експерименталните условия (температура 1000° С и продължителност 10 h) и изцяло се е получил ZnFe₂O₄. Цинковият ферит кристализира в кубична сингония и изчисленият параметър на кристалната му решетка на базата на рентгенофазовия анализ е 8,442 Å, която стойност е много близка до представените данни в литературата [24,25,26]. Взаимодействието между CdO и Fe₂O₃ също протича изцяло и полученият CdFe₂O₄ е хомогенен еднофазен образец.

Мьосбауеровият спектър на ZnFe₂O₄ (както и на CdFe₂O₄) представлява дублет. Цинковият ферит има следните параметри на свръхфините взаимодействия: изомерно отместване IS спрямо α-Fe – 0,34±0,01 mm/s и квадруполното разцепване QS – 0,36±0,02 mm/s. Не се наблюдават остатъчни линии на секстета от Fe₂O₃, което е също потвърждение за пълното протичане на твърдофазната реакция между изходните оксиди.

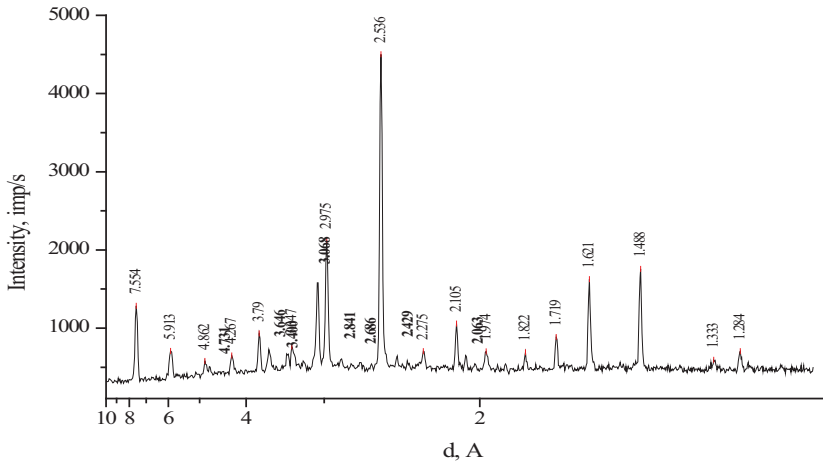
Цинкът в цинковия кек е свързан основно под формата на цинков ферит. В табл. 1 е представен химичният състав на кека за основните компоненти, като разликата от общия цинк и сярноразтворимия цинк се пада главно на феритния цинк, а именно 9,35%.

Таблица 1. Химичен състав на изследвания цинков кек

Zn _{общ}	Zn _{H₂SO₄}	Zn _{H₂O}	S _{об.}	Zn _{SO₄}	S _s	Pb
16,15	4,80	4,25	6,78	5,77	1,1	6,2

Цинковият кек е охарактеризиран с използването на рентгенофазов анализ (фиг. 1) и чрез диференциално-термичен и термогравиметричен анализ (фиг. 2).

Цинковият кек е сравнително кристален образец, чийто спектър включва линиите на ZnFe₂O₄, PbSO₄, ZnSO₄·xH₂O и SiO₂. Дифракционните максимуми, принадлежащи на основната фаза в цинковия кек (ZnFe₂O₄) са (в Å): 4,862; 2,975; 2,536; 2,429; 2,105; 1,719; 1,621; 1,488; 1,333; 1,284.



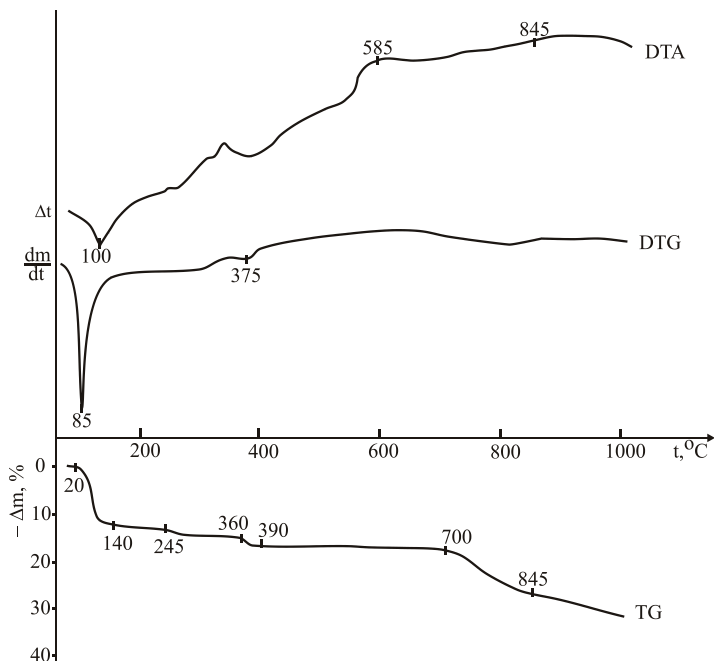
Фигура 1. Дифрактограма на цинковия кек

Определеният фазов състав на кристалните фази на базата на рентгенофазовия анализ е следният (в мас. %): $ZnFe_2O_4$ – 58,7; $ZnSO_4 \cdot xH_2O$ – 14,8; $PbSO_4$ – 7,7; SiO_2 – 6,3; $CaSO_4$ – 6,1; други – 6,4.

Химичният състав на цинковия кек показва, че една част от цинка в него е във водоразтворима форма. Общото съдържание на Zn (16,15%) е ниско за директното подаване на Zn кек за велцуване. Наличието на 5,77% сулфатна сяра (S_{SO_4}) показва, че една част от цинка би могъл да премине в ZnS при редукцията на $ZnSO_4$ при използване на велцуването като метод на преработка.

От дериватограмата на Zn кек (фиг. 2) е видно, че при температура до 140°C се отделя влагата от кека. Наблюдаваната известна загуба на масата в температурния интервал 245–390° С вероятно се дължи на отделяне на кристализационна вода. Над 700° С масата на пробата намалява. Основната причина за това е дисоциацията на $ZnSO_4$.

При извличането на синтезираните $ZnFe_2O_4$, $CdFe_2O_4$ и промишления цинков кек чрез обикновено нагряване се забелязват почти еднакви стойности при използването на 7 и 10,5% H_2SO_4 , докато при 14% H_2SO_4 степента на извличане се увеличава значително (табл. 2). Всички опити са проведени при продължителност 1 h, което съответства на методиката, която се прилага в заводската практика, за определяне на цинка, разтворим в 7% разтвор на H_2SO_4 .



Фигура 2. Дериватограма на цинковия кек

При конвенционалното нагряване се постига повърхностно загряване на пробите и генерираната топлина не прониква в целия обем на материала, а от там и степента на извличане на цинка и кадмия от пробите е ниска.

Микровълновото нагряване при извличането е по-ефективно, защото енергията генерирана от магнетрона се трансформира в топлинна енергия, а тя прониква в целия обем на изследвания материал. Микровълните причиняват загряване, само когато се абсорбират. Полярните молекули на материала абсорбират микровълните и се привеждат в движение, като следват микровълните, вибриращи според честота. Това води до молекулярно триене и до нагряване на пробата. Вътрешното обемно генериране на топлина създава условия за възникване на положителен температурен градиент. Създава се топлинно поле, характеризиращо се с по-висока температура на вътрешните, централни слоеве в сравнение с повърхността на материалите. При класическите

начини на предаване на топлината към изследвания материал, температурата на повърхността е по-висока от тази в центъра и съществува отрицателен температурен градиент. Обработване на феритите и кека чрез МН е съпроводено с равномерно вътрешно загряване и незначителни вътрешни напрежения и дефекти.

Всички това доказва по-високата ефективност на този вид нагряване, като при проведените изследвания се получава и технологичен ефект. При микровълновото нагряване посочената температура се постига за много по-малко време, в сравнение с обикновеното нагряване и степента на извличане на цинка и кадмия се повишава.

Таблица 2. Резултати от извличането на $ZnFe_2O_4$, $CdFe_2O_4$ и цинков кек при обикновено (КН) и микровълново нагряване (МН)

C _{H₂SO₄} об. %	Степен на извличане η , %					
	ZnFe ₂ O ₄ , η_{Zn}		CdFe ₂ O ₄ , η_{Cd}		Zn кек, η_{Zn}	
	КН	МН	КН	МН	КН	МН
7	4,4	7,5	12,0	24,0	9,6	14,6
10,5	4,9	7,6	21,0	25,0	11,5	16,3
14	8,4	12,7	23,8	44,0	12,5	17,6

Получените резултати за степента на извличане на цинка и кадмия от феритите са средни стойности от по 3–5 паралелни опита за всяка проба.

Резултатите за извличането на кадмия са значително по-високи спрямо получените за цинка от $ZnFe_2O_4$ и цинковия кек. Това дава основание да се направи изводът, че $CdFe_2O_4$ е по-нестабилен в сравнение с $ZnFe_2O_4$. При използване на микровълново извличане се получава по-висока степен на извличане на полезните метали и за двата ферита всравнение с конвенционалното нагряване. Въпреки, че тази разлика не е особено голяма, то трябва да се има предвид, че даже 1% по-висока степен на пряко извличане на цинка може да доведе до значителни технологични и икономически ползи.

През последните години в различни технологии разтворимостта на полезните компоненти се увеличава чрез използване на метода на механичната активация (МА) [27]. Има сведения, че разтворимостта на $ZnFe_2O_4$ се повишава чрез механохимично третиране [28].

Установено е [29], че част от механичната енергия, отвеждана от твърдото тяло по време на активацията се усвоява от него във вид на

нови повърхностни, линейни и точкови дефекти, а химичните свойства на кристалите се определят от наличните в тях дефекти. МА не се свежда просто до смилане на твърдото тяло, а се съпровожда от кристалохимични и структурни превръщания в него [20,29], при което голяма част от отвежданата енергия се оказва натрупана в неговия обем, а това се дължи на преминаването на веществото частично в аморфно състояние.

В тази връзка чрез прилагане метода на механоактивиране е проверена разтворимостта на цинка и кадмия от смесения ферит $Zn_{0,5}Cd_{0,5}Fe_2O_4$, както и на проби от цинковия кек с посочения химичен състав след отстраняване на вода – и сярноразтворимият цинк.

Анализът на резултатите (табл. 3) показва, че степента на извличане (η) на Zn и Cd от механично обработените проби в 7% разтвор на H_2SO_4 значително надвишава степента на извличане на Zn и Cd от изходните проби.

Таблица 3. Резултати от извличането след механоактивация (МА) на $Zn_{0,5}Cd_{0,5}Fe_2O_4$ и Zn кек

№	Вид на пробата	Време на МА, min	Степен на извличане на Zn, %	Степен на извличане на Cd, %
1	$Zn_{0,5}Cd_{0,5}Fe_2O_4$	0	1,8	1,9
2	$Zn_{0,5}Cd_{0,5}Fe_2O_4$	60	3,6	6,2
3	$Zn_{0,5}Cd_{0,5}Fe_2O_4$	120	7,0	11,1
4	$Zn_{0,5}Cd_{0,5}Fe_2O_4$	600	40,3	49,7
5	Цинков кек	0	0,9	-
6	Цинков кек	60	7,1	-
7	Цинков кек	120	7,6	-
8	Цинков кек	600	13,6	-

Времето на МА оказва съществено влияние върху разтворимостта на цинка и кадмия. С увеличаване продължителността на механичното третиране се увеличава и количеството на Zn и Cd, преминали в разтвора. При продължителност на МА от 600 min съдържанието на Zn и Cd в разтвора при извличане на смесения ферит нараства приблизително 25 пъти, а при извличането на цинковия кек съдържанието на Zn и Cd в разтвора нараства около 20 пъти.

Експерименталните резултати показват, че след механична обработка в планетарна мелница, разтворимостта на феритите се изменя

значително и затова този процес може да се проведе при относително по-меки условия. Предполага се, че една от причините за това поведение на феритите е механоактивацията. Съчетаването на механоактивиране и/или едновременно механоактивиране и извличане в класическия хидрометалургичен процес може да увеличи извличането на цинка и да се даде гъвкавост при третиране на различни цинкови угарки и полупродукти с високо съдържание на желязо.

Лесно осъществима препоръка за практиката е намаляване размера на отворите на ситата за пресяване на угарката. По този начин ще се увеличи надситовата фракция и по-голяма част от угарката ще премине през мелниците. Увеличаването на повърхността и натрупването на енергия в получените нови частици ще спомогнат за увеличаване степента на прякото извличане на цинка с всички благоприятни последици от това: намаляване на количеството на цинковия кек; намаляване разходите за неговото преработване; включване на повече желязо в неутралния цикъл, което благоприятства утаяването на примесите; намаляване или напълно избягване внасянето на $FeSO_4$; намаляване общото количество на твърдите отпадъци със съответния екологичен ефект и др.

ИЗВОДИ

1. Чрез рентгенофазов анализ е показано, че синтезираните в лабораторни условия $ZnFe_2O_4$, $CdFe_2O_4$ и $Zn_{0.5}Cd_{0.5}Fe_2O_4$ по класическата керамична технология са еднофазни образци.
2. Резултатите от микровълновото и конвенционалното нагряване показват, че степента на извличане на металите от $ZnFe_2O_4$, $CdFe_2O_4$ и цинков кек се повишава в полза на микровълновото нагряване.
3. Механичното активиране чрез смилане в планетарна мелница на цинков кек и $Zn_{0.5}Cd_{0.5}Fe_2O_4$ води до многократно повишаване степента на извличане на Zn и Cd достигайки 20–25 пъти в сравнение с нетретираните проби.

БЛАГОДАРНОСТ

Това изследване е извършено с помощта на финансирането по проект НИ11-ХФ-007 на Пловдивски университет „Паисий Хилендарски“.

ЛИТЕРАТУРА

1. B. S. Boyanov, M. P. Sandalski and K. I. Ivanov, *Zinc Sulfide Concentrates and Optimization of their Roasting in Fluidized Bed Reactor*, World Academy of Science, Engineering and Technology, 73 (2011) 420–427.
2. S. Nikolov, B. Boyanov, N. Moldovanska and R. Dimitrov, *Mössbauer Spectroscopy Study on the Oxidation of Sulfide Zinc Concentrate Rich in Marmatite*, *Thermochimica Acta*, 380 (2001) 37–41.
3. И. Костов, *Минералогия*, София, „Наука и изкуство“, 1973.
4. T. T. Chen and J. E. Dutrizac, *Mineralogical Changes Occurring During the Fluid-Bed Roasting of Zinc Sulfide Concentrates*, *Journal of Metallurgy*, 56 (2004) 46–51.
5. J. W. Graydon, and D. W. Kirk, *Mechanism of ferrite formation from iron sulfides during zinc roasting*, *Metallurgical transactions. B, Process metallurgy*, 19 (1988) 777–785.
6. S. A. Degterov, E. Jak, P. C. Hayes and A. D. Pelton, *Experimental study of phase equilibria and thermodynamic optimization of the Fe-Zn-O system*, *Metallurgical and Materials Transactions B*, 32 B (2001) 643–657.
7. В. Каролева, *Металургия на тежките цветни метали, т. 2*, ДИ „Техника“, София, 1986, 99–113
8. P. Lessidrenski, I. Gruev, A. Apostolov, S. Stoyanova and E. Bekrieva, *Jarosite technology for zinc production at the lead and zinc complex and optimization of the reagent mode*, *Proceedings of the 4th International Conference ZINC 2006*, Plovdiv, Bulgaria, 11–12 September, 2006, 213–216.
9. T. R. A. Davey, G. Willis and G. Mervin, *Review of developments in 1979–1980*, *Journal of Metals*, 33 (1981) 52–66.
10. C. Arslan and F. Arslan, *Thermochemical Review of Jarosite and Goethite Stability Regions at 25 and 95° C*, *Turkish J. Eng. Env. Sci.*, 27 (2003) 45–52.
11. D. Filippou and G. P. Demopoulos, *Steady-state modeling of zinc-ferrite hot-acid leaching*, *Metallurgical and Materials Transactions B*, 28B (1997) 701–711.

12. F. J. Tamargo, M. San and M. R. Valcarcel, *Asturiana de zinc: More than thirty years of experience with the Jarosite process*. The Canadian Institute of Mining, Metallurgy and Petroleum, Montreal, Canada (1996) 93–100.
13. M. R. C. Ismael and J. M. R. Carvalho, *Iron recovery from sulphate leach liquors in zinc hydrometallurgy*, Minerals Engineering 16 (2003) 31–39.
14. A. R. Gordon and R.W. Pickering, *Improved leaching technologies in the electrolytic zinc industry*, Metallurgical Transactions B, 6B (1975) 43–53.
15. M. Loan, O. M. G. Newman, R. N. G. Cooper, J. B. Farrow and G. M. Parkinson, *Defining the paragoethite process for iron removal in zinc hydrometallurgy*, Hydrometallurgy, 81 (2006) 104–112.
16. Г. И. Журавлев, *Химия и технология ферритов*, „Химия“, Ленинград, 1983, 27–31.
17. R. Dimitrov and B. Boyanov, *Investigation of Solid State Interactions in the Systems $ZnO-\alpha-Fe_2O_3$, $ZnFe_2O_4-CuO$ and $ZnFe_2O_4-CaO$* , Rudarsko-Metalurski Zbornik, 31, 1 (1984) 67–80.
18. T. Havlik, B. Friedrich and S. Stopic, *Pressure leaching of EAF dust with sulphuric acid*, World of Metallurgy, 57 (2004) 113–120.
19. K. Hirakoso, K. Watanabe, R. Baba and T. Nagai, *Fundamental studies on zinc ferrite*, Memories of the Faculty of Engineering, Hokkaido University, 30 (1955) 40–57, <http://hdl.handle.net/2115/37792>.
20. Y. Zhang, X. Li, L. Pan, Y. Wei and X. Liang, *Effect of mechanical activation on the kinetics of extracting indium from indium zinc ferrite*, Hydrometallurgy, 102 (2010) 95–100.
21. Е. Г. Аввакумов, *Механические методы активации химических процессов*, Новосибирск, „Наука“, 1986.
22. I. Mitov, V. Mitrov, E. Lefterova and Tz. Koleva, *Tribochemical synthesis of zinc ferrite*, Tribology Letters, 2 (1996) 417–426.
23. V. V. Boldyrev, *The use of mechanochemistry in „dry“ technological processes*, Sorovsky educational journal, 12 (1997) 47–52.

24. A. Z. Juhasz, *Aspects of mechanochemical activation in terms of comminution theory*, Colloids and Surfaces A: Physicochemical and Engineering Aspects, 141 (1998) 449–462.
25. V. V. Boldyrev, S. V. Pavlov and E. L. Goldberg, *Interrelation between fine grinding and mechanical activation*, Int. J. Miner. Process, 44–45 (1996) 181–185.
26. A. M. Gismelseed, K. A. Mohammed, N. M. Widatallah, A. D. Al-Rawas, M. E. Elzain and A. A. Yousif, *Structure and magnetic properties of the $Zn_xMg_{1-x}Fe_2O_4$ ferrites*, Journal of Physics: Conference Series 217 (2010) 012138.
27. J. Philip, G. Gnanaprakash, G. Panneerselvam, M. P. Antony, T. Jayakumar and B. Raj, *Effect of thermal annealing under vacuum on the crystal structure, size and magnetic properties of $ZnFe_2O_4$ nanoparticles*, Journal of Applied Physics, 102 (2007) 054305.
28. B. P. Ladgaonkar, P. N. Vasambekar and A. S. Vaingankar, *Effect of Zn^{2+} and Nd^{3+} substitution on magnetization and AC susceptibility of Mg ferrite*, Journal of Magnetism and Magnetic Materials, 210 (2000) 289–294.
29. P. Balaz, *Mechanical activation in hydrometallurgy*, Int. J. Mineral Processing, 72 (2003) 341–345.

WASTE TONERS AND CARTRIDGES – UTILIZATION OPTION

G. Patronov, D. Tonchev

*Department of Chemical Technology,
Plovdiv University „Paisii Hilendarski“, Plovdiv 4000, Bulgaria
E-mail: patron@uni-plovdiv.bg*

ABSTRACT

The present investigation involves determining the ash content and calorific effect of waste toners and cartridges. Non-magnetic, magnetic and mixed waste toners, waste cartridges and printer bodies were analysed.

Values obtained for the ash content varied between 1,6% and 45,5%, and values obtained for calorific effects varied between 35,44 MJ/kg and 22,33 MJ/kg for waste cartridges and magnetic toner, respectively. Results of the analysis were compared with those for conventional fossil fuels and biomass. Odours and harmful gases, emitted during combustion, reduce the possibilities for utilization of these waste products. Eventual combustion of the wastes should be carried out under appropriate conditions in convenient reactors and should be accompanied by purification of exhaust gases. The emitted heat could be used to produce process steam or electricity.

Key words: *waste toner, ash content, calorific effect, waste cartridges*

INTRODUCTION

The increasing consumption of electrical devices and electronics as a result of technological innovation and market expansion led to the

generation of significant quantities of electronic waste worldwide (mainly in Europe, USA and Australia). Their volume increased by 3–5% annually for the last few years is estimated at 20–30 mil t per year [1, 2]. A large proportion of them refer to the waste toners and cartridges. The U. S. only amount of waste toners ranges from 9 000 to 25 000 t per year [3, 4]. Complicated chemical composition, development of new technologies and pressure from environmental organizations lead to search for alternatives for processing and recycling of these waste materials with minimal environmental impact. Waste toner can be incorporated into asphalt binder for example [4]. Waste cartridges may include the following components: steels – 40%, plastics – 35%, Fe_3O_4 – 5%, Al – 12% and toner – 8% [5]. A model composition of the waste toner is presented in Figure 1 [6].

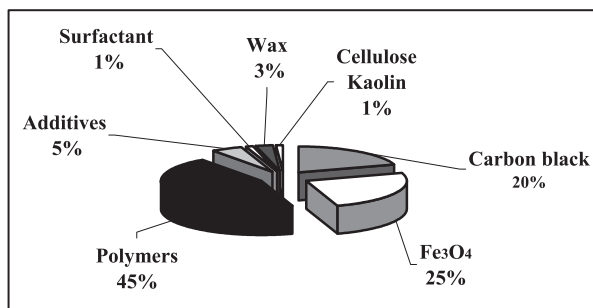


Figure 1. A model composition of the waste toner.

This study aims at determining the ash content and calorific effect of waste toners, waste cartridges and printer bodies with a view to eventual utilization by incineration.

EXPERIMENTAL

Samples of non-magnetic, magnetic and mixed waste toners, as well as plastic parts of the waste cartridges and printer bodies were analyzed. Samples of the waste toners were selected randomly at different times from different locations. Mixtures of non-magnetic and magnetic toners in different weight proportions are prepared and tested for better comparability of results.

Analyses were carried out under the current state standards. Lack of moisture is characteristic for these materials.

The ash content was determined by ignition at 850 °C to constant weight. Calorific effects were determined using an automated isoperibolic calorimeter KL – 10 (type Berthelot). The analysis consists of samples combustion in oxygen atmosphere in the calorimetric bomb, submerged in water and measuring the increase of the water temperature. The calorific effect Q is automatically calculated by the formula:

$$Q = \frac{K(\Delta t - k) - c}{m}, J / g \quad (1)$$

where,

K is the heat capacity of the calorimeter, $J/^\circ\text{C}$;

Δt – temperature change during the main period $^\circ\text{C}$;

k – correction for heat exchange between calorimeter and environment $^\circ\text{C}$;

c – corrections for additional heat effects, J ;

m – mass of the sample, g .

The bombe calorimeter was calibrated against benzoic acid [7].

RESULTS AND DISCUSSION

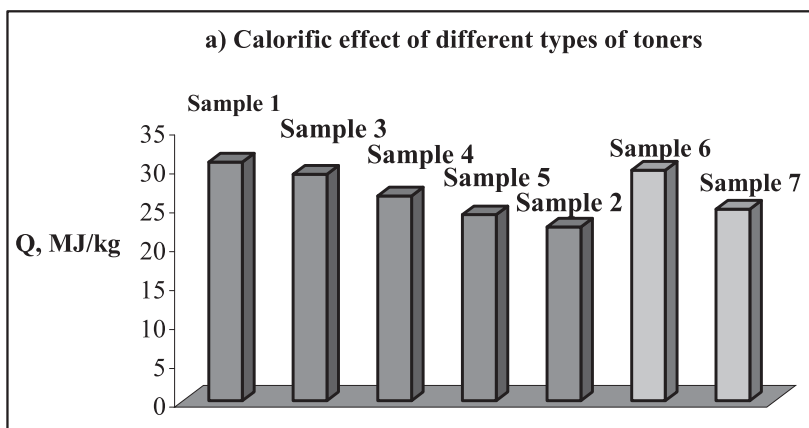
Results of the analysis (samples 1–9) are presented in Table 1 and Figures 2, 3. These results are compared with those for conventional fossil fuels (coal, briquettes) and biomass obtained from our further research (samples 10–14).

The results for samples 15 and 16 are literature data [7].

Numbers 3–5 of samples in Table 1 were artificially made by mixing non-magnetic and magnetic toners in a certain ratio to better comparability of results and more accurate analysis of the possibilities for utilization of waste toner incineration. Values obtained for ash content are ranging between 1,6% and 45,5%, and calorific effect between 35,44 MJ / kg and 22,33 MJ / kg for waste cartridge and magnetic toner respectively. As seen, the results for waste toners, cartridges and printer bodies are similar and higher than these values for conventional fossil fuels (coal, briquettes) and biomass. Odours and harmful gases emitted during combustion are limiting the possibilities for utilization of these waste products as a fuel. In addition, as shown by the results, some waste toners were characterized by high ash content.

Table 1. Moisture content, ash and calorific effect of different samples

№	Sample	Moisture, %	Ash, %	Calorific effect, MJ/kg
1.	<i>Non-magnetic toner (nm)</i>	-	3,4	30,70
2.	<i>Magnetic toner (m)</i>	-	45,5	22,33
3.	<i>Mixed toner nm:m=3:1</i>	-	13,6	29,13
4.	<i>Mixed toner nm:m=1:1</i>	-	25,1	26,35
5.	<i>Mixed toner nm:m=1:3</i>	-	35,1	23,92
6.	<i>Waste toner I</i>	-	12,8	29,65
7.	<i>Waste toner II</i>	-	28,4	24,65
8.	<i>Waste cartridge</i>	-	1,6	35,44
9.	<i>Waste printer body</i>	-	6,7	31,76
10.	<i>Coal briquette (c)</i>	12,3	14,6	19,78
11.	<i>Biomass briquette (b)</i>	8,9	11,1	16,60
12.	<i>Mixed briquette (c+b)</i>	12,1	14,3	17,93
13.	<i>Wood pellets</i>	7,3	0,6	19,51
14.	<i>Black coal</i>	15,9	12,7	22,96
15.	<i>Anthracite</i>			32,5 – 34,0
16.	<i>Coke</i>			28,0 – 31,0



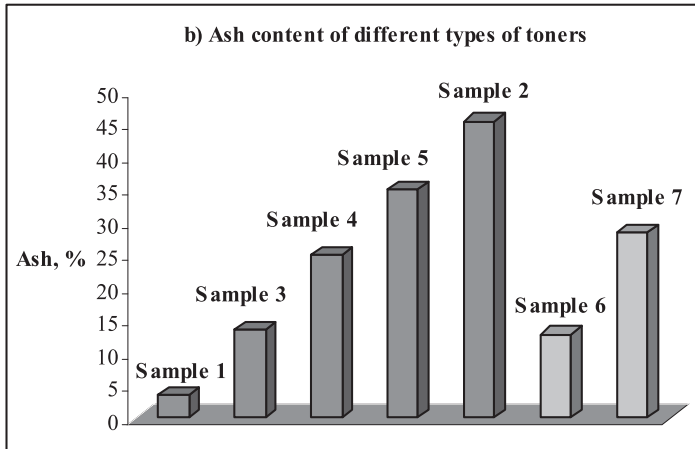


Figure 2. Visual comparison of the results of calorific effect (a) and ash content (b) of different types of toners: sample 1 – non-magnetic toner; sample 2 – magnetic toner; sample 3 – mixed toner nm:m=3:1, sample 4 – mixed toner nm:m=1:1, sample 5 – mixed toner nm:m=1:3, sample 6 – waste toner I, sample 7 – waste toner II.

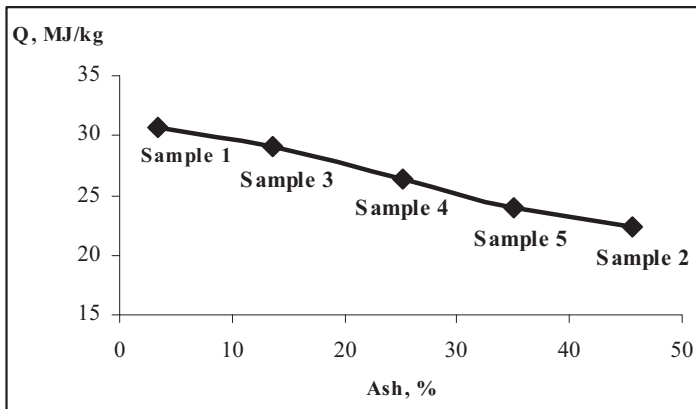


Figure 3. Calorific effect versus the ash content of non-magnetic, magnetic and mixed toners.

CONCLUSION

Waste toners, waste cartridges and printer bodies reveal high calorific effects. This energy is enough to be utilized as a fuel. Combustion of these wastes should be carried out under appropriate conditions in the reactors and accompanied by purification of exhaust gases. The released heat could be used to produce process steam or electricity.

REFERENCES

1. H.-Y. Kang, J. M. Schoenung, *Resources, Conservation and Recycling* 45 (2005) 368-400.
2. B. H. Robinson, *Science of the Total Environment*, 408 (2009) 183–191.
3. Ahmadi et al., *Journal of Cleaner Production*, 11 (2003) 573–582.
4. Y. Yildirim et al., *Resources, Conservation and Recycling*, 42 (2004) 295–308.
5. J. Ruan et al., *Journal of Hazardous Materials*, 185 (2011) 696–702.
6. Shaffert R. M., *Electrophotography*, Focal Press, London, 1980.
7. O. Kubaschewski and C. Alcock, *Metallurgical Thermochemistry*, Pergamon Press, Oxford – New York – Paris, fifth ed. 1979

RISK ASSESSMENT OF CYCLODODEC-2-EN-1-YL ETHERS IN THE ENVIRONMENT

As. Kolev¹, Y. Koleva²

*¹Atmospheric Vacuum Distillation-1, LUKOIL Neftochim Burgas
E-mail address: asekolev@yahoo.com*

*²Department of Organic Chemistry, University „Prof. Assen Zlatarov“,
1 Prof. Yakimov str., 8010 Bourgas, Bulgaria
E-mail address: ykoleva@btu.bg*

ABSTRACT

Environmental pollutants are continuously being emitted from anthropogenic activities in large amounts. They move throughout the ecosystem by a variety of processes and are eventually degraded or accumulated somewhere in the environment. The chemical diversity of pollutants and the variations in behaviour, both with respect to transport, degradation, accumulation (fate) and toxicity (effects) has introduced the field of risk assessment. It needs to be based on an interdisciplinary approach involving monitoring of exposure concentrations in the natural environment, laboratory scale fate and effect studies and predictive models designed to establish a quantitative link between sources, exposure levels, and risk of effects of potential hazardous pollutants. The aim of this work is to predict risk assessment of some new synthesized chemicals (cyclododec-2-en-1-yl ethers) in the environment.

Key words: *Risk assessment, persistence, bioaccumulation, toxicity, cyclododec-2-en-1-yl ethers*

INTRODUCTION

New chemicals are continuously being introduced to the environment either directly (primary emission) or indirectly as an unintended result of the use. The pollution caused by synthetic organic chemicals has brought about severe lessons to human beings. Persistent toxic substances (PTS) in the environment have become an important issue affecting the survival and development of human in the 21st century [1].

Environmental risk assessment (ERA) involves evaluating the potential for persistence, accumulation and toxicity of chemicals in the environment in order to manage these risks to protect the environment and the organisms living in it [2]. One major group of organic substances of concern is called PBTs (Persistent, Bioaccumulative, Toxic substances). PBTs are persistent because they remain unchanged for a relatively long time in the environment. Moreover, these chemicals are not easily metabolized or excreted and therefore tend to accumulate in organisms [3]. These chemicals also hold toxic properties and hence are harmful to wildlife and the ecosystem [4].

Scientific and regulatory activity in environmental (ecological) risk assessment continues to progress globally. In Europe, the REACH programme, together with new requirements for the ERA of human pharmaceuticals, represent significant developments in regulatory ERA procedures for industry. The Organisation for Economic Co-operation and Development (OECD), for example, has been developing in vitro and in vivo mammalian and wildlife test guidelines for assessing the developmental and reproductive effects of chemicals in the environment [5, 6].

It is evident that ecological risk assessment (ERA) for the synthetic organic compounds can provide a precaution against the pollution [1]. ERA includes three primary phases as defined by U.S. Environmental Protection Agency (US EPA): problem formulation, analysis, and risk characterization [7]. It is obvious that data on physicochemical properties, environmental behavior and ecotoxicology of organic compounds, are indispensable for the ERA. However, the data have three aspects of problems: 1) Lack of the data [8]; 2) Large expense of testing [9]; 3) Uncertainty in data [10].

Molecular structures are internal factors governing the physicochemical properties, environmental behaviour and ecotoxicology of organic compounds. Compounds with similar molecular structures should have similar physicochemical properties, environmental fate and ecotoxicological effects, i.e., there are inherent relations between molecular structures and their physicochemical properties, environmental behavioral and ecotoxicological parameters [11]. Thus, (Q) SARs can fill the data gap for physicochemical, environmental behavioral and ecotoxicological parameters of organic compounds; they also can decrease

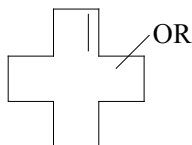
experimental expenses and reduce the extent of experimental testing (especially animal testing). Furthermore, (Q)SARs can be used as supporting tools to evaluate the adequacy of the available empirical data of organic compounds, which is also one of the four specific functions of (Q)SARs for ERA [12]. Thus (Q)SAR technology is of great importance to ERA of organic compounds [13].

Among the numerous compounds used in perfume industry nowadays, methoxy – and ethoxycyclododecanes as well as (2-methoxyethoxy) – and (2-ethoxyethoxy) cyclododecanes hold an important position. The commonly accepted procedures for the preparation of these compounds are multi-stage, and some of the reaction steps are associated with the formation of highly-toxic, explosive, or expensive chemicals. The cyclododec-2-en-1-yl ethers are derived by the catalytic substitution reaction between isomeric cyclododec-2-en-1-yl acetates [14] and primary aliphatic alcohols in the presence of $\text{Pd}^0[\text{PPh}_3]_4$ [15]. The new synthesized chemicals as the cyclododec-2-en-1-yl ethers can be introduced to the environment which need to be explored the environmental risk assessment of these compounds.

The aim of this work is to predict the potential for persistence, bioaccumulation and toxicity of some new synthesized chemicals (cyclododec-2-en-1-yl ethers) in the environment.

MATERIALS AND METHODS

Compound Data. Some new synthesized chemicals (cyclododec-2-en-1-yl ethers) are presented in Tables 1 [15].



R represents: CH_3 , C_2H_5 , $\text{C}_2\text{H}_4\text{OCH}_3$ or $\text{C}_2\text{H}_4\text{OC}_2\text{H}_5$.

Criteria used by the PBT Profiler. The PBT Profiler is a screening-level tool that provides estimates of the persistence, bioaccumulation, and chronic fish toxicity potential of chemical compounds. It is designed to be used when data are not available. In order to help interested parties make informed decision on a chemical's PBT characteristics, the PBT profiler automatically identifies chemicals that may persistent in the environment and bioaccumulate in the food chain. These chemicals are identified using thresholds published by the Environmental Protection Agency (EPA) [16].

Persistence criteria. The PBT Profiler combines the persistence criteria for water, soil, and sediment and highlights chemicals with an estimated half-life ≥ 2 months and < 6 months as persistent and those with an estimated half-life ≥ 6 months as very persistent. The half-life in air is not used in the PBT Profiler's Persistence summary (chemicals with an estimated half-life > 2 days are considered as persistent). The PBT Profiler uses 30 days in a month for its comparisons.

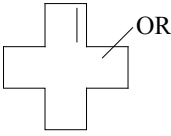
Bioaccumulation criteria. The PBT Profiler combines the bioaccumulation criteria and highlights chemicals with a BCF (bioconcentration factor) ≥ 1000 and < 5000 as bioaccumulative and those with a BCF ≥ 5000 as very bioaccumulative.

Toxicity criteria. To highlight a chemical that may be chronically toxic to fish, the PBT profiler uses the following criteria: Fish ChV (Chronic Value) > 10 mg/l (low concern), Fish ChV = 0.1 – 10 mg/l (moderate concern) and Fish ChV < 0.1 mg/l (high concern).

RESULTS AND DISCUSSION

The results of the estimation of cyclododec-2-en-1-yl ethers for persistence, bioaccumulation and toxicity are presented in Table 1.

Table 1. PBT Profiler Estimate of Cyclododec-2-en-1-yl Ethers

№	Cyclododec-2-en-1-yl ethers 	Persistence		Bioaccumulation	Toxicity
		Media (water, soil, sediment, air) Half-life (days)	Percent in Each Medium	BCF	Fish ChV (mg/l)
1	R = -CH ₃	15; 30; 140; 0.046	13%; 70%; 17%; 0%	1,000	0.003
2	R = -C ₂ H ₅	38; 75; 340; 0.042	5%; 58%; 37%; 0%	2,200	0.0017
3	R = -C ₂ H ₄ OCH ₃	38; 75; 340; 0.042	11%; 74%; 15%; 0%	680	0.005
4	R = -C ₂ H ₄ OC ₂ H ₅	38; 75; 340; 0.042	8%; 61%; 32%; 0%	1,400	0.003

The PBT profiler uses a well-defined set of procedures to predict the persistence, bioaccumulation, and toxicity of chemical compounds when

experimental data are not available. The persistence, bioaccumulation, and fish chronic toxicity values estimated by the PBT profiler are automatically compared to criteria published by EPA.

Persistence is the ability of a chemical substance to remain in an environment in an unchanged form. The longer a chemical persists, the higher the potential for human or environmental exposure to it. The individual environmental media for which a chemical's persistence is usually measured or estimated are air, water, soil, and sediment.

The PBT Profiler expresses persistence in individual medium half-lives in air, water, soil, and sediment measured in days. These half-lives are for reactivity-based persistence only. The EPA has established a series of proposed thresholds for persistence based on the efforts of scientists, regulators, and other interested parties worldwide in helping to identify and regulate chemicals that may present the greatest health and environmental risks [16].

Cyclododec-2-en-1-yl ethers from Table 1 are expected to be found predominantly in soil and their persistence estimate is based on their transformation in this medium. Half-life of compound 1 in soil, 30 days, does not exceed the EPA criteria. Therefore, ether 1 is estimated not to be persistent in the environment. While half-life of compounds 2–4 in soil, 75 days, exceeds the EPA criteria of $>$ or $=$ 2 months (and $<$ or $=$ 6 months). Therefore, these ethers are estimated to be persistent in the environment.

Humans, domestic animals, and wildlife are more likely to be exposed to a chemical if it does not easily degrade or is dispersed widely in the environment. The structural characteristics that enable a chemical to persist in the environment can also help it to resist metabolic breakdown in people or wildlife.

Bioaccumulation is the process by which the chemical concentration in an aquatic organism achieves a level that exceeds that in the water, as a result of chemical uptake through all possible routes of exposure. Biomagnification refers to the concentration of a chemical to a level that exceeds that resulting from its diet. Bioaccumulation includes both biomagnification and bioconcentration. In general, chemicals that have the potential to bioconcentrate also have the potential to bioaccumulate [16].

Bioconcentration in fish can be readily measured in the laboratory and is frequently used to predict the importance of bioaccumulation, which is much more complicated to determine. The potential for bioconcentration in fish is expressed as its bioconcentration factor, or BCF. The prediction of BCF is based on a chemical's octanol/water partition coefficient and one or more chemical structure-based correction factors, if applicable [16].

The estimated bioconcentration factor (BCF) for compounds 1, 2 and 4 from Table 1, exceeds the EPA bioconcentration criteria ($>$ or $=$ 1,000). The PBT Profiler estimates that ethers have the potential to bioconcentrate in fish and aquatic organisms and are expected to bioaccumulate in the food chain because it exceeds the BCF criteria. While the estimated bioconcentration factor (BCF) for compound 3,680, does not exceed the EPA bioconcentration criteria. Therefore, the PBT Profiler estimates that ether 3 is not expected to bioaccumulate in the food chain because it does not exceed the BCF criteria.

PBT chemicals are those that persist in the environment, bioconcentrate in aquatic organisms, and may bioaccumulate in humans, birds, and wild mammals. Exposure to PBT chemicals will result in chronic exposures which, in turn, leads to chronic toxicity [16].

The PBT Profiler estimates that cyclododec-2-en-1-yl ethers are chronically toxic to fish (Table 1). It is important to note that ethers may also be toxic to other aquatic organisms. Some aquatic organisms, such as daphnids, may be more sensitive to both acute and chronic exposures to ethers. The four ether compounds are with high toxicity (Fish ChV $<$ 0.1 mg/l), which can be explained by metabolic transformation. A possible mechanism of cyclododec-2-en-1-yl ethers is to act as proelectrophiles by monooxygenase activation, which can be converted to acceptors of Michael-type [17]. Michael-type addition provides a means of covalent adduct formation at an electrophilic center, without any leaving group.

Chemicals can have a variety of toxic properties, resulting in a diverse array of adverse health effects. According to the EPA, the toxicity rating of a potential PBT chemical is based on repeated exposures which result in human or environmental toxicity. Adverse impacts can include mutagenic damage to DNA, cancer, neurological toxicity, reproductive toxicity, developmental toxicity, or immune system damage, among others [18].

CONCLUSION

For the environmental risk assessment of toxic organic chemicals, (Q)SARs play an important role in filling the data gap of environmental endpoints, decreasing experimental expense, reducing and replacing testing (especially animal testing), and assessing the uncertainty of experimental data. The analyses of results of this work have been shown that the cyclododec-2-en-1-yl ethers are persistent for some media (one exception is compound 1), bioaccumulative (without compound 3) and they are high toxic to fish. The high toxicity of the four ether compounds can be explained by their metabolic transformation (monooxygenase activation).

REFERENCES

1. Macleod, M., T. E. Mckone, K. L. Foster, R. L. Maddalena, T. F. Parkerton, D. Mackay, *Environmental Science & Technology*, 2004, 38, 6225–6233.
2. ECETOC. Risk assessment of PBT chemicals. Technical Report No. 98. European Centre for Ecotoxicology and Toxicology of Chemicals, Brussels, Belgium, 2005 (<http://www.ecetoc.org>).
3. Devillers, J., S. Bintein, D. Domine, *Chemosphere*, 1996, 33, 1047–1065.
4. Candido, A., The CBR approach in measuring toxicity of narcotic chemicals, MSc Toxicology and Environmental Health Institute for Risk Assessment Sciences (IRAS), Utrecht University.
5. Vos, J. G., E. Dybing, H. Greim, O. Ladefoged, C. Lambré, J. V. Tarazona, I. Brandt, A. D. Vethaak, *Critical Reviews in Toxicology*, 2000, 30, 71–133.
6. Gourmelon, A., J. Ahtiainen, *Ecotoxicology*, 2007 16, 161–167.
7. U. S. Environmental Protection Agency. Guidelines for ecological risk assessment. In Risk Assessment Forum. Washington: U. S. Environmental Protection Agency, 1998, 63, 26846–26924.
8. Verhaar, H. J. M., J. Solbe, J. Speksnijder, C. J. Van Leeuwen, J. L. M. Hermens, *Chemosphere*, 2000, 40, 875–883.
9. Enterprise & Industry Directorate General and Environment Directorate General. European Commission, REACH in brief. 2002, September. Available online at: <http://ecb.jrc.it/REACH/>
10. Linkov, I., M. R. Ames, E. A. C. Crouch, F. K. Satterstrom, *Environmental Science & Technology*, 2005, 39, 6917–6922
11. Tunkel, J., K. Mayo, C. Austin, A. Hickerson, P. Howard, *Environmental Science & Technology*, 2005, 39, 2188–2199.
12. Cronin, M. T. D., J. D. Walker, J. S. Jaworska, M. H. I. Comber, C. D. Watts, A. P. Worth, *Environmental Health Perspectives*, 2003, 111, 1376–1390.
13. JingWen, C., L. XueHua, Y. HaiYing, W. YaNan and Q. XianLiang, *Science in China Series B: Chemistry*, 2008, 51, 593–606.
14. Kolev, A., M. Skumov and E. Balbolov, *Reaction Kinetics and Catalysis Letters*, 2003, 78, 325–330.

15. Kolev, A., E. Balbolov, *Annual Assen Zlatarov-Burgas*, 2011, XL, 34–36.
16. Criteria used by the PBT Profiler: <http://www.pbtprofiler.net/criteria.asp>; Girard, J. E., Chapter 14. Organic chemicals in the environment, In *Principles of Environmental Chemistry*, 2nd ed., Jones & Bartlett Publishers, LLC, 2010, 402–439.
17. Lipnick, R. L, *The Science of the Total Environment*, 1991, 109/110, 131–153.
18. Persistent, Bioaccumulative and Toxicants, *Science & Environmental Health Network*. Available online at: <http://www.saferchemicals.org/PDF/PBT-Factsheet.pdf>

АНТИОКСИДАНТЕН КАПАЦИТЕТ НА ПЛОДОВЕ НА ЧЕРНА БОРОВИНКА

*Р. Динкова, М. Георгиева, К. Василев, К. Михалев,
Н. Йончева, Х. Динков*

*УХТ–Пловдив, Катедра „Консервиране и хладилна технология“,
4000 Пловдив; e-mail: rada_d@abv.bg*

ABSTRACT

Methanol extracts from the fruits of black bilberry (*Vaccinium myrtillus* L.) with different regions (Trojan, Velingrad) of plant material, were analysed for their content of total polyphenols and anthocyanins and antioxidant capacity (DPPH-and FRAP-assay). The correlations between the content of total polyphenols and antioxidant capacity of the analysed samples were good ($R = 0.98-0.99$). The results show that the content of anthocyanins in the extracts contributes significantly to their antioxidant capacity, which is higher in the fruits from the region of Velingrad.

Key words: *Vaccinium myrtillus* L., polyphenols, anthocyanins, DPPH, FRAP

ВЪВЕДЕНИЕ

Множество *in vitro* изследвания показват, че полифенолите на ягодоплодните са мощни хранителни антиоксиданти [1–3]. Въпреки, че все още предстои научното доказване на вероятните механизми, съществуват убедителни доказателства за връзката между антиоксидантната активност на полифенолите на ягодоплодните и човешкото здраве [4].

Антиоксидантната активност зависи в голяма степен от вида на ягодоплодните, като обикновено диворастящите видове имат по-висок общ антиоксидантен потенциал от култивираните [5]. В последно време, обаче, има съобщения за значителни вариации в съдържанието на антоциани при популациите на диворастящи ягодоплодни видове, в частност черна боровинка [6, 7].

Целта на настоящата разработка е да се оценят полифенолното съдържание и антиоксидантния капацитет на плодове на черна боровинка в зависимост от произхода на растителния материал.

МАТЕРИАЛИ И МЕТОДИ

За аналитични цели са използвани следните реактиви: DPPH [2,2-дифенил-1-пикрилхидразил], TPTZ [2,4,6-три(2-пиридил)2-триазин] и Trolox [(±)-6-хидрокси-2,5,7,8-тетраметилхроман-2-карбоксилна киселина] (Sigma-Aldrich, Steinheim, Германия); реактив на Folin-Ciocalteu (FC-реактив) (Merck, Darmstadt, Германия); галова киселина монохидрат (Fluka, Buchs, Швейцария). Всички останали реактиви и разтворители са с аналитична чистота.

Използвани са плодове на черна боровинка (*Vaccinium myrtillus* L.) от находища в районите на Велинград и Троян. Плодовете са набрани (реколта 2009 г.) от предварително маркирани растения в средата на характерния за съответния район беритбен период и са транспортирани до лабораторията в рамките на 24 h. След сортиране за отстраняване на незрели, презрели или наранени плодове, разфасовките (~200 g) са поставени в полиетиленови пликове, замразени (-25°C) и съхранявани в замразено състояние (-18°C).

Подготовката на пробите е осъществена в съответствие със схемата от Фигура 1. Приблизително 100 g плодове са размразени при стайна температура и са смлени с пасатор MR 300 Minipimer compact (Braun, Kronberg, Germany). 25 g от плодовата каша са хомогенизирани с 40 mL подкиселен метанол (2300 µL 37% HCl в 1L метанол) в лабораторен дезинтегратор MPW-309 (Mechanika precyzyjna, Warsaw, Poland) за 2 min. Сместа е прехвърлена в ерленмайрова колба от 250 mL с общо 210 mL подкиселен метанол. След престояване в продължение на едно денонощие в хладилни условия (10°C) съдържанието на колбата е филтрирано през нагънат филтър. След изпаряване под вакуум (40°C), концентратът е прехвърлен в мерителна колба от 100 mL и съдържанието е доведено до марката с подкиселена вода (pH 1.5). Полученият базов екстракт (40 mL) е допълнително екстрахиран с етил

ацетат (40 mL) трикратно. Комбинираните екстракти са изпарени под вакуум. Сухият остатък е разтворен в 4 mL метанол – фракция 1. Аналогично е приготвена фракция 2, като са използвани 40 mL от базовия екстракт при pH 7.0. Екстракцията и фракционирането са осъществени трикратно.

ЧЕРНИ БОРОВИНКИ

РАЗМРАЗЯВАНЕ

СМИЛАНЕ

ЕКСТРАКЦИЯ

БАЗОВ ЕКСТРАКТ

(антоциани, фенолни киселини и неантоцианови флавоноиди)

Анализи: TMA; TPP; DPPH; FRAP

ФРАКЦИОНИРАНЕ

ФРАКЦИЯ 1

(фенолни киселини)

Анализи: TPP; DPPH; FRAP

ФРАКЦИЯ 2

(неантоцианови флавоноиди)

Анализи: TPP; DPPH; FRAP

Фигура 1. *Схема на опитната постановка*

Анализите на общи полифеноли (TPP), общи мономерни антоциани (TMA), радикалоулавяща способност (DPPH-тест) и металоредуцираща способност (FRAP-тест) са осъществени в съответствие с методите описани в [8]. Представените резултати са средноаритметични стойности от най-малко три паралелни определения, като коефициентите на вариация са по-малки от 5%.

РЕЗУЛТАТИ И ОБСЪЖДАНЕ

Данните за съдържанието на общи полифеноли и общи мономерни антоциани и антиоксидантния капацитет на изследваните проби са представени в Таблица 1.

Като цяло, антиоксидантният капацитет и полифенолното съдържание на базовите екстракти са значително по-високи от тези на фракциите. Наличието на синергизъм при антиоксидантното действие, вероятно, съществено допринася за установените резултати. Съществуват добри корелационни зависимости ($R = 0.98-0.99$) между съдържанието на общи полифеноли и антиоксидантния капацитет на изследваните проби.

Таблица 1. Съдържание на общи мономерни антоциани (ТМА) и общи полифеноли (ТРР) и стойности на антиоксидантния капацитет (DPPH и FRAP) на екстрактите от плодове на черна боровинка в зависимост от района на произход

Анализиран показател	Район на произход на плодовете					
	Базов екстракт	Троян		Базов екстракт	Велинград	
		Фракция 1	Фракция 2		Фракция 1	Фракция 2
ТМА (mg CGE ¹ /100 g)	628.4	-	-	853.2	-	-
ТРР (mg GAE ² /100 g)	1075.4	168.8	146.2	1087.5	121.7	74.4
DPPH (μmol TE ³ /100 g)	6725.0	846.3	813.8	7750.0	850.0	631.3
FRAP (μmol TE ³ /100 g)	7644.4	1295.6	1060.0	10652.8	970.6	555.3

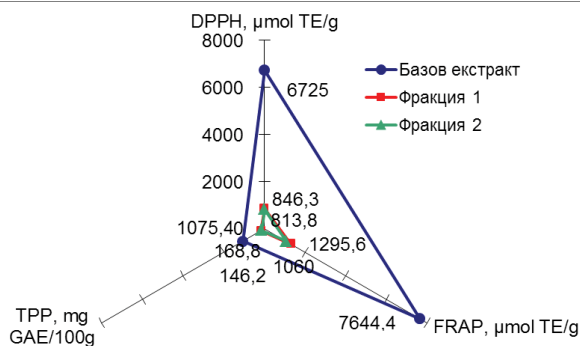
¹Резултатите са изразени като еквиваленти на цианидин 3-глюкозид.

²Резултатите са изразени като еквиваленти на галова киселина.

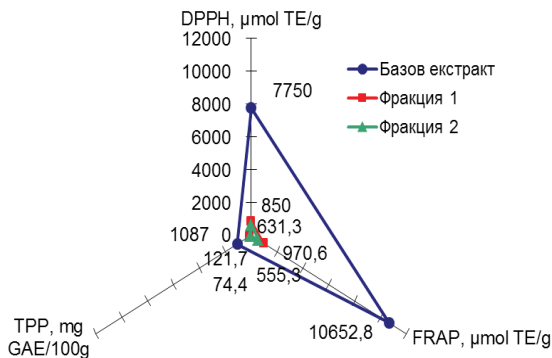
³Резултатите са изразени като еквиваленти на Trolox (водоразтворим аналог на витамин Е).

Интересно е да се отбележи наличието на 15.2–39.4% по-високи стойности на антиоксидантния капацитет при базовите екстракти на плодовете от района на Велинград в сравнение с тези от района на Троян. Този факт може да се обясни с 35.8% по-високото съдържание на общи антоциани при първата проба, тъй като няма съществена разлика в общото полифенолно съдържание. Наличието на подобна зависимост на антоциановото съдържание от произхода е установено наскоро при черните боровинки в Латвия [7] и Финландия [6].

A



B



Фигура 2. Радарна диаграма на антиоксидантния капацитет на екстрактите от плодове на черна боровинка в зависимост от района на произход: A – Троян; B – Велинград.

За комплексното характеризиране на общия антиоксидантен капацитет е приложен подходът на Terashima et al. [9], като радарната диаграма (Фигура 2) е построена на база стойностите за съдържание на общи полифеноли (TPP), металоредуцираща (FRAP) и радикалоулавяща (DPPH) способност. Съществено значение за активността на екстрактите от плодове на черна боровинка имат полифенолни анти-

оксиданти, действащи едновременно като донори на водородни атоми (DPPH-тест) и електрони (FRAP-тест).

ИЗВОДИ

Получените резултати показват, че антоциановото съдържание и антиоксидантния капацитет на екстрактите от плодове на черна боровинка съществено зависят от произхода, което вероятно се дължи на различия в почвените и климатични условия.

БЛАГОДАРНОСТ

Представеното изследване е финансово подпомогнато от фонд „Научни изследвания“ към МОМН (Проект № ДО02-334/20.12.2008 г.).

ЛИТЕРАТУРА

1. Jakobek, L., Šeruga, M., Novak, I., Medvidović-Kosanović, M. (2007). Flavonols, phenolic acids and antioxidant activity of some red fruits. *Deutsche Lebensmittel-Rundschau*, 103, 369–378.
2. Moyer, R. A., Hummer, K. E., Finn, C. E., Frei, B., Wrolstad, R. E. (2002). Anthocyanins, phenolics, and antioxidant capacity in diverse small fruits: *Vaccinium*, *Rubus*, and *Ribes*. *Journal of Agricultural and Food Chemistry*, 50, 519–525.
3. Kähkönen, M. P., Hopia, A. I., Heinonen, M. (2001). Berry phenolics and their antioxidant activity. *Journal of Agricultural and Food Chemistry*, 49, 4076-4082.
4. Heinonen, M (2007). Antioxidant activity and antimicrobial effect of berry phenolics – a Finnish perspective. *Molecular Nutrition and Food Research*, 51, 684–691.
5. Wu, X., Beecher, G. R., Holden, J. M., Haytowitz, D. B., Gebhardt, S. E., Prior, R. L. (2004). Lipophilic and hydrophilic antioxidant capacities of common foods in the United States. *Journal of Agricultural and Food Chemistry*, 52, 4026–4037.
6. Lähti, A. K., Riihinen, K. R., Kainulainen, P. S. (2008). Analysis of anthocyanin variation in wild populations of bilberry (*Vaccinium*

- myrtillus L.) in Finland. *Journal of Agricultural and Food Chemistry*, 56, 190–196.
7. Burdulis, D., Ivanauskas, L., Dirse, V., Kazlauskas, S., Razukas, A. (2007). Study of diversity of anthocyanin composition in bilberry (*Vaccinium myrtillus* L.) fruits. *Medicina (Kaunas)*, 43, 971–977.
 8. Йончева, Н., Георгиева, М., Иванов, Г., Михалев, К., Кондакова, В. (2010). Профил на антиоксидантния капацитет на плодове от различни видове диворастящи ягодоплодни. *Journal of Mountain Agriculture on the Balkans*, 13, 1475–1481.
 9. Terashima, M., Nakatani, I., Harima, A., Nakamura, S., Shiiba, M. (2007). New method to evaluate water-soluble antioxidant activity based on protein structural change. *Journal of Agricultural and Food Chemistry*, 55, 165–169.

ЛИПИДЕН СЪСТАВ НА СЕМЕНА ОТ КИПАРИС

*М. Ангелова-Ромова, М. Златанов,
Г. Антова, О. Тенева*

*ПУ „П. Хилендарски“, кат. Химична технология,
ул. Цар Асен 24, 4000 Пловдив, E-mail: maioan@uni-plovdiv.bg*

ABSTRACT

The lipid composition of cypress (*Cupressus*) seeds was investigated. The seeds contain 27.3% glyceride oil. The total quantity of phospholipids was 0.9%. Sterols general amounts 2.2% were found to be. In the tocopherol fraction (328 mg/kg) γ -tocopherol predominated (91.3%). Fatty acid composition of triacylglycerols was identified. In the triacylglycerols the main component were oleic, linoleic, linolenic and palmitic acids. The oxidation stability of cypress seeds oil was 3.5 h.

Key words: *Cypress seeds, glyceride oil, fatty acids, phospholipids, sterols, tocopherols.*

ВЪВЕДЕНИЕ

Кипарисът представлява вечно зелено дърво, което е широко разпространено както в северното, така и в южното полукълбо. У нас растат шест вида от рода *Juniperus* (хвойна), два от които са защитени. Използва се основно като декоративен вид в парковете и градините [4].

Листата на кипариса се използват за извличане на екстракти с противовъзпалително действие, които намират приложение в рецептури на паста за зъби и някои други продукти [14,17]. Глицеридното масло от семената на кипариса също има противовъзпалително и противопаразитно действие, поради което то намира приложение във фармацевтиката [14,17]. Съдържанието на глицеридно масло в семената достига до 40.0%, но информацията за състава му е оскъдна [15,17]. Според *Aitzemüller* [5] основните компоненти в мастнокиселинния състав на кипарисовото глицеридно масло са: линолова (24.0%), линоленова (33.6%), олеинова (15.4%), палмитинова (6.7%), стеаринова (4.1%) и сциаденова киселина (7.9%). Според други автори количеството на рядко срещаната сциаденова киселина ($C_{20:3}$), която има качества, аналогични на арахидоновата киселина ($C_{20:4}$) е в количество 3.0 – 3.5%. [15,17].

Цел на настоящата работа е да се изследва липидния състав на семена от кипарис, отглеждан у нас, по отношение на неговия мастнокиселинен състав и съдържанието на биологичноактивни вещества в тях.

МАТЕРИАЛИ И МЕТОДИ

За провеждане на изследванията са използвани семена от кипарис (род *Juniperus*) от региона на Южна България, реколта 2010 година.

Общото количество на липидите е определено тегловно, след екстракция с n-хексан в апарат на Соксле [1]. За охарактеризиране на глицеридното масло са използвани стандартни методики за анализ на липиди.

Общото количество на фосфолипиди е определено спектрофотометрично при 700 nm, след минерализиране на маслото [2]. Съдържанието на стеролите е определено спектрофотометрично, след осапунване на маслото и последващо им изолиране чрез тънкослойна хроматография [13].

Количеството и индивидуалният състав на токофероловата фракция са установени директно в маслото чрез високоефективна течностна хроматография с флуоресцентна детекция [8], а мастнокиселинният състав – чрез газова хроматография [9,10].

Оксидантната стабилност е определена кондуктометрично на база индукционния период с апарат „Rancimat“ при температура 100°C и скорост на продухване с въздух 20 dm³/h [7].

РЕЗУЛТАТИ И ДИСКУСИЯ

Съдържанието на глицеридно масло в семената от кипарис и на основните биологичноактивни компоненти в него – фосфолипиди, стероли и токофероли, които определят хранителната му стойност и биологична ценност са представени в Таблица 1.

Таблица 1. Съдържание на глицеридно масло и на биологичноактивни компоненти в маслото от кипарисови семена.

Компоненти	Съдържание
Масло в семената, % тегл.	27.3
Фосфолипиди в маслото, % тегл.	0.9
Стероли в маслото, % тегл.	2.2
Токофероли в маслото, mg/kg	328

Изследваните семена са сравнително богати на глицеридно масло (27.3%), което е близко до това в други видове растителни масла – слънчогледово, соево, рапично, където количеството му съответно е – 35.0 – 45.0%, 18.0 – 20.0% и 40.0 – 45.0% [16].

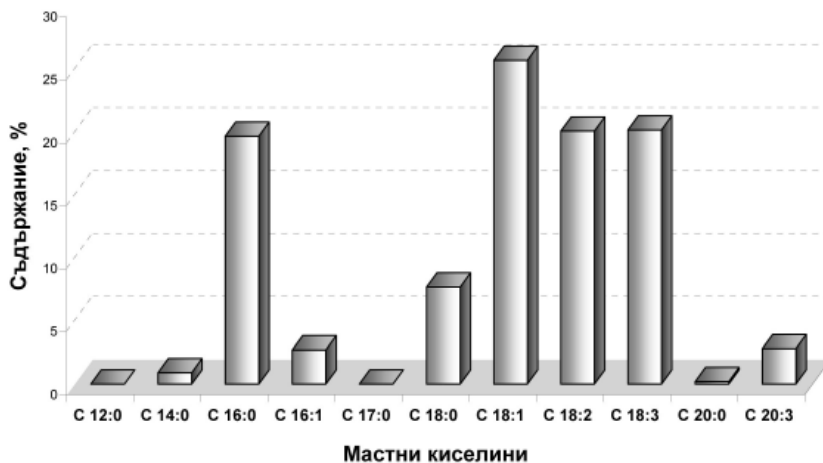
Съдържанието на фосфолипиди в масло от семената на кипарис (0.9%) съответства на това в други видове растителни масла, където то е в рамките на 0.8 – 2.0% [6,11].

Количеството на стеролите в изследваното масло (2.2%) е значително по-високо от това в други растителни масла (0.3 – 1.0%) [11,12].

Токоферолите в анализираното масло са сравнително малко – 328 mg/kg, докато в слънчогледовото масло са около 600 – 1000 mg/kg, а в соевото 650 – 1300 mg/kg [11,16].

Мастнокиселинният състав на глицеридно масло от семена на кипарис показва, че олеиновата (25.7%), линоловата (20.1%), линоленовата (20.2%) и палмитиновата (19.7%) киселини са основни компоненти в триацилглицероловата фракция (Фигура 1).

Фигура 1. *Мастнокиселинен състав на глицеридно масло от семена на кипарис*



За разлика от други растителни масла, където една мастна киселина е преобладаваща, в състава на изследваното масло количествата на палмитинова ($C_{16:0}$), олеинова ($C_{18:1}$), линолова ($C_{18:2}$) и линоленова ($C_{18:3}$) киселини са от еднакъв порядък, около 20.0%. В мастнокиселинният състав е установено наличието на сциаденова киселина ($C_{20:3}$) – 2.8%, което е по-ниско от това при предишни изследвания на този вид масла – 3.0 – 7.9% [5,15,17].

В изследваното глицеридно масло съдържанието на ненаситените мастни киселини преобладава (71.5%), като в най-голям процент са полиненаситените киселини (43.1%). Количеството на наситените (28.5%), главно палмитинова и стеаринова киселина и мононенаситените (28.4%), основно олеинова киселина са от еднакъв порядък. Установено е наличието на значителен процент палмитолеинова киселина ($C_{16:1}$) – 2.7% при 0.1 – 1.2% в други растителни масла [11,16].

Съставът на токофероловата фракция на изследваното масло е представен в Таблица 2. Идентифицирани са основните класове токофероли, като преобладаващ е γ -токоферол – 91.3%. Това определя кипарисовото масло като гама-тип, подобно на сусамовото масло [11].

Таблица 2. *Индивидуален състав на токофероловата фракция на кипарисово масло.*

Токофероли	Съдържание, %
α – Токоферол	5.8
α -3 – Токотриенол	0.2
β – Токоферол	сл.
γ – Токоферол	91.3
δ – Токоферол	2.7

Оксидантната стабилност на кипарисовото масло е 3 h 50 min, което показва, че тя е два – три пъти по-ниска, в сравнение с тази на други сурови растителни масла, като слънчогледово, соево и др. (12 – 24 h) [3]. Ниската стабилност е резултат от наличието на висок процент полиненаситени мастни киселини (главно линолова и линоленова) в триацилглицероловата фракция и сравнително ниското съдържание на токофероли в маслото.

ЗАКЛЮЧЕНИЕ

Изследваните кипарисови семена са богати на глицеридно масло (27.3%), като съставът му е различен от този на други растителни масла. То е специфично по отношение на своя мастнокиселинен състав, от една страна поради съотношението между ненаситени и наситени мастни киселини (71.5% : 28.5%) и от друга страна поради еднаквото съотношение между моно-, ди – и триненаситените мастни киселини. В мастнокиселинния състав на изследваните семена от кипарис е установено и наличието на есенциалната мастна киселина – сциадонова (C_{20:3}) в количество 2.8%. Оксидантната стабилност на глицеридното масло е сравнително ниска, поради ненаситения му характер и ниското съдържание на токофероли.

БЛАГОДАРНОСТИ

Изследванията са проведени с финансовата подкрепа на Фонд „Научни изследвания“ към МОН (договор ДВУ 02–38) и Дирекция „Научно производствена дейност“ към ПУ „Паисий Хилендарски“.

ЛИТЕРАТУРА

1. Бабачев Н. И., Неделчева Л. Б., (1974). Методи за анализ в масло-сапунената промишленост, изд. „Техника“, София.
2. Бешков М., Иванова Л., (1972). Определяне на фосфолипиди в липидни смеси, *Научни трудове на ВИХВП*, Пловдив, 20, 3, 231–234.
3. Попов А., Янишлиева Н., (1976). Автоокисление и стабилност на липидите, изд. на БАН, София.
4. Adams R. P., (2004). *Junipers of the World: The Genus Juniperus*, Trafford Publishing Co., Vancouver, Canada.
5. Aitzetmüller K., (1995). Seed Oil Fatty Acids – SOFA Database Retrieval, Unpublished Results, [http://sofa.bfel.de/...](http://sofa.bfel.de/)
6. Ajana H., Perrin J. L., Prevot A., (1986). Studies on phospholipid separations from vegetable oils by HPLC – comparison with thin-layer chromatography, *Rev. Franc. Corps Gras*, 33, 19–26.
7. Animal and vegetable fat and oils – Determination of Oxidation stability (Accelerated oxidation test), ISO 6886, 1996.
8. Animal and vegetable fats and oils – Determination of tocopherols and tocotrienols by HPLC method, ISO 9936, 1997.
9. Animal and vegetable fat and oils – Preparation of methyl esters of fatty acids, ISO 5509, 2000.
10. Animal and vegetable fat and oils – Determination of methyl esters of fatty acids (Gas chromatographic method), ISO 5508, 2000.
11. Codex standard for named vegetable oils, *CODEX-STAN 210 – 1999 (Amendment 2005, 2011)*.
12. Homberg E., Bielefeld B., (1989). Sterinsusammensetzung und Steringehalt in 41 verschiedenen pflanzlichen und tierischen Fetten, *Fat. Sci. Technol*, 91, 1, 23–27.
13. Ivanov S., Bitcheva P., Konova B., (1972). Methode de determination chromatographique et colorimetrique des phytosterols dans les huiles vegetales et les concentres steroliques, *Rev. Fr. Corps Gras*, 19, 3, 177–180.
14. Lai L. T., Naiki M., Yoshida S. H., German J. B., Gershwin M. E., (1994). Dietary Platycladus orientalis seed oil suppressed antierythrocyte autoantibodies and prolongs survival of NZB mice, *Clin Immunol Immunopathol.*, 71, 3, 293–302.

15. Munavu R. M., Odhiambo D., (1984). Physiological characterization of Nonconventional vegetable oils for fuel in Kenya, *J. Sci. Technol. (Kenya)*, 5, 45–52.
16. O'Brien R. D., (2004). Fats and oils: Introduction to the technology of oils and fats, ed. „Union of the producers of vegetable oils and oil's products in Bulgaria“, Sofia.
17. Pierre-Leandri C., Fernandez X., Lizzani-Cuvelier L., Loiseau A. et al., (2003). Chemical composition of cypress essential oils: Volatile constituents of leaf oils from seven cultivated Cupressus species, *JEOR*, 15, 4, Jul/Aug 2003.

FATTY ACIDS COMPOSITION AND FAT SOLUBLE VITAMINS CONTENT OF BIGHEAD CARP (*ARISTICHTHYS NOBILIS*)

A. Merdzhanova, D. Dobreva, M. Stancheva

*Medical University of Varna, 55 Marin Drinov St., 9000 Varna
a.merdzhanova@gmail.com*

ABSTRACT

In the present study fatty acid composition and fat soluble vitamins content were analyzed in two season's samples (spring and autumn) freshwater bighead carp (*Aristichthys nobilis*).

Analysis of fatty acid methyl esters was performed by gas chromatography system with MS detection. Vitamins A, D₃ and E were analyzed simultaneously using RP-HPLC system. The sample preparation procedure includes saponification and liquid-liquid extraction of the unsaponifiable matter.

The fatty acid and vitamins contents of the investigated fish species showed significant seasonal changes. The spring bighead carp characterized with saturated fatty acid (SFA) (37.5%) and mono unsaturated fatty acids (MUFA) (22.1%), and poly unsaturated fatty acids (PUFA) (40.4%), including essential omega 3 fatty acids (23.0%). The autumn samples showed higher SFA (40.5%) and MUFA (34.8%), and lower PUFA (24.6%), due to reduced omega 3 fatty acids (9.7%).

Similar amounts of alpha-tocopherol were found in two season's fish samples – 1097.0 $\mu\text{g}\cdot 100\text{g}^{-1}\text{ww}$ for spring and 1051.8 $\mu\text{g}\cdot 100\text{g}^{-1}\text{ww}$ for autumn bighead carp. The higher amounts of all-trans retinol (15.7 $\mu\text{g}\cdot 100\text{g}^{-1}\text{ww}$) and cholecalciferol (8.0 $\mu\text{g}\cdot 100\text{g}^{-1}\text{ww}$) were found in spring fish samples, while in autumn bighead carp were found – 9.0 $\mu\text{g}\cdot 100\text{g}^{-1}\text{ww}$ and 5.4 $\mu\text{g}\cdot 100\text{g}^{-1}\text{ww}$, respectively.

Key words: *Aristichthys nobilis*, fatty acids, retinol, alpha-tocopherol, cholecalciferol

INTRODUCTION

Fish tissue is considered as a valuable source of proteins, fats, vitamins and minerals, which are very important for human health and might be obtained from the diet. Many studies suggest that fish is one of the most important dietary sources of vitamin A (all-trans-retinol), vitamin D₃ (cholecalciferol) and vitamin E (alpha-tocopherol) and also essential fatty acids (FA), but their contents depend on the fish species and season of catch. Therefore we need to determine their contents in the edible parts of fishes [1, 2].

Aquaculture in Bulgaria is mainly fresh water. One of the most farming warm-water fishes in our country are carps family (about 50% of total aquaculture production). After common carp, the bighead carp (*Aristichthys nobilis*) is another highly bred member of this family – in freshwater farms and dam lakes [3].

There is limited information in the scientific literature about the nutritive composition, especially about vitamins, on bighead carp edible tissue.

The aim of this study was to determine and compare fat soluble vitamins content and fatty acids composition in bighead carp raw fillets in two seasons – spring and autumn.

MATERIALS AND METHODS

Collection of samples

Samples of Bighead carp fish species were caught from Pyasachnik Dam Lake (Plovdiv region), Spring and Autumn 2010. Three specimens of

each fish sample were used as a material for FA and vitamin analysis. The fishes were filleted with the skin and the samples were homogenized using kitchen homogenizer. The raw material was used for the determination of fat soluble vitamins content and FA composition.

Lipid extraction and fatty acid analysis

The samples of freshly prepared homogenate ($5.000 \pm 0.001\text{g}$) were extracted in triplicate with chloroform:methanol (1:2 v/v) according to Bligh and Dyer procedure [4]. The chloroform layers were evaporated until dryness and quantified gravimetrically. Total lipid content of edible tissue was determined for each group ($n = 3$) and the results were presented as g per 100 g wet weight ($\text{g}\cdot 100\text{g}^{-1}\text{ww}$).

The dry residue of the chloroform fraction was methylated by base-catalyzed transmethylation using 2M KOH in methanol and n-hexane [5]. The hexane layer was separated and analyzed by GC-MS. All chemicals used in the experiments were analytical grade (Merck, Germany; Sigma-Aldrich, Germany).

Gas chromatography was performed by a model FOCUS Gas Chromatograph with auto sampler A3000, equipped with Polaris Q MS detector (Thermo Scientific, USA). The capillary column used was a TR-5 MS, 30 m length, 0.25 mm i.d. Helium was used as a carrier gas at a flow rate 1 ml/min. Peaks were identified according to two parameters: Retention Time (RT) based on available FAME mix standard (SUPELCO F.A.M.E. Mix C4 – C24) and mass spectra (ratio m/z) – compared to internal Data Base (Thermo Sciences Mass Library, USA). The recovery rates were calculated utilizing the external standard method. The results were expressed as FA % of total FA.

Extraction of fat soluble vitamins and HPLC analysis

The sample preparation includes several steps: an aliquot of the homogenized sample ($1,000 \pm 0.005\text{g}$) was weighed into a glass tube with a screw cap and 1% of methanolic L-ascorbic acid and 1M methanolic potassium hydroxide were added. Six parallel samples of fish edible tissue were prepared and saponified at 80°C for 20 min. The interested components were extracted with n-hexane and the extract was evaporated under nitrogen

[6]. The dry residue was dissolved in methanol and injected (20 μ l) into the liquid chromatography system.

Three fat soluble vitamins were analyzed simultaneously using reversed phase high performance liquid chromatography (RP-HPLC) system (Thermo Scientific Spectra SYSTEM) equipped with analytical column ODS2 Hypersil™ 250x4, 6 mm, 5 μ . All-trans retinol and cholecalciferol were detected by UV, alpha-tocopherol by fluorescence detection. The mobile phase was composed 97:3 = MeOH:H₂O, flow rate 1ml.min⁻¹. The qualitative analysis was performed by comparing the retention times of pure substances: at λ_{\max} = 325 nm for retinol; λ_{\max} = 265 nm for cholecalciferol and alpha-tocopherol fluorescence at λ_{ex} = 288 nm and λ_{em} = 332 nm. The quantitation was done by the method of external calibration comparing the chromatographic peak areas of the corresponding standards (Retinol, Supelco; DL-alpha Tocopherol, Supelco; Cholecalciferol, Supelco). The results were expressed as μ g per 100g wet weight (μ g.100g⁻¹ww). All chemicals used in the experiments were for liquid chromatography (Sigma-Aldrich, Germany).

Statistical analysis

The data were analyzed using Graph Pad Prism 5 software. Two-way ANOVA (nonparametric test) and student t-test statistical analysis was employed for the calculations. The differences were considered significant at $p < 0.05$.

RESULTS AND DISCUSSION

Total lipid content and FA composition

The lowest total lipid amount was found in spring bighead carp (3.80 \pm 0.09g.100⁻¹g ww), whereas the autumn's samples presented the highest content (7.33 \pm 0.25g.100⁻¹g ww). Our results are higher for both season than presented by Vujkovic *et al.* (1999) and Hadjinikolova *et al.*, 2008 [7, 8].

The typical FA composition of freshwater fish species is a result from the FA composition of their food – phytoplankton and other aquatics plants [2, 7, 9]. Vujkovic *et al.* were found a relative pattern MUFA>SFA>PUFA in bighead carp from local fish farm for both seasons – spring and autumn [2]. A deflection of this pattern was observed for spring bighead carp in our

investigation, in which PUFA content was significantly higher than SFA ($p < 0.001$) and MUFA ($p < 0.001$) (PUFA > SFA > MUFA). Significantly higher quantities in SFA compared to MUFA ($p < 0.001$) and PUFA ($p < 0.001$) were found for the autumn bighead carp ($p < 0.05$) (SFA > MUFA > PUFA) (Fig. 1).

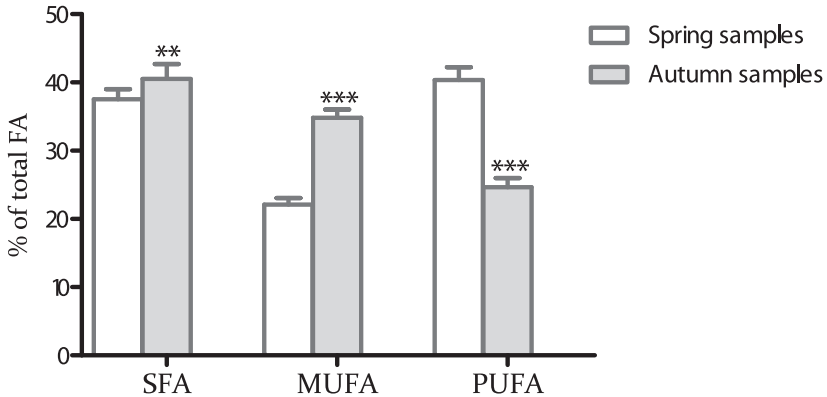


Figure 1. Fatty acid composition in both season's bighead carp raw fillets
*** $p < 0.001$ and ** $p < 0.05$

Many authors found out a great variation in FA content with predomination of palmitic (C16:0) and stearic (C18:0) SFA among the fish species [2, 7]. Our results also revealed that in all studied fish species the dominating SFAs were palmitic, stearic and myristic acid (Table 1). The highest level of palmitic acid was measured for autumn sample (28.10%), which is in agreement with the results of Vujkovic et al. who found highest levels of palmitic and stearic acid in autumn bighead carp and silver carp species. Similar results were obtained by other authors [7, 10, 11].

Among MUFAs the highest levels were found for oleic acid followed by palmitoleic acid in two seasons studied fish species. The highest levels of erucic acid were measured in the spring carp. It may be supposed that the low MUFA levels in spring bighead carp are related to the lower concentrations of palmitoleic and oleic acids (Table 1). Few studies reported that the oleic acid is the main MUFA in freshwater fish species. According to Mieth and Vujkovic the highest levels of oleic acid were measured in autumn bighead carp fillets (up to 34.6%) compared to spring samples [7, 11]. Our results showed the same trends for this FA (Table 1).

Table 1 *Fatty Acid profile in bighead carp species (spring and autumn (mean ± SD) ⁺*

Fatty acid % of total FA	Bighead carp Spring 2010	Bighead carp Autumn 2010
<i>Saturated Fatty Acid</i>		
C 12:0	2.10±0.50	1.00±0.05
C 14:0	2.96±0.70	2.30±0.45
C 16:0	14.70±1.20	28.10±1.65***
C 17:0	0.79±0.05	0.60±0.08
C 18:0	9.11±1.05	5.50±0.80***
C 20:0	2.09±0.72	0.55±0.05
C 21:0	0.00	0.09±0.01
C 22:0	2.56±0.70	0.55±0.04
C 23:0	0.46±0.02	0.15±0.01
C 24:0	2.04±0.90	1.50±0.30
<i>Monounsaturated Fatty Acid</i>		
C 14:1	1.65±0.50	0.75±0.10
C 16:1	5.25±0.90	10.50±1.05***
C 17:1	0.76±0.06	0.15±0.01
C 18:1 omega9	10.21±1.18	22.35±1.60***
C 20:1	1.30±0.35	0.50±0.03
C 22:1 omega9	1.91±0.60	0.30±0.02
C 24:1	1.04±0.25	0.25±0.02
<i>Polyunsaturated Fatty Acid</i>		
C 18:3 omega6	0.00	0.20±0.01
C 18:2 omega6	4.55±1.05	9.58±1.15***
C 18:3 omega3	2.21±0.54	0.80±0.10

C 20:5 omega3	5.81±0.80	2.55±0.75***
C 20:4 omega6	7.99±1.00	3.75±0.85***
C 20:3 omega6	1.55±0.45	0.65±0.10
C 20:2	1.60±0.40	0.60±0.05
C 20:3 omega3	1.85±0.50	0.58±0.02
C 22:6 omega3	13.15±1.05	5.71±0.70***
C 22:2	2.14±0.81	0.35±0.05

*** $p < 0.001$; + all samples analyzed in triplicate

Four major PUFAs were identified as dominant: C22:6 omega3, linoleic (LA, C18:2 omega 6), C20:5 omega3 and arachidonic acid (ARA, C20:4 omega 6) (Table 1). Significant amounts of the biologically important PUFAs such as C22:6 omega3, C18:2 omega6, C20:5 omega3 and C20:4 omega6 were found in all studied fish samples. The highest levels of C22:6 omega3 and EPA were measured in the spring fish fillets (33.00% and 22.80% of total PUFAs) whereas in autumn its level significantly decreased (23.00% and 10.20% of total PUFAs) (Table 1). A possible explanation is that nutrition spectrum of this fish species, which consumes only natural food, strongly depends on the availability of phyto – and zoo-plankton, which is rich on omega3 PUFA (DHA and EPA) [8, 9]. DHA and EPA metabolism strongly influenced by water temperature, which is higher in autumn, and this leads to decrease in their values [2]. For both season the C20:4 omega6 levels in studied fish species were lower than those of C22:6 omega3 (Table 1). The bighead carp feed predominantly with pelagic phytoplankton, which contains low levels of C20:4 omega6. This freshwater food chain from phytoplankton via zooplankton to fish is one of the main reasons for accumulation of significant amounts of omega6 PUFAs.

The studied spring bighead carp is characterized with relatively high levels of omega3 FA and low levels of omega6 FA (Table 2). This ratio changed in autumn's samples – omega6 PUFAs increases at the expense of reduction on omega3 PUFAs. These results are in agreement with Vujkovic et al., who observed similar changes in autumn silver carp and bighead carp [7].

Table 2. PUFA/SFA and omega6/omega3 ratios, total sum of omega3 and omega6 FA content

Fatty acid % of total FA	Bighead carp Spring 2010	Bighead carp Autumn 2010
Omega 6	14.10	14.13
Omega 3	23.02	9.65***
Omega 6/omega3	0.61	1.46
PUFA/SFA	1.08	0.61

*** $p < 0.001$

The omega6/omega3 FA ratio has been suggested to be an useful indicator for comparing the relative nutritional value of a given fish. According to the UK Department of Health, a ratio within 0.20–1.50 would constitute a healthy human diet and values higher than 1.50 would be harmful and may promote cardiovascular diseases [13]. For studied freshwater fish the omega6/omega3 FA ratio (Table 2) was within the recommended range. Values for PUFA/SFA ratio greater than 0.45 are recommended [13]. Our results are in agreement with this requirement and highest and most balanced PUFA/SFA ratio was observed in spring fish samples whereas the lowest value was found for autumn's (Table 2).

Vitamins content

The results from the determination of vitamins A, D₃ and E content in both seasons' fish samples are given in table 3 as µg per 100g wet weight (µg.100g⁻¹ ww).

Table 3. Fat soluble vitamins content in bighead carp fillets, µg.100g⁻¹ ww (mean ± SD)⁺

Vitamin	Season	
	Spring	Autumn
Vitamin A	15.66±1.91	8.97±1.40**
Vitamin D ₃	8.00±0.99	5.40±0.30***
Vitamin E	1097.03±44.06	1051.80±37.11

*** $p < 0.001$ and ** $p < 0.05$; + all samples analyzed in triplicate

The amounts of vitamin A ($p < 0.005$) and vitamin D₃ ($p < 0.001$) were higher in the spring sample of bighead carp fillets (table 3). Their contents correlated with PUFAs values. For vitamin E were observed the same relations but the differences in contents in two seasons are not significant. The three fat soluble vitamin contents did not correspond to the total lipid's amounts.

There is no information in the scientific literature about the content of vitamins in bighead carp edible tissue. The data for common carp (fish on the same family) about retinol, cholecalciferol and alpha-tocopherol contents in fish fillets given by others were of the same order of magnitude as ours [14, 15, 16, 17].

Karatas et al were measured 125 $\mu\text{g}\cdot 100\text{g}^{-1}\text{ww}$ retinol and 1200 $\mu\text{g}\cdot 100\text{g}^{-1}\text{ww}$ alpha-tocopherol in the edible tissue of common carp [14]; in the Czech food composition database for the same fish were given values of 44 $\mu\text{g}\cdot 100\text{g}^{-1}\text{ww}$ for retinol and 630 $\mu\text{g}\cdot 100\text{g}^{-1}\text{ww}$ for alpha-tocopherol in raw carp fish fillets [15]. Almost the same data was presented in the Slovak Food Composition Data Bank – 44 $\mu\text{g}\cdot 100\text{g}^{-1}\text{ww}$ for vitamin A and 630 $\mu\text{g}\cdot 100\text{g}^{-1}\text{ww}$ for Vitamin E in raw carp fish tissue [16].

The Whole Food Catalog database was given a value of 4 $\mu\text{g}\cdot 100\text{g}^{-1}\text{ww}$ for retinol, 14 $\mu\text{g}\cdot 100\text{g}^{-1}\text{ww}$ for cholecalciferol, which is in a good agreement with our findings, whilst a much higher value for alpha-tocopherol (2000 $\mu\text{g}\cdot 100\text{g}^{-1}\text{ww}$) compared to our results was indicated [17].

CONCLUSION

Our study presented fatty acids composition and fat soluble vitamin contents on two seasons' bighead carp. The fatty acid and vitamins contents showed seasonal changes.

Spring bighead carp have lower SFA (37.5%) and MUFA (22.1%), and highest PUFA (40.4%), especially omega 3 fatty acids (23.0%). In contrast autumn samples showed higher SFA (40.5%) and MUFA (34.8%), and lower PUFA (24.6%), due to reduced omega 3 fatty acids (9.7%). Omega6/omega 3 ratio increased in autumn samples (up to 1.46) due to reduction of omega 3 PUFA during this period. More balanced PUFA/SFA ratio was obtained for the spring bighead carp (1.08).

All-trans retinol (15.7 $\mu\text{g}\cdot 100\text{g}^{-1}\text{ww}$) and cholecalciferol (8.0 $\mu\text{g}\cdot 100\text{g}^{-1}\text{ww}$) were found in higher amounts in spring fish samples. Similar differences were

not observed of alpha-tocopherol contents – 1097.0 $\mu\text{g}\cdot 100\text{ g}^{-1}\text{ww}$ for spring samples and 1051.8 $\mu\text{g}\cdot 100\text{g}^{-1}\text{ww}$ for autumn bighead carp.

Spring catches species are better sources of omega 3 FA and vitamin A and vitamin D₃. Bighead carp edible tissue in two seasons is rich on fat soluble vitamins and unsaturated fatty acids, which makes it a desirable item in the human diet.

REFERENCES

1. Anderson J., Young L., Fat-Soluble Vitamins, *Food and Nutrition series, Colorado State University*, 2008, 9.315
2. Tocher D., Metabolism and functions of lipids and fatty acids in teleost fish, *Review Fishery Science*, 2003, 11,107–184
3. National Strategic Plan for Fisheries and Aquaculture, 2007 – 2013. Ministry of Agriculture and Forestry, National Agency for Fisheries and Aquaculture, Bulgaria
4. Bligh E., Dyer W. J., A rapid method of total lipid extraction and purification, *Canadian Journal of Biochemistry and Physiology*, 1959, 37, 913–917
5. EN ISO 5509:2000, Animal and vegetable fats and oils – Preparation of methyl esters of fatty acids
6. Dobрева D. A., Galunska B., Stancheva M., Liquid chromatography method for the simultaneous quantification of fat soluble vitamins in fish tissue, *Scripta Scientifica Medica, Varna Medical University*, 2011, 43, 1, 276–279.
7. Vujkovic G., Karlovic D., Vujkovic A., Vorosbaranyi I. and Jovanovic B., Composition of muscle tissue lipids of Silver carp and Bighead carp, *Journal of the American Oil Chemists' Society*, 1999, 76, 4, 475–480
8. Hadjinikolova L., Nikolova L. and Stoeva A., Comparative investigations of the nutritive value of carp fish meat (*Cyprinidae*), growt at organic aquaculture conditions, *Bulgarian Journal of Agricultural Science*, 2008, 14 (2), 127–132
9. Steffens W., Wirth M., Freshwater fish – an important source of n-3 polyunsaturated fatty acids: a review, *Archivies of Polish Fisheries*, 2005, 13, 1, 5–16

10. FAO/WHO Scientific and ethical challenges in agriculture to meet human needs; <http://www.fao.org/docrep/003/X8576M/x8576m05.htm>
11. Mieth G., Wirth M., Friedrich M., Steffens W., Lieder U., Lipid Content and Fatty Acids Composition of Silver Carp (*Hypophthalmichthys molitrix* /Val./), *Cyprinida Lipid Content, 1st Report, Die Nahrung*, 1989, 33:91–93
12. Simopoulos A., Importance of the Ratio of Omega-6/Omega-3 Essential Fatty Acids: Evolutionary Aspects. Omega-6/Omega-3 Essential Fatty Acid Ratio: The Scientific Evidence, *World Review Nutrition Dietetics*, 2003, 92, 1–22
13. Culyer A., Supporting research and development in the NHS: a report to the Minister of Health, *London, HMSO, ISBN: 0113218311*, 1994
14. Karatas F., Obek E., Karatepe M., Saydam S, Saatci Y., An Investigation of Vitamin Levels of the Carp (*Cyprinus carpio* L.) Muscle Tissue Subjected to Thiazole Copper (II) Complex, *Pakistan Journal of Biological Sciences*, 2002, 5: 54–56
15. Czech food composition database, 2011; <http://www.czfcdb.cz/en/food/?id=239>
16. Slovak Food Composition Data Bank, 2010; <http://www.pbd-online.sk/en#>
17. Whole Food Catalog database, 2009; http://wholefoodcatalog.info/food/carp%28cultured,_raw%29/nutrients/

ORGANOCHLORINE PESTICIDES AND POLYCHLORINATED BIPHENYLS IN FRESHWATER FISH

St. Georgieva, M. Stancheva, L. Makedonski

*Department of Chemistry, Medical University – Varna,
Marin Drinov 55, 9002 Varna, Bulgaria,
e-mail: stanislavavn@mail.bg*

ABSTRACT

Organochlorine pesticides (OCPs) and polychlorinated biphenyls (PCBs) were determined in muscle tissue of three freshwater fish species: common carp (*Cyprinus carpio*), grass carp (*Ctenopharyngodon idella*) and bighead carp (*Hypophthalmichthys nobilis*). Fish samples were collected in 2010 from the Pyasachnik Dam Lake. The OCPs and PCBs were analysed in order to evaluate the status and potential sources of pollution in area of the lake. The species were selected because of their importance to local human fish consumption.

The fifteen congeners of PCBs, p,p'-DDT and its two main metabolites p,p'-DDE and p,p'-DDD were determined by capillary gas chromatography system with MS detection. DDTs were the predominant organohalogenated contaminants in all species, with the p,p' – DDE contributing to more than 67% to the total DDTs. All samples of muscle tissue examined contained detectable levels of p,p'-DDE and p,p' – DDD. The residues of p,p' – DDT were not detected in all samples. The sum of the individual PCB congeners

was determined lower than those found in similar fish species from other aquatic ecosystems.

Key words: *organochlorine pesticides; polychlorinated biphenyls; fish; Bulgaria*

INTRODUCTION

Organochlorine pesticides (such as DDT and its metabolites DDE and DDD) and polychlorinated biphenyls (PCBs) are widely distributed environmental pollutants. They characterised by a high bioaccumulation potential in food chains and therefore may pose a serious threat to upper trophic levels of aquatic communities [1]. Chlorinated pesticides such as DDT are effective pest control chemicals, which were used in agriculture worldwide in the past and are still in use in many developing countries (malaria eradication, etc.). Polychlorinated biphenyls are group of chemicals primarily used in transformers, capacitors, paints and printing inks, and also in many other industrial applications. DDTs and PCBs are readily accumulated by aquatic organisms [2], and although banned decades ago, remain a concern in many aquatic systems [3].

Data on the presence and distribution of organohalogenated contaminants in fish and especially edible fish species are therefore important not only from ecological, but also human health perspective. In biological systems, several of these chemicals are potentially carcinogenic and may cause alternations in endocrine, reproductive and nervous systems [4]. Once released into the aquatic environment, these chemicals biomagnify in the food web, and consequently high trophic level organisms may accumulate high concentration in their fatty tissues [5, 6].

The Pyasachnik Dam Lake is located 50 km from Plovdiv, Bulgaria. It is the largest dam lake in this region. Its water are used for water-supply and irrigation. Potential sources of pollution are agricultural activity along the dam and long-range atmospheric transport. To our knowledge, no studies carried out on levels of organohalogenated pollutants in fish in this aquatic ecosystem.

The aim of the present study was to investigate the presence of organochlorine pesticides (DDT and its metabolites DDE and DDD) and poly-

chlorinated biphenyls (PCBs) in several fish species from Pyasachnik Dam Lake.

MATERIALS AND METHODS

Sampling

Three freshwater fish species: common carp (*Cyprinus carpio*), grass carp (*Ctenopharyngodon idella*) and bighead carp (*Hypophthalmichthys nobilis*) were obtained from fishermen along the Pyasachnik Dam Lake between May and June 2010. The samples were transferred immediately to the laboratory in foam boxes filled with ice and were stored in a freezer (-18°C) until analysis.

The species were selected for their importance to local human fish consumption. Common carp is omnivorous – can eat water plants, but prefer to scavenge the bottom for insects, crustaceans, crayfish and benthic worms. The grass carp is herbivorous – adults of the species feed primarily on aquatic plants. Bighead carp is primarily filter feeder and preferentially consume zooplankton but also phytoplankton and detritus.

DDTs and PCBs analysis

The analytical method for determination of residues of OCP and PCB was based on BDS EN 1528:2001. Briefly, the edible tissues of fish were homogenized and sub-samples of 20 g were taken for extraction. Each sample was spiked with internal standards PCB 30 and PCB 204. These standards were used to quantify the overall recovery of the procedures. The OCs were extracted with hexane / dichloromethane (3/1, v/v) in Soxhlet apparatus. After lipid determination, the extract was cleaned-up on a glass column packed with neutral and acid silica. PCBs and OCPs were eluted with 80 ml n-hexane followed by 50 ml n-hexan/dichloromethane (80:20). The eluates were concentrated to near dryness and reconstituted in 0.5 ml in hexane.

Gas chromatographic analysis of the DDTs and PCBs were carried out by GC FOCUS (Thermo Electron Corporation, USA) using POLARIS Q Ion Trap mass spectrometer and equipped with an AI 3000 autosampler. Experimental MS parameters are the following: the Ion source and Transfer line temperatures were 220°C and 250°C, respectively. The splitless Injector temperature was 250°C. For DDTs determination the oven was programmed as follows: 60°C (1 min), 30°C/min to 180°C, 5°C/min to 260°C, 30°C/min to 290°C with a final hold for 3.0 min. The PCBs experimental temperature program – 90°C for 1 min, then programmed 30°C/min to 180°C, 2°C/min to

270°C, 30°C/min to 290°C with a final hold for 3.0 min. Splitless injections of 1 µl were performed using a TR-5ms capillary column coated with cross-linked 5% phenyl methyl siloxane with a length of 30 m, 0.25 mm ID and a film thickness of 0.25 µm. Helium was applied as carrier gas at a flow of 1 ml/min. The selectivity of the IT-MS/MS method was based on the appropriate selection of parent ions for the detection of each analyte by mass spectrometry extracted ion mode.

Pure reference standard solutions (EPA 625/CLP Pesticides Mix 2000 µg/ml – Supelco and PCB Mix 20 – Dr. Ehrenstorfer Laboratory), were used for instrument calibration, recovery determination and quantification of compounds. Measured compounds were p,p'-DDT, p,p'-DDD and p,p'-DDE, PCB congeners: IUPAC № 28, 31, 52, 77, 101, 105, 118, 126, 128, 138, 153, 156, 169, 170, 180).

The detection limit of the method (LOD) varied from 2 to 5 ng/g lipid weight for PCBs and from 1 to 5 ng/g for the DDT and its metabolites. The recoveries were within 73–108 %. Recoveries were determined by adding known amounts of PCBs and DDTs standards (at three levels of concentrations) to empty samples before extraction. The RSD values with five times repeatedly determined was less than 16%.

The quality control was performed by regular analyses of procedural blanks and certified reference materials: BCR – 598 (DDTs in Cod liver oil) and BB350 (PCBs in Fish oil) – Institute for Reference Materials and Measurements, European commission.

RESULTS AND DISCUSSIONS

DDT and its metabolites

Lipid contents and concentrations of p,p'-DDE, p,p'-DDD and p,p'-DDT found in muscle of selected fish species, average of duplicate measurements, are present in Table 1. In the environment DDT metabolised slowly and the metabolite DDE is particularly persistent compound [7]. The metabolite p,p'-DDE constituted more than 67% of the ΣDDTs for each species, followed by p,p'-DDD (12 – 32%). The concentrations of p,p'-DDE in common carp, grass carp and bighead carp muscle samples were 18.81, 7.45, 20.42 ng/g ww (wet weight), respectively. DDE concentration found in common carp of the present study is lower then concentration levels of carp from the Kahramanmaras, Turkey (4–156 ng/g ww) [8].

Table 1. Lipids (%) and concentrations of DDTs (ng/g wet weight) in freshwater fish

fish compound	common carp (<i>Cyprinus carpio</i>)	grass carp (<i>Ctenopharyngodon idella</i>)	bighead carp (<i>Hypophthalmichthys nobilis</i>)
Lipids, %	8.39	3.24	0.66
p,p' – DDE	18.81	7.45	20.42
p,p' – DDD	9.15	3.27	2.95
p,p' – DDT	0.00*	0.00	0.00
Σ DDTs (ng/g ww)	27.06	10.72	23.37

*Values below LOD were set to zero.

In our study the p,p'-DDE / p,p'-DDT ratio in the muscle of the investigated species correlated with exposure to DDT in the past (high p,p'-DDE concentrations and low p,p'-DDT content). Another metabolite of DDT, p,p'-DDD, was also found, but in lower amounts than p,p'-DDE. The p,p'-DDT in all analyzed fish species were found under limit of detection of the method.

ΣDDTs (sum of p,p'-DDE, p,p'-DDD and p,p'-DDT) in common carp, grass carp and bighead-carp muscle samples were measured 27.06, 10.72, and 23.37 ng/g ww, respectively (Table 1). The concentrations of DDTs in common carp samples from Pyasachnik Dam Lake were found lower than those reported by Erdogru, Ö., 2005 for carp and nose carp from the Kahramanmaras, Turkey (4.5 – 170 and 8.4 – 246 ng/g ww, respectively) [8], and those reported by Covaci, A. et al., 2006 from Danub Delta (2 847 ng/g lipid weight) [9]. Grass carp and bighead carp sampled from Pearl River Delta, China (Kong et al., 2005) [10] were found to contain 7.4 – 20.57 ng/g ww and 1.5 – 25.33 ng/g ww DDTs, respectively.

PCBs contamination

The concentrations of individual PCBs congeners found in different fish species are summarized in Table 2. The most persistent PCB congeners (PCB 138, 153 and 180) were found only in fish tissues of common carp and bighead carp, but with a lower contribution to PCBs than reported for similar species from other rivers and lakes in Europe [8, 11]. They are defined by WHO as important for evaluating the risk to human health and are called indicator PCBs, such as PCBs 28, 52, 101, 118 (noted with * in Table 2).

ΣPCBs (sum of 15 congeners) were found in detectable levels in muscle tissues of common carp (7.52 ng/g ww), grass carp (0.98 ng/g ww) and of bighead carp (1.65 ng/g ww). The contamination degree with PCBs of the freshwater fish samples from the Pyasachnik Dam Lake were lower than PCB levels found in other countries. The average PCB levels in common carp from Lake Zemplinska Sirava (Slovak Republic) were identified 33.41 mg/kg fresh weight [11]. ΣPCB concentrations found by Erdogru et al., 2005 [8] in carp and wels muscle from the Kahramanmaras, Turkey ranged between nd – 4.8 and 0.39 – 42.3 ng/g ww, respectively.

Table 2. Concentrations of individual PCBs congeners (ng/g wet weight) in freshwater fish

compound	fish	common carp (<i>Cyprinus carpio</i>)	grass carp (<i>Ctenopharyngodon idella</i>)	bighead carp (<i>Hypophthalmichthys nobilis</i>)
PCB 28*+31		1.29	0.98	0.69
PCB 52*		nd	nd	0.08
PCB 77		nd	nd	nd
PCB 101*		nd	nd	nd
PCB 105		nd	nd	nd
PCB 118*		nd	nd	nd
PCB 126		nd	nd	nd
PCB 128		nd	nd	nd
PCB 138*		1.12	nd	0.02
PCB 153*		0.94	nd	0.19
PCB 156		nd	nd	nd
PCB 169		nd	nd	nd
PCB 170		1.96	nd	nd
PCB 180*		2.21	nd	0.67
Σ PCBs (ng/g ww)		7.52	0.98	1.65

*nd – not detection, * Indicator PCBs*

Other freshwater fish species – barbel and chub from rivers of the North of Luxembourg contained Σ PCBs ranging from 29.6 to 158.2 ng/g ww and from 21.7 to 195.3 ng/g ww, respectively – reported by Boscher, A. et al., 2010 [12].

CONCLUSIONS

In present study the analysis of fish tissues of carp, grass carp and big-head carp showed a mean total load of DDT pollutants 27.06, 10.72, and 23.37 ng/g ww, respectively. DDTs were the predominant organohalogenated contaminants in all species, with the p,p – DDE contributing to more than 67% to the total DDTs. In all samples DDT was present only in the form of its metabolites p,p' – DDE and p,p' – DDD, suggesting previous contamination.

The highest residue concentrations of PCBs quantified in our study were found in muscle tissue of common carp 7.52 ng/g ww. The residues of PCBs in bighead carp and grass carp were found lower. The very low levels of PCBs observed in fish tissues correspond with the fact that no industrial activities that lead to the spread of persistent organic pollutants in the area of Pyasachnik Dam Lake.

In general, concentrations of DDTs and PCBs in fish species: carp, grass carp and bighead carp from the Dam Lake Pyasachnik were found lower than levels measured in the same fish species from rivers and lakes in Europe and Asia.

ACKNOWLEDGMENT

This study was financed by the National Science Fund, Ministry of Education and Science of Bulgaria (Project DVU 440/2008).

REFERENCES

1. Fisk A. T., Hobson K.A., Norstrom R. J. *Environ Sci Technol*, 35 (2001) 732–8.
2. Gray J. S. *Marine Pollution Bulletin* 45 (2002) 46–52
3. Smith A. G., Gangoli S. D., *Food Chem. Toxicol*, 40 (2002) 767–779.
4. Langer P., Kocan A., Tajtakova M., Petrik J., Chovancova J., Drobna B., et al. *J Occup Environ Med*, 45 (2003) 526– 32.
5. Serrano R., Simal-Julian A., Pitarch E., Hernandez F., Varo I., Navarro J. C., *Environmental Science and Technology*, 37 (2003) 3375–3381.
6. Storelli M. M., Marcotrigiano G. O. *Chemosphere*, 62, 375–380 (2006)
7. Ferreira M., Antunes P., Gil O., Vale C., Reis-Henriques M. A. *Aquatic Toxicology*, 69 (2004) 347–357
8. Erdogruł Ö., Covaci A., Schepens P. *Environment International*, 31 (2005) 703–711.
9. Covaci A., Gheorghe A, Hulea O, Schepens P. *Environmental Pollution*, 140 (2006) 136–149.
10. Kong K. Y., Cheung K. C., Wong C. K. C., Wong M.H. *South China Water Research* 39 (2005) 1831–1843
11. Šalgovicova D., Zmetacova Z., *Journal of Food and Nutrition Research* Vol. 45, 2006, No. 4, pp. 171–178
12. Boscher A., Gobert S., Guignard C., Ziebel J., L’Hoste L., Gutleb A. C., Cauchie H.-M., Hoffmann L., Schmidt G. *Chemosphere*, 78 (2010) 785–792

НАУЧНИ ТРУДОВЕ
том 38, кн. 5, 2011

Химия

Предпечатна подготовка: Цветелина Сотирова
Печат и подвързия: УИ „Паисий Хилендарски“

ISSN 0204–5346

